Department of Electrical and Computer Engineering

Control of a Multilevel Inverter for Wind Energy Conversion System with Energy Storage and Condition Monitoring Options

Md. Liton Hossain

This thesis is presented for the Degree of
Doctor of Philosophy
of
Curtin University

April 2020

Declaration

I, myself, declare here that as far my knowledge, this thesis contains no conflict of interest with any other thesis's previously published by any third person or party except the cited ones.
This thesis contains also no materials which have been published or accepted for the award of any other degree in any university.

Signature:

Md Liton Hossain

Date: 27/11/2020

Abstract

Wind energy has become the second most common source of renewable energy in the world which plays a vital role in the modern power sector. There have been several design and implementation constraints when converting and utilizing this energy effectively. These constraints and challenges could be resolved by designing a more effective and efficient wind energy conversion system (WECS). The most critical section of WECS is the power electronic converter (PEC), which has brought a tremendous enhancement to industrial applications. The PEC consists of a rectifier and inverter. The conventional inverter reduces the machine's operational lifetime, creates synchronization issues with the grid, and produces low output voltage with high total harmonic distortion in their output voltages. Multilevel inverter (MLI) is an emerging technology which has brought about a technological revolution in high-power and medium-voltage industrial applications by overcoming the drawbacks of a conventional inverter. The performance of the MLI is solely dependent on its topology and the controller. Cascaded half bridge inverter (CHBI) is one of the most promising topologies among MLIs, since it requires the least components during fabrication. However, the CHBI requires a large number of isolated dc sources, which restrict it being coupled with a dc-link. As such a generalized three-phase CMLI based on conventional inverter is proposed in this thesis, which requires four non-isolated series-connected dc-link capacitors and is easily coupled with the rectifier. However, the three-phase CMLI suffers from voltage balancing issues across the non-isolated series-connected dc-link capacitors. Therefore, a space vector pulse width modulation (SVPWM) controller is proposed in this thesis, which controls the three-phase CMLI and balances the voltages across the dc-link capacitors. In addition, the proposed SVPWM controls the rectifier and minimizes the ripples of the dc-link voltage. A complete WECS along with rectifier, three-phase CMLI, and SVPWM has been designed and simulated in the MATLAB software environment. An experimental setup of the WECS has also been developed to validate the simulation results in which a synchronous generator plays the role as a wind generator.

The WECS may encounter various faults within the switching devices of the three-phase CMLI and the dc-link capacitors, which contribute to the significant loss of revenue. If these faults are not monitored and detected in the early stages, they may lead to catastrophic failures to the WECS. Since most wind power plants are located in remote areas or offshore, reliable condition monitoring, fault diagnosis, and asset management systems need to be developed to monitor the condition of the WECS in real-time to ensure system reliability. This thesis proposes an algorithm to monitor the condition of the WECS in real-time. The proposed

algorithm is designed and simulated in the MATLAB software environment, which is tested and validated through the developed WECS hardware. The condition of the WECS could be monitored remotely. This thesis proposes an industrial internet of things (IoT) algorithm to monitor the condition of the WECS remotely over IoT. An industrial IoT experimental setup has been developed to validate the proposed algorithm.

In summary, this thesis:

- proposes a new three-phase cascaded multilevel inverter,
- presents a simplified but yet effective space vector pulse width modulation,
- suggests two real time algorithms to monitor the condition of switching devices and dc-link capacitor over IoT.
- validating simulation analysis through experimental measurements.

Acknowledgments

First and foremost, I would like to thank my Almighty Allah (God) for his mercy and blessing upon me throughout my Ph.D. research. I would also like to take an opportunity to express immense gratitude to my supervisor, Associate Professor Dr. Ahmed Abu-Siada, who supported by all means in my research. It would not be easy to achieve my research goal without his active guidance, advice and encouragement. I am also grateful to my co-supervisor, Associate Professor S. M. Muyeen for his efforts. Moreover, I am thankful to Professor Dr. Frede Blaabjerg (Aalborg University, Aalborg, Denmark) and Professor Dr. Zulkifilie Ibrahim (Universiti Teknikal Malaysia Melaka) for their effective research collaboration.

Besides, I am thankful to the departmental technical staffs, Mark Fowler, Russell Wilkinson, Zibby Cielma, Joshua and Scott for their friendly and helpful attitude while conducting different experiments.

Moreover, I would like to acknowledge the contribution of the Curtin International Postgraduate Research Scholarship (CIPRS), Curtin Strategic International Research Scholarship (CSIRS), and Curtin HDR Completion Scholarship in supporting this research.

Finally, I would like to express immense gratitude to my parents, siblings, other family members and friends for their encouragement and help.

Table of Contents

List of Figures

List of Tables

List of Publications

It is acknowledged that most of the results from this work has been published in the following journal articles and conferences.

Journal articles

1. **Md Liton Hossain**, A. Au-Siada, S. M. Muyeen, Md Mubashwar Hasan, Md Momtazur Rahman, "Industrial IoT based Condition Monitoring for Wind Energy Conversion System", accepted in 24.06.2020, CSEE Journal of Power and Energy Systems (SCI Indexed, Q2, IF: 3.115).
2. **Md Liton Hossain**, A. Au-Siada, S. M. Muyeen, Zulkifilie Ibrahim, Frede Blaabjerg "Design and Validation of a Generalized Multilevel Inverter with Simplified Switching Technique", Electric Power Components and System, Vol.0, No: 0, Page: 1-15, 07 April 2020 (Q2, SCIE Indexed, IF: 0.888).
3. **Md Liton Hossain**, Abu-Siada A, Muyeen SM. Methods for Advanced Wind Turbine Condition Monitoring and Early Diagnosis: A Literature Review. Energies. 2018; 11(5):1309. (Q3, SCIE Indexed, IF: 2.707).
4. Md Liton Hossain, A. Au-Siada, S. M. Muyeen, Md Mubashwar Hasan, "Topologies, Controllers, Applications and Future Challenges of Multilevel Inverters: A Comprehensive Review", under review, Journal of Energy Storage in August 2020 (SCI Indexed, IF: 5.129).

Conference Papers

1. **Md Liton Hossain**, A. Abu-Siada and S. M. Muyeen, "A Hybrid Multilevel Power Electronic Inverter and Fault Location Identification of Switching Devices," 2018 Condition Monitoring and Diagnosis (CMD), Perth, WA, 2018, pp. 1-4 (IEEE Xplore indexed).
2. **Md Liton Hossain**, "A Review on Wind Turbine Condition Monitoring and Fault Diagnosis", Proceedings of One Curtin International Postgraduate Conference, 2017/12.

List of Abbreviations

WECS	Wind energy conversion system
PEC	Power electronic converter
MLI	Multilevel inverter
DCLI	Diode clamped inverter
CCLI	Capacitor clamped inverter
CHBI	Cascaded h-bridge inverter
IoT	Internet of things
WPAN	Wireless personal area network
WLAN	Wireless local area network
LTE	Long-term Evolution
WiMAX	Worldwide interoperability for microwave
GPRS	General packet radio service
GSM	Global system for mobile communication
PI	Proportional integral
THIPWM	Third harmonic injection pulse width modulation
CMLI	Cascaded multilevel inverter
SVPWM	Space vector pulse width modulation
DFIG	Doubly fed induction generators
PWM	Pulse width modulation
ac	Alternating current
VSC	Voltage source converter
CSI	Current source inverter
THD	Total harmonic distortion
2LI	2-level inverter
NPCI	Neutral point clamped inverter
FCLI	Flying capacitor clamped inverter
HMI	Hybrid multilevel inverter
SC-HB	Hybrid switch capacitor h-bridge
QHNPC	Quadrupled hybrid neutral point clamped
FCCT	Forward converter cascaded transformer
SPWM	Sine pulse width modulation
SHE	Selective harmonic elimination

UPS	Uninterruptible power system
FFT	Fast Fourier transform
PCB	Printed circuit board
IGBT	Insulated gate bipolar transistor
SCADA	Supervisory control and data acquisition
NDT	Non-destructive testing
WT	Wind turbine
RFID	Radio frequency identification
IP	Internet protocol
BLE	Bluetooth low energy
IPv4	Internet protocol version 4
IPv6	Internet protocol version 6
6LoWPAN	IPv6 low power wireless personal area network
CoAP	Constrained application protocol
MQTT	Message Queuing Telemetry Transport
XMPP	Extensible Messaging and Presence Protocol
AMQP	Advanced Message Queuing Protocol
HTTP	Hypertext Transfer Protocol
XML	Extensible Markup Language
CMS	Condition monitoring system
IDE	Integrated development environment
LCD	Liquid crystal display
UART	Universal Asynchronous Receiver/Transmitter
AFL	Adafruit FONA Library
SSL	Software Serial Library
LCL	Liquid Crystal Library
SC13LI	Switched-Capacitor 13-Level Inverter
BCMLI	Binary cascaded multilevel inverter
HNLI	hybrid nine-level inverter

Chapter I
Introduction

1.1 Background to the study

With the rapid growth of the world population, energy consumption is increasing day by day, demanding increased energy production. To meet the increasing demand for energy consumption, there is increased pressure on sourcing fossil fuels (petroleum, coal and natural gas, etc.), which have been the dominant energy resources since the industrial revolution [1]. However, excessive use of fossil fuels to meet this demand is creating a range of adverse environmental effects (skin cancer, global warming, acid rain, air pollution, etc.) [2]. These serious environmental outcomes are prompting scientists and engineers to search for alternative sources of energy. Renewable energy sources (hydro, wind, solar, biothermal, etc.) are currently the most common alternative energy sources – these are unlimited, cost-effective, environment friendly and, unlike fossil fuels, they have no adverse effect on the environment [3]. Wind energy has recently become the second most common renewable energy source and is attracting considerable in-depth research. In 2019, wind energy contributed 6% of total world energy, which has made it the second most dominating renewable energy source in the world [4]. However, to keep the production curve on an upward trend and make wind energy a truly competitive resource in the global market against fossil fuels, many constraints need to be resolved by designing mechanical and electrical subsystems, controllers, and condition monitoring for wind energy conversion systems (WECS). Condition monitoring for WECS has become an essential aspect of energy industry practice as this helps improve wind farm reliability, overall performance and productivity [5]. If not detected and rectified in the early stages, some faults can be catastrophic, causing significant loss of revenue along with interruptions to businesses that rely on wind energy. The failure of WECS results in system downtime and repair or replacement expenses that significantly reduce annual income. Such failures call for more systematised operation and maintenance schemes to ensure the reliability of WECS. Condition monitoring of WECS plays an important role in reducing maintenance and operational costs and increases system reliability.

1.2 Research problem

WECS is a complex electromechanical system that consists of several components and subsystems such as blades, generator, full-scaled power electronic converter (PEC), and controllers [6]. The full-scaled power electronic converter (PEC) consists of two-stage power conversions – the AC/DC stage, which converts input ac power to intermittent dc power, and

the DC/AC stage, which converts the intermittent dc power to ac output power [7]. The AC/DC converter (rectifier) produces low frequency harmonic ripples in the intermittent DC power, which is a challenging task to minimise [8]. On the other hand, multilevel inverter (MLI) topologies, such as diode clamped inverters (DCLI) [9], capacitor clamped inverters (CCLI) [10] and cascaded h-bridge inverters (CHBI) [11], are among the many DC/AC converters developed recently which increase output power, deliver to load and improve the qualities of output waveforms. However, to produce them-level in the output voltage, 6(m-2) clamping diodes, and 3(m-2) clamping capacitors are required for DCLI and CCLI respectively [12], and these increase the complexity, cost and size of the WECS. This issue can be resolved by adopting a CHBI topology that does not employ any clamping diodes or capacitors. However, the main drawback of CHBI is the requirement for several non-isolated dc sources, which restricts it from being coupled with a rectifier and increases the management complexity as well as overall cost [13].

In addition, WECS suffer various types of faults during operation, which need to be monitored to reduce system downtime. There are several offline condition-monitoring techniques mentioned in the literature, such as vibration, temperature, strain, and electrical signals to ensure the reliability of WECS [5]. Condition monitoring based on electrical signals is one of the most dominating techniques widely applied. The technique has some attractive advantages over others, including ease of implementation, cost-effectiveness, non-intrusiveness, early-stage fault detection abilities, fault location identification, and fault mode identification. On the other hand, the condition of the WECS could also be monitored online. Online condition monitoring has caused a tremendous revolution in industrial applications, where remote users can monitor the condition of industrial devices over the internet of things (IoT) [14]. The internet protocols and standards for developing IoT projects are mainly divided into three major categories such as wireless local area network (WLAN), wireless personal area network (WPAN), and cellular network [15]. The WPAN uses a low rate standard (IEEE 802.14.4) and WLAN has a limited bandwidth standard (IEEE 802.3). The cellular networks which are second-generation (2G), third-generation (3G), fifth-generation (5G), worldwide interoperability for microwave (WiMAX), Long-term Evolution (LTE), global system for mobile communication (GSM), and general packet radio service (GPRS), have faster data rates, wide coverage and appropriate bandwidths, and are becoming the mainstream of industrial IoT.

1.3 Summary of research problems

In summary, the investigated research problems that have not been solved yet in the literature include:

- Conventional AC/DC converter produces low frequency harmonic ripples that affects the overall performance of WECS.
- Conventional CHBI requires several isolated DC sources which restricts it from being coupled with a rectifier and increases the management complexity as well as overall cost.
- The WECS may encounter various faults within the switching devices of the three-phase CMLI and the dc-link capacitors, which contribute to the significant loss of revenue.

1.4 Research objectives

The sole objectives of this thesis are outlined below:

1. Proposing a three-phase cascaded multilevel inverter (CMLI) and a simplified space vector pulse width modulation (SVPWM) controller.
2. Developing a complete WECS hardware prototype.
3. Proposing a SVPWM-based algorithm and an industrial internet of things (IoT) algorithm to monitor the condition of dc-link capacitor and semiconductor switching devices in the three-phase CMLI remotely and in real time.
4. Developing an industrial IoT hardware prototype integrated with the WECS hardware to monitor the condition of the system in real time.

1.5 Motivation for the research

Wind energy production has increased from 300 GW in 2013 to 597 GW in 2019 [16], [17]. According to the World Wind Energy Association, wind energy contributed 6% of the total world electricity generation in 2019, which is a significant share of renewable power generation worldwide [4]. This makes wind energy the second most common source of renewable energy in the world after hydropower and is playing a significant role in the revolution in the modern power sector. According to statistics from the world energy agency, wind energy contributed 4% of the global energy in 2018, and it forecasts this to be tripled by the year 2024 [18]. However, to implement this ambitious forecast, several challenges need to

be overcome by designing proper mechanical, electrical, and control systems for WECS, especially power electronic converters and controllers [19], [20]. The conventional power electronic converters produce ripples in the dc-link voltage, has a low-quality output, and suffers from voltage imbalance across the dc-link capacitors [21]. Hence, proposed controllers and topology will be designed and developed to resolve these issues.

Switching devices and power electronic converter's capacitors are the most fragile elements with failure rates of 30% and 21% respectively [22]. In addition, about 20% of the malfunctions within WECS are due to failures in the power electronic converters [5]. If such faults are not identified and rectified in the early stages, they may result in disastrous consequences and a loss of revenue [23]. Hence, the proposed algorithm will be designed and developed to monitor the condition of the dc-link capacitors and semiconductor switching devices in the three-phase CMLI. Since most wind power plants are located in remote areas or offshore, where the environmental conditions are harsher, a reliable online condition-monitoring technique needs to be developed to investigate the current status of the WECS in real-time to ensure system reliability. Online condition monitoring has brought tremendous change to industrial applications, where remote users can monitor the condition of industrial devices over the internet of things (IoT) [24]. The International Data Corporation shows current spending and forecasting on IoT and related projects in the period 2016–2022, will go beyond AUD $6 trillion [25]. The details of the IoT techniques have been described in the literature. Hence, the proposed industrial IoT algorithm will be designed and implemented to monitor the condition of WECS remotely in real-time over the internet.

1.6 Methodology

The methodologies employed in this research are described briefly here:

- **Literature review**: The author has conducted an extensive review of the literature on WECS and condition monitoring. The review papers are totally 292 which are included in the reference section. Critical constraints and challenges are highlighted to design and implement WECS. The literature review helps in the design of the proposed controllers, topology, and algorithms for WECS.
- **Modelling and simulation**: The three-phase cascaded multilevel inverter and simplified SVPWM have been designed in MATLAB/SIMULINK software environment which require insulated gate bipolar transistor (IGBT), capacitors, dc source, induction motor, PI controller and embedded coder. The model has been simulated and performances have been

investigated. The condition monitoring algorithms have been designed and simulated in the MATLAB software environment, while the industrial IoT algorithm has been designed in proteus software. The algorithm has been simulated and performances have been investigated.

- **Experimental development**: An experimental prototype of WECS has been developed, which includes a computer, digital signal processing board, driver circuit, synchronous generator, power electronic converter, and motor, etc. Industrial IoT hardware has been developed and includes an Arduino board, SIM800 module, global system for mobile application (GSM), general packet radio service (GPRS), and an internet-based server.

1.7 Research contributions

The main contributions of the thesis given here extend the knowledge of existing literature.

1. Proposed 3-phase cascaded MLI

The proposed 3-phase cascaded MLI does not require any clamping capacitor or diodes, such as the diode clamped inverter (DCLI) [26] or capacitor clamped inverter (CCLI) [27], and this decreases the cost and complexity of the implementation. In addition, it does not require any DC voltage source, such as a cascaded h-bridge inverter (CHBI) [11], [28], [29], [30]. Authors of [31] propose a cascaded multilevel inverter (CMLI) using a two-level configuration. However, this CMLI requires two series-connected 3-phase rectifiers, which increase the implementation cost, size, and complexity. The proposed 3-phase cascaded MLI has the ability to be coupled with a single rectifier through series connected dc-link capacitors.

2. Proposed SVPWM controller

The key challenge of the PI-based SVPWM technique for controlling a 3-phase cascaded MLI is the large number of triangles exhibiting different numbers of switching vectors, which makes the selection of switching vectors quite difficult. The MLI's performances depend significantly on the selection of these switching vectors [32]. The 5-level space vector diagram includes 16 triangles in each sector and 125 switching vectors, which increases the complexity of its implementation. Moreover, triangles have an unequal number of switching vectors which cause a voltage imbalance across dc-link capacitors. Hence, the conventional SVPWM controller has been simplified and proposed in this thesis by omitting lower-weighted switching vectors. This not only reduces the switching vector's complexity but also balances the voltages across the dc-link capacitors. It is to be noted that omitting such low-level contributed switching vectors does not significantly affect the performance of the 3-phase cascaded MLI.

3. Proposed condition monitoring algorithm

The PEC suffers from various types of faults, which interrupt the continuous power flow. If these faults are not detected and corrected in the early stages, these faults may lead to catastrophic scenarios with a significant negative impact on the power sector. This thesis presents an algorithm to facilitate condition monitoring of switching devices in the three-phase CMLI and dc-link capacitors.

4. Industrial IoT algorithm

Since most wind power plants are in remote areas or offshore, where the environmental conditions are harsh, a reliable online condition monitoring and fault diagnosis technique need to be developed to monitor the condition of the WECS in real-time to ensure system reliability. Online condition monitoring has enabled remote users to monitor the condition of industrial devices over the internet of things (IoT) [24]. However, there are several challenges to developing industrial IoT projects, such as data encrypt-ability, security, privacy, etc. To resolve these challenges, there are more than 123 standards and technologies published in the literature on the development of IoT projects [33], which need to be strictly maintained to develop IoT projects. The standards of internet protocols are mainly divided into three categories – wireless personal area network (WPAN), wireless local area network (WLAN), and cellular network protocols [15]. WPAN uses low rate standards (IEEE 802.14.4) and WLAN has limited bandwidth standards (IEEE 802.3). Cellular networks such as second-generation (2G), third-generation (3G), fifth-generation (5G), Long-term Evolution(LTE), worldwide interoperability for microwave (WiMAX), general packet radio service (GPRS), global system for mobile communication (GSM) have faster data rates, wider coverage, and appropriate bandwidth, which is becoming the mainstream for the industrial IoT. The global system for mobile communication (GSM) and general packet radio service (GPRS) are promising techniques for monitoring the condition of WECS.

1.8 Original contributions of the thesis

The original contributions of this thesis are outlined below:

- New three-phase CMLI with four non-isolated series-connected dc-link capacitors
- Novel simplified SVPWM controller
- New SVPWM based algorithm and Industrial IoT algorithm

1.9 Thesis outline

This thesis is divided into five chapters and outlines of the remaining chapters are given below:

- Chapter 2 presents a comprehensive review of the literature on WECS and its condition monitoring. The picture of wind energy is highlighted, which describes its current status and development.
- Chapter 3 presents a design for WECS, which proposes three-phase CMLI, and a SVPWM controller. The proposed three-phase CMLI, with non-isolated series -connected dc-link capacitors, inverts the dc-link capacitors 'voltage to three-phase staircase ac voltage, which suffers from voltage balancing issues over the non-isolated capacitors. The proposed SVPWM controller controls the three-phase CMLI and balances the dc-link voltage over non-isolated capacitors. The WECS has been designed and simulated in the MATLAB software environment. An experimental hardware prototype has been developed, which validates the simulated results.
- Chapter 4 proposes and implements an algorithm to monitor the condition of the dc-link capacitor and switching devices of the three-phase CMLI for WECS. Another industrial IoT algorithm is proposed and implemented to monitor the condition of the dc-link capacitor and switching devices of the three-phase CMLI for WECS in real-time over the internet. A local area network (LAN) view is also presented to monitor the condition of the dc-link capacitor and switching devices of the three-phase CMLI for WECS in real-time.
- Chapter 5 represents the key findings and recommendations for future work and challenges.

Summary

Power electronic converter topology and its controller play a vital role in wind energy conversion systems. This thesis proposes a three-phase CMLI with series-connected dc-link capacitor to improve output performance; a simplified SVPWM controller to balance the dc-link voltages; an condition monitoring algorithm and an industrial IoT algorithm to monitor the condition of the switching devices and dc-link capacitors. An entire overview of the thesis is given in Fig. 1.

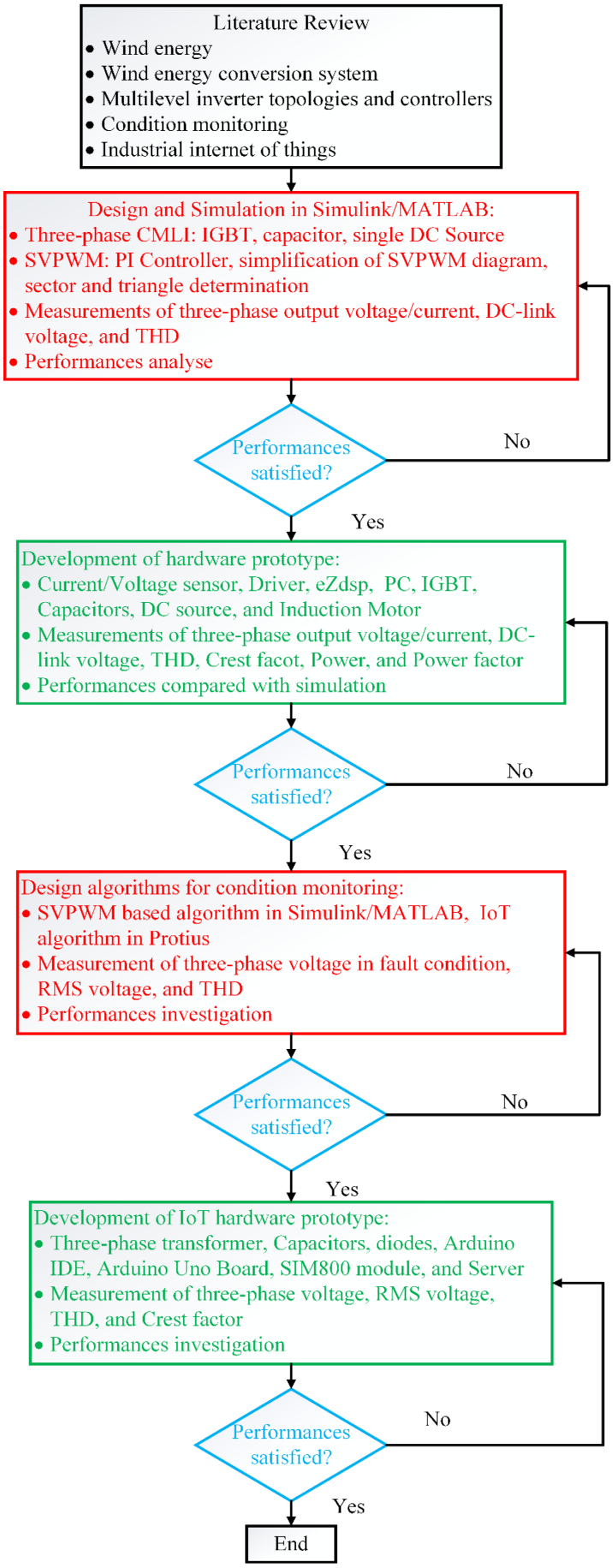

Fig. 1. Flow chart of the stages in this thesis.

Chapter II
Review of Multilevel Power Electronic Converter Topologies and Condition Monitoring Technique for Wind Energy Conversion System

2.1 Introduction

With the rapid growth of the world population, energy consumption is increasing day by day, demanding increased energy production. To meet this demand, pressure is increasing on fossil fuels such as petroleum, coal, oil shale, and natural gas, which have been the dominant sources of energy since the industrial revolution [1]. The excessive use of fossil fuels causes a range of adverse effects on the world environment, such as skin cancer, global warming, acid rain, and air pollution [2]. These serious environmental outcomes are prompting scientists and engineers to search for alternate sources of energy. Renewables, such as hydro, wind, solar, and biothermal energy, are infinite, cost-effective, and environmentally safe [3]. Renewable energy production is increasing worldwide, and Fig. 2-1 indicates this growth as a global total in recent years [16], [17], [4]. The current percentage of renewable energy compared to World Energy is 17%, while it was 14.5% in 2013. With the increase of renewable energy production, wind energy production is also showing an upward curve (Fig. 2-1).

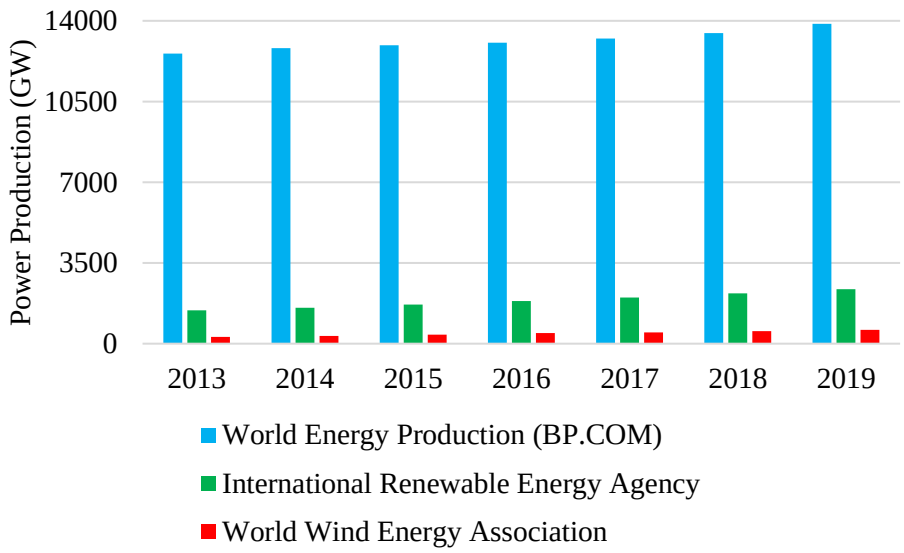

Fig. 2-1. World total energy, renewable energy and wind energy production (GW/annum)

Wind energy production is currently 597 GW, up from 300 GW in 2013. According to the note of World Wind Energy Association, wind energy contributes 6% of total world electricity generation in 2019, which is a significant share of total renewable power generation [4]. This significant share in the global market makes wind energy the second

most common source of renewable energy after hydro energy, causing a revolution in the modern power sector.

Figure 2-2 presents a snapshot comparing the contribution of renewable energies, such as hydro, wind, solar, biothermal, and others. According to Australian government energy statistics, renewable energy generation in 2018 is 21% of total energy production as shown in Fig. 2-3, up from 17.3% in 2016 [34]. Fig. 2-4 shows the contribution of all renewable sources in Australian renewable power generation, where it was indicated that wind energy contributes as the second dominating renewable source in Australia as well [34].

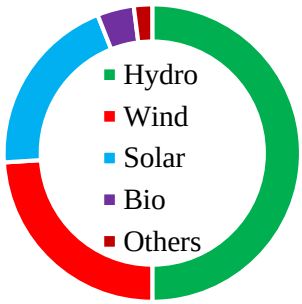

Fig. 2-2. World renewable energy production

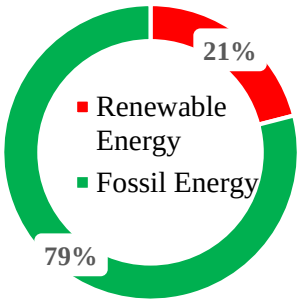

Fig. 2-3. Australian energy production

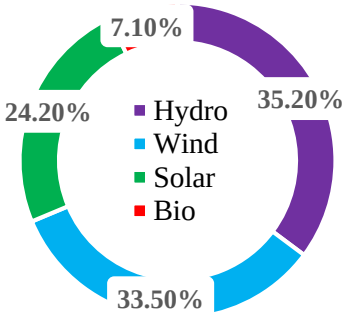

Fig. 2-4. Australian renewable energy production.

According to statistics from the world energy agency 2018, wind energy contributes 4% of total world energy, and it forecasts that this percentage will be tripled by 2024 [18]. However, before wind energy as a resource can be a serious competitor for fossil fuels, many constraints need to be resolved including improved designs for the mechanical and electrical subsystems for WECSs (WECS) [19].

2.2 Wind Energy Conversion System

A wind energy conversion system (WECS) is a complex electromechanical system that consists of several components and subsystems. The major components include the blade, generator, power electronic converter and controllers as shown in Fig. 2-5.

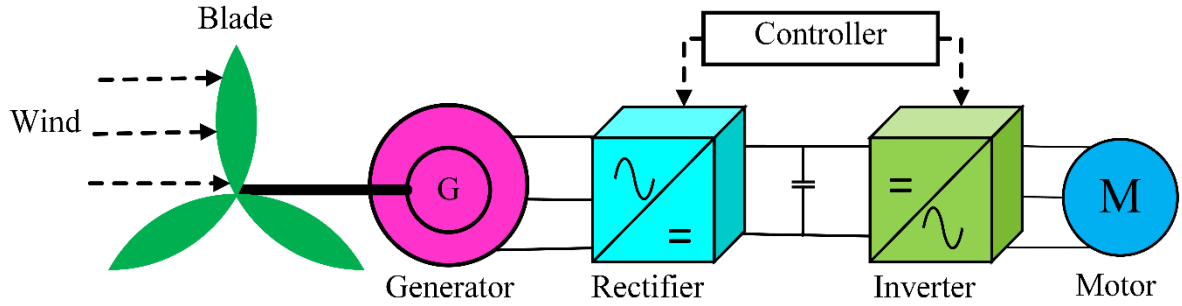

Fig. 2-5. Block diagram of a WECS.

According to literature in the field of aerodynamics, wind power depends on rotor diameter and wind speed in cubic metres, which is why the size of commercial wind turbines during the last couple of years have increased. These large turbines require less installation and maintenance costs [20]. Various combinations of power converters and generators with different control techniques have been developed to obtain the desired full variable operation of WECSs (WECS) [5], [24] which increase conversion efficiency, decrease mechanical stresses on the wind turbines, and improve power quality of electrical grid [35].

Various types of generators, such as wound rotor induction generators, squirrel-cage induction generators, and synchronous generators can be employed in a WECS [36]. A wind turbine system that uses the wound rotor induction generator (also known as doubly-fed induction generators (DFIG)) requires a coupling transformer, which increases the complexity and cost of the system [37]. The squirrel-cage induction generator runs at a fixed speed, and variable wind speeds may cause faults for this type. An adaptive control scheme is presented in [38] to ensure the reliable operation of the permanent magnet synchronous generator under different operating conditions. This type

of generator is interfaced with the grid through a full-scale power electronic converter (PEC) [39].

The full-scaled power electronic converter (PEC) is given much attention in this thesis due to its flexibility and faster response, which facilitate the integration of various sources of renewable energy and improve power system reliability [40]. Various PEC topologies have been suggested to suit several applications, such as battery energy storage [41], [42], [43], photovoltaic [44], [45], electric vehicle [46], [47], and power conditioning [48].

The PEC consists of two-stage power conversions – an AC/DC stage, which converts input ac power to intermittent dc power, and a DC/AC stage which converts the intermittent dc power to ac output power. The AC/DC converter (rectifier) produces low-frequency harmonic ripples in the intermittent dc power, which presents quite a challenge to minimize [8]. Using a bulky electrolytic capacitor to suppress such ripples restricts the efficiency and power density of the converter. Authors [49] present a controller to eliminate such voltage ripples. However, the AC/DC converter exhibits poor dynamic performances due to the low bandwidth of the controller during ripple suppression. Authors [50] propose an optimised design for PEC with extended controller bandwidth. In addition, a new discrete function minimization technique has been presented to avoid the current distortion, maintain near unity power factor operation and achieve better dynamic response [51]. A pulse width modulation controller has been presented to suppress the ripples of the output voltage of a buck single-stage bidirectional AC/DC converter [52]. In this technique, minimum commutations have been maintained to guarantee the closeness of the three voltage levels to the output reference voltage, hence minimizing the output voltage ripples.

On the other hand, the controllers have brought a revolution in the field of medium-voltage and high-power multilevel inverters (MLI), which is one of the new trends in DC/AC converters. The MLIs have several advantages over conventional inverters that include less stress on switching devices, less harmonic distortion, more utilisation of the dc-link capacitor's voltage, and better power quality [53].

2.3 Multilevel Inverter

The main concept of the MLI is the generation of a desired sinusoidal (staircase) output voltage waveform by producing several output voltages levels from input dc sources as shown in Fig. 2-6. Inverter which is called n-level inverters, produces n-level

output voltage waveforms with respect to the dc source negative terminal (Fig. 2-6). In order to increase the number of levels in the waveform of the output voltage, the required MLI's structure must be optimised [54], [55], [28]. Several multilevel inverter (MLI) topologies have been proposed in the literature, which is classified as depicted in Fig. 2-7.

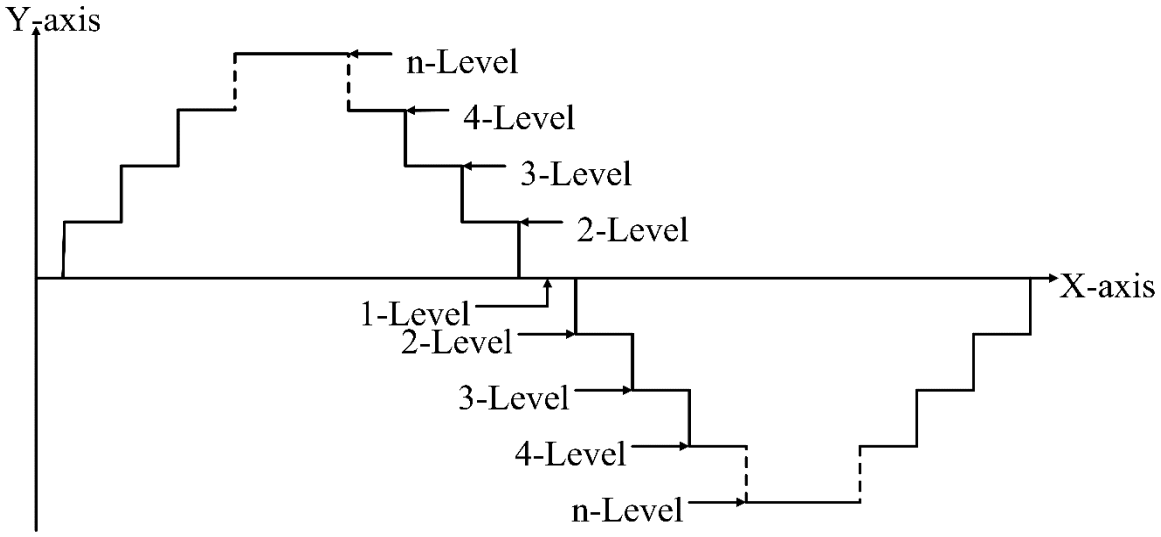

Fig. 2-6. Staircase waveform of an n-level inverter.

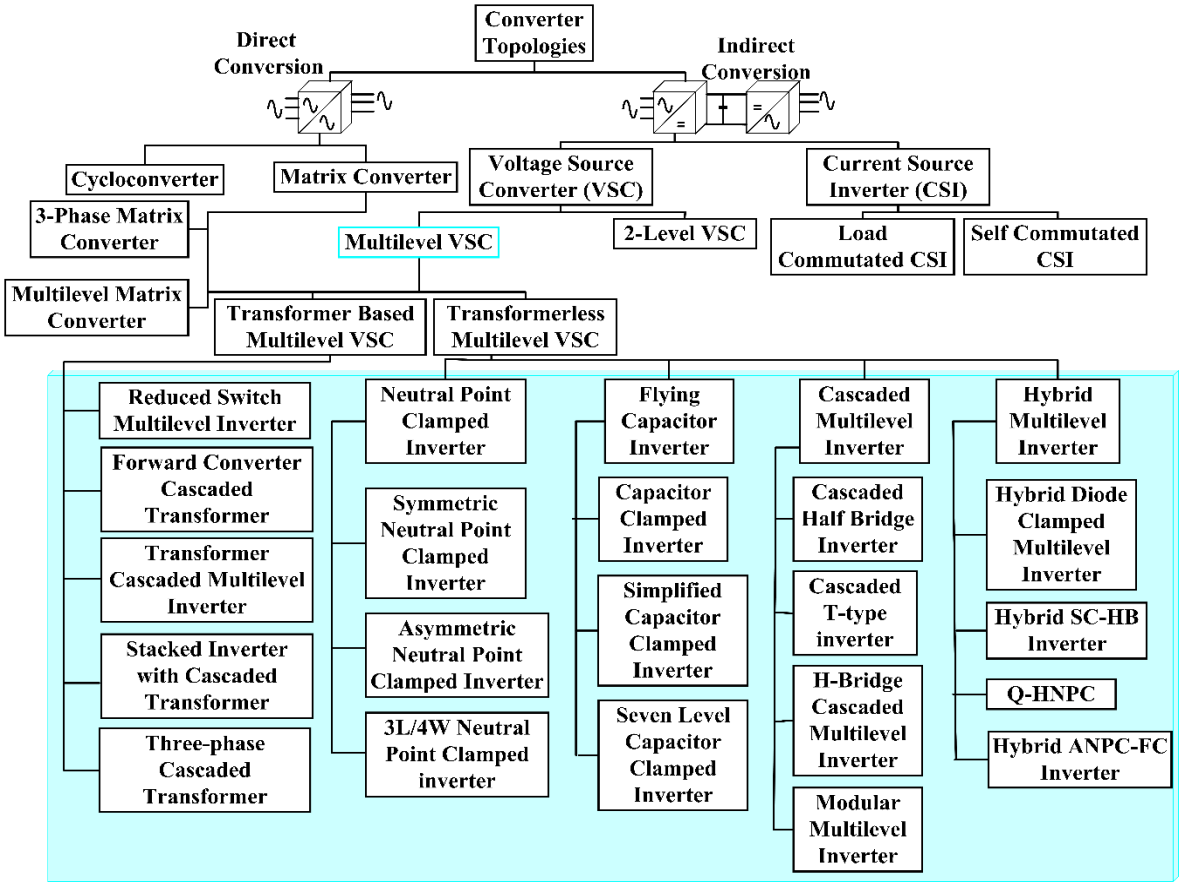

Fig. 2-7. Classification of MLI topologies.

According to the literature, AC power is converted through direct and indirect conversion [56]. For direct conversion, the converter, such as cycloconverter or matrix converter, is directly connected between the supply and the load [57], [58], [59]. This form of conversion is not beneficial to high-power industrial applications due to its poor dynamic performance. Indirect power conversion is done through energy storage devices, such as a voltage source converter (VSC) or current source inverter (CSI), which results in better dynamic performance when compared to the direct conversion method. Current source inverters, such as load commutated CSI and self-commutated CSI, suffer from low power factor and distorted input current, which are avoided by the VSC [60]. VSCs are divided into two categories: conventional 2-level and multilevel converters.

It has been reported that the 2-level VSC comprises drawbacks, such as reducing the driven machine's operational life and creating synchronisation issues with the grid [61], [62]. Moreover, the 2-level VSC produces low peak-peak output voltage and high total harmonic distortion (THD), while exhibiting high switching losses [63]. To reduce harmonic distortion, a bulky filter must be connected to the output terminals of the 2-level VSC, which increases the cost as well as the size of the converter. Hence, a multilevel VSC has been developed as a solution to produce a high-voltage level waveform, high output power, and low THD.

The key challenge associated with most traditional MLIs, such as multilevel matrix converters, transformer-based converters or transformer-less converters, is the requirement of a huge number of semiconductor devices and related components, which increases the complexity of the circuit and reduces its reliability when compared to the 2LI [29], [64], [13], [30]. This has motivated researchers to develop new inverter structures, such as the reduced switching multilevel inverter [65], forward converter cascaded transformer [66], transformer-based cascaded multilevel inverter [67], stacked inverter with cascaded transformer [68], three-phase cascaded transformer [69], neutral point clamped inverter (NPCLI) [70], flying capacitor clamped inverter (FCCLI) [71], cascaded multilevel inverter (CMLI) [72] and hybrid multilevel inverter (HMLI) [73]. These multilevel inverter topologies are presented in subsection 2.4. There are several modulation techniques recently developed to control the performance of MLIs [74]. Some of the modulation techniques are described in subsection 2.5.

2.4 Multilevel Inverter Topologies

The topologies of a multilevel voltage source inverter are mainly classified into three categories: transformer-less MLIs, transformer-based MLIs and matrix MLIs. In addition to these three types, there have been a few other MLI topologies recently developed based on modifying the infrastructure of these basic three topologies. The main topologies are presented below along with recent trends and advancements.

2.4.1. Transformer-less Multilevel Inverter

Transformer-less multilevel inverter topologies can be sorted into four categories including neutral point clamped inverter (NPCLI), cascaded multilevel inverter (CMLI), flying capacitor clamped multilevel inverter (FCMLI), and hybrid multilevel inverter (HMLI).

2.4.1.1. Neutral Point Clamped Inverter

The neutral point clamped inverter (NPCLI) has been initially developed as a 3-level topology in 1981 as shown in Fig. 2-8(a) [75]. This topology has been rapidly advanced and developed for high-power applications. An m-level 3-phase NPCLI typically consists of 6(m-1) number of semiconductors switching devices, 6(m-2) number of clamping diodes, and (m-1) series-connected dc-bus capacitors.

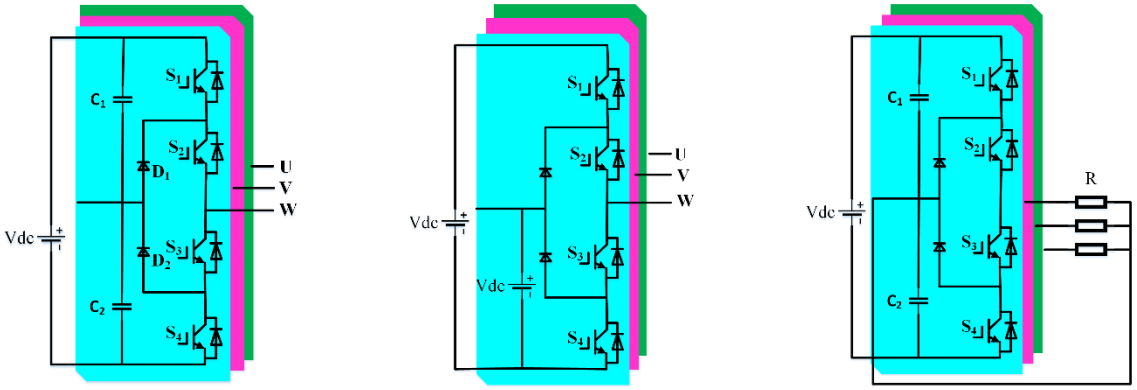

(a) (b) (c)

Fig. 2-8. (a) 3-level NPCLI (b) Asymmetrical NPCLI (c) 3-phase 4-wire NPCLI.

The qualities of the output voltage waveforms are improved with the increase of the number of levels which enrich the voltage waveform to be closest to an ideal sinusoidal voltage waveform. In the NPCLI topology shown in Fig. 2-8(a), the voltage across the dc bus is shared equally through the series-connected dc-link capacitors, C_1 and C_2. The zero-level output voltage of the NPCLI is generated when switches S_3 and S_4 are in on mode, while switches S_1 and S_2 are in the opposite condition. A voltage level

($V_{dc}/2$) is generated when S_2 and S_3 are operating in toggle mode with S_1 and S_4. On the other hand, the full dc-link voltage (V_{dc}) is obtained when switches S_1 and S_2 are in ON mode, while switches S_3 and S_4 are in OFF. The key components of the 3-level NPCLI are the clamping diodes D_1 and D_2, which distinguish the NPCLI from the conventional 2-level inverter. These two clamping diodes clamp the full switching voltage by sharing the dc-bus voltage equally. When both switches S_1 and S_2 are in ON mode, switch S_3 blocks the dc-bus voltage across C_1, and S_4 blocks the dc-bus voltage across C_2.

An asymmetrical NPCLI with two dc input sources as shown in Fig. 2-8(b) was then proposed in the literature [76]. This structure allows bidirectional electrical power flow and facilitates the active and reactive power management between dc and ac ports. A three-phase four-wire NPCLI as shown in Fig. 2-8(c) is proposed to handle symmetrical/asymmetrical load to improve the transformation efficiency and to balance the neutral point voltage [77]. The main drawback of the NPCLI is the requirement of a huge number of clamping diodes, which makes the NPCLI very complex and bulky to implement and control [78], [79].

2.4.1.2. Flying Capacitor Clamped Multilevel Inverter

The flying capacitor clamped multilevel inverter (FCMLI) has recently been developed as an alternative topology to the DCLI, where clamping diodes are normally replaced with clamping capacitors [80], [81] as shown in Fig. 2-9(a) [82], [83].

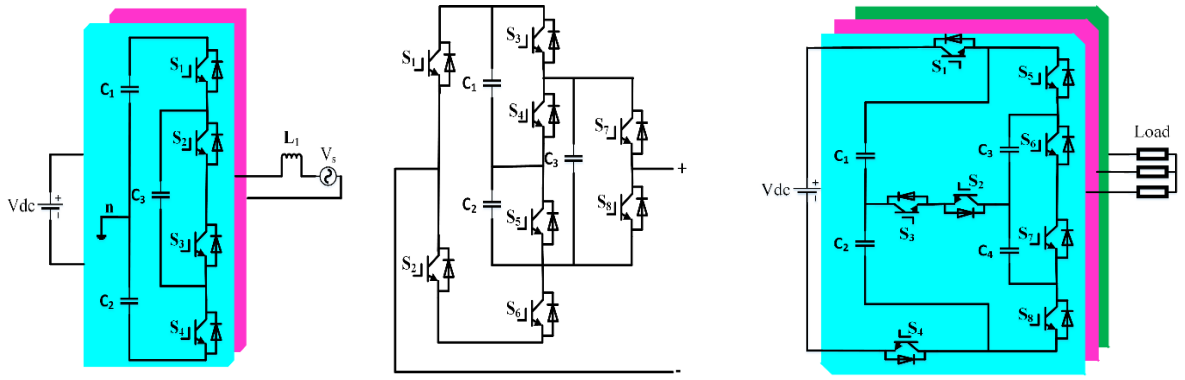

Fig. 2-9. (a) 3-level FCMLI (b) Simplified capacitor clamped inverter (c) 7-level FCMLI.

The structure of the topology appears almost the same as the NPCLI, but the inverter utilizes dc side capacitors in the shape of a ladder instead of the clamping form of diodes. Phase redundancies have been created by balancing the voltage levels across the clamping capacitors. Voltage synthesis of the FCMLI is more reliable than in the

NPCLI, while the voltage increment between two adjacent legs of capacitor, estimates the sizing step of the voltage. The FCMLI requires 3(m-2) clamping capacitors in order to produce the output voltage waveform of m-levels. This represents half of the required clamping devices in the NPCLI topology. The inverter still requires the same number of switching devices as in the NPCLI, but only two dc-bus capacitors.

Similar to the NPCLI and as shown in Table 1, the zero levels in the output voltage of the inverter is generated when the two switches S_3 and S_4 are in ON mode, while switches S_1 and S_2 are turned to OFF. A voltage level of $V_{dc}/2$ is generated when S_2 and S_3 are operating in toggle mode with switches S_1 and S_4. The full dc-link voltage (V_{dc}) is obtained when switches S_1 and S_2 are in ON mode, while switches S_3 and S_4 are in OFF mode.

A five-level FCMLI is presented based on a bridge modular switched capacitor topology, shown in Fig. 2-9(b) [71]. This topology features reduced semiconductor switching losses and fewer components compared to the topology shown in Fig. 2-9(a). A seven-level FCMLI is presented for medium-voltage high-power industrial applications as shown in Fig. 2-9(c). This structure has less active switches and components, and low control circuit complexity [84].

Although the complexity of the FCMLI, due to the clamping devices, is reduced compared to the NPCLI, the control technique for all clamping capacitor inverters is complicated. This topology suffers from generating the same voltage levels for all clamping capacitors.

2.4.1.3 Cascaded Multilevel Inverter

Baker and Bannister propose a cascaded multilevel inverter (CMLI), known later as a cascaded h-bridge inverter (CHBI) as depicted in Fig. 2-10(a) [85], [86]. This topology is simple and free of any clamping diode or capacitor. The several single h-bridges are connected in series, which facilitates its modular structure. In such a topology, there is no voltage balancing issue and high output voltage and power can be achieved with reduced harmonic content by applying the same modulation technique for all h-bridge cells. The output voltage could be calculated by summing up the voltages produced by each cell.

One of the benefits of the topology is that it needs fewer components compared to the above two MLI topologies. A self-balanced cascaded h-bridge with binary ratio is presented using a single dc source per phase as shown in Fig. 2-10(b) [87]. Several identical hybrid inverter modules are cascaded to develop a single-phase, m-level grid -

tied inverter [88] as shown in Fig. 2-10(c). This topology needs a small filter to eliminate voltage and current ripples.

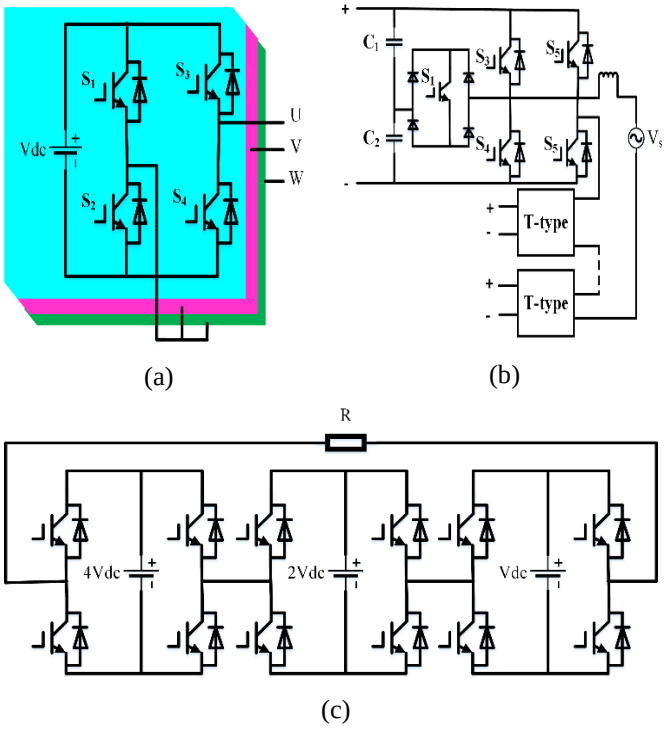

Fig. 2-10. (a) CHBI (b) Cascaded T-type inverter (c) H-bridge cascaded MI.

2.4.1.4. Hybrid Multilevel Inverter

The hybrid multilevel inverter is normally developed by modifying the topologies mentioned above. There have been several hybrid structures recently presented in the literature, such as the hybrid clamped inverter and the hybrid switch capacitor h-bridge inverter. The hybrid clamped inverter shown in Fig. 2-11(a) combines the features of the flying capacitor inverter and the neutral point clamped inverter [89].

This topology has been constructed in such a process so that it can balance the voltage across each level for standard power industry applications as well as high-power industry applications. The hybrid switch capacitor h-bridge (SC-HB) inverter consists combining of the traditional series capacitor inverter and the modified switched-capacitor inverter systems as shown in Fig. 2-11(b). This topology reduces the required number of semiconductor switches and isolated dc voltage sources, and hence reduces the system's size and cost compared to the conventional topology [90]. Moreover, the hybrid SC-HB inverter can produce the input voltage as a double without using any transformer and it eliminates the need for any complicated method to balance capacitor voltage. A quadrupled hybrid neutral point clamped (Q-HNPC) converter as shown in Fig. 2-11(c)

is proposed which increases the number of levels in the output voltage waveform without significantly increasing the number of active components [91].

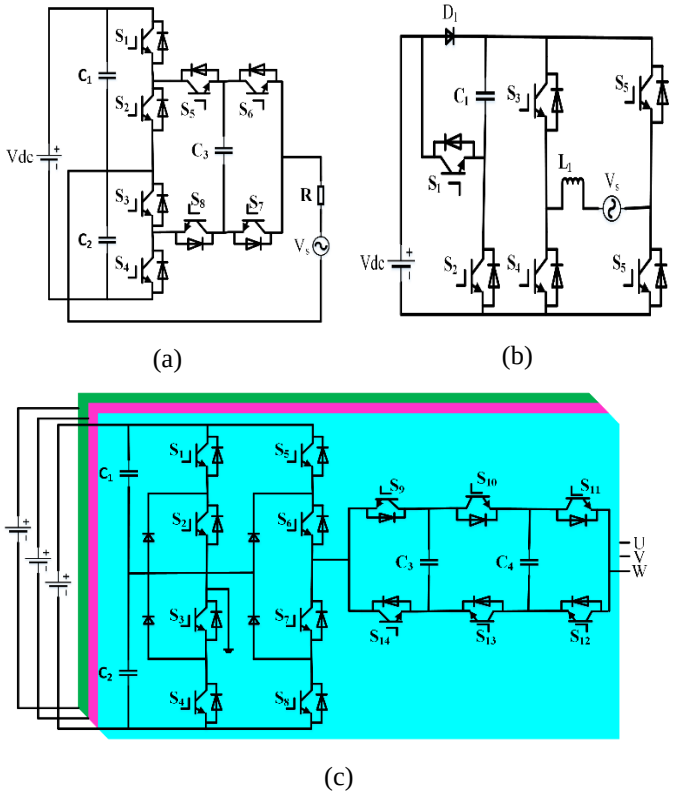

Fig. 2-11. (a) Hybrid clamped inverter (b) Hybrid SC-HB inverter (c) Q-HNPC.

There are other topologies presented in the literature [92], [11]. The common complexity of MLI is due to the large number of semiconductors switching devices, which increases the system's cost and size, complicate the control system, and increase the fault probability. Much research effort has been invested and published in the literature to overcome these issues. For instance, a new cascaded h-bridge inverter with only two switching devices and two freewheeling diodes was proposed in [93]. Bulkiness is another major problem of the multilevel inverter due to the use of input phase-shifting transformers [11]. In this regard, a high-frequency cascaded h-bridge inverter with galvanic isolation is presented which reduces the size and weight of the inverter [94]. However, this topology raises the problem of using a large number of switching devices again. The voltage balancing problems are solved using two bidirectional buck-boost DC–DC converter stages for a 5-level diode-clamped multilevel inverter [95], which increases the complexity including additional semiconductor switching devices, sensors, inductors, and controllers.

2.4.2. Transformer-Based Multilevel Inverter

Transformer-based multilevel inverters are presented to reduce the required number of isolated dc sources for the multilevel inverters. A reduced number of switches cascaded transformer-based 3-level MLI is presented as shown in Fig. 2-12(a) [65], which does not require any h-bridge.

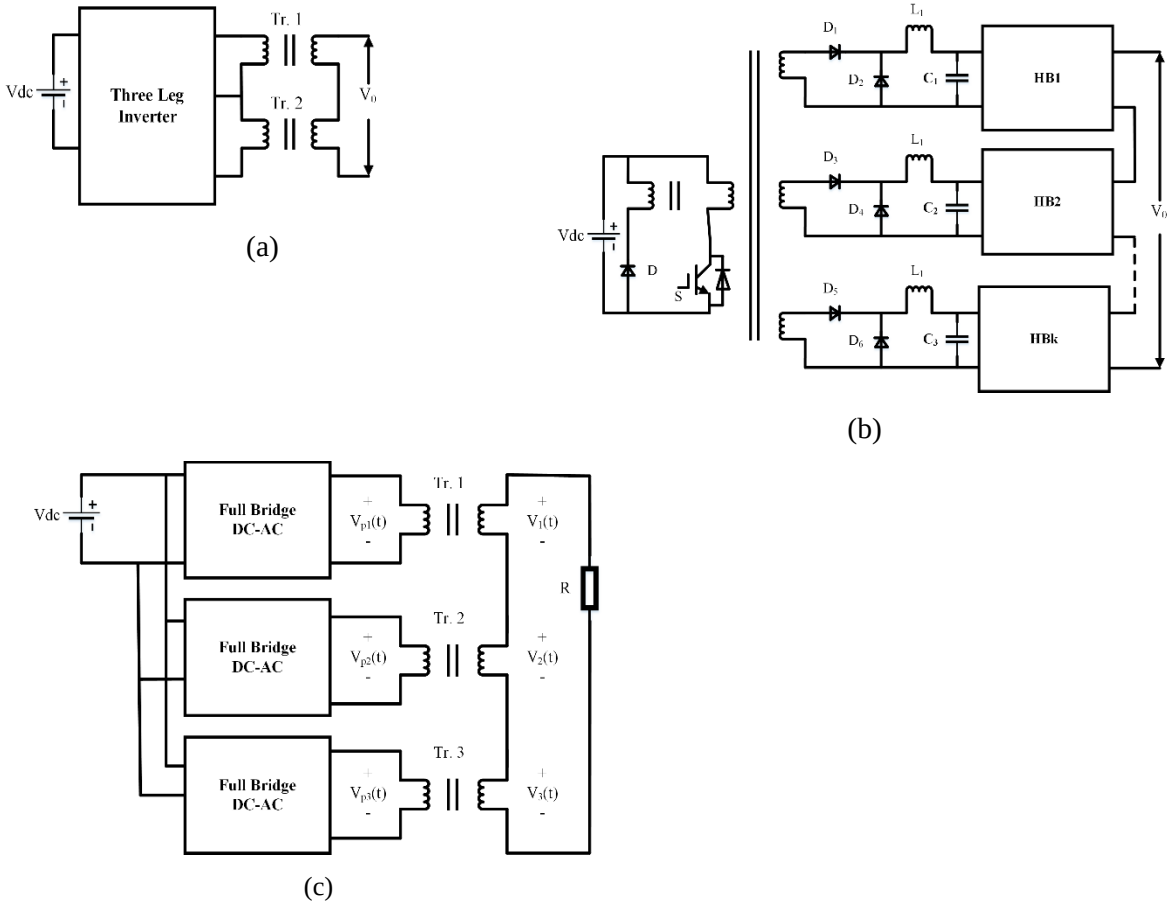

Fig. 2-12. (a) RS multilevel inverter (b) FCCT (c) Transformer-based cascaded MI.

This MLI can generate 5-levels by setting equal ratio turns for the two transformers and this can be modified and implemented for a higher number of levels.

A 15-level cascaded inverter in asymmetrical structure, using only one dc source, is called a forward converter cascaded transformer (FCCT) as shown in Fig. 2-12(b) is presented in [66]. This inverter consists of a forward buck converter, an h-bridge , and a cascaded transformer along with a primary winding.

The buck converter is made using a transformer with isolation, which consists of one primary winding, one tertiary winding connected to a diode, and one secondary winding. However, this topology of a buck converter is not well-suited for high-power industrial applications because of having a large number of passive elements and a multi-

winding transformer. Moreover, the topology has the latest compensator, which has to be modelled and optimised to stabilise the waveform of the output voltage for several forward converters. A technique is developed to implement balanced power distribution by applying a new asymmetric ratio 6:7:8:9 between the transformer stages as shown in Fig. 2-12(c) [67]. The technique minimizes the deviation error and provides balanced power distribution.

2.4.3. Multilevel Matrix Converter

The Multilevel Matrix Converter is an emerging power conversion topology suitable for high-voltage medium-power industrial drive applications. The topology is constructed from direct/indirect multilevel conversion structures, such as a neutral point clamped inverter and an h-bridge inverter. This converter can produce multiple levelled output voltage waveforms and can achieve high volumes of active power transfer at unity input power factor operation [96]. However, these advantages call for a large number of semiconductors switching devices, which increase the cost as well as complexity for implementation.

2.4.4 Summary of the Multilevel Inverter Topologies

Transformer-based multilevel inverters must require a transformer, which makes the multilevel structure bulky and difficult to implement. The transformer-less multilevel inverters are free from any bulky transformer. Despite the attractive advantages of the capacitor clamped topologies, such as reduced voltage stresses on the semiconductor devices and capacitors, and the possibility of high-voltage operation with low switching frequency, these topologies have not been popular recently, mainly because they require a large number of capacitors [97], [98]. The diode-clamped inverter has been extended to a higher number of voltage levels, such as four [99], five [100], and more [101]. Although these topologies have higher voltage and power ratings along with reduced switching frequency, these features are not enough to attract industrial applications due to the large number of clamping diodes required to block the capacitor voltage along with the voltage balancing issues across these capacitors. The cascaded multilevel inverters have recently become more promising and could be applied in the case of WECS. A summary of the latest topologies proposed in recent literature with their advantages and limitations is given in Table 2-1.

Table 2-1. A summary of recent topologies.

Topologies	References	Advantages and Applications	Limitations
MLDCL-MLI	[71]	✓Simple developed structure ✓Capacitor voltage auto-balancing	Requires a high number of isolated DC voltage sources
T-type MLI	[72]	✓Simple developed structure ✓Reduction of FPGA chip-source utilization	Difficult to share equal load among the symmetric sources
SSPS-MLI	[73]	✓Equal load distribution is possible ✓Power quality improvement for induction motor drive	Difficult to employ trinary configuration
SCSS-MLI	[74]	✓Simple developed structure ✓Reduced switching losses	✓Symmetric configuration is mandatory ✓Equal load distribution abilities are not available
CBSC-MLI	[75]	✓Non-isolated DC sources are required ✓Wide range variable frequency ac drive	✓Equal load distribution abilities are not available ✓Switches require different rated voltage
PUC Topology	[76], [77]	✓Simple developed structure ✓ Efficient for various dc/ac power systems, e.g., renewable energy, micro-grids, electrical vehicles, etc.	✓Complicated control algorithm ✓Needs isolated dc sources
MLM-MLI	[78]	✓Requires non-isolated DC voltage sources ✓Simple developed structure	✓Requires both unidirectional and bidirectional semiconductor switches
TCHB	[79]	✓Produces a boost output voltage ✓Reduced size of the DC-link	✓Complicated Voltage balancing across capacitors for a high number of levels
RV Topology	[80], [102]	✓Requires non-isolated DC voltage sources ✓Single DC-link voltage feeds all three-phase voltages	✓Equal load distribution abilities are unavailable ✓Asymmetric source configurations are difficult

2SELG-MLI	[82]	✓Requires non-isolated DC voltage sources ✓Power smoother for wind power system	✓Equal load distribution abilities are not available
MLDCL	[83]	✓Simple developed structure ✓Reduced number of semiconductor switches and gate driver modules	✓THD is relatively high ✓Requires higher numbers of isolated DC voltage sources
BSC MLI	[84]	✓Small in size ✓Reduced number of switching devices ✓It can control the load currents effectively	✓Equal load distribution abilities are not available ✓Asymmetric sources configurations are not available
MCMLI	[85]	Reduced number of components	✓Employs large number of clamping diodes
CHB with MS MLI	[86]	✓Simple developed structure ✓It minimizes harmonics of motor current	✓THD is relatively high ✓High switching frequency cannot be employed
Modified PUC	[87]	✓Improved total blocking voltage, switch ratings	✓Needs large number of shielded dc voltage sources
New 5L MLI	[88]	✓Reduced switching count, and hence low switching losses and THD ✓It maximizes power flow to the grid	✓Requires a large number of diodes and capacitors for clamping ✓Difficult voltage balancing for a high number of levels
RSC-SMLI	[89]	✓Reduced switching count and gate drivers	Requires a huge number of dc sources
SC13LI	[103]	✓Requires single dc source ✓13-level output voltage ✓Gain is 6 ✓Self-voltage balancing ability	Produce single phase output only Low dc power input
BCMLI	[104]	Size and cost of the system is reduced greatly by keeping 15-level output, galvanic isolation	It requires dual rectifier and transformer which make the system bulky.
HNLI	[105]	Increases the peak phase fundamental voltage	Requires higher number of switching devices

2.5 Multilevel Modulation Controller

The main purpose of the modulation controllers in MLIs is to synthesize the desired waveform of output voltage as closest as possible to an ideal sinusoidal voltage waveform. A number of pulse width modulation (PWM) controllers have been developed in the last three decades for industrial applications [106]. These have several advantages, such as the quality of the output waveforms, system losses, and efficiencies, which have been greatly affected by these modulation controllers [107]. A brief classification of multilevel modulation controllers is given in Fig. 2-13. These modulation controllers are reviewed below.

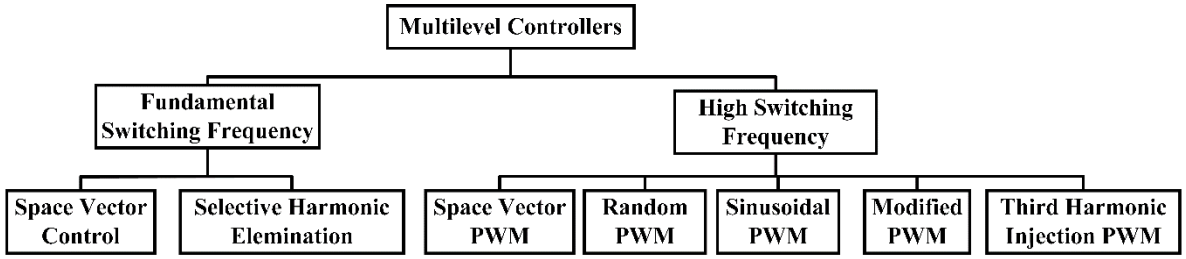

Fig. 2-13. Classification of multilevel modulation controllers.

2.5.1. Sine Pulse Width Modulation

Sine pulse width modulation (SPWM) is the simplest PWM controller, which bears attractive features in industrial applications. The basic principle of the SPWM is to compare a low-frequency sinusoidal wave with a high-frequency rectangular wave to produce control pulses [108]. The control signal diagram is shown in Fig. 2-14(a).

When the instantaneous value of the sinusoidal waveform is larger when compared to the instantaneous value of the triangular waveform, the generated control pulse signal is of a high level (1). Otherwise, it turns into a low level (0) as shown in Fig. 2-14(b). The ratio of the sinusoidal waveform amplitude and the carrier waveform amplitude is called the modulation index, which is applied to control the magnitude of the inverter output voltage waveform.

Despite many attractive features, the SPWM does have a few limitations which restrict the wide application of this controller in industry [109]. An SPWM attenuates the fundamental frequency component, which increases the THD. THD could be reduced by increasing the switching frequency, but this will be on the account of increasing the switching losses. Moreover, this controller is only applicable to a conventional two-level inverter. The modified concept of the SPWM is the multi-carrier SPWM, which overcomes some drawbacks of the conventional SPWM, such as reducing the harmonic

distortion in the output waveforms, functioning at low frequencies, increasing the dc-bus voltage utilisation and reducing the stresses on switching devices [110].

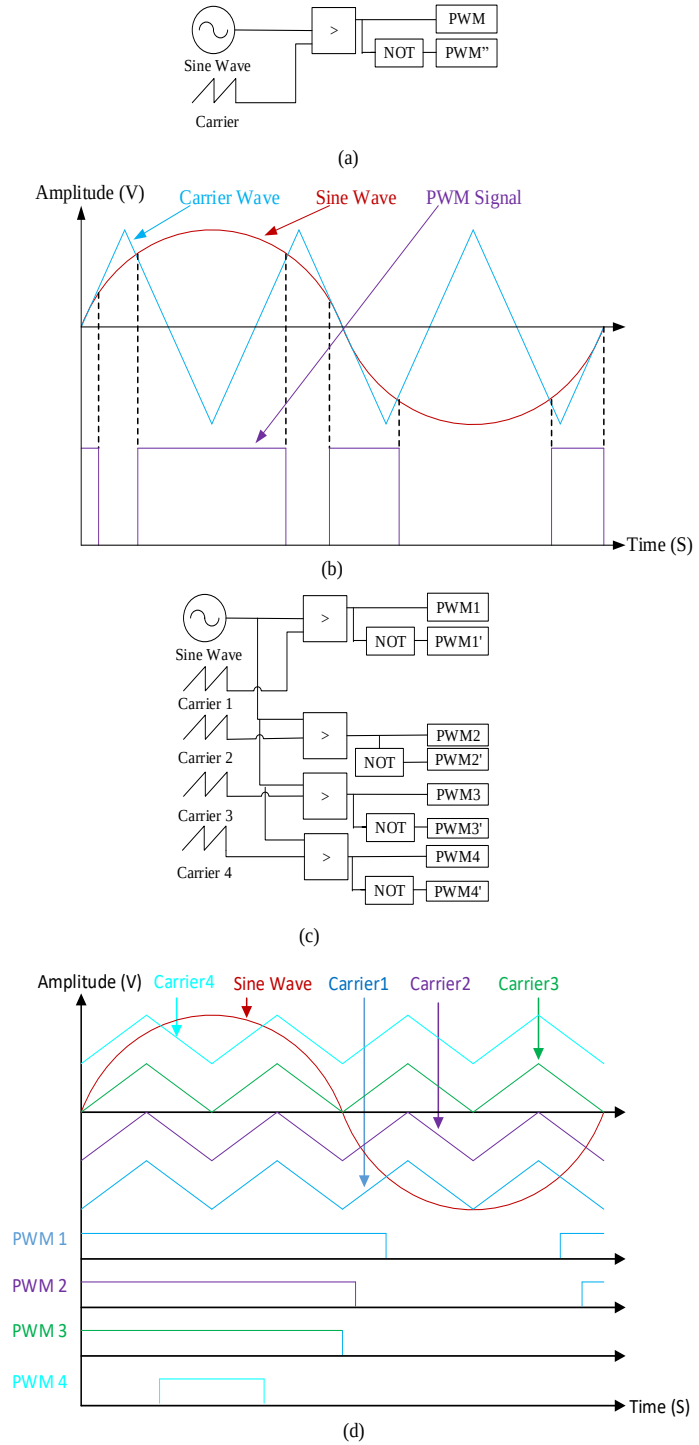

Fig. 2-14. (a) Block diagram of SPWM control pulse generation (b) Control pulse generation of SPWM (c) Block diagram of multi-carrier SPWM control pulse generation (b) Control pulse generation of multi-carrier SPWM.

The basic principle of the multi-carrier SPWM is the utilisation of several triangular carrier signals of either different amplitudes or phases, which are then

compared with only one sinusoidal waveform to generate the control pulses. For an m-level inverter to generate the control pulses, (m-1) triangular carrier waveforms are required, where m is defined as the level numbers in the output voltage. Each carrier is operated at the symmetrical frequency and peak-to-peak magnitude. The control signal diagram is shown in Fig. 2-14(c) and the generated control pulse signals are shown in Fig. 2-14(d). A modified concept of the SPWM by injecting third harmonic component into the sinusoidal waveform is proposed in [111]. The third harmonic voltage is not presented in the waveform of the output voltage, which is the key benefit of this controller. On the other hand, the critical limitation of the modified modulation controller is that does not have any well-established procedure to determine how much a third harmonic component should be added to the SPWM.

Another modified concept of the SPWM has the ability to shift the first significant harmonic content back. The frequency of the harmonic content is twice the switching frequency, which reduces the THD more than the conventional SPWM proposed in [112]. However, this controller produces high switching frequency stresses on the semiconductor switching devices and the harmonic distortion remains high on the input side.

2.5.2. Selective Harmonic Elimination Pulse Width Modulation

Selective harmonic elimination (SHE) is a modulation controller that can determine the correct switching angles to control power electronic converters [113]. This controller is a non-carrier based PWM in which the switching angles are determined from a pre-offline calculation. This controller eliminates up to (m-1) number of low order harmonic contents from the waveform of output voltage, which minimizes the THD. The eliminated low order harmonic contents remain constant if all switching angles are not equal to or greater than 90°. However, if this condition is not fulfilled and the switching angles become more than 90°, this controller will be unfitted for practical applications. In [114], a new selective harmonic elimination pulse width modulation controller is proposed for a transformer-less static synchronous compensator system by employing a cascaded h-bridge inverter. This proposed controller produces low harmonic contents in the output voltage with optimised switching angles that do not affect the main structure of the inverter. The main difficulty of this controller lies in the optimisation of the switching angles, which complicates its practical implementation.

2.5.3. Space Vector Pulse Width Modulation

Recently, space vector pulse width modulation (SVPWM) has brought considerable advancement to the variable frequencies drive applications due to its superior performance [115]. SVPWM provides the lowest amount of harmonic ripples in the output waveforms when compared to other modulation controllers and is well suited for hardware implementation [106]. The utilisation of DC-bus voltage is increased by 15.5% when SVPWM is employed.

A new SVPWM for a 3-level inverter that reduces the execution time significantly is proposed in [116]. The three-level SVPWM diagram is categorised into six (6) two level SVPWM diagrams. A new general space vector PWM for cascaded h-bridge inverters based on a generalisation of dwell-time calculation is proposed in [117]. A dead band hysteresis is also introduced to eliminate level jumping of the output voltage waveform. This controller requires a separate set of equations for the calculation of ON times to determine the odd and even number of the triangles. The complexity of the control algorithm arises here to determine the rotating reference vector location, the calculation of ON times, and the selection of the vector's switching states.

The existing 2-level SVPWM diagram for a 3-phase conventional voltage source inverter is in the shape of a hexagon, which comprises six sectors [118]. Each sector represents an equilateral triangle, each side of which is equal in length and the height is $h=\sqrt{3}/2$. Each sector also has $(m-1)^2$ number of triangles, where m is defined as the number of levels. The 2-level space vector diagram has a total of m^3 switching state vectors, which is represented in the α-β reference frame as presented in Fig. 2-15(a).

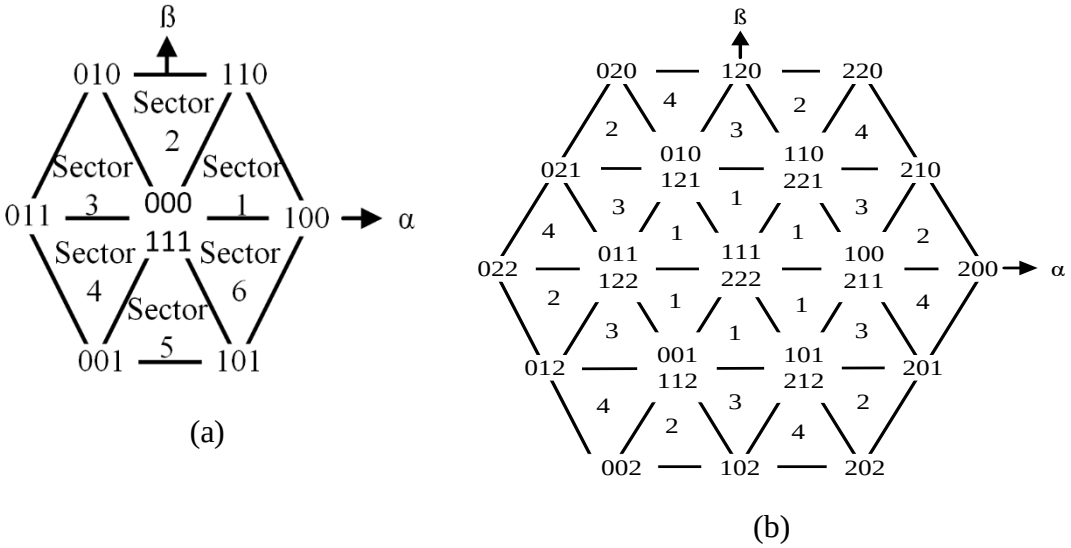

Fig. 2-15. Space vector diagram (a) 2-level (b) 3-level.

The 2-level SVPWM diagram has been extended to the multilevel SVPWM(SVPWM) diagram during the last three decades [119]. The multilevel SVPWM diagram is also divided into 6 sectors in which each sector is divided into 2(m-1) triangles with a total of m^3 switching state vectors [120]. A 3-level SVPWM diagram has 4 triangles for each sector and 27 switching state vectors [121] as shown in Fig. 2-15(b). The 3-level SV diagram could be extended and applied to any higher level of a multilevel inverter.

Despite of the several advantages, the SVPWM has considerable high number of triangles as well as switching vectors. The number of switching vectors are increasing with the increase of number of levels which make the system complex for implementation. The details of this modulation scheme have been described in Chapter 3.

2.5.4. Random Pulse Width Modulation

The main purpose of random pulse width modulation is to reduce the harmonic distortion from the inverter output voltage [122], [123]. However, it reduces the magnitude of the fundamental frequency component and has rapid deterioration of the operational quality at low modulation index values. It also produces additional stresses and switching losses to the semiconductor devices due to the random carrier frequency.

2.5.5. Other Recent Pulse Width Modulation Controllers

Apart from the above mentioned three controllers, other modulation controllers have been presented in the literature of the last few years. Selective harmonic elimination pulse width modulation (SHEPWM) is an offline computation controller that restricts the dynamic performance of the converter. Authors of [124] proposed a new PWM controller based on space vector control (SVC) and nearest vector control (NVC) without a modulator, which significantly reduces the computation complexity and provides high dynamic performance. The nearest voltage level control (NLC) instead of nearest vector control is proposed to achieve the appropriate relation of output voltage [125], which is easily able to detect a close voltage level. An algorithm for modulation of adaptive duty cycle has been presented for a 9-level asymmetric CHBI in [126]. A summary of recent pulse with modulation controllers is given in Table 2-2.

Table 2-2. A summary of recent MLI modulation controllers

Topologies	References	Advantages	Limitations
H-PWM	[115]	✓ Reducing the losses ✓ Easy to implement ✓ Efficiency improved ✓ Applicable for higher level	✓ THD is higher for constant switching frequency ✓ Modification is needed to apply hybrid MLI
SHE-PWM	[116],[127]	✓ Eliminates most dominant low order selected harmonics ✓ Output filter size can be reduced	✓ It's not applicable as a control loop controller ✓ It is not recommended for higher level of inverter ✓ Reduces efficiency
OACT	[117]	✓ Very low switching frequency and excellent dynamic performance	✓ Switching losses and cost increases with the increase of levels
DCC	[118]	✓ Excellent working behaviour even under abnormal conditions ✓ High efficiency and reliability	✓ High average switching frequency ✓ Reduces efficiency for high switching frequency ✓ Complicated algorithm
SWFSTSM	[119]	✓ Facilitates easy to control for the inverter	✓ Output voltage profile contains low order harmonics
MPC	[120]	✓ Significant Voltage and current THD reduction ✓ Improves efficiency	✓ Large number of iterations required to determine the switching states

2.6 Applications of MLI Topologies and Modulation Schemes

MLIs have been utilised successfully in the modern industry due to their superior performance [128]. Although MLIs were initially developed to reduce the harmonic

ripple of the output voltage of a conventional 2-level inverter, their industrial applications have been extended across a wide range due to their unique features, such as inherent voltage boosting, continuous input current, power factor compensation, active power, and the significant reduction they introduce to the line current harmonic contents in meeting electricity grid standards. MLIs have recently been utilised in several applications, including industrial control processes [129], power quality improvement devices [130], traction loads [131], renewable energy integration [131], uninterruptible power system [132], and the mining and marine electric power sector [11], [128]. Among the topologies mentioned in section 2.3, CHBIs have widespread applications in the modern industry due to their high-voltage and high-power capability (13.8 kV and 30 MVA) [133]. CHBIs are widely used in flexible AC transmission systems (FACTS), active electronic filters, reactive power compensation, PV power conversion systems, static synchronous compensators and uninterruptible power systems (UPS) [134], [135], [136], [137], [138], [139], [140], [141], [142], [143], [144]. Diode-clamped multilevel inverters are used in conventional high-power AC motor drives and regenerative applications, such as conveyor belts, fans, mills, pumps, mining industries like oil and gas, back-to-back configurations and chemical industries [145], [146], [147], [148], [149], [150], [151], [152], [153]. Flying capacitor multilevel inverters (FCMLIs) are mainly used in high bandwidth applications and high switching frequency applications; for example, in traction load drives. Hybrid multilevel converter topologies have been applied in power electronic drives, flexible AC transmission systems [154], [155], [156], industrial drives, and high-voltage dc transmission. One of the most fragile areas where the application of multilevel technologies has been explored in depth is renewable energy conversion systems, such as wind turbine, solar energy, and fuel cells [157]. A novel CoolMosfet-based diode-clamped inverter has been applied to a transformer-less solar inverter to mitigate the issue of leakage current [158]. In order to obtain the lowest cost, high efficiency, ease of control, and secure reliability, a capacitor clamped dc to dc boost converter topology by using least number of components has been proposed which is applied to interface the low voltage PV module with the grid [159].

2.7 Future Trends and Challenges of MLI

The MLI is an established solution in several industries due to its distinctive proven advantages. However, despite these, there are several arguments against them and

challenges for their sustainable developments, which are briefly discussed in section 2.7.1 and contributions of this thesis in MLI in section 2.7.2.

2.7.1. Recent Trends and Future Challenges

MLIs mainly operate at average switching frequencies ranging between 500 and 700 Hz [160], which produces low harmonic orders. These harmonics are the main hindrance to achieving the desired high levels of efficiency which is the major challenge for these converters. This problem can be overcome by developing a higher-level inverter.

Switching and conduction losses are important factors during the design stage of the MLI because of the multiple series-connected devices. The most attractive MLI topologies will be those that have less switching devices and feature a voltage sharing ability among these devices. A comparison has been presented based on the switching and conduction losses of existing MLI topologies in [161], [162]. In addition to the conduction and switching losses, THD is another challenge for MLIs. Although much research effort has been invested in mitigating the harmonics issue of MLIs [163], [163], [164], further investigation is still required to fully resolve the harmonic distortion without sacrificing output power and efficiency. Reliability is another key challenge for the ongoing development of MLIs, since several faults may take place within the inverter, such as switching device faults, capacitor faults, and printed circuit board faults. Although some MLIs have some fault tolerance, it has become mandatory to monitor the condition of all inverter components in order to detect and diagnose incipient faults and take proper and timely remedial action [165], [5].

2.7.2. Contribution of This Thesis

This thesis proposes a novel three-phase cascaded multilevel inverter along with simplified space vector pulse width modulation (SVPWM) which can produce better quality output waveforms with reduced harmonics. The details of the three-phase cascaded multilevel inverter and SVPWM controller will be discussed in chapter 3.

2.8 Condition Monitoring of WECSs

Wind turbines are usually installed in remote areas or offshore and operate under harsh environmental conditions. This makes wind turbines more prone to failures. According to some statistical studies [22], most wind turbine failures take place in the

gearbox followed by faults in the power electronic converters. Faults such as open and short circuit faults in the switching devices and DC-link capacitors interrupt the continuity of the power flow. Switching devices and capacitors are the most fragile components of power electronic conversion systems [166], [167]. A survey report conducted of over 200 products from 80 different companies shows that the failure rates for capacitors and semiconductor switching devices are 30% and 21%, respectively [22]. In addition, about 20% of the malfunctions in WECSs are due to failures in the power electronic converters [5]. Some of these faults can be catastrophic with significant loss of revenue, resulting in interruptions to businesses that rely mainly on wind energy. If not detected and rectified at early stages, some faults can be catastrophic with significant loss or revenue along with interruption to the business relying mainly on wind energy. To avoid such consequences, the implementation of reliable condition monitoring and fault diagnosis techniques has become essential for all critical components in an electricity grid including wind turbines [168], [169], [170], [171]. The condition of the WECS could be monitored online and offline. Different types of faults in WECS are discussed in section 2.8.1. Offline condition monitoring techniques are discussed in section 2.8.2., while online condition monitoring techniques are discussed in section 8.3.

2.8.1 Faults in WECSs

A WECS is subject to several types of faults in various components as shown in Fig. 2-16. These faults are discussed below.

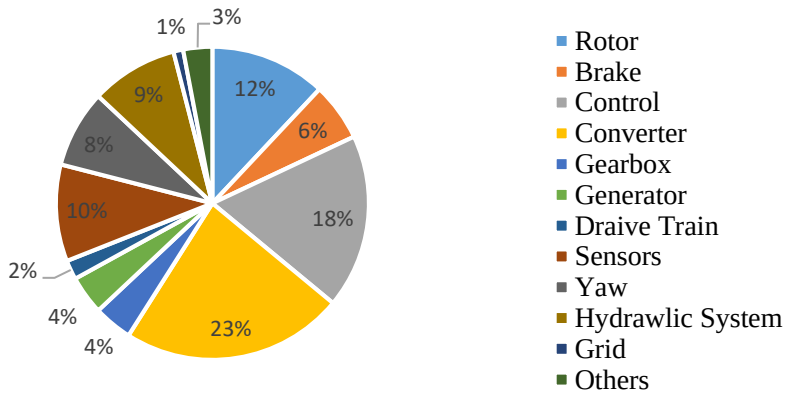

Fig. 2-16. Failure rate within the components of WECS [172].

2.8.1.1. Rotor

The rotor of a wind turbine consists of blades and a hub, and is subject to various mechanical faults, including rotor asymmetry, fatigue, cracks, increased surface roughness, reduced stiffness, and the deformation of blades [173]. Incorrect blade pitch angle and blade

mass imbalance are the main causes of rotor asymmetry [174]. Fatigue is caused by material ageing and variable wind speeds on the blades. Long-term fatigue causes a reduction in the stiffness of the blades and leads to cracks on the surface. Blade surface roughness is usually caused by icing, pollution, exfoliation and blowholes. As rotor faults are accompanied by a change in the blade material structure, these faults can be diagnosed using acoustic emission and vibration sensors. It is possible to use acoustic emissions to detect emerging structural changes by inserting sensors in the blades [175]. If these faults develop to a certain level that contributes abnormal vibrations in the blades, then information from vibration sensors can be utilised in fault diagnosis.

2.8.1.2. Gearbox

Gearbox faults represent approximately 35% of the overall faults in wind turbines [5]. Failure in the gearbox and bearing depends on various factors such as material defects, design, manufacturing and installing errors, surface wear, torque overloads, misalignment and fatigue. The most common gearbox failures include tooth abrasion, tooth crack, breakage, fracturing, and surface fatigue initiated by the debris from bearing failures [176]. These faults may cause an abnormal temperature increase in the bearing and the lubrication oil, and this can be used as an indication of such faults.

2.8.1.3. Main Shaft

The failure of the mechanical shaft may be from corrosion, misalignment, cracks and coupling failures [177]. These faults affect the normal rotation of the shaft as well as other subsystems connected to the shaft. Hence, the torque transmitted via the drivetrain will be affected and may lead to vibrations at certain characteristic frequencies in the gearbox, rotor and generator [178]. Shaft misalignment affects the amplitude of the fundamental frequency of the vibration of the gearbox, rotor, and generator; hence, shaft faults can be detected and analysed by capturing vibration, torque, and electrical signals [177]. The analysis is conducted using frequency analysis such as the Fast Fourier Transform methodology (FFT).

2.8.1.4. Hydraulic Systems

The hydraulic system delivers hydraulic power to drive the motors used to adjust the blade pitch angle [179], maximizes wind power generation by adjusting yaw position and controls the mechanical brake to ensure the safety of the wind turbine [180]. This system is subject to oil leaks and sliding valve blocking faults. Pressure and level sensor signals are used to diagnose these faults.

2.8.1.5. Mechanical Brake

A mechanical brake typically has three main components – the disc and calipers, the hydraulic mechanism, and the three-phase AC motor. The hydraulic mechanism is used to drive the calipers, and the motor is used to power the hydraulic mechanism [181]. The brake is usually mounted on the main shaft. It is used to prevent over speed of the rotor and even to force the shaft to stop in case of the failure of critical components. The brake is also applied to the yaw subsystem to stabilise the bearing. The disc may be cracked due to overshoot of mechanical stress on the brake and overheating. Faults in the mechanical brake can be diagnosed through temperature and vibration monitoring.

2.8.1.6. Tower

The wind turbine tower faults are mainly occurred due to structural damages such as cracks and corrosions. These faults may be caused due to several factors including improper installation, loading, poor quality control during the manufacturing process, lightning, fire and earthquakes. Time and frequency domain analysis techniques can reveal the health condition of the tower [182].

2.8.1.7. Electric Machine

Two types of faults may take place in the electrical machine – mechanical and electrical faults. Electrical faults comprise open circuit, stator/rotor insulation damage, and electrical imbalance. Broken rotor bar, air gap eccentricity, bent shaft, bearing failure, and rotor mass imbalance are the main mechanical faults. The most common fault reported in the literature is the short-circuiting between turns of the coils in the wind turbine generator [183]. These faults can be detected through shaft displacement detection, torque measurement, and vibration analysis. A temperature sensor can be used to detect winding faults [36]. Stator open-circuit faults alter the spectra of the stator line currents and instantaneous power [184]. Since rotor electrical imbalance causes shaft vibration, vibration signals can be used to monitor electrical imbalance [178]. Stator electrical imbalance can be detected from the change in the harmonic content of electrical signals [183].

2.8.1.8. Power Electronic Converter

The reliability of the power electronic converter becomes more complex with the increase of the wind turbine power rating. According to the literature, about 20% of WECS failure is due to the failure of power electronic converters as can be seen in Fig. 2-16 [178]. Temperature, vibration, and humidity are the three main factors that cause failures in power electronic converters [185]. There are three main converter components

in which faults normally occur: capacitors, printed circuit boards (PCB), and insulated gate bipolar transistors (IGBT) as shown in Fig. 2-17. Capacitor faults include open/short circuits, electrode materials migrating across the dielectric and forming conductive paths, dielectric breakdown, and an increased dissipation factor.

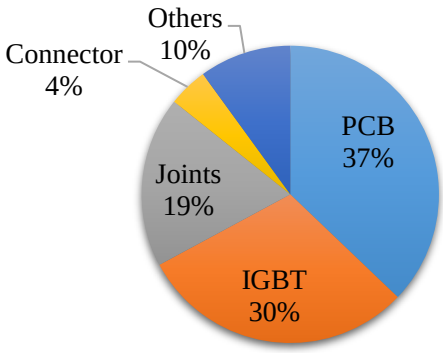

Fig. 2-17. Failure rates in power electronic converters for wind turbine systems [186].

Faults in PCBs include broken buried metal lines, corrosion or cracked traces, component misalignment, board delamination, and cold-solder joints. The failure modes of the IGBT modules include bond wire lift-off, short circuits, gate misfiring, solder fatigue, and cracks [187]. Thermo-sensitive electrical parameters, such as the collector-emitter saturation voltage, gate-emitter threshold voltage, on-state resistance and internal thermal resistance are used to monitor the degradation of IGBT modules.

2.8.1.9. Sensors

Faults within the WECS may also take place in the sensors mounted at various locations to measure certain parameters such as temperature, voltage, current and torque transducers. More than 14% of WECS faults occurs in these sensors [188]. Faults such as malfunction/physical failure, malfunction of the data processing/communication software [175] may cause performance degradation, and failure in the control system and mechanical and electrical subsystems, may lead to shutting down the wind turbine. Encoder faults in an induction motor drive are detected by measuring the mean and standard deviation of the rotor speed signal [189]. The correlation between rotor position and stator current are used to detect encoder faults by using the wavelet transform [190].

2.8.1.10. Control System

The control system plays a vital role in regulating the operations of the wind turbine. Faults in the control system can be categorised as hardware or software failures. Hardware failures include sensor faults, actuator faults, failure of the control board and communication links. Model-based methods can be used to detect hardware failures. The

software failures include buffer overflow, resource leaks, and out of memory. These faults can be detected using diagnosing codes in the software.

2.8.2. Signals of Offline Condition Monitoring for WECS

2.8.2.1. Vibration

Vibration analysis is one of the powerful tools currently used to monitor the mechanical integrity of wind turbines [190]. Vibration sensors installed on the casing of the wind turbine are used to detect faults within various wind turbine components such as the gearbox, bearing, rotor and blade, tower, generator and main shaft [191]. There are three main types of vibration sensors: displacement sensors, velocity sensors and accelerometers. The signals from the accelerometer carry the accelerated fault information out, and the amplitude of the accelerated signal demonstrates the fault severity level [192]. Installation of vibration sensors and the required data acquisition devices increase the wiring complexity and capital cost of the technique. In addition, it is quite difficult to insert the sensors on the surface or into the body of the components. Moreover, if the sensors and data acquisition devices fail to provide signals, this may lead to the failure of the wind turbine control, mechanical and electrical subsystems. Vibration signals are not capable of detecting incipient faults due to low signal-to-noise ratio (SNR).

2.8.2.2. Acoustic Emission

Acoustic emission sensors mounted on critical areas emit sound signals, which are used to detect structural defects in the blades, gearbox, and bearings [193]. The signal received from small structural changes indicates incipient structural damage or defect such as fatigue, cracks, reduced stiffness and increased surface roughness [194]. Unlike vibration analysis, this technique can detect incipient faults at an early stage. However, it requires a large number of sensors, which increases the cost and complexity of the technique.

2.8.2.3. Strain

Fibre optic strain sensors are normally mounted on the surface of the wind turbine blade. The signal collected from the sensors provides information about the structural defects of the blades [195]. This technique can detect small structural changes, requires low sampling frequency, and has consistent performance over distances.

2.8.2.4. Torque and Bending Moment

There are two torque sensors, namely rotary torque and reaction torque sensors. Rotary torque sensors measure the torque signals whereas reaction torque sensors measure the bending moment signals. The electrical signals of a generator can also be used to calculate the torque that omits the requirement for sensors and reduces the capital costs [196]. Signature extraction of the torque signal identifies mechanical failures. The frequency spectrum derived from the generator torque signal is also used to detect mechanical faults in the generator [197].

2.8.2.5. Temperature

Temperature data are mainly used to detect faults within the generators, bearings, gearbox, and power converters [198]. A cost-effective wind turbine thermal model is developed to diagnose the faults through temperature analysis based on the Supervisory Control and Data Acquisition (SCADA) signal [199], [200]. The SCADA signal provides reach information regarding faults in the wind turbine system with suitable signal processing methods. An electro-thermal model of DFIG is presented that reduces the cost of fault prevention and diagnosis for the wind turbine system [201]. SCADA data control sets are used to prevent and diagnose wind turbine faults by analysing the machine's temperature [202]. A generalised model is presented based on SCADA data analysis of ambient temperature and wind speed to predict faults in the wind turbine [203]. The performances of the model are compared with a real 1.5 MW DFIG-based wind turbine system that shows more effective results than the conventional one. Although the technique is considered reliable and cost-effective, its implementation is a bit complex. This technique cannot identify incipient faults and it is hard to identify the root cause and source of the temperature variation. Temperatures detected using thermal sensors may rise due to faulty components nearby. Hence, the technique is unable to detect accurate fault locations. In addition, the thermal sensors are quite fragile in harsh environments.

2.8.2.6. Lubrication Oil Parameters

Lubrication oil parameters such as viscosity level, water content, particle count and identification, pressure, and temperature are measured to detect defects in the gearbox and bearings at early stages [204]. The condition of the lubrication oil can be monitored in two ways – offline or online [205]. In offline monitoring, an oil sample is taken for condition testing, typically every six months [201]. This may cause an interruption to the overall system. In online oil monitoring, oil sensors to detect levels, dissolved particles, viscosity and temperature are utilised to reflect the condition of the oil in real-time [201].

2.8.2.7. Non-Destructive Testing

Non-destructive testing (NDT) techniques such as X-ray inspection, infrared thermography, ultrasonic scanning, and tap tests are used to detect hidden damage in composite materials [203], [206]. However, the implementation of the NDT techniques usually requires expensive instruments.

2.8.2.8. Electrical Signal-Based Methods

Electrical signal-based methods are widely used to detect various faults due to their distinctive advantages [189]. For example, the magnitude of certain harmonic components in an electrical current signal can be used to detect faults at early stages. Stator and rotor currents and stator voltages are measured to monitor the condition of the generator [207]. A stator and rotor current based data technique is proposed to identify faults within the doubly-fed induction generator (DFIG) [208]. Power signals calculated from voltage and current signals is used to detect rotor electrical imbalance as reported in [209]. Stator open circuit faults in DFIGs is detected using power and current spectra [185]. A mechanical fault or structural defect usually induces a vibration of the component that can modulate generator electrical signals. This modulated signal involves fault-related information of the mechanical components [210]. The P-amplitude of the generator electrical signal indicates a rotor imbalance due to increased blade surface roughness or yaw misalignment [211].

Electrical power spectral density indicates the reduction of blade stiffness [212]. Bearing failure can be extracted by analysing the phase and amplitude spectra of the generator's current signals, which can be used to identify the development of bearing failures at an early stage [213]. Electrical signals are also used to detect faults in the gearbox and power electronic converter [210]. Compared to other signals, electrical signal-based condition monitoring methods have significant advantages in terms of ease of implementation, less complex hardware, less cost, more reliability, and potential. The typical faults and associated signals have been summarised in Table 2-3. A summary of signals with their advantages and limitations is shown in Table 2-4.

Table 2-3. Summary of Faults and Signals

Component	Faults Occurred	Signals Monitored
Rotor	1. Fatigue and Crack 2. Surface roughness 3. Asymmetries 4. Reduced stiffness 5. Deformation	1. Vibration and AE 2. Strain 3. Torque 4. Electrical 5. NDT
Gearbox	1. Gear tooth abrasion 2. Tooth crack and tooth breakage 3. Tooth fracturing	1. Vibration and AE 2. Torque and Electrical 3. Temperature, oil parameters
Bearing	1. Surface roughness 2. Fatigue, Crack, Breakage 3. Outer/inner race 4. Ball and cage	1. Vibration and AE 2. Electrical 3. Temperature 4. Oil parameters
Main shaft	1. Corrosion and crack 2. Misalignment, Coupling failure	1. Vibration and torque 2. Electrical
Hydraulic system	1. Oil leakage 2. Sliding valve blockage	Pressure level
Mechanical Brake	1. Disc/caliper wear 2. Disc crack and motor failure 3. Hydraulic section failure	1. Vibration 2. Temperature 3. Electrical
Tower	1. Corrosion and crack 2. Structural damage	Vibration
Generator	1. Open/short circuit 2. Insulation damage 3. Imbalance and bent shaft 4. Rotor bar brok 5. Bearing failure 6. Air gap eccentricity	1. Vibration 2. Torque 3. Temperature 4. Oil parameters 5. Electrical
Power Converter	1. Capacitor 2. PCB 3. Semiconductor	1. Temperature 2. Electrical
Sensors	1. Sensor 2. Data processing hardware 3. Communication 4. Software malfunction	All related signals
Control system	1. Sensor 2. Actuator 3. Controller 4. Communication 5. Software malfunction	All related signals

Table 2-4. Summary of different signals of condition monitoring for wind turbine (WT)

Signals Monitored	Advantages	Limitations
Vibration	1. Mostly dominated technique 2. Reliable 3. Ability to detect incipient fault 4. Standardised (ISO10816)	1. Expensive and intrusive 2. Wiring complexity 3. Difficulties of sensor's installation 4. Subject to sensor failures 5. Inability to detect incipient faults
Acoustic Emission	1. Able to detect an early-stage fault 2. High signal-to-noise ratio 3. Good for low-speed operation 4. Frequency range far from load perturbation	1. Expensive 2. Complex 3. Very high sampling rate required
Strain	1. Ability to detect small structural changes 2. A requirement of low sampling frequency 3. Consistent performance over transmitting distance	1. Complex 2. Intrusive 3. Expensive
Torque and Bending moment	1. Direct measurement of rotor load 2. No requirement of sensors 3. Cost-effective	Intrusive
Temperature	1. Cost-effective 2. Reliable 3. Standardised (IEEE 841)	1. Embedded temperature detector required 2. Inaccurate fault locations 3. Sensors are quite fragile in a harsh environment
Lubrication Oil	1. Early-stage fault detection 2. Direct characterisation of bearing condition	1. Limited to bearings with closed-loop oil 2. Supply system 3. Expensive for online operation
Non-Destructive Testing	Ability to detect hidden damages in composite materials	Requires expensive instruments
Electrical Signals	1. Widely used technique 2. Early-stage fault detection 3. Less hardware complexity 4. Cost-effective 5. More reliability 6. No additional sensor needed 7. Non-intrusive 8. Easy to implement	1. Displacement based rather than force based 2. Difficult to detect incipient faults 3. Sometimes low signal-to-noise ratio

2.8.3. Online Condition Monitoring Technique

Technological development is accelerating and bringing the world to such a level where everyone and everything will be connected over the internet. Such technological development is providing secure communication and data exchange to connect machine to machine, machine to human, machine to objects, human to object at any time and in any place. This development is called the internet of things (IoT). The main idea behind the IoT is to establish self-governing, independent connections among physical devices, which is secure enough to allow data exchange in real time throughout the world [214].

The IoT platform has already connected billions of devices such as smartphones, computers, laptops, tablets, sensors, cars, home/work appliances, and many other handy embedded devices all over the world [215], [216], [217], [218]. Some smart phones nowadays have various built-in sensors that can sense objects and capture information, take decisions from this captured information, and transmit this to an authenticated internet server [219].

2.8.3.1. Internet of Things

A general scenario of IoT is presented in Fig. 2-18. With the advancement of technologies, data processing power and internal storage capacity, IoT devices have been extended rapidly which broadens IoT applications. Nowadays, different objects around the world can be fitted with barcodes or radio frequency identification (RFID) tags, which are easy for IoT smart devices such as barcode readers, smart phones, and RFID embedded scanners to scan and read [220], [221].

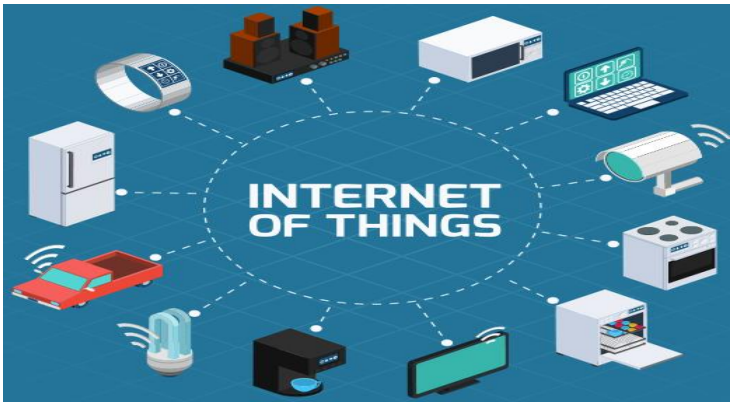

Fig. 2-18. Basics of the IoT network

An IoT device consists of a sensor with a processing unit, a network, and the cloud as shown in Fig. 2-19. The smart sensor device is used to sense physical objects and to

collect information from them. Different types of smart sensors are applied to sense information from physical objects.

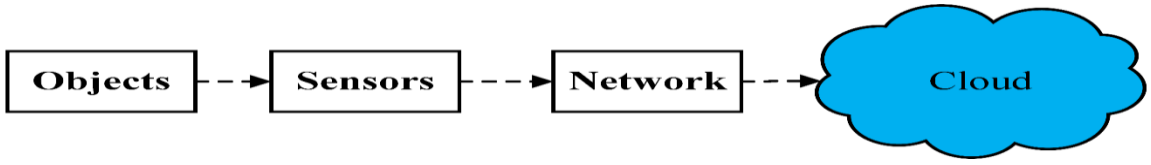

Fig. 2-19. Basic block diagram of the IoT

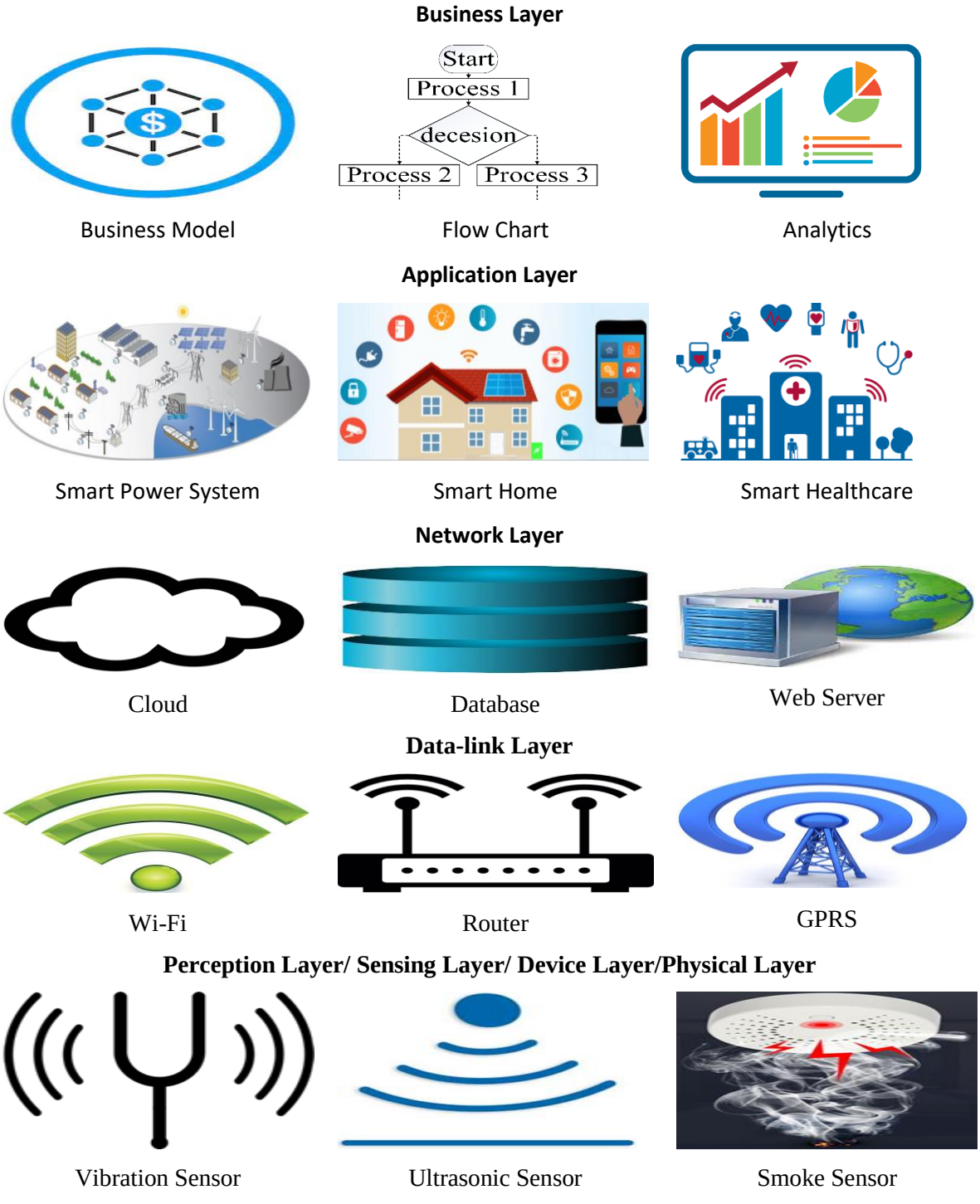

Fig. 2-20. IoT architecture

This sensed information can include things like humidity, motion, vibration, temperature, chemical composition, electrical signals and so on. The processing unit is used to make sense of the information from the objects. The network is used to transmit the information to the authenticated cloud server.

2.8.3.2. IoT Architecture

The IoT is structured using five layers – the perception layer, data-link layer, network layer, application layer, and business layer – as shown in Fig. 2-20 [222], [223], [224].

Researchers have conducted studies and literature surveys covering several IoT internet protocols (IPs) for each layer with appropriate workability under constrained environments and how these protocols have been applied to lead the communication flow effortlessly without any interruption. These protocols have certain standards, which need to be fulfilled to process data over network boundaries [225]. The details of these layers are described here.

2.8.3.2.1. Perception Layer

The perception layer consists of physical elements (smoke, temperature, vibration, pressure, and so on), and their corresponding sensor devices (smoke sensors, temperature sensors, vibration sensors, pressure sensors, and so on). This layer is also called the physical layer, device layer, or sensing layer. The sensors identify physical elements and collect information from or about them, such as their orientation, location, motion, humidity, pressure, and so on, using RFID tags, barcodes, or other identification methods [226]. The collected information is linked to the network layer for processing and secure transferal. RFID technology identifies the object and converts its identity into an electronic serial number using radio waves tagged on the objects [227], [228]. RFID technology is cost-effective and easy to implement [229]. The RFID system includes a reader, an access controller, an antenna, software, tags and a server [230]. The tags could be used in different contexts such as distribution, patient monitoring, military applications and so on.

A barcode is a method which encodes via visualise information. The visualised information contains optical codes that are readable by a specific machine (barcode scanner, image scanner). The barcode consists of black and white bars which become a line of text in a computer through the barcode scanner [231]. There are mainly two types of barcodes – 1D and 2D [232]. A 1D code consists of several vertical black and white lines. This code structure is popular since any barcode scanner can read it. The 2D

barcode consists of several vertical and horizontal lines which is a bit more complex to read. Only specific image scanners can read this type of code. The 2D code can hold more information (up to 2,000 characters) within less space compared to the 1D code (20–25 characters).

2.8.3.2.2. Data-link Layer

The data-link layer establishes a connection between the perception layer and the network layer. Several internet protocols, such as Bluetooth low energy (BLE), ZigBee, Wi-Fi, Z-wave, Dash7, Home plug GP, and so on, are utilised to build an initial interface in the perception layer and the network layer [233], [234].

Bluetooth is a wireless technology like Wi-Fi, which is used to exchange data between electronic devices over short distances (10 to 100 metres) [235]. It uses ultra-high frequency (UHF) radio waves with a short wavelength (2.4 to 2.485 GHz). A large number of electronic devices can be connected through Bluetooth technology.

Wi-Fi is basically a wireless technology that allows electronic devices to connect to the internet. It is a trademark name of the Wi-Fi alliance which uses IEEE 802.11 standards to transfer information [236]. A large number of electronic devices such as computers, laptops, tablets, smart-phones, and many other embedded electronic devices can be integrated using Wi-Fi. The authors of [237] show that Bluetooth devices require less power compared to Wi-Fi devices.

ZigBee is a wireless technology created by ZigBee alliance in 2001, which is used to enhance the functionality of sensor-based networks over short distances [238]. The ZigBee alliance uses IEEE the 802.15.4 standard to develop this device, which is highly flexible, needs less power, is cost-effective, scalable and reliable [233]. This technology is normally used in healthcare monitoring, home automation, agriculture, and many other smart devices.

Home plug GP is a low data rate communication protocol used for broadband power line communications [239]. This protocol is secure, reliable and very interoperable with IEEE 1901 devices.

DASH7 is an open-source protocol combining an actuator network protocol and wireless sensor protocol [240]. This protocol is a low data rate protocol that transfers data up to 167 kbits/s. A summary of these technologies is presented in Table 2-5.

Table 2-5. A summary of perception layer technologies

Parameters	BLE	Wi-Fi	Z-Wave	ZigBee	Home Plug	GP Dash7
Standardisation	IEEE 802.15.1	IEEE 802.11	IEEE 802.15.4	IEEE 802.15.4	IEEE 1901-2010	ISO/IEC 18000-7
Supported Networks	WPAN	LAN	LR-PAN	LR-PAN	WPAN	WSAN
Frequency	2.4 GHz	2.4/5 GHz	ISM, 915 MHz	2.4GHz ISM	28 MHz	68/433/915 MHz
Data rate	1 Mb/s	1 Gb/s	9.6/40 Kb/s	250 Kb/s	3.8 Mb/s	Up to 167 kb/s
Topologies	Mesh and star	Mesh and ethernet	mesh	Mesh only	Ethernet	Node-to-node, star, tree

2.8.3.2.3. Network Layer

The network layer stores the incoming information from the data-link layer to the database, cloud, web server, and so on. This layer is also called the service management layer since it manages the incoming information and stores it into directories.

Table 2-6. A summary of network layer protocols

Parameter	IPv4	IPv6	RPL	6LoWPAN
Interoperability	Low	Low	High	High
Security	IPSec	IPSec	Confidentiality and integrity of message	Secure authorisation
standardisation	IETF	ETF	IETF ROLL group	IEEE 802.15.4
Application	source host to router	Secure end-to-end data processing for multiple IP users	Building, home, Urban, and Industrial automation	Smart grid meters, building, home, and thread automation
Scalability	×	√	×	√
Communication network	Packet-switching	Packet-switching	P2P, P2M, and M2P	processing capability limited

The network layer uses a number of standard protocols, such as internet protocol version 4 (IPv4), internet protocol version 6 (IPv6), a routing protocol for low-power and lossy networks (RPL), and IPv6 low-power wireless personal area network (6LoWPAN) [241], [242]. These protocols are summarised in Table 2-6.

2.8.3.2.4. Application Layer

The application layer employs information globally from the middle-ware layer according to different protocols. The application layer includes smart homes, healthcare, the defence sector, power systems, intelligent transportation, and others. The range of protocols used in the application layer includes the constrained application protocol

(CoAP), Extensible Messaging and Presence Protocol (XMPP), Message Queuing Telemetry Transport (MQTT), Hypertext Transfer Protocol (HTTP), Advanced Message Queuing Protocol (AMQP), and so on [243], [244], [245]. CoAP is a specialised application layer protocol used to communicate among constrained devices. This protocol is especially suitable for local area networks. The protocol could be translated easily to HTTP during web integration by fulfilling special requirements, such as very low overheads, simplicity and multicast support, which are important requirements for the IoT [246]. The MQTT protocol consists of a message broker and a number of clients. The broker is a server that receives all incoming messages from clients and sends them to authenticated clients [247]. The client can be any range of devices from a micro-controller to a fully-fledged server, which connects the MQTT broker by executing an MQTT library over a network. MQTT is a lightweight constrained protocol, which is especially applicable for cloud/remote communication. A performance investigation has been conducted, which shows that the MQTT-SN protocol is 30% faster compared to CoAP for the same payload [248]. XMPP is an application layer protocol developed by the eponymous open-source community in 1999 based on Extensible Markup Language (XML), which facilitates real-time data communication among network entities [244]. The protocol is normally applicable for file transfer, video, signalling, gaming and so on. The XMPP protocol provides better security, faster response, and scalability which is especially suitable for IoT applications. AMQP is an open-source application layer protocol, which facilitates queuing, orientation of message, reliability, routing, and security [249]. HTTP is an application layer protocol used to transmit hypertext information between web clients and servers [250]. The hypertext information is encrypted as a link so that the web clients can access encrypted information easily by clicking or touching the link. A brief comparison of these protocols is summarised in Table 2-7.

2.8.3.2.5. Business Layer

This layer designed a business model, and the graphical results of the analysis applied in various sectors depend on the extracted information from the application layer. Success of the IoT depends solely on this layer since it determines all the actions and strategies to achieve the goals.

Table 2-7. A summary of protocols of the application layer

Parameter	CoAP	MQTT	AMQP	XMPP	HTTP
Year	2010	1999	2003		1997
Real Time	√	√	×	√	√
Synchronous/ Asynchronous	Both	Asynchronous only	Asynchronous only	Both	Both
QoS	Higher	Higher	Higher	Lower	Lower
Power Consumption	Lower	Lower	Higher	Higher	higher
Bandwidth	Lower	Lower	Higher	Higher	Higher
Client-Broker or Client-Server	Both	Client-Broker only	Both	Both	Client-Server only
Request to Response/ Publish to Subscribe	Both	Publish to Subscribe	Both	Publish to Subscribe	Request to Response
Header Size	4 byte	2 byte	8 byte	8 byte	Undefined
Encoding	Binary	Binary	Binary	Binary	Text
Licensing	Open-Source	Open-Source	Open-Source		Free
Security	DTLS	TLS/ SSL	TLS/ SSL	TLS/ SSL	TLS
Protocol	UDP	TCP	TCP	TCP	TCP/UDP
Interoperability	Higher	Lower	Lower	Lower	Higher

2.9 Industrial Internet of Things

Wireless sensor networks are formed of spatially autonomous dedicated sensors, which are used to monitor and record the physical condition of objects (vibration, sound, pressure, temperature, humidity, speed, etc) and organise these monitored and recorded data at a central location. Wireless sensor network technologies have gained huge popularity in industrial applications, such as healthcare, security, air transport, military, manufacturing, and so on [233]. These technologies are continually expanding and developing, which motivates new research and investment in them.

The International Data Corporation shows the current spending and forecasts for the IoT and IoT-related projects for 2016–2022, which indicates that the spending will go beyond $6 trillion by 2022 as shown in Fig. 2-21 [25]. There are more than 123 standards and technologies published in the literature to develop the IoT projects [33]. The internet protocols and standards for developing IoT projects are mainly divided into three categories, such as wireless personal area networks (WPAN), wireless local area networks (WLAN) and cellular networks [15]. WPAN uses a low rate standard (IEEE 802.14.4) and WLAN has a limited bandwidth standard (IEEE 802.3).

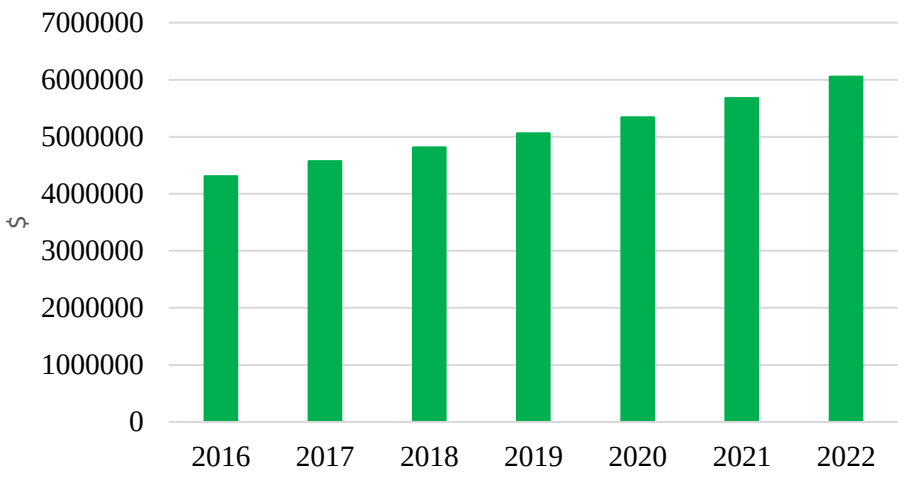

Fig. 2-21. Spending and forecast for the IoT

The cellular networks such as second-generation (2G), third-generation (3G), fifth-generation (5G), Long-term Evolution (LTE), worldwide interoperability for microwave (WiMAX), general packet radio service (GPRS), and global system for mobile communication (GSM) have faster data rates, wider coverage, and appropriate bandwidth, which is becoming the mainstream for the industrial internet of things (IoT). Nowadays, the general packet radio service (GPRS) and global system for mobile communication (GSM) are widely applied to develop industrial IoT projects.

2.10 Application and Future Challenges of IoT

IoT has a wide range of applications in our daily life, such as in smart cities, smart homes, smart transportation, smart healthcare, smart industries and so on. However, there have been so many constraints to implement IoT in every sector of our lives. The existing applications and challenges of IoT are discussed in section 2.10.1 and contribution of the thesis regarding IoT system for wind energy conversion system is hinted in section 2.10.2.

2.10.1 Existing Application of IoT and Future Challenges

Many houses in modern cites are now integrated with the internet of things. The IoT is applied to monitor air quality, traffic information, power line switches, etc. Smart homes are being designed with the help of IoT, which facilitates the detection of emergencies, monitoring energy consumption, and protecting homes from suspicious activities. The IoT helps us to design and develop smart transport systems, which facilitate efficient consumer control of smart transport and collecting information

(transport law enforcement, arrival and departure schedules, unexpected delays, and so on) [233]. The healthcare sector uses IoT to monitor patient conditions and scheduled drug intake. IoT is also applied to develop smart industries, which is called the industrial internet of things (IoT). The application of IoT is increasing at such a speed that it will cover every sphere of life in the near future. Despite the tremendous features of IoT, it faces many issues and challenges during its implementation, such as interoperability, standardisation, information confidentiality, network security, object security, and safety [233], [251]. Different manufacturing companies follow their own fabrication process to develop IoT devices, which restrict interoperability between objects. Hence, the standardisation of IoT devices is required to render interoperability among the devices, which is a great challenge. Another challenge for IoT devices is in naming and identity. A large number of IoT devices have connected each other which requires unique name and identity on the internet. To resolve this issue, a systematic and robust technique is required to identify and assign each device separately on the internet, which is quite a challenging task. Information confidentiality is important in IoT since different barcodes (1-D, 2-D, QR, RFID) attached to products ensure product details. Unauthorised information needs to be restricted during product labelling. Network security is another challenge for IoT devices, since data has been transferred via wired mediums or wireless mediums. The entire data transmission system needs to be secure to make sure that no data is being lost or interfered with.

2.10.3 Contribution of This Thesis in WECS Condition Monitoring

The wind energy conversion system (WECS) is mainly located in remote areas where the environment is harsher in condition. The WECS experiences various types of faults particularly in the dc-link capacitor and switching devices of the multilevel inverter. These faults, if not detected and rectified at early stages, they may lead to catastrophic failures to the WECS and continuity of power supply. This thesis proposes a new algorithm embedded into the SVPWM controller to identify the fault location in real- time. Since most wind power plants are in remote areas or offshore, WECS condition monitoring needs to be developed over the internet of things (IoT) to ensure system reliability. A novel industrial IoT algorithm is developed which can monitor the WECS remotely over IoT. The details of the SVPWM embedded algorithm and industrial IoT algorithm will be discussed in chapter 4.

Summary

WECS plays a significant role in the modern power sector. An extensive literature review has been conducted on WECS, which mainly focuses on full-scale power electronic converters and condition monitoring techniques. A summary is given here through the following points.

According to the World Wind Energy Association, wind energy contributed 6% of total world electricity generation in 2019, which is a significant share of world renewable power generation. This share in the global market makes wind energy the second most common source of renewable energy generation after hydropower in the world, resulting in a revolution in the modern power sector. According to statistics from the World Energy Agency in 2018, wind energy contributed 4% of global energy, and it forecasts this will triple by 2024. These achievements and forecasts attract new researchers to join the research into wind energy, motivating them to build their careers with deep sound knowledge and investigations.

The rectifier is one of the parts of the power electronic converter that produces ripples in output waveforms, and it is quite a challenging task to minimize these. Researchers have proposed different controllers to minimize these ripples, which result in poor dynamic performance, low efficiency, and low-power density. Hence, a controller has to be developed to suppress these ripples without sacrificing the performance of the rectifier.

The MLI is another part of the power electronic converter which has several advantages over conventional 2LI, such as less stress on switching devices, less harmonic distortion, more utilisation of the DC-link voltage, and better power quality. Better performance depends on a suitable topology and controller. Several MLI topologies have been discussed in this section, including transformer-based converters and transformer-less converters, which require a huge number of semiconductor devices and related components compared to the 2LI. Transformer-based multilevel inverters require a transformer which makes the multilevel structure bulky and difficult to implement. The transformer-less multilevel inverters are free of this bulky transformer. These include the neutral point clamped inverter (NPCLI), flying capacitor clamped inverter (FCCLI), and cascaded multilevel inverter (CMLI). Despite the attractive advantages of the capacitor clamped topologies, such as reduced voltage stresses on the semiconductor devices and capacitors, and the possibility of high-voltage operation with low switching frequency, these topologies have not been popular in the industry mainly because they require a large number of capacitors. Though diode-clamped inverters have higher voltage and power ratings along with reduced

switching frequency, these features are not enough to attract industrial applications due to the large number of clamping diodes required to block the capacitor voltage along with the voltage balancing issues across these capacitors. Cascaded multilevel inverters have become a promising topology, since they do not require any clamping diodes or capacitors. However, a cascaded MLI requires several non-isolated DC sources that restrict it to being coupled with a rectifier. Hence, a cascaded MLI has to be designed which resolves this issue without compromising performance.

A number of pulse width modulation techniques have been discussed in this thesis such as sinusoidal pulse width modulation (SPWM), selective harmonic elimination pulse width modulation (SHEPWM), and SVPWM(SVPWM). Despite having many attractive features, SPWM produces higher harmonic distortion, higher switching losses, and lower efficiency. The main difficulty with SHEPWM lies in the proper optimisation of the switching angles, which complicates its practical implementation. SVPWM(SVPWM) has brought considerable advancement to the variable frequencies drive application due to its superior performance, including the lowest harmonic distortion in its output waveforms, being well-suited for hardware implementation, and 15% increased DC-bus voltage utilisation. The key challenge in implementing the SVPWM technique is the large number of triangles exhibiting a different number of switching vectors, which makes the selection of switching vectors quite difficult.

The condition of the WECS needs to be monitored to maintain continuous power flow. Due to the global trend in generating electrical energy through renewable energy resources, especially from wind, the reliability of such systems has become a priority for stakeholders of transmission and distribution networks. As such, reliable condition monitoring and fault diagnosis techniques have to be adopted to detect any incipient faults in these systems to avoid potential consequences. This thesis presents a comprehensive review of the common faults, signals and signal processing methods for condition monitoring and fault diagnosis in WECS. The advantages and limitations of each technique have been highlighted. The review shows that there is still a significant research gap in developing comprehensive, cost-effective, real-time condition monitoring techniques for WECSs.

Since the majority of wind turbine plants are located in remote areas that often include harsh environmental conditions, online condition monitoring techniques need to be developed with the application of the internet in real-time for these wind turbine plants. With advancements in power electronics, communication technology, and sensor accuracy, reliable online condition monitoring for wind turbines will be viable in the near future.

Online condition monitoring has become popular nowadays and can be utilised to monitor the condition of WECS via the internet of things.

Chapter III
Design and Implementation of Proposed Controllers and Three-Phase CMLI for the WECS

3.1 Introduction

A block diagram of the wind energy conversion system (WECS) is depicted in Fig. 3-1, which proposes a three-phase cascaded multilevel inverter (CMLI), and a space vector pulse width modulation (SVPWM) controller. Apart from this proposed duo, the block diagram consists of several components and subsystems such as the blade, generator, rectifier, and motor. Aerodynamic force strikes the wind turbine blade, which rotates causing the wind generator to produce three-phase power [252]. An aerodynamic wind turbine model is described in section 3.2. The rectifier converts the wind-generated three-phase ac voltage to dc-link voltage, which contains ripples [50]. The SVPWM controller controls the rectifier as well as suppresses the ripples from the dc-link voltage, which is described in section 3.3. The proposed three-phase cascaded multilevel inverter (CMLI) with four series connected dc-link capacitors inverts the dc-link voltage to three-phase staircase ac voltage, which is described in section 3.4. The three-phase CMLI suffers from voltage balancing issues across the dc-link capacitors. The proposed SVPWM controller controls the three-phase CMLI and balances the dc-link voltage over non-isolated capacitors, which is described in section 3.5. The inverted three-phase staircase output voltages are fed to the three-phase squirrel cage induction motor. The proposed controller (SVPWM) and three-phase CMLI for WECS are designed in the MATLAB/Simulink software and a hardware prototype is developed to validate the simulated results, which are described in section 3.6.

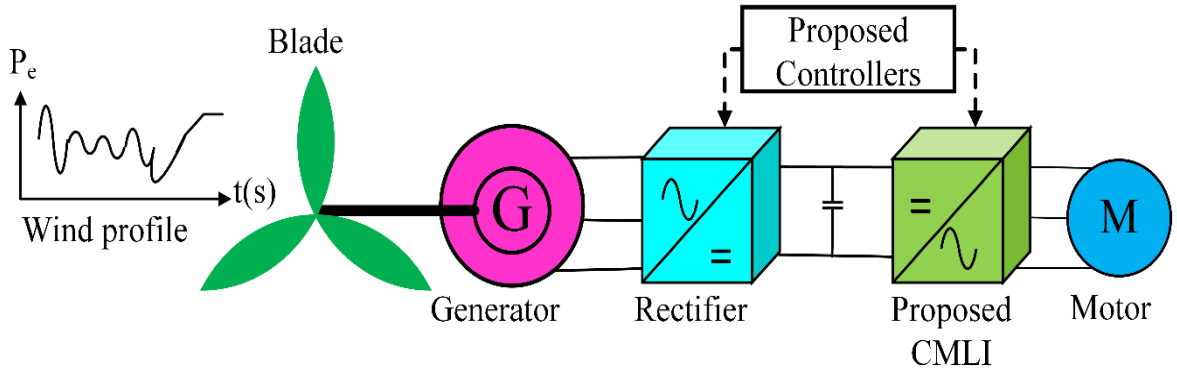

Fig. 3-1. Block diagram of proposed controllers and three-phase CMLI for the WECS.

3.2 Wind Turbine Model

Aerodynamic force hits the wind turbine blade at a perpendicular angle, which causes it to rotate (v). The rotation of the blade sweeping across its area (A) produces mechanical power (P_m), which is used to drive a generator to produce electrical power. The produced mechanical output power of any wind generator is presented in equation (1) [253].

$$P_m = \frac{1}{2}\rho A v^3 C_p\big(\lambda(t), \beta(t)\big) \tag{1}$$

Here ρ is called air density which is 1.225 kg/m^3, $C_p\big(\lambda(t), \beta(t)\big)$ is the mechanical power coefficient, which is a function of the tip speed turn ratio $\lambda(t)$, and pitch angle of blade $\beta(t)$. The tip speed turn ratio λ(t) is the ratio of tip speed of blade (T_S) to wind speed (v) as in equation (2) [254].

$$\lambda = \frac{T_s}{v} = \frac{\omega_r R}{v} \tag{2}$$

Where, ω_r is wind turbine rotor speed, and R is the rotor radius of the wind turbine. The power coefficient $C_p(\lambda, \beta)$ of a wind turbine generator could be designed by using equation (3) [255].

$$C_p(\lambda, \beta) = C_1\left(\frac{C_2}{\lambda_i} - C_3\beta - C_4\right)e^{\frac{-C_5}{\lambda_i}} + C_6\lambda \tag{3}$$

The aerodynamic torque produced by the drivetrain is expressed in equation (4) [256].

$$\tau_a(t) = \frac{1}{2}\rho\pi R^2 \frac{v^2}{\omega_r(t)} C_p\big(\lambda(t), \beta(t)\big) \tag{4}$$

Based on Betz's law, the blade of the wind turbine cannot capture all the power; therefore, the power coefficient, $C_p(\lambda, \beta)$ should be well-defined to describe the efficiency of a wind turbine to produce electricity. The C_p is determined by the ratio of actual electric power to total wind power, which flows into the wind turbine's blades.

The developed torque in the turbine by the maximum captured aerodynamic power is expressed in equation (5) [257].

$$\tau_{aopt} = \frac{P_{mmax}}{\omega_{ropt}} = K_{opt}\omega_{ropt}^2 \tag{5}$$

Where

$$K_{opt} = \frac{1}{2}\pi\rho R^5 \frac{C_{pmax}(\lambda_{opt})}{\lambda_{opt}^3},\ \omega_{ropt} = \frac{\lambda_{opt} v}{R} \tag{6}$$

The existing controller, which ensures convergence to the optimum (Q) operating point at a steady state, is applied for the generator reference torque based on the nonlinear control law of the form.

$$T_{g\_ref} = K_{opt}\omega_r^2 \tag{7}$$

However, control law (7) requires enough knowledge regarding turbine parameters and atmospheric condition, K_{opt} which depends on characteristics $C_p(\lambda, \beta)$, blade radius R, and air density ρ.

3.3 Space Vector Pulse Width Modulation (SVPWM) Controller

The 3-phase ac voltage produced by the wind generator is converted into intermittent dc-link voltage using the rectifier, which requires 6 bi-directional switching devices (S_1-S_6) as shown in Fig. 3-2. This converted dc-link voltage contains ripples, which restrict obtaining the desired input voltage for the three-phase CMLI. The space vector pulse width modulation (SVPWM) controller is applied to suppress these ripples and improve power quality. In the controller, the output voltage of the AC/DC converter (V_{dc}) is measured using a voltage sensor, which is compared to the reference signal (V*). The error signal (e = V*-V_{dc}) contains minimum ripples and is supplied to the PI controller to produce a modulated reference signal (V_m*). Then, V_m* is fed to the SVWM controller to generate pulses which control the rectifier. The entire process of minimizing the ripples from the dc-link voltages has been depicted in Fig. 3-2.

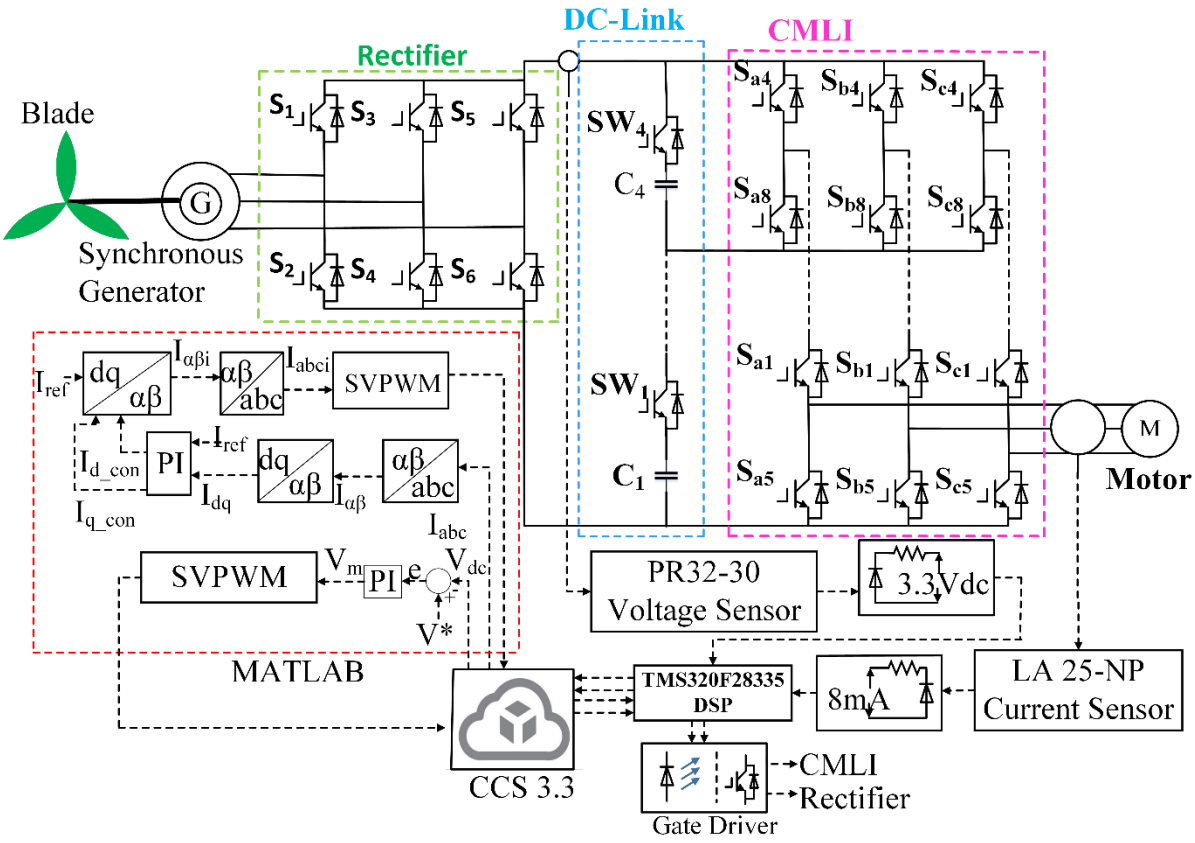

Fig. 3-2. The proposed controllers and three-phase CMLI for the WECS

3.4 Proposed Three-Phase Cascaded Multilevel Inverter

The conventional three-phase two-level inverter (2LI) consists of six insulated gate bipolar transistors (IGBTs), a squirrel cage induction motor, and a dc source (V_{dc}) as shown in Fig. 3-3 [258]. The 2LI is functioned properly when the upper switches of transistors (S_{a1}, S_{b1} and S_{c1}) are switched to 'ON'; the lower switches of transistors (S_{a2}, S_{b2}, and S_{c2}) are switched to 'OFF' and vice versa. A constant dc-link voltage is set as the input voltage of three-phase inverter. It produces the output three phase ac voltages by using the concept of switching functions. Each phase leg is operated independently. Each switching function takes the value of '1' if the upper switch is turned to 'ON' and the value of '0' if the lower switch is turned to 'OFF' and vice versa. The three-phase output voltages produced by this inverter which are V_a, V_b, and V_c at points A, B, and C respectively are fed to the three-phase induction motor.

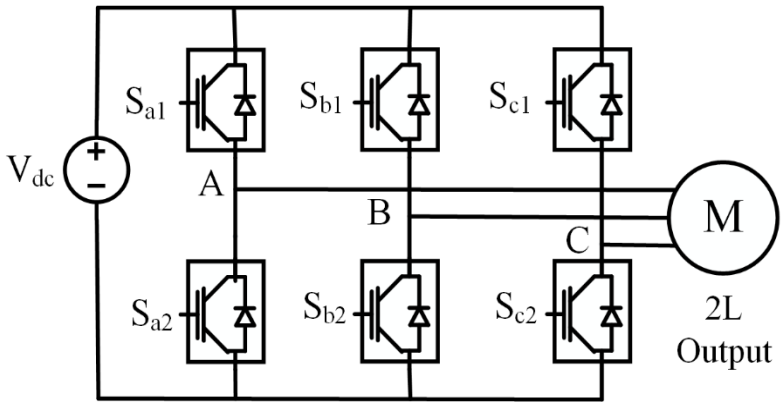

Fig. 3-3. Three-phase two-level inverter (2LI)

A three-phase 3-level CMLI is developed by cascading two 2Lis, which is depicted in Fig. 3-4. Each phase of the conventional 2LI consists of two IGBT as shown in Fig. 3.3. The middle point of the two IGBT is connected to the collector of the upper IGBT of another 2LI.

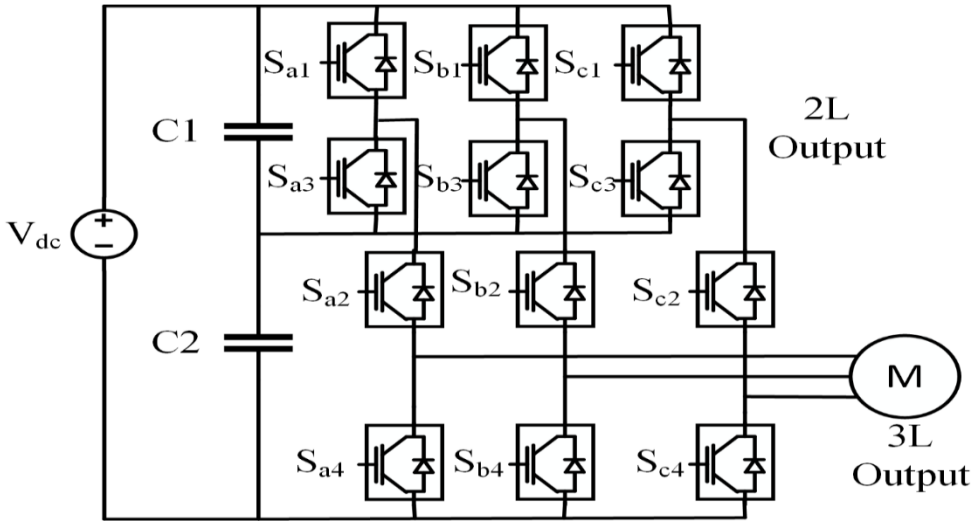

Fig. 3-4. Proposed three-phase 3-level CMLI

The middle point of another 2LI inverter is connected to the load. One three-phase 2-level inverter is connected in cascade to the other three-phase inverter that's why; this topology is called three-phase cascaded multilevel inverters (CMLI). The three phase 3-level cascaded multilevel inverter consists of 12 switching devices and 2 dc-link voltage sources as shown in Fig. 3.4. This topology is free from any clamping diodes and capacitors that greatly reduced the complexity of multilevel inverter. Zero levels in the output voltage of the three-phase CMLI as depicted in Fig. 3.4 is generated when the two switches S_{a3} and S_{a4} are turned on while switches S_{a1} and S_{a2} are turned off. A voltage level of $V_{dc}/2$ is generated when S_{a2} and S_{a3} are operating in a toggle mode with S_{a1} and S_{a4}. On the other hand, the full dc-link voltage (V_{dc}) is obtained when S_{a1} and S_{a2} are turned on while S_{a3} and S_{a4} are turned off. Each phase produces 3-level output voltages of 0, Vdc/2, and Vdc according to the state of the four IGBTs.

A three-phase 4-level CMLI can be implemented by cascading the three-phase 3-level CMLI and the 2LI. The three-phase 4-level CMLI consists of 18 switching devices and 3 dc-link voltage sources. It requires an additional 6 IGBTs and a dc source compared to 3LCMLI. Similarly, a three-phase 5-level CMLI is developed and proposed here by cascading the three-phase 4-level CMLI and the 2LI without any neutral point connection as shown in Fig. 3-5.

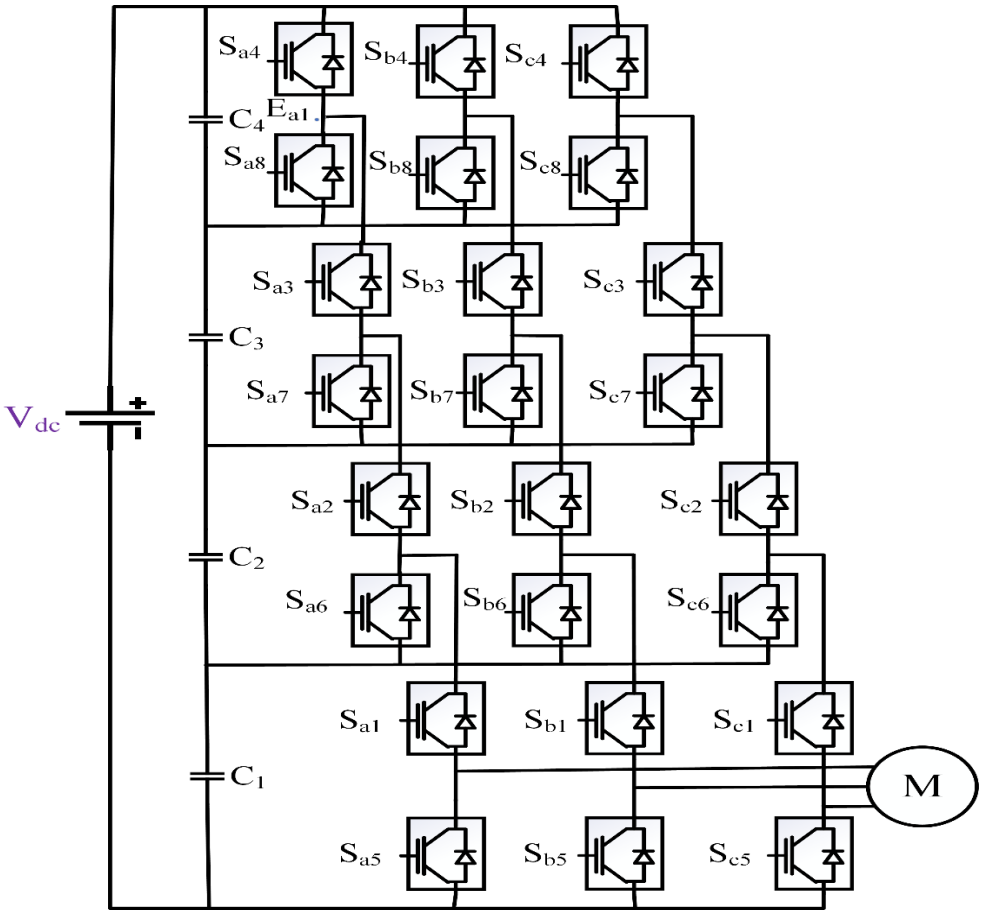

Fig. 3-5. Proposed three-phase 3-level CMLI

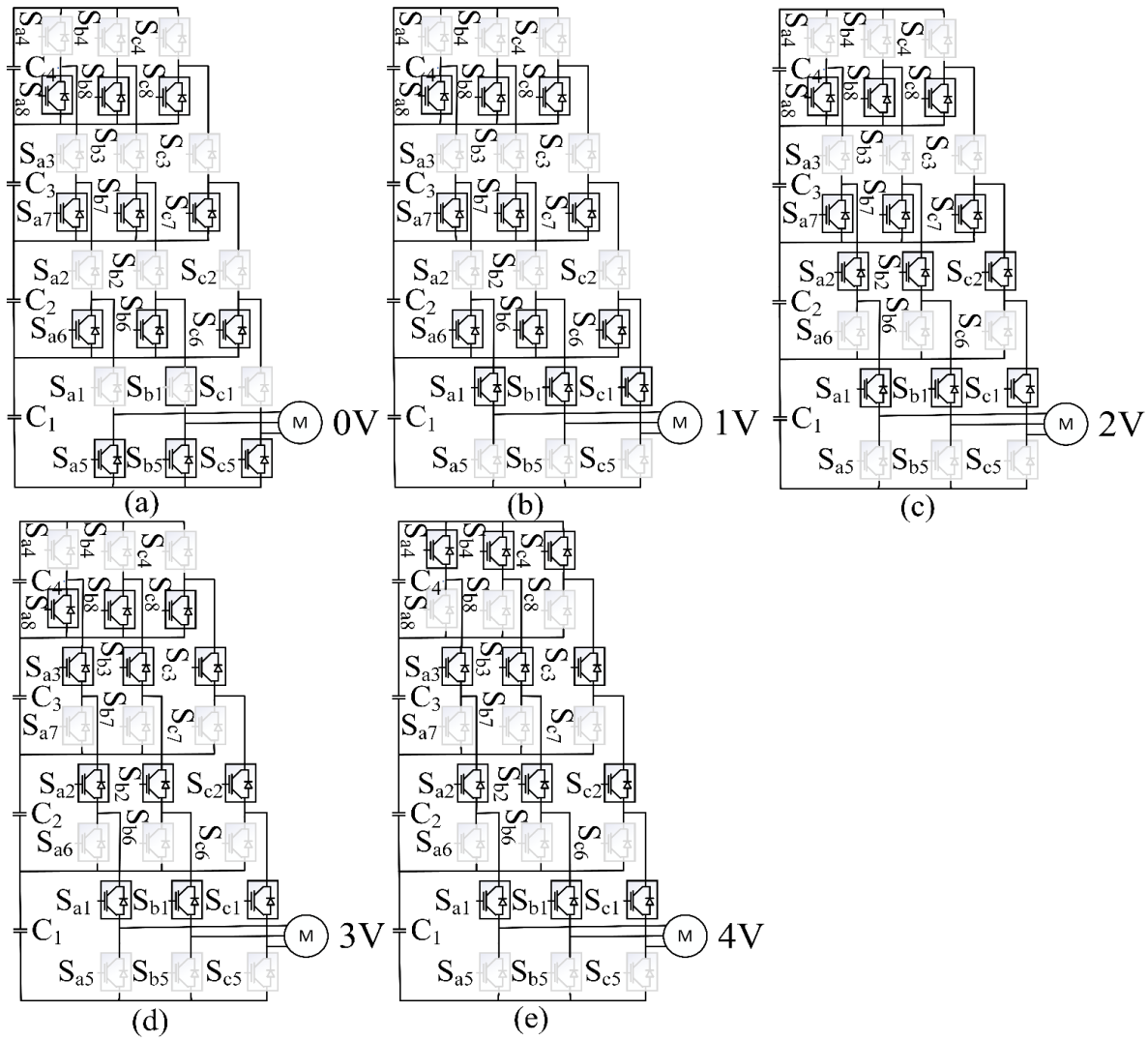

Fig. 3-6. Switching pattern for producing multilevel voltage (a) 0V (1-level) (b) 1V (2-level) (c) 2V (3-level) (d) 3V (4-level) (e) 4V (5-level)

The converted dc-link voltage with minimum ripples is fed to the proposed three-phase 5-level CMLI as presented in Fig. 3-2. The proposed three-phase 5-level CMLI consists of 24 switching devices and 4 dc-link capacitors (C_1-C_4). The voltages produced across these capacitors are V_{c1}, V_{c2}, V_{c3} and $V_{c4,}$ which are considered equal in amplitude ($V_{c1}=V_{c2}=V_{c3}=V_{c4}=V$). If switches S_{a5}, S_{a6}, S_{a7}, and S_{a8} are switched to ON while S_{a1}, S_{a2}, S_{a3}, and S_{a4} are switched to OFF, the output voltage is OV (1-level) as shown in Fig. 3-6(a). If S_{a1}, S_{a6}, S_{a7}, and S_{a8} are switched to ON while S_{a2}, S_{a3}, S_{a4}, and S_{a5} are switched to OFF, the output voltage is 1V (2-level) as depicted in Fig. 3-6(b). If S_{a1}, S_{a2}, S_{a7}, and S_{a8} are switched to ON while S_{a3}, S_{a4}, S_{a6}, and S_{a5} are switched to OFF, the output voltage is 2V (3-level) as shown in Fig. 3-6(c). If S_{a2}, S_{a2}, S_{a3}, and S_{a8} are switched to ON while S_{a4}, S_{a5}, S_{a6}, and S_{a7} are switched to OFF, the output voltage is 3V (4-level) as presented in Fig. 3-6(d). If switches S_{a1}, S_{a2}, S_{a3},

and S_{a4} are switched to ON while S_{a5}, S_{a6}, S_{a7}, and S_{a8} are switched to OFF, the output voltage is 4V (5-level) as shown in Fig. 3-6(e). Hence, the three-phase CMLI produces a staircase output voltage of 0, 1V, 2V, 3V and 4V which is summarized in Table 3-1.

Table 3-1. The switching sequence of 5-level CMLI

Switching sequence for phase A								Terminal Voltage
S_{a1}	S_{a2}	S_{a3}	S_{a4}	S_{a5}	S_{a6}	S_{a7}	S_{a8}	
1	1	1	1	0	0	0	0	4V
0	1	1	1	1	0	0	0	3V
0	0	1	1	1	1	0	0	2V
0	0	0	1	1	1	1	0	1V
0	0	0	0	1	1	1	1	0

3.5 Proposed SVPWM Controller

Several controllers have been proposed in the literature for multilevel inverter topologies [55]. Among them, the space vector pulse width modulation features several unique advantages including low total harmonic distortion, high output voltage, high switching frequency and self-voltage balancing ability that makes it a suitable candidate for the CMLI proposed in this thesis [106]. The conventional SVPWM controller diagram is a hexagon divided into 6 sectors [259]. Each sector is comprised of an equilateral triangle that has unity of sides and height (h=√3/2). The diagram comprises m^3 switching states presented in $\alpha\beta$ reference frame, where m is defined as the number of levels in the output voltage waveform. The conventional SVPWM controller diagram has been extended to a multilevel SVPWM controller diagram [115]. The diagram is also divided into six sectors, which include $(m\text{-}1)^2$ triangles and m^3 switching vectors in each sector. A conventional 5-level SVPWM controller diagram is shown in Fig. 3-7 [260].

As shown in Fig. 3-7, there are two different types of triangles in the 5-level SVPWM diagram. These are: type 1 (denoted by 1, 2, 4, 5, 7, 9, 10, 12, 14, and 16) and type 2 (denoted by 3, 6, 8, 11, 13, and 15). Type 1 triangles have their base at the bottom and type 2 at the top. The reference vector (V_{ref}) shown in Fig. 3-8 is rotating in either anti-clockwise or clockwise direction to determine the switching vectors of type 1 and type 2 triangle respectively as shown in Fig. 3-9. The triangle numbers Δ_n could be determined using two variables of P_1 and P_2, that

are normally dependent on the position of the reference vector $(I_\alpha,\ I_\beta)$ as shown in Fig. 3-10. These two variables are calculated as below:

$$P_1 = int\left(I_\alpha + \frac{I_\beta}{\sqrt{3}}\right) \quad (8)$$

$$P_2 = int\left(\frac{I_\beta}{h}\right) \quad (9)$$

P_1 presents a part of sector between two adjacent lines ($y + \sqrt{3} = \sqrt{3}P_1$ and $\sqrt{3}x = \sqrt{3}(P_1 + 1)$) joining the vertices, which are separated by distance (h) and inclined at 120^0 with respect to α −axis. $P_1 = 0$ reveals that point I_{ref} is under line A_1A_2 while $P_1 = 1$ implies that point I_{ref} is between the two lines A_1A_2 and A_3A_5.

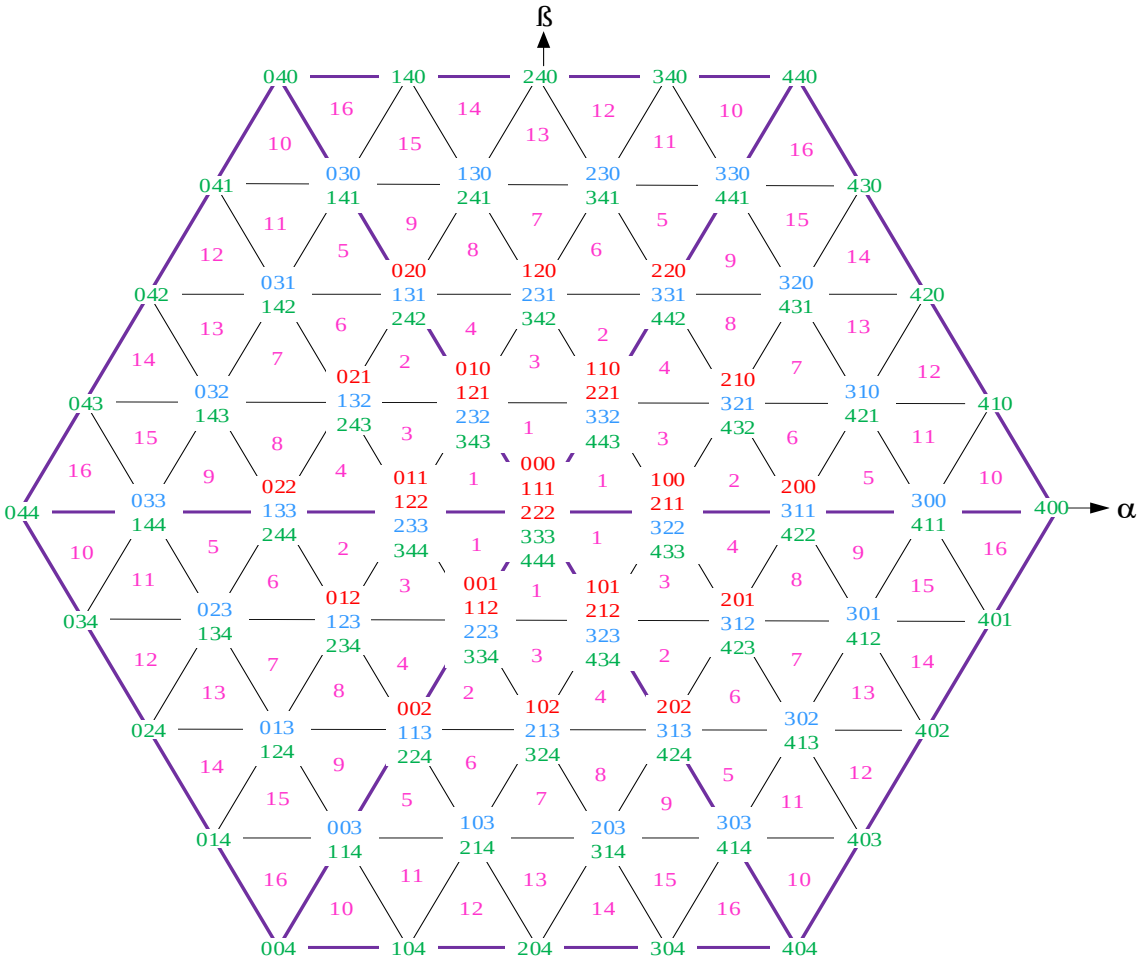

Fig. 3-7. Conventional 5-level SVPWM controller diagram.

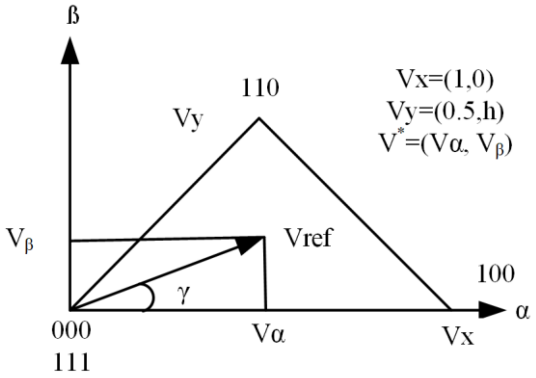

Fig. 3-8. Determination of the reference vector location.

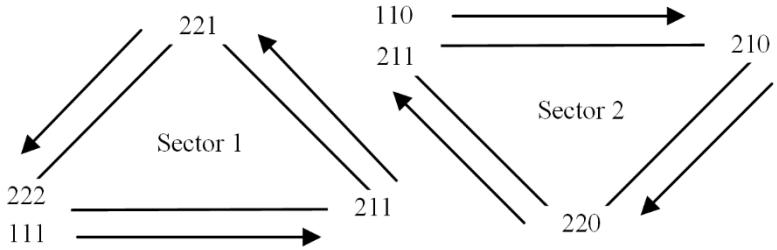

Fig. 3-9. Rotation of vectors

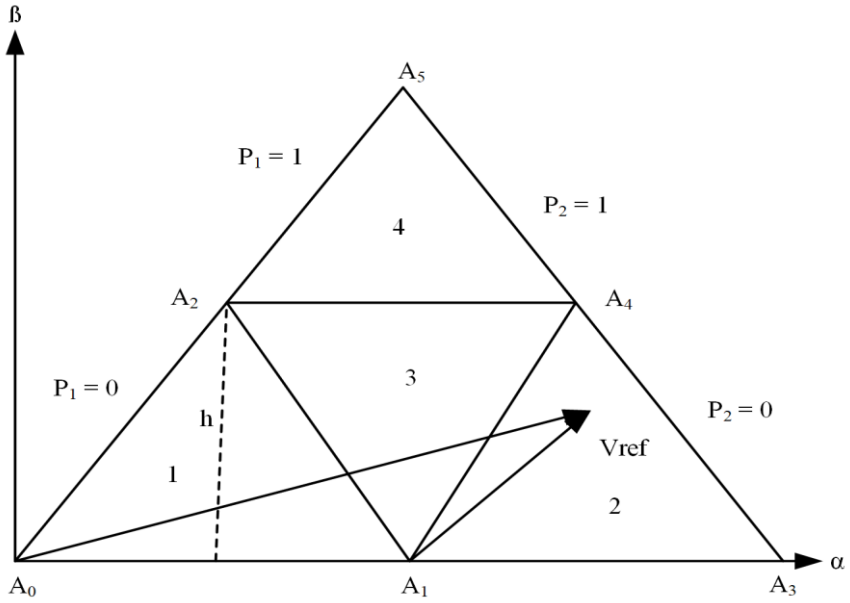

Fig. 3-10. Triangle number determination

On the other hand, P_2 is presented as another part of the sector between the two defined lines ($y = h.P_1$ and $y = h.(P_1 + 1)$) joining the vertices, which are separated by distance (h) and parallel to α −axis. $P_2 = 0$ implies that point I_{ref} is between lines A_0A_3 and A_2A_4, while this point is located above line A_2A_4 when $P_2 = 1$. Geometrically, the values of P_1 and P_2 indicate the intersection of two regions that are either a rhombus or triangle. In addition, point I_{ref} lies in (a) triangle 1 if $P_1 = 0$, and $P_2 = 0$, (b) rhombus $A_1A_3A_4A_2$ if $P_1 = 1$ and $P_2 = 0$, and (c) triangle

4 if $P_1 = 1$ and $P_2 = 1$. The same calculation could be used for any number of levels. In Fig. 3-10, the reference vector is located in the rhombus $A_1A_3A_4A_2$. This rhombus consists of two (2) triangles which are triangle 2 and triangle 3. Point I_{ref} could be positioned in any of these two (2) triangles. Let $(I_{\alpha i},\ I_{\beta i})$ is the coordinates of point I_{ref} with respect to point A_1 achieved as:

$$I_{\alpha i} = I_{\alpha} - P_1 + .5P_2 \quad (10)$$

$$I_{\beta i} = I_{\beta} - P_2 h \quad (11)$$

In (3) and (4), $(I_{\alpha i}/I_{\beta i})$ is the tangent of the line between the origin of the reference vector, and the rhombus which is compared to the tangent of the diagonal point of rhombus ($\sqrt{3}$). The tangent comparison is conducted through the inequality $I_{\beta i} \leq \sqrt{3} I_{\alpha i}$ for determining a small vector I^Z and an accurate triangle number Δ_n . If $I_{\beta i} \leq \sqrt{3 I}_{\alpha i}$, the triangle number Δ_n is obtained as:

$$\Delta_n = P_1^2 + 2P_2 \quad (12)$$

$$I_1 = I_{\alpha i} \quad (13)$$

$$I_2 = I_{\beta i} \quad (14)$$

If $I_{\beta i} > \sqrt{3} I_{\alpha i}$, the triangle number is obtained as:

$$\Delta_n = P_1^2 + 2P_2 + 1 \quad (15)$$

$$I_1 = 0.5 - I_{\alpha i} \quad (16)$$

$$I_2 = h - I_{\beta i} \quad (17)$$

The above equations offer a simple guide to arranging the triangles and facilitate ease of identification and can be extended to any number of desired levels. The on-time calculation is the same for all sectors as given below.

$$T_a = T_s \left[I_1 - \left(\frac{I_2 T_s}{2h} \right) \right] \quad (18)$$

$$T_b = T_s \left[\frac{I_2}{h} \right] \quad (19)$$

$$T_0 = T_s - T_a - T_b \quad (20)$$

where $T_s = 1/2f_s$, f_s is the switching frequency.

The space vector diagram consists of 16 number of triangles in each sector and 125 number of switching vectors, which makes the controller complex and difficult to implement. Moreover, the triangles have an unequal number of switching vectors, which causes a voltage imbalance across the dc-link capacitors. Vectors (000 to 111) basically contribute to the performances of the conventional 2-level diagram, while vectors (111 to 222), (222 to 333) and vectors (333 to 444) respectively contribute to the performances of the 3-level, 4-level and 5-level SVPWM controllers.

In this thesis, the switching vectors for 2-level and 3-level controllers are omitted, which not only reduce the switching vector's complexity, but also balance the voltages of the dc-link capacitors. It is to be noted that omitting such low level contributed switching vectors do not significantly affect the performance of the CMLI.

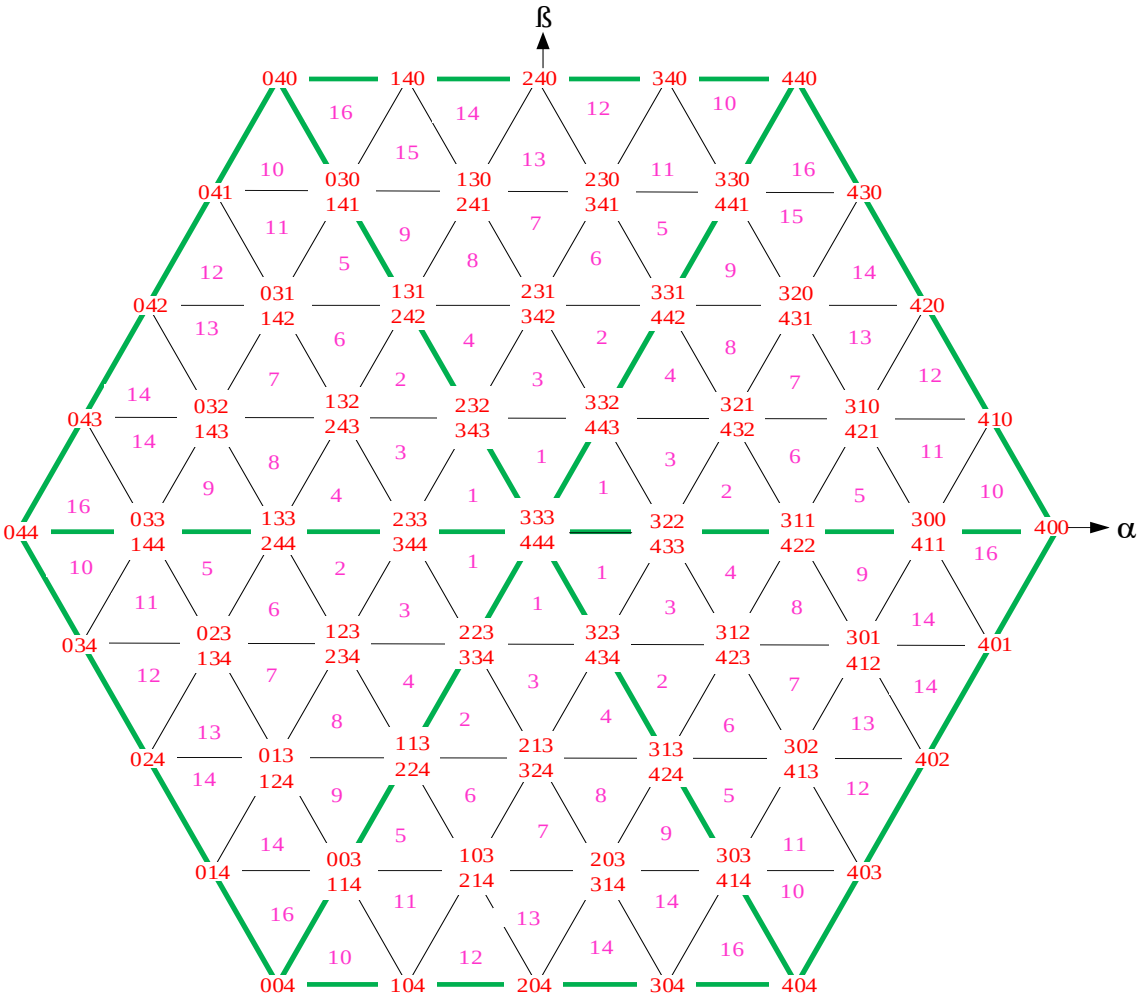

Fig. 3-11. Proposed simplified 5-level SVPWM controller diagram

This is attributed to the fact that low level contributed switching vectors are of least contribution to the performance of the CMLI, while the switching vectors of high-level contribution dominate the CMLI performance. The conventional SVPWM controller diagram, as shown in Fig. 3-7, consists of three types of switching vectors marked by three different colour bands (red, blue and green). The switching vectors marked by red bands in triangle 1 (e.g. 000, 100, 110, 111, 211, 221, 222) and triangle 2 (e.g. 100, 200, 210, 211) in sector 1 are completely redundant. On the other hand, the green colour-coded switching vectors of triangle 1 (e.g. 333, 433, 443, 444) and triangle 2 (e.g. 422, 432, 433) in sector 1 are mandatory for the formation of the triangles. The blue colour-coded switching vectors (e.g. 322) are redundant

for triangle 1 but mandatory for triangle 2 in sector 1. From this point of view, it can be concluded that green colour-coded switching vectors are mandatory for the formation of the triangles, while the red colour-coded switching vectors are completely redundant, and the blue colour-coded ones are either redundant or mandatory for the formation of the triangles in the SVPWM controller diagram. Hence, the 5-level SVPWM controller diagram has been simplified by omitting red colour-coded switching vectors as shown in Fig. 3-11.

The proposed simplified diagram comprises 98 switching vectors instead of 127 switching vectors in the case of the conventional SVPWM controller diagram. Moreover, only four switching vectors are enough to create a triangle. The elimination of the lower weighted switching vectors for triangle 1 has been shown in Fig. 3-12. These four high weighted switching vectors are selected from the simplified diagram to execute the control pulses for the CMLI.

Hence, this thesis proposes a proportional integral (PI)-based SVPWM controller to balance the dc-link voltage over non-isolated capacitors and control the three-phase CMLI. In the proposed controller, the 3-phase output currents are measured and transformed to the dq reference frame using Clarke and Park's transform. The dq reference signal (I_{ref}) is compared to the dc-link current (I_{dc}) and the resultant error signal is supplied to the PI controller as per the equations below.

$$I_{ref} = I_r \sin \omega t \tag{21}$$

$$I_{d\_con} = k_p\left(I_d - I_{ref}\right) + k_i \int \left(I_d - I_{ref}\right) dt \tag{22}$$

$$I_{q\_ref} = 0 \tag{23}$$

$$I_{q\_con} = k_p\left(I_q - I_{q\_ref}\right) + K_i \int \left(I_q - I_{q\_ref}\right) dt \tag{24}$$

$$I_{\alpha i} = I_{d\_con} \left(\cos \theta - I_{q\_con} \sin \theta\right) \tag{25}$$

$$I_{\beta i} = I_{d\_con} \left(\sin \theta + I_{q\_con} \cos \theta\right) \tag{26}$$

The angle (θ_i), and magnitude (I_i^*) are determined from the following equations.

$$\theta_i = \tan^{-1}\left(\frac{\mathrm{I}_{\beta \mathrm{i}}}{\mathrm{I}_{\alpha \mathrm{i}}}\right) \tag{27}$$

$$I_i^* = \sqrt{\mathrm{I}_{\alpha \mathrm{i}}^2 + \mathrm{I}_{\beta \mathrm{i}}^2} \tag{28}$$

The sector number (s) is obtained by applying the following equation.

$$s = \mathrm{floor}\left(\frac{\theta_i}{\pi/3}\right) + 1 \tag{29}$$

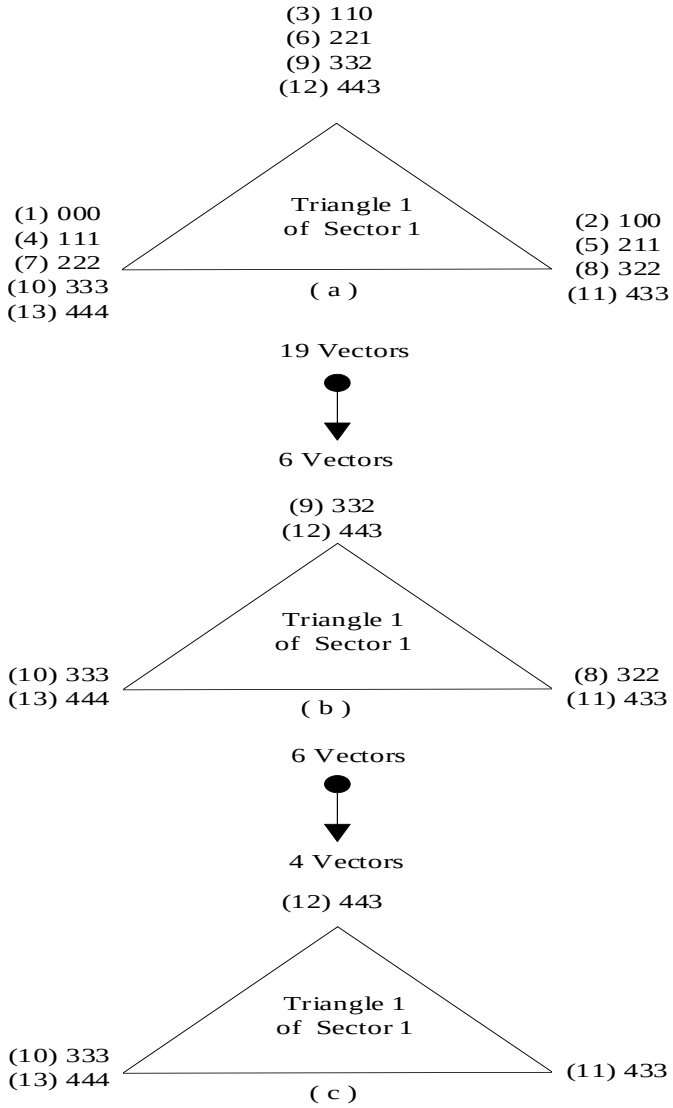

Fig. 3-12. Process of omitting lower weighted switching vectors for triangle 1

A comparison of the proposed number of switching vectors based on the simplified SVPWM controller and the conventional SVPWM controller is shown in Table 3-2.

Table 3-2. Comparison of switching vectors in SVPWM controllers

Switching Vectors of SVPWM		
No. of Levels	Conventional	Proposed
3	27	26
4	64	56
5	125	98

This comparison reveals the advantage of the proposed simplified SVPWM controller, particularly when a higher number of levels is required in the output voltage waveform. From Table 3-2, the proposed 5-level SVPWM controller diagram reduces the 27 switching vectors

in the conventional SVPWM controller. The proposed switching vectors for triangle 1 of the proposed SVPWM controller are shown in Table 3-3.

Table 3-3. Proposed switching vectors

Sec.	Tri. No.	Switching Vectors	Sec.	Tri. No.	Switching Vectors
1	1	$I_{333}\rightarrow I_{433}\rightarrow I_{443}\rightarrow I_{444}$	2	1	$I_{333}\rightarrow I_{343}\rightarrow I_{443}\rightarrow I_{444}$
	2	$I_{322}\rightarrow I_{422}\rightarrow I_{432}\rightarrow I_{433}$		2	$I_{332}\rightarrow I_{342}\rightarrow I_{442}\rightarrow I_{443}$
	3	$I_{332}\rightarrow I_{432}\rightarrow I_{433}\rightarrow I_{443}$		3	$I_{332}\rightarrow I_{342}\rightarrow I_{343}\rightarrow I_{443}$
	4	$I_{332}\rightarrow I_{432}\rightarrow I_{442}\rightarrow I_{443}$		4	$I_{232}\rightarrow I_{242}\rightarrow I_{342}\rightarrow I_{343}$
	5	$I_{311}\rightarrow I_{411}\rightarrow I_{421}\rightarrow I_{422}$		5	$I_{331}\rightarrow I_{341}\rightarrow I_{441}\rightarrow I_{442}$
	6	$I_{321}\rightarrow I_{421}\rightarrow I_{422}\rightarrow I_{432}$		6	$I_{331}\rightarrow I_{341}\rightarrow I_{342}\rightarrow I_{442}$
	7	$I_{321}\rightarrow I_{421}\rightarrow I_{431}\rightarrow I_{432}$		7	$I_{231}\rightarrow I_{241}\rightarrow I_{341}\rightarrow I_{342}$
	8	$I_{331}\rightarrow I_{431}\rightarrow I_{432}\rightarrow I_{442}$		8	$I_{231}\rightarrow I_{241}\rightarrow I_{242}\rightarrow I_{342}$
	9	$I_{331}\rightarrow I_{431}\rightarrow I_{441}\rightarrow I_{442}$		9	$I_{131}\rightarrow I_{141}\rightarrow I_{241}\rightarrow I_{242}$
	10	$I_{300}\rightarrow I_{400}\rightarrow I_{410}\rightarrow I_{411}$		10	$I_{330}\rightarrow I_{340}\rightarrow I_{440}\rightarrow I_{441}$
	11	$I_{310}\rightarrow I_{410}\rightarrow I_{411}\rightarrow I_{421}$		11	$I_{330}\rightarrow I_{340}\rightarrow I_{341}\rightarrow I_{441}$
	12	$I_{310}\rightarrow I_{410}\rightarrow I_{420}\rightarrow I_{421}$		12	$I_{230}\rightarrow I_{240}\rightarrow I_{340}\rightarrow I_{341}$
	13	$I_{320}\rightarrow I_{420}\rightarrow I_{421}\rightarrow I_{431}$		13	$I_{230}\rightarrow I_{240}\rightarrow I_{241}\rightarrow I_{341}$
	14	$I_{320}\rightarrow I_{420}\rightarrow I_{430}\rightarrow I_{431}$		14	$I_{130}\rightarrow I_{140}\rightarrow I_{240}\rightarrow I_{241}$
	15	$I_{330}\rightarrow I_{430}\rightarrow I_{431}\rightarrow I_{441}$		15	$I_{130}\rightarrow I_{140}\rightarrow I_{141}\rightarrow I_{241}$
	16	$I_{330}\rightarrow I_{430}\rightarrow I_{440}\rightarrow I_{441}$		16	$I_{030}\rightarrow I_{040}\rightarrow I_{140}\rightarrow I_{141}$

Sec.	Tri. No.	Switching Vectors	Sec.	Tri. No.	Switching Vectors
3	1	$I_{333}\rightarrow I_{343}\rightarrow I_{344}\rightarrow I_{444}$	4	1	$I_{333}\rightarrow I_{334}\rightarrow I_{344}\rightarrow I_{444}$
	2	$I_{232}\rightarrow I_{242}\rightarrow I_{243}\rightarrow I_{343}$		2	$I_{233}\rightarrow I_{234}\rightarrow I_{244}\rightarrow I_{344}$
	3	$I_{233}\rightarrow I_{243}\rightarrow I_{343}\rightarrow I_{344}$		3	$I_{233}\rightarrow I_{234}\rightarrow I_{334}\rightarrow I_{344}$
	4	$I_{233}\rightarrow I_{243}\rightarrow I_{244}\rightarrow I_{344}$		4	$I_{223}\rightarrow I_{224}\rightarrow I_{234}\rightarrow I_{334}$
	5	$I_{131}\rightarrow I_{141}\rightarrow I_{142}\rightarrow I_{242}$		5	$I_{133}\rightarrow I_{134}\rightarrow I_{144}\rightarrow I_{244}$
	6	$I_{132}\rightarrow I_{142}\rightarrow I_{242}\rightarrow I_{243}$		6	$I_{133}\rightarrow I_{134}\rightarrow I_{234}\rightarrow I_{244}$
	7	$I_{132}\rightarrow I_{142}\rightarrow I_{143}\rightarrow I_{243}$		7	$I_{123}\rightarrow I_{124}\rightarrow I_{134}\rightarrow I_{234}$
	8	$I_{133}\rightarrow I_{143}\rightarrow I_{243}\rightarrow I_{244}$		8	$I_{123}\rightarrow I_{124}\rightarrow I_{224}\rightarrow I_{234}$
	9	$I_{133}\rightarrow I_{143}\rightarrow I_{144}\rightarrow I_{244}$		9	$I_{113}\rightarrow I_{114}\rightarrow I_{124}\rightarrow I_{224}$
	10	$I_{030}\rightarrow I_{040}\rightarrow I_{041}\rightarrow I_{141}$		10	$I_{033}\rightarrow I_{034}\rightarrow I_{044}\rightarrow I_{144}$
	11	$I_{031}\rightarrow I_{041}\rightarrow I_{141}\rightarrow I_{142}$		11	$I_{033}\rightarrow I_{034}\rightarrow I_{134}\rightarrow I_{144}$
	12	$I_{031}\rightarrow I_{041}\rightarrow I_{042}\rightarrow I_{142}$		12	$I_{023}\rightarrow I_{024}\rightarrow I_{034}\rightarrow I_{134}$
	13	$I_{032}\rightarrow I_{042}\rightarrow I_{142}\rightarrow I_{143}$		13	$I_{023}\rightarrow I_{024}\rightarrow I_{124}\rightarrow I_{134}$
	14	$I_{032}\rightarrow I_{042}\rightarrow I_{043}\rightarrow I_{143}$		14	$I_{013}\rightarrow I_{014}\rightarrow I_{024}\rightarrow I_{124}$
	15	$I_{033}\rightarrow I_{043}\rightarrow I_{143}\rightarrow I_{144}$		15	$I_{013}\rightarrow I_{014}\rightarrow I_{114}\rightarrow I_{124}$
	16	$I_{033}\rightarrow I_{043}\rightarrow I_{044}\rightarrow I_{144}$		16	$I_{003}\rightarrow I_{004}\rightarrow I_{014}\rightarrow I_{114}$

Sec.	Tri. No.	Switching Vectors	Sec.	Tri. No.	Switching Vectors
5	1	$I_{333}\rightarrow I_{334}\rightarrow I_{434}\rightarrow I_{444}$	6	1	$I_{333}\rightarrow I_{433}\rightarrow I_{434}\rightarrow I_{444}$
	2	$I_{223}\rightarrow I_{224}\rightarrow I_{324}\rightarrow I_{334}$		2	$I_{323}\rightarrow I_{423}\rightarrow I_{424}\rightarrow I_{434}$
	3	$I_{223}\rightarrow I_{323}\rightarrow I_{324}\rightarrow I_{334}$		3	$I_{323}\rightarrow I_{423}\rightarrow I_{433}\rightarrow I_{434}$
	4	$I_{323}\rightarrow I_{324}\rightarrow I_{424}\rightarrow I_{434}$		4	$I_{322}\rightarrow I_{422}\rightarrow I_{423}\rightarrow I_{433}$
	5	$I_{113}\rightarrow I_{114}\rightarrow I_{214}\rightarrow I_{224}$		5	$I_{313}\rightarrow I_{413}\rightarrow I_{414}\rightarrow I_{424}$
	6	$I_{113}\rightarrow I_{213}\rightarrow I_{214}\rightarrow I_{224}$		6	$I_{313}\rightarrow I_{413}\rightarrow I_{423}\rightarrow I_{424}$
	7	$I_{213}\rightarrow I_{214}\rightarrow I_{314}\rightarrow I_{324}$		7	$I_{312}\rightarrow I_{412}\rightarrow I_{413}\rightarrow I_{423}$
	8	$I_{313}\rightarrow I_{314}\rightarrow I_{324}\rightarrow I_{424}$		8	$I_{312}\rightarrow I_{412}\rightarrow I_{422}\rightarrow I_{423}$
	9	$I_{313}\rightarrow I_{314}\rightarrow I_{414}\rightarrow I_{424}$		9	$I_{311}\rightarrow I_{411}\rightarrow I_{412}\rightarrow I_{422}$
	10	$I_{003}\rightarrow I_{004}\rightarrow I_{104}\rightarrow I_{114}$		10	$I_{303}\rightarrow I_{403}\rightarrow I_{404}\rightarrow I_{414}$
	11	$I_{103}\rightarrow I_{104}\rightarrow I_{114}\rightarrow I_{214}$		11	$I_{303}\rightarrow I_{403}\rightarrow I_{413}\rightarrow I_{414}$
	12	$I_{103}\rightarrow I_{104}\rightarrow I_{204}\rightarrow I_{214}$		12	$I_{302}\rightarrow I_{402}\rightarrow I_{403}\rightarrow I_{413}$
	13	$I_{203}\rightarrow I_{204}\rightarrow I_{214}\rightarrow I_{314}$		13	$I_{302}\rightarrow I_{402}\rightarrow I_{412}\rightarrow I_{413}$
	14	$I_{203}\rightarrow I_{204}\rightarrow I_{304}\rightarrow I_{314}$		14	$I_{301}\rightarrow I_{401}\rightarrow I_{402}\rightarrow I_{412}$
	15	$I_{303}\rightarrow I_{304}\rightarrow I_{314}\rightarrow I_{414}$		15	$I_{301}\rightarrow I_{401}\rightarrow I_{411}\rightarrow I_{412}$
	16	$I_{303}\rightarrow I_{304}\rightarrow I_{404}\rightarrow I_{414}$		16	$I_{300}\rightarrow I_{400}\rightarrow I_{401}\rightarrow I_{411}$

3.6 Results and Discussion

3.6.1. Simulation Results and Discussion

The proposed three-phase CMLI, and SVPWM controller for WECS have been designed in the MATLAB/SIMULINK software environment as shown in Fig. A (1), A (2), and A (3) in the Appendix. The length (l), tip speed ratio (λ), and power coefficient (C_p) of the wind turbine blade are set to 26m, 8 and 0.48; respectively [261].

The maximum power point tracker is shown in Fig. 3-13. The generator produces maximum power when the average wind speed is 12 m/s. The wind and generator speed have been displayed in Fig. 3-14. The three-phase voltage and current waveforms of the synchronous generator are presented in Fig. 3-15. The generated output peak-peak voltage and current are 480V and 2.5A respectively, which are pure sinusoidal. The total harmonic distortion (THD) depicted in Fig. 3-16 assures their pure sinusoidal natures.

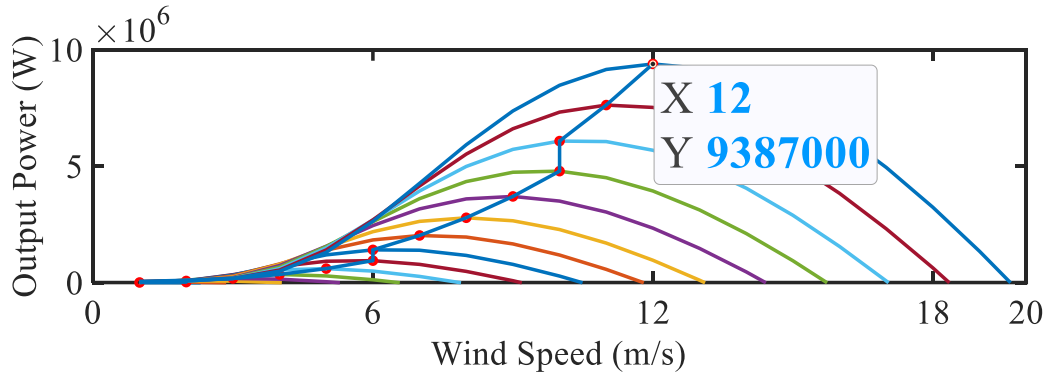

Fig. 3-13. Maximum power point tracker

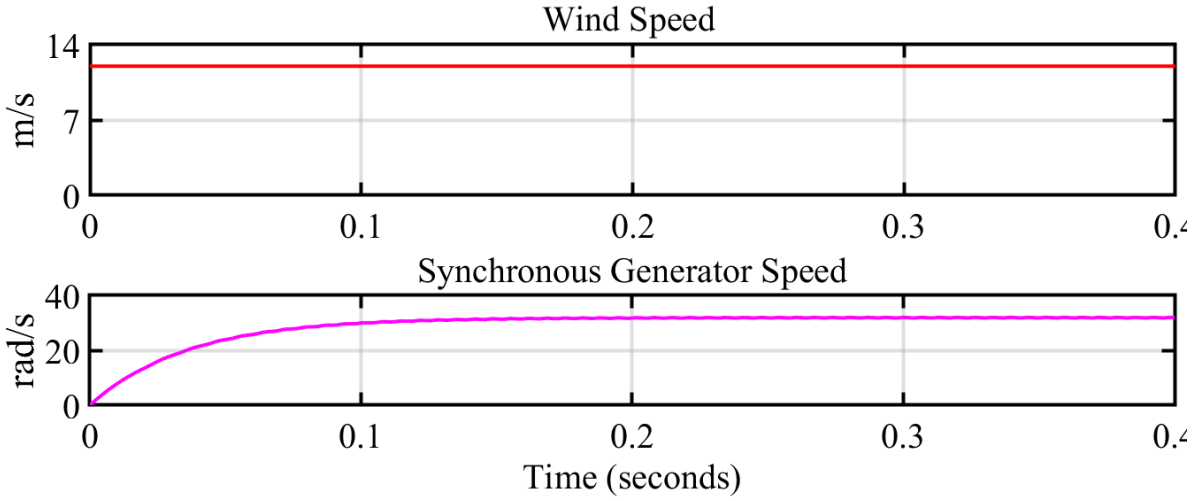

Fig. 3-14. Wind and synchronous generator speed

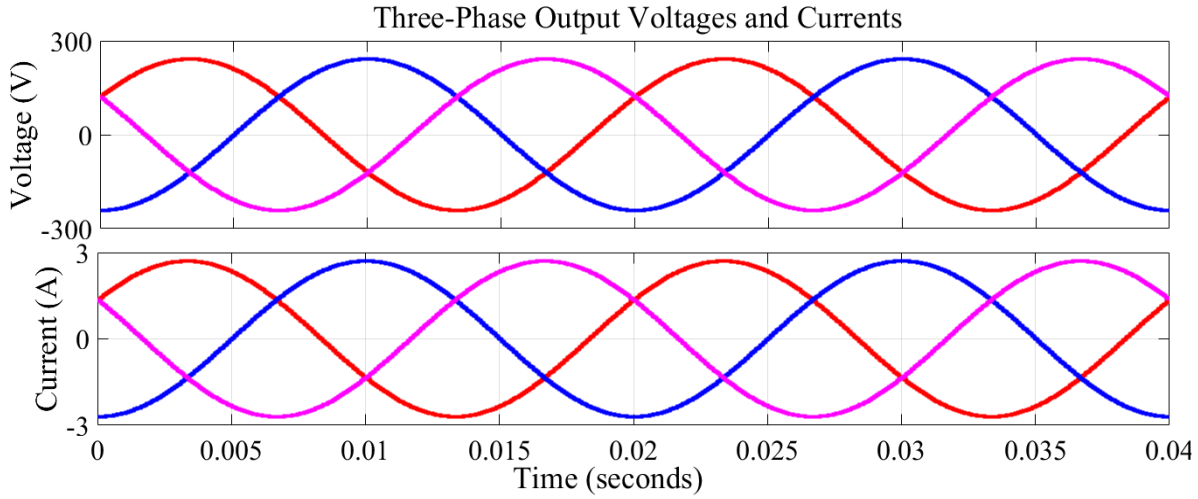

Fig. 3-15. Three-phase output voltage and current of the three-phase synchronous generator

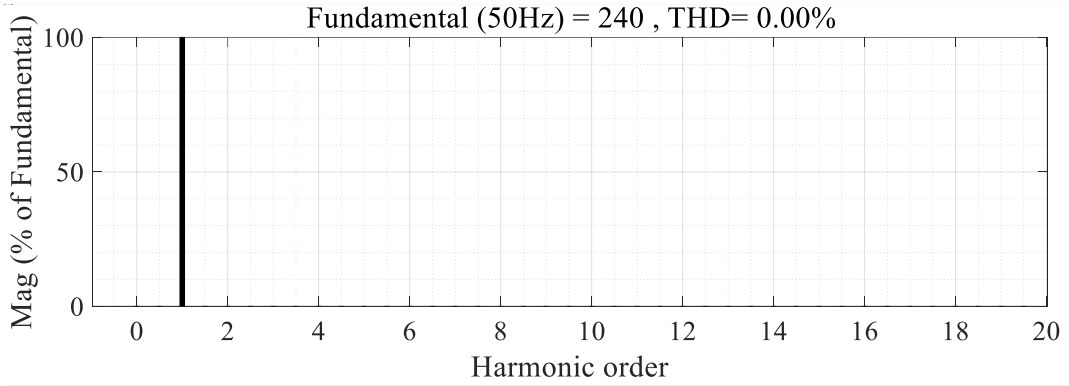

Fig. 3-16. THD of the three-phase output voltages and currents of the three-phase synchronous generator

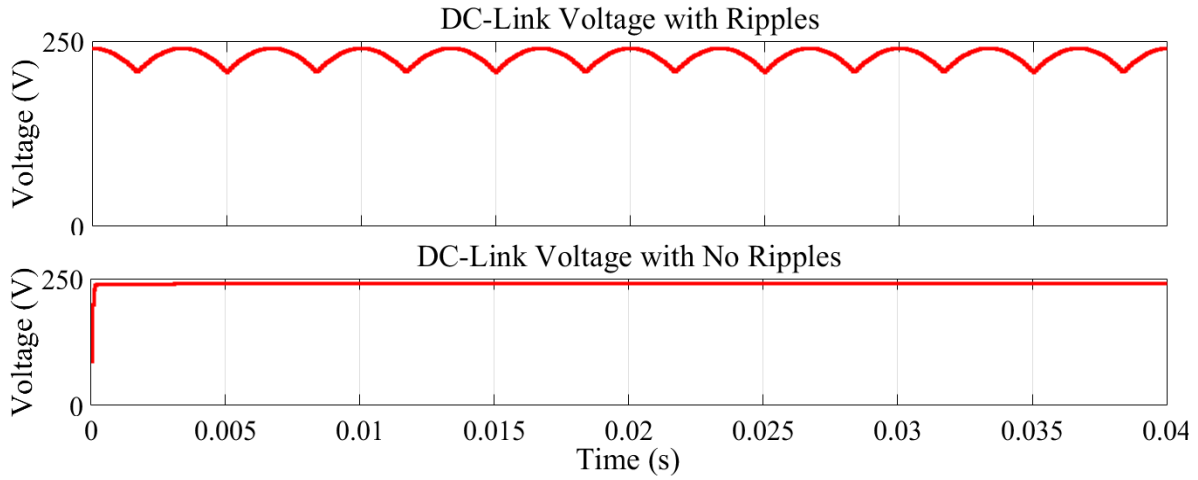

Fig. 3-17. dc-link voltage without the controller and with the SVPWM controller

The generated three-phase output waveforms are converted to DC-link voltage using a three-phase uncontrolled rectifier. The obtained output voltage of the uncontrolled three-phase rectifier constitutes ripples as presented in Fig. 3-17, which need to be minimized. The SVPWM controller has been practiced for the three-phase rectifier to suppress the ripples from

the dc-link voltage. The obtained output voltage of the controlled rectifier is shown in Fig. 3-17, where the ripples are minimized.

The output dc-link voltage of the three-phase rectifier is fed to the input of the three-phase CMLI, which suffers voltage unbalancing issues across the dc-link capacitors as presented in Fig. 3-18. Due to the voltage unbalancing issues across the dc-link capacitors, three-phase output voltage and current waveforms distort from their sinusoidal behaviour as depicted in Fig. 3-19. The THD of these distorted three-phase waveforms is increased as shown in Fig. 3-20, which indicates the deviation from the sinusoidal behaviour.

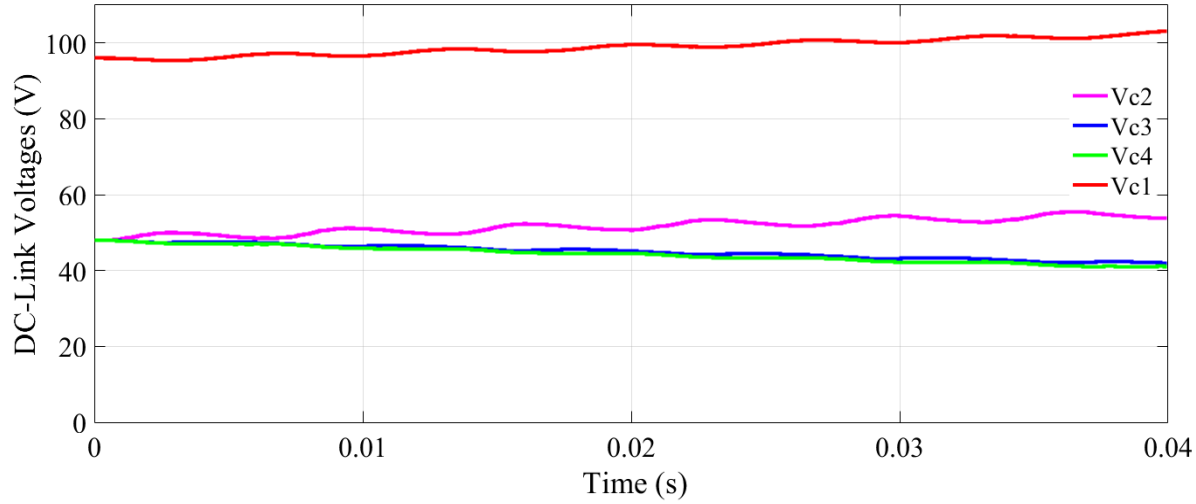

Fig. 3-18. Unbalanced dc-link voltages across dc-link capacitors

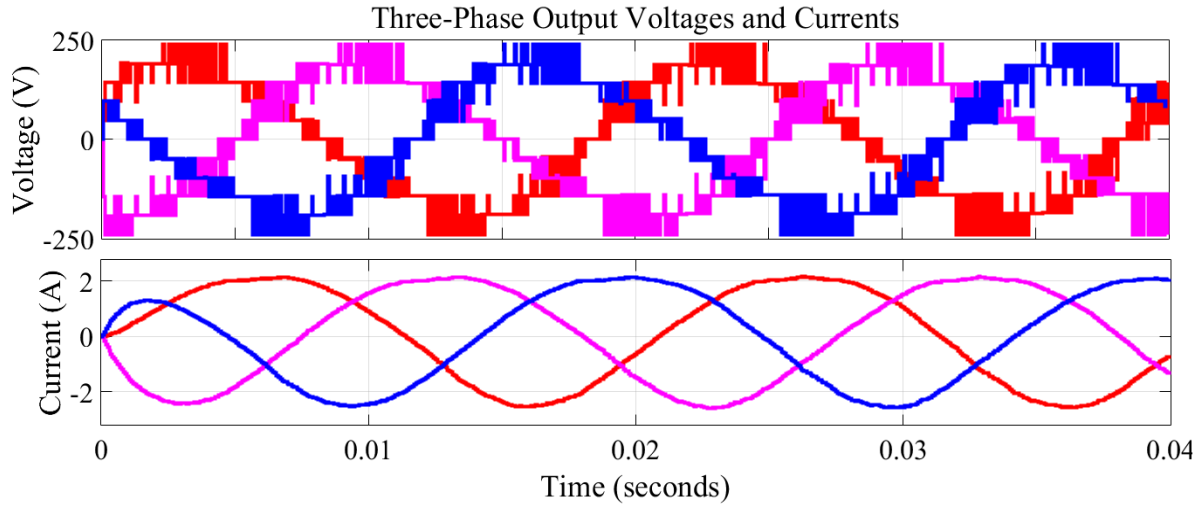

Fig. 3-19. Unbalanced three-phase voltage and current of the CMLI due to unbalanced dc-link voltages

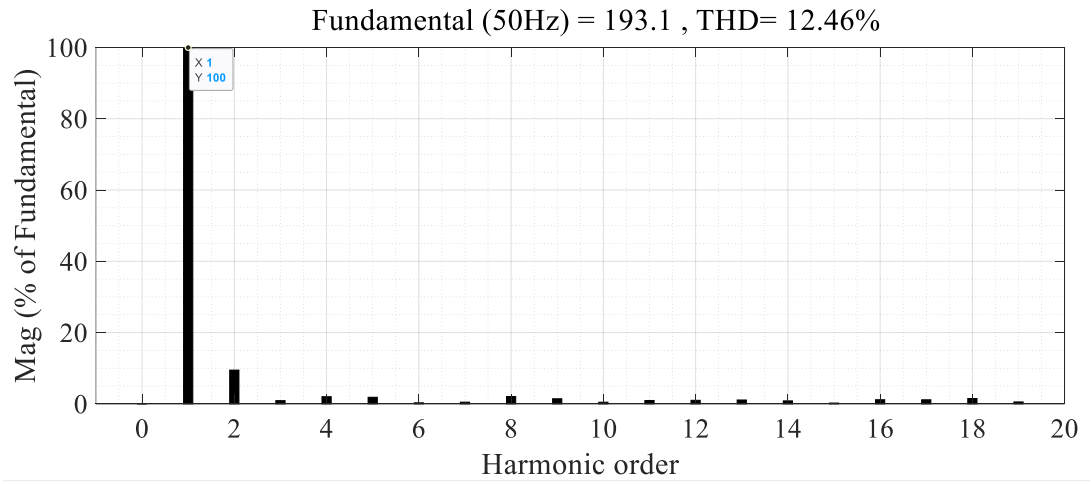

Fig. 3-20. THD of unbalanced three-phase voltage and current of the CMLI

To resolve the voltage balancing issues as well as to control the three-phase CMLI, the proposed PI-based SVPWM controller has been applied. The proposed PI-based SVPWM controller resolves the voltage balancing issues, which are presented in Fig. 3-21. The sampling frequency for both the rectifier and three-phase CMLI is set to 5000 Hz. The obtained output voltage and current waveforms of the CMLI are also showing almost sinusoidal natures as depicted in Fig. 3-22. The output voltage waveform comprises five staircase levels; 0V, 60V, 120V, 180V, and 240V. The THD of the three-phase output voltage and current waveforms as shown in Fig. 3-23 is reduced to around 5.69, which indicates almost sinusoidal natures as well as satisfying the IEEE519 standard on harmonics [262].

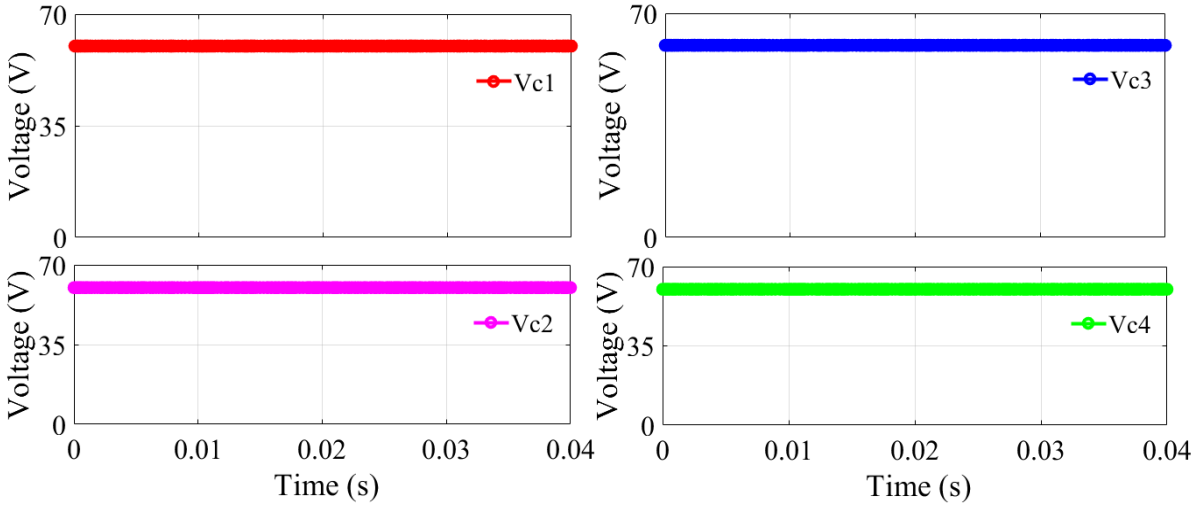

Fig. 3-21. Balanced dc-link voltages across dc-link capacitors applying SVPWM controller

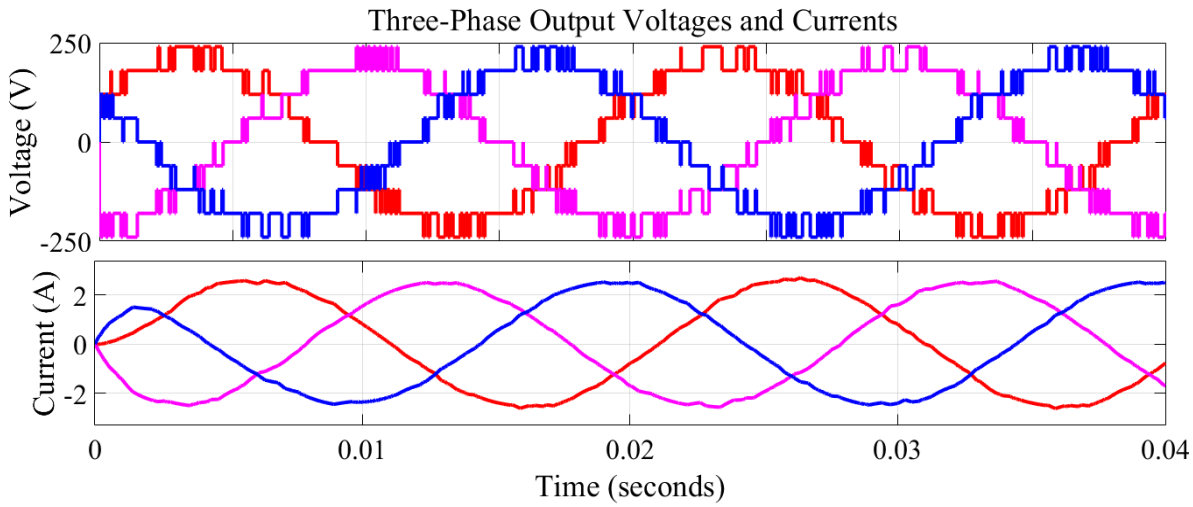

Fig. 3-22. Balanced three-phase voltage and current of the CMLI applying SVPWM controller

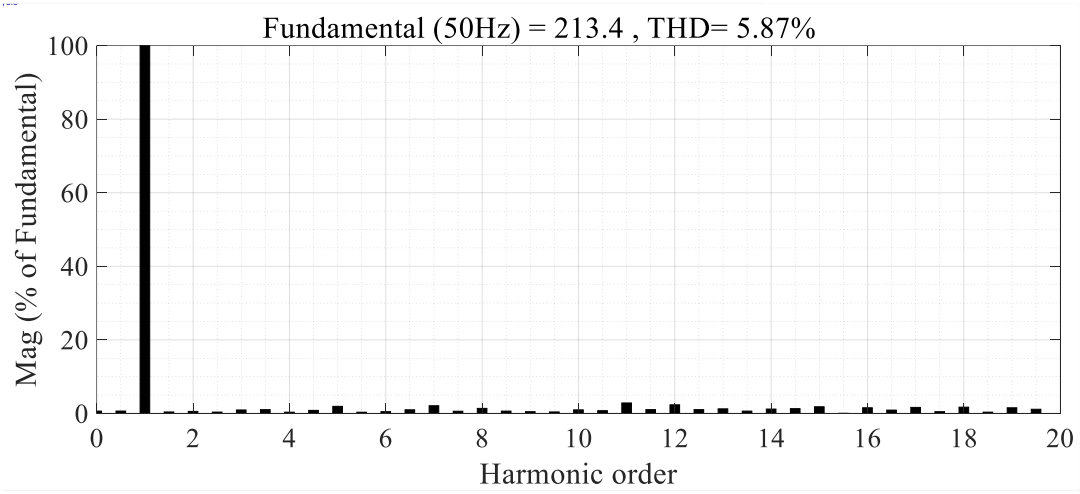

Fig. 3-23. THD of balanced three-phase voltage and current of the CMLI

The simulated results show the robustness of the proposed SVPWM controller and three-phase CMLI.

3.6.2. Experimental Results

An experimental setup has been developed as depicted in Fig. 3-24 for validating the simulation result. The experimental prototype consists of a synchronous generator, insulated gate bipolar transistor (IGBT, Dual N Channel, 155 A, 2 V, 511 W, 1.2 kV), voltage sensor (PR32-30), current sensor (LA 25-NP), digital signal processing board (TMS320F28335), 3-phase squirrel cage induction motor (380V, 1.6/3.1A, 0.4/1KW, 0.64/0.76), 3-phase gate driver (5/15V), and DC supply (GPC-3030D, 0/30V, 0/3A). The three-phase input voltage is scaled down to half of the simulated three-phase voltage due to the limitation of ratings of hardware capacity and lab facility.

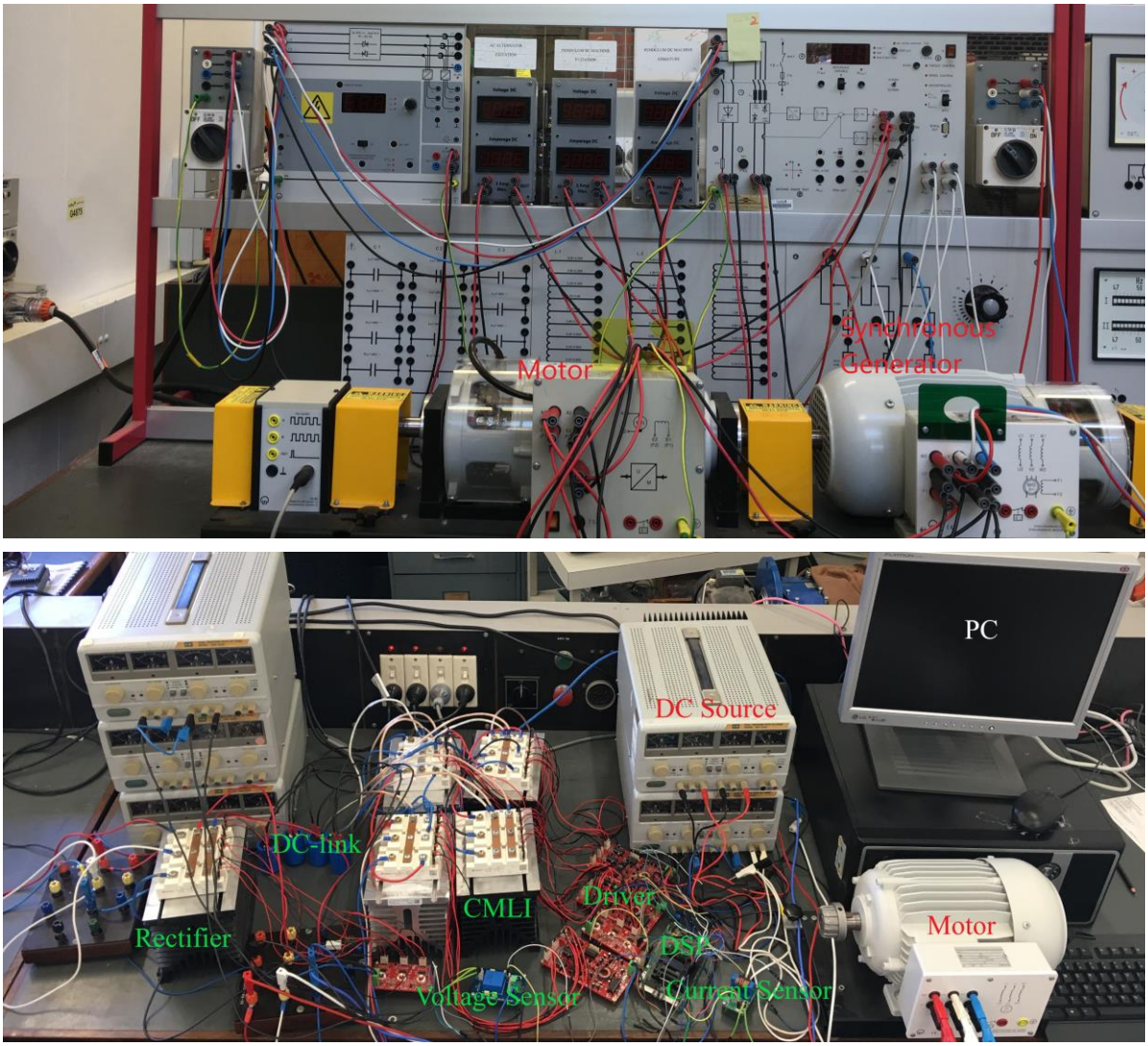

Fig. 3-24. Experimental setup of proposed controllers and three-phase CMLI for the WECS

The three-phase line-to-line voltages (V_{ab}, V_{bc}, and V_{ca}) and phase currents (I_a, I_b, and I_c) of the synchronous generator are presented in Fig. 3-25 and 3-26, which are symmetrical in the simulated results. The real trend of total harmonic distortion (THD) presented in Fig. 3-27 is around 6% which satisfies the IEEE519 standard on harmonics [262].

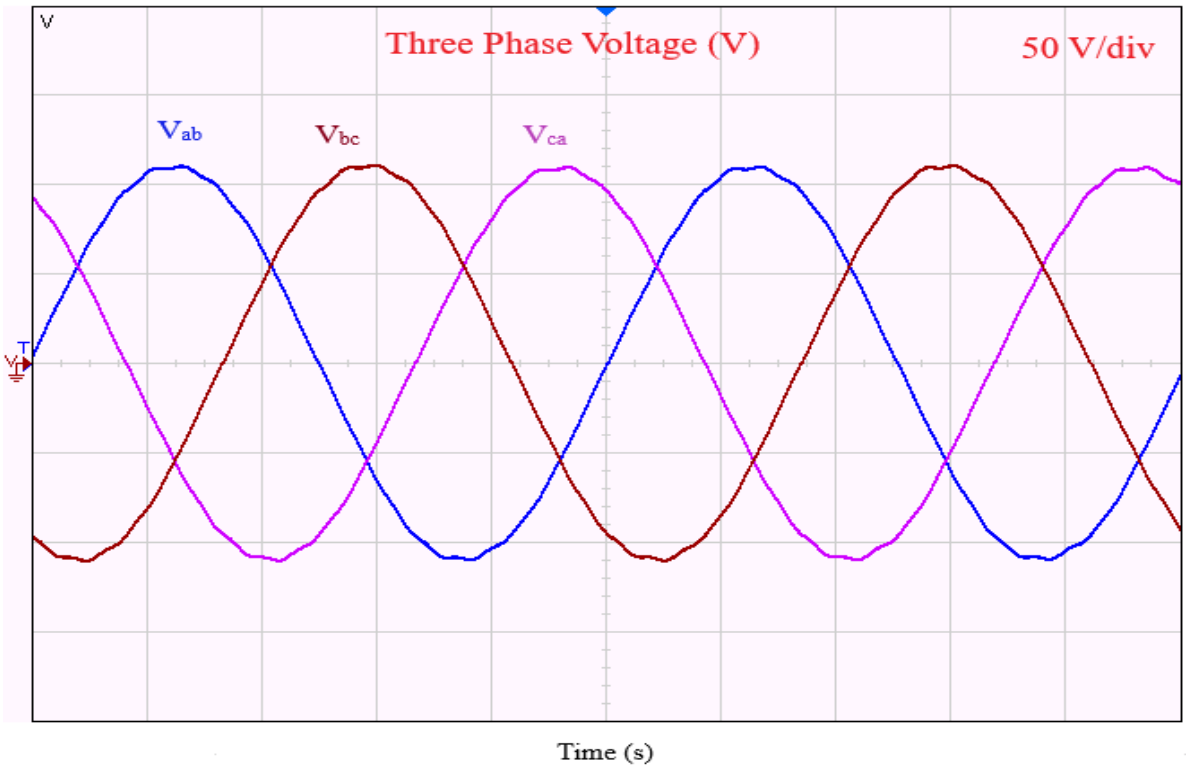

Fig. 3-25. Three-phase output voltage of the synchronous generator

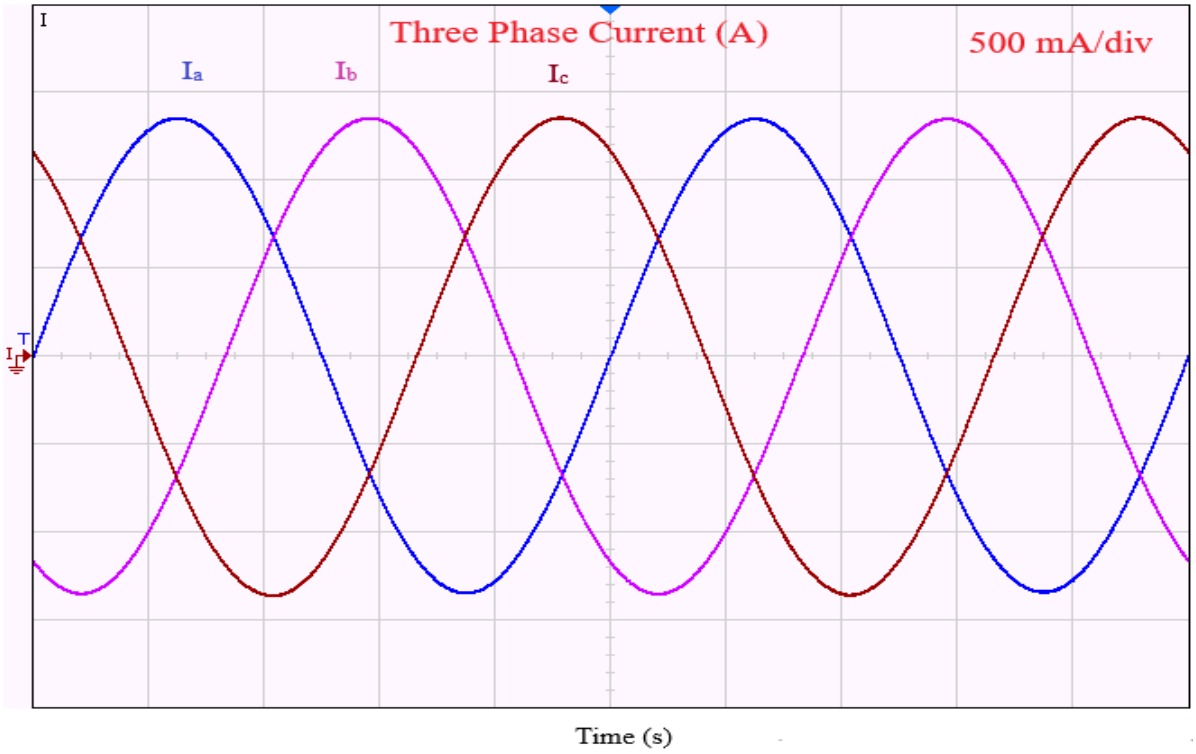

Fig. 3-26. Three-phase output current of the synchronous generator

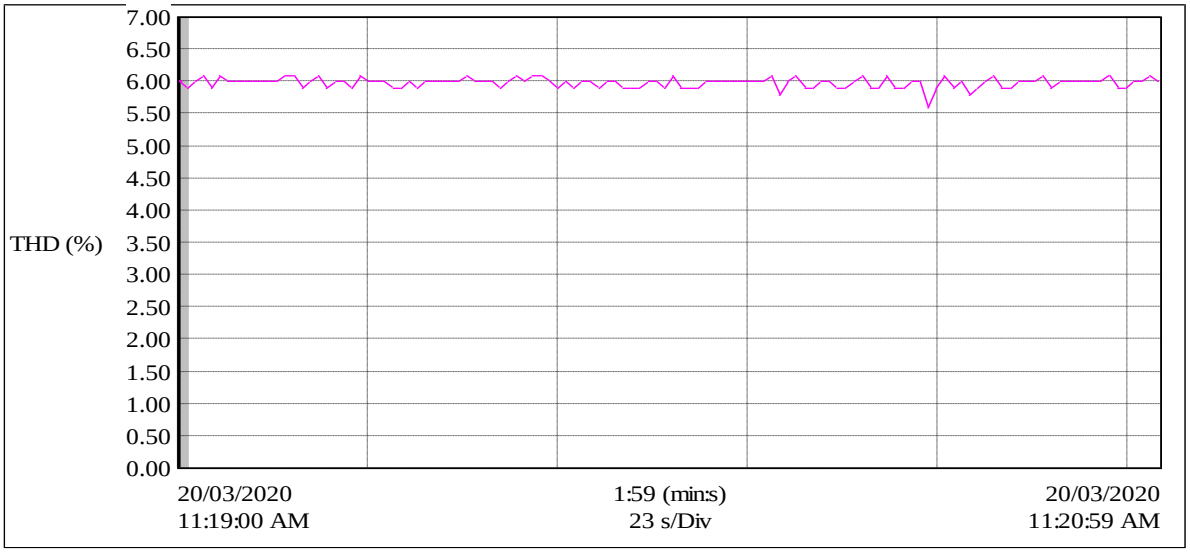

Fig. 3-27. THD of the three-phase output voltages of the synchronous generator

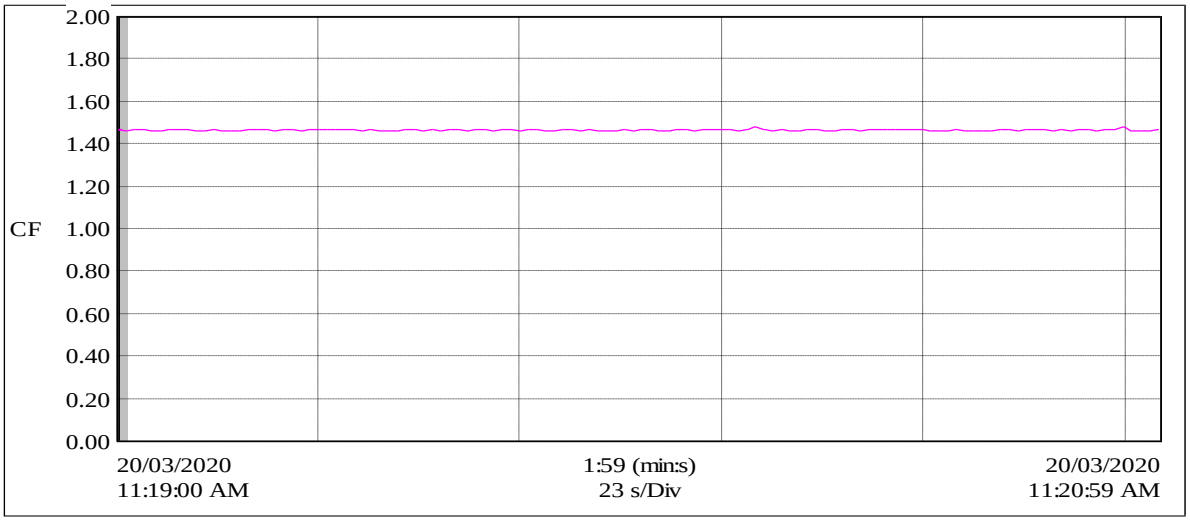

Fig. 3-28. Crest factor of the three-phase output voltages of the synchronous generator

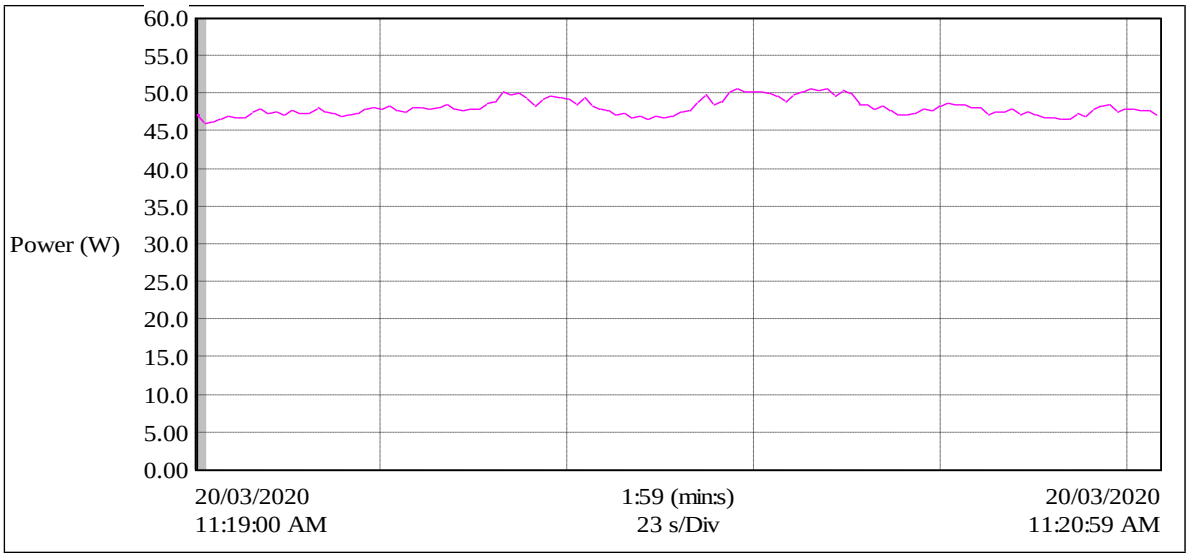

Fig. 3-29. Output power of the synchronous generator

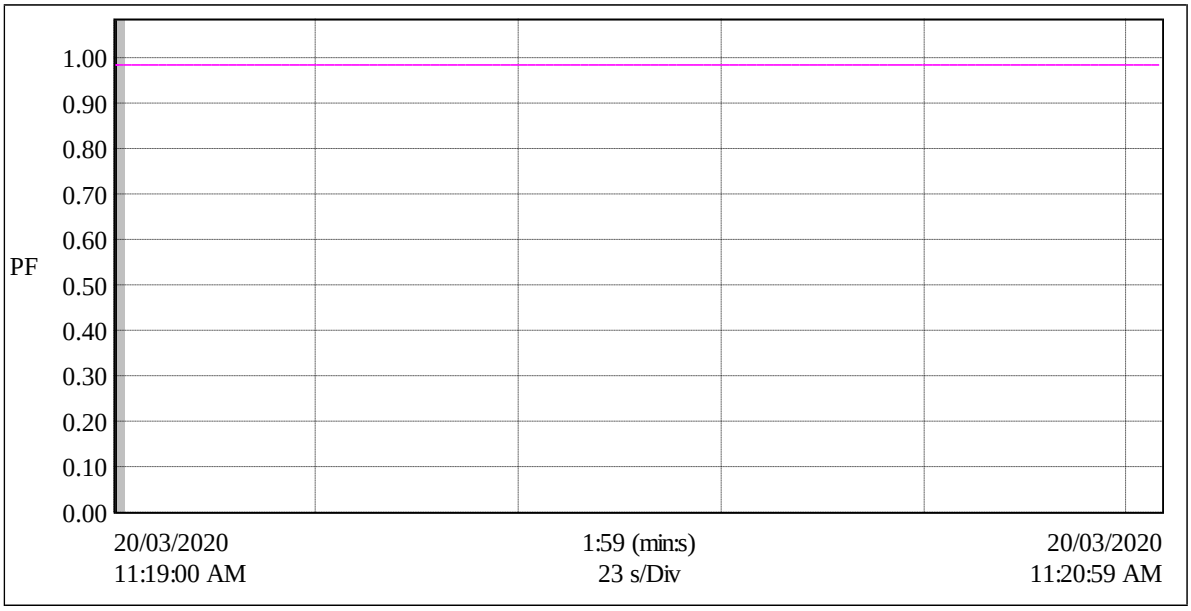

Fig. 3-30. Power factor of the synchronous generator

The voltage crest factor is close to √2 as depicted in Fig. 3-28, which indicates the almost sinusoidal nature of the output voltage. The output power and power factor are around 47W and 0.98 as presented in Fig. 3-29 and 3-30 respectively. The power factor is close to unity which is the desired power factor for the proposed system.

The SVPWM controller is designed in the MATLAB/Simulink software environment. Code composer studio (ccs 3.3) has been installed and interfaced with Simulink. The SVPWM controller model is linked to the code composer studio, which converts the model into C source code. The C source code is uploaded to the digital signal processor (DSP) control board (TMS320F28335). The DSP generates firing pulses across the specified general-purpose input/output (GPIO) pins with a magnitude of 3.3V each. The firing pulses are connected to the 3-phase gate driver, which boosts the firing pulse voltages to 15V. The boosted firing pulses control the rectifier's IGBTs (S_1 to S_6). The voltage sensor captures the dc-link ripple voltages from the AC/DC converter. The voltage sensor converts the DC-link ripple voltage (120V) to 3.3V, which is fed to the DSP board through an analogue to digital conversion pins. The DSP board sends the converted dc-link ripple voltage to the SVPWM controller model.

The SVPWM controller is employed, and the generated dc-link voltage is presented in Fig. 3-31. The experimental dc-link output voltage is ripple free and similar to the simulated results, which validates the SVPWM controller.

This experimental output voltage has been fed to the input of the proposed three-phase CMLI. The proposed SVPWM controller is designed in the MATLAB/Simulink software environment. Code composer studio (ccs 3.3) has been installed and interfaced with Simulink.

The proposed SVPWM controller is linked to the code composer studio, which converts the model into C source code. The C source code is uploaded to the digital signal processor (DSP) control board (TMS320F28335). The DSP generates firing pulses across the specified general-purpose input/output (GPIO) pins with a magnitude of 3.3V each. The firing pulses are connected to the 3-phase gate drivers which boost the firing pulse voltages to 15V.

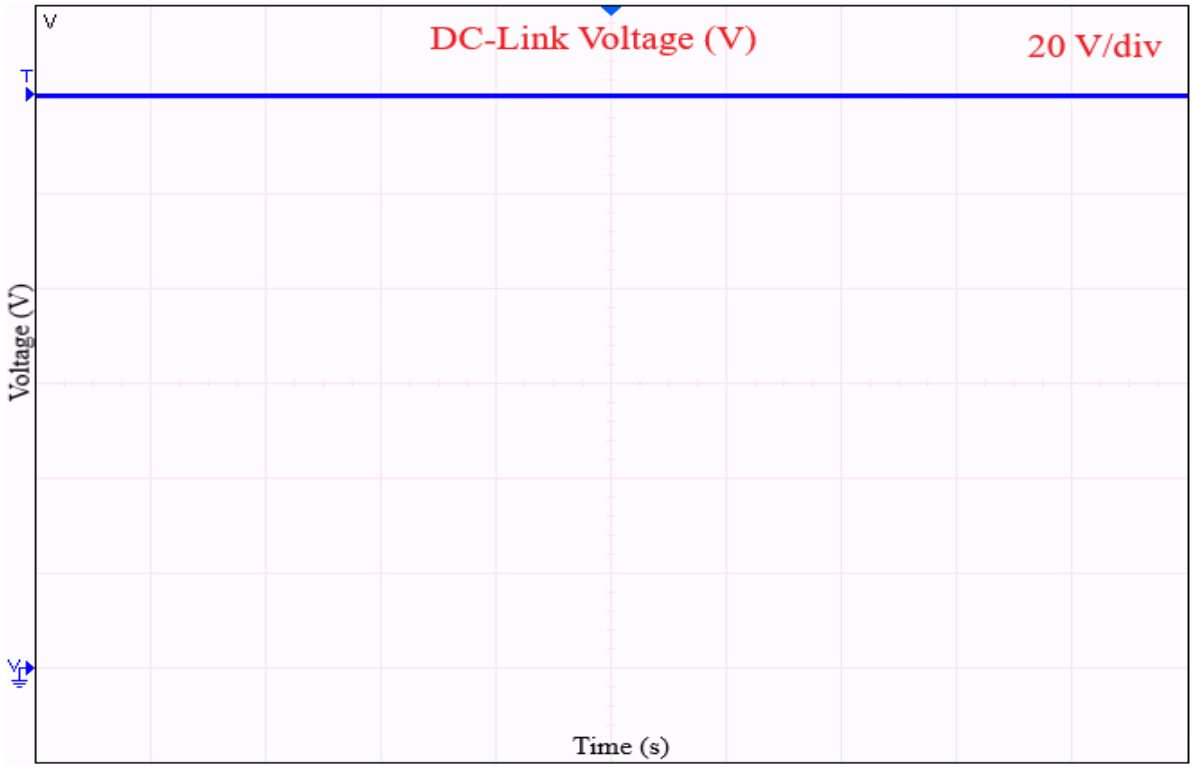

Fig. 3-31. Experimental DC-link voltage applying the PI-based THIPWM controller

The boosted firing pulses control the IGBTs of CMLI (S_{a1} to S_{a8}, S_{b1} to S_{b8} and S_{c1} to S_{c8}). The current sensor captures the output current of the three-phase CMLI and converts the captured current to 3.3A, which is fed to the DSP board through an analog to digital conversion pins. The DSP board sends the converted current to the proposed SVPWM controller. Shifter and scaler blocks are used to revert the current signal to its original shape. The complete hardware setup of the proposed three-phase CMLI and SVPWM has been shown in Fig. 3.24. The experimental three-phase line to line output voltages (V_{ab}, V_{bc}, and V_{ca}) and phase currents (I_a, I_b, and I_c) of the three-phase CMLI are presented in Fig. 3-32, and 3-33 respectively. The three-phase output voltages show staircase output waveforms with 5-levels (0V, 30V, 60V, 90V, and 120V) which are in a balanced condition. The proposed SVPWM controller has balanced the dc-link voltage over non-isolated capacitors. The three-phase output currents are also in balanced condition and similar to the simulated results. These results reveal the excellent performance of the proposed SVPWM controller and three-phase CMLI.

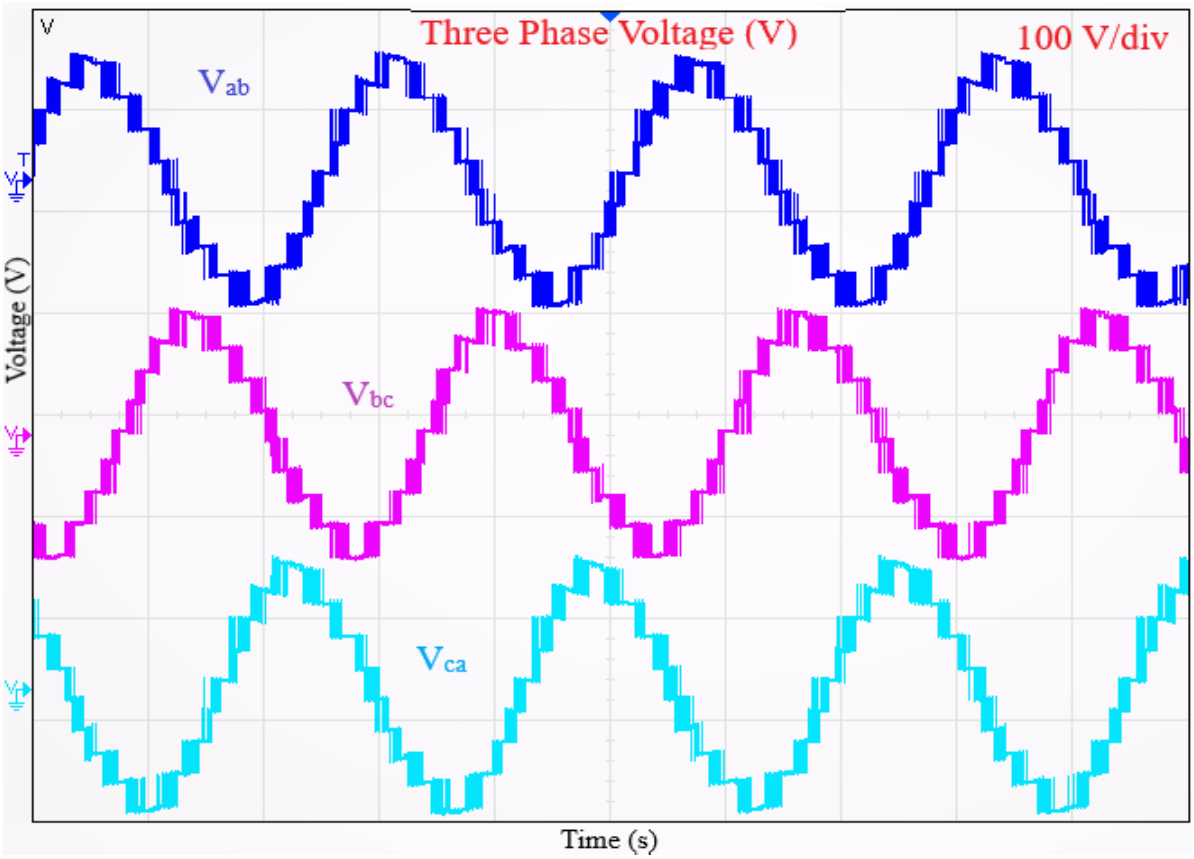

Fig. 3-32. Balanced three-phase output voltage of the three-phase CMLI

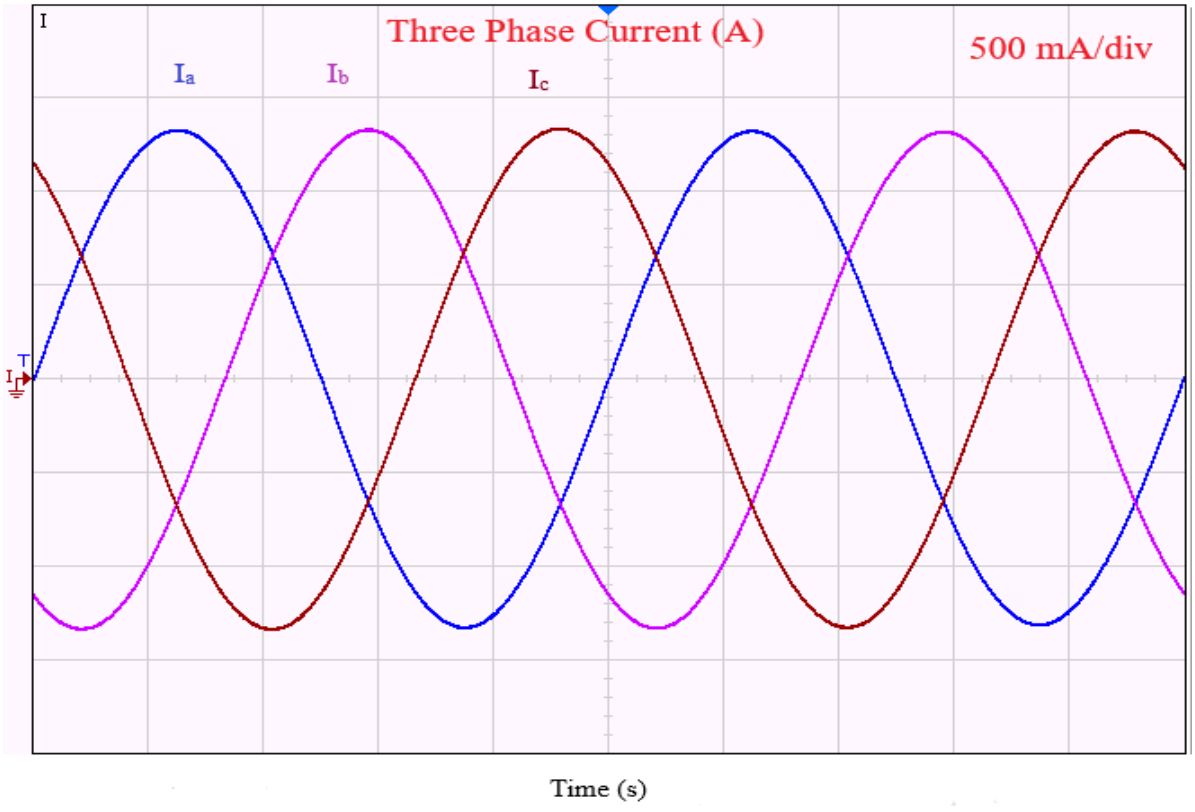

Fig. 3-33. Balanced three-phase output current of the three-phase CMLI

The real trend of total harmonic distortion (THD) presented in Fig. 3-34 is around 6% which satisfies the IEEE519 standard on harmonics [262].

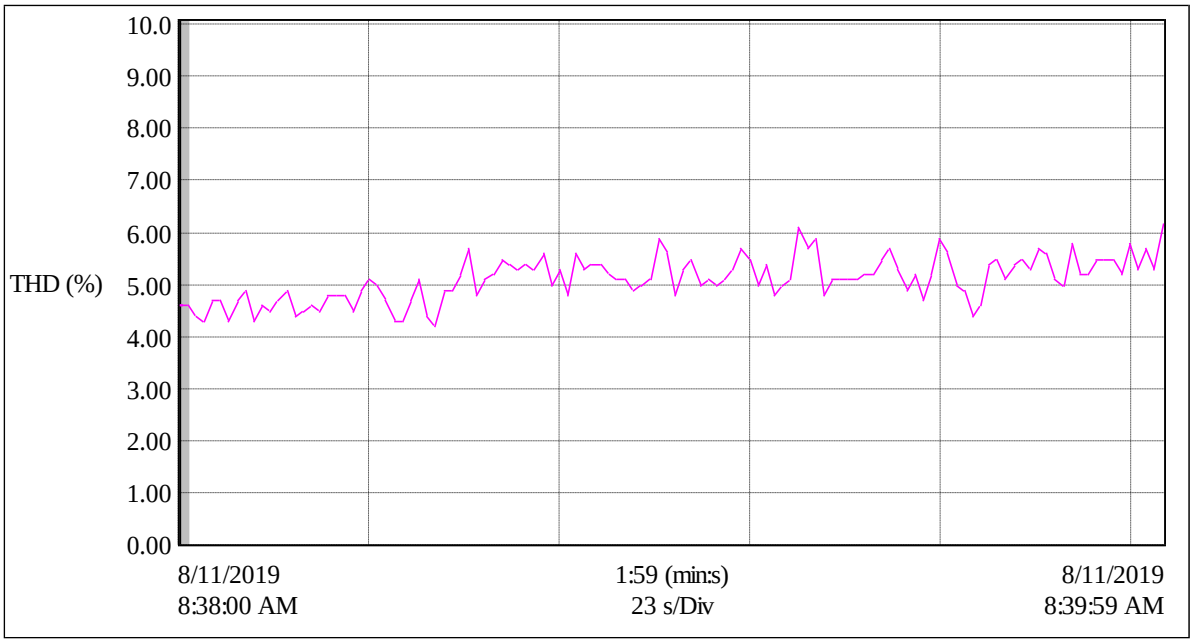

Fig. 3-34. Real trend of the voltage THD of the three-phase CMLI

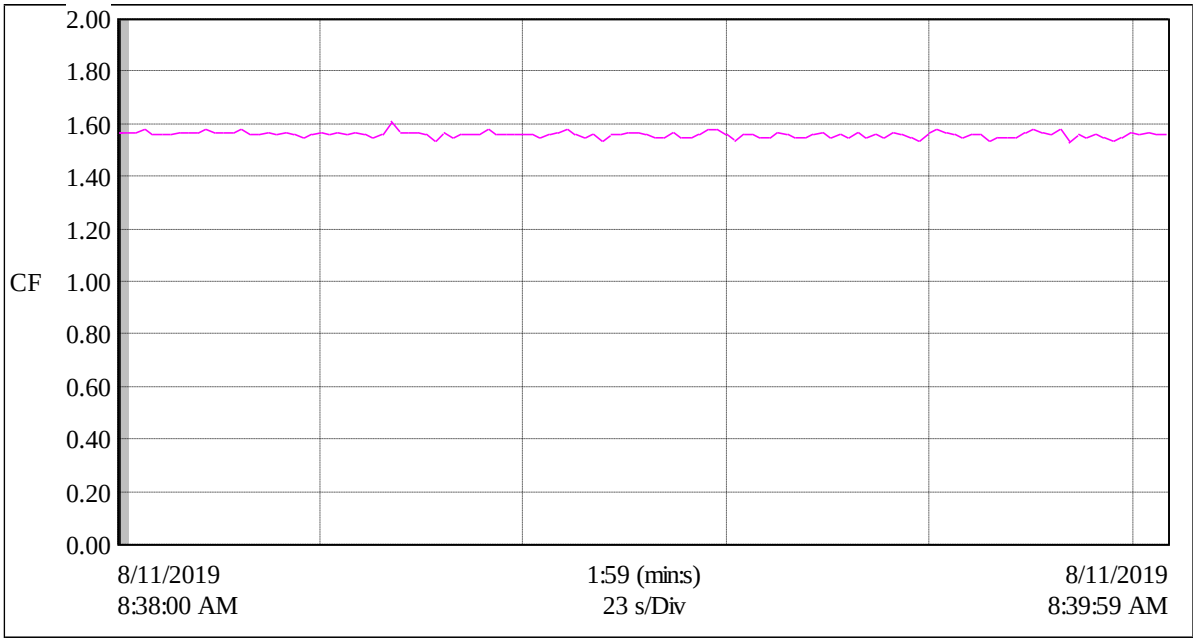

Fig. 3-35. Real trend of the voltage crest factor of the three-phase CMLI

The voltage crest factor is close to √2 as shown in Fig. 3-35, which indicates the almost sinusoidal nature of the voltages. The output power and power factor are 42.5W and 0.76 as presented in Fig. 3-36, and 3-37 respectively. The output power factor of the proposed CMLI is 0.76 due to the machine rated power factor available in the laboratory. This power factor can

be increased to a value close to unity using a power factor correction scheme such as a capacitor bank as shown in Fig. 3-38 [263].

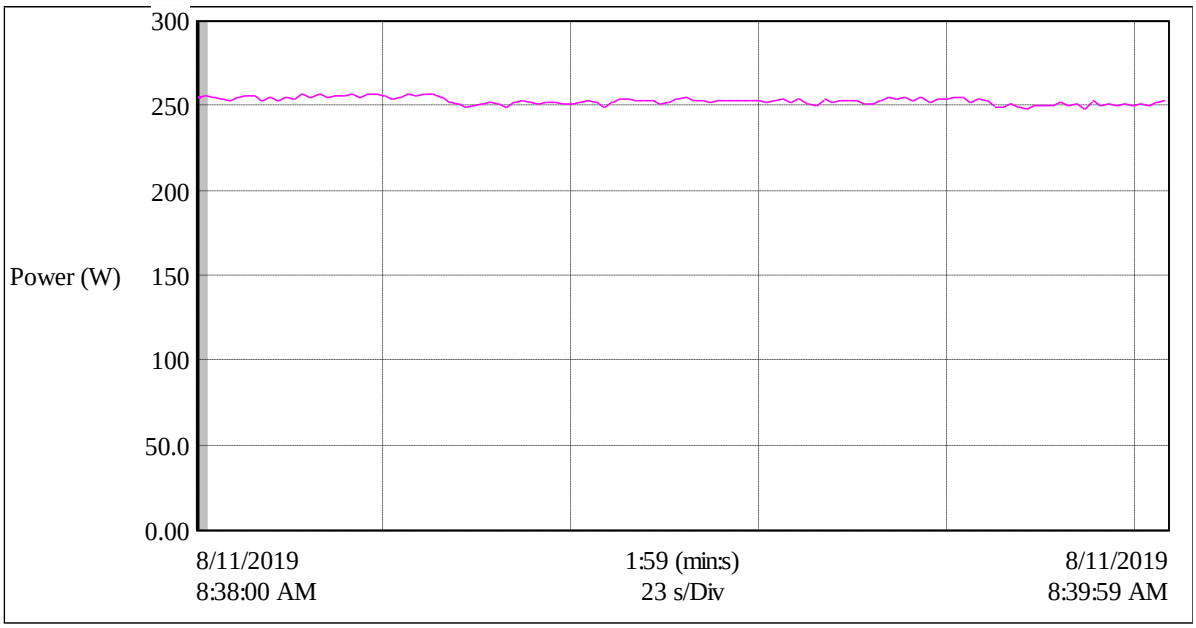

Fig. 3-36. Output power of the three-phase CMLI (8W/div)

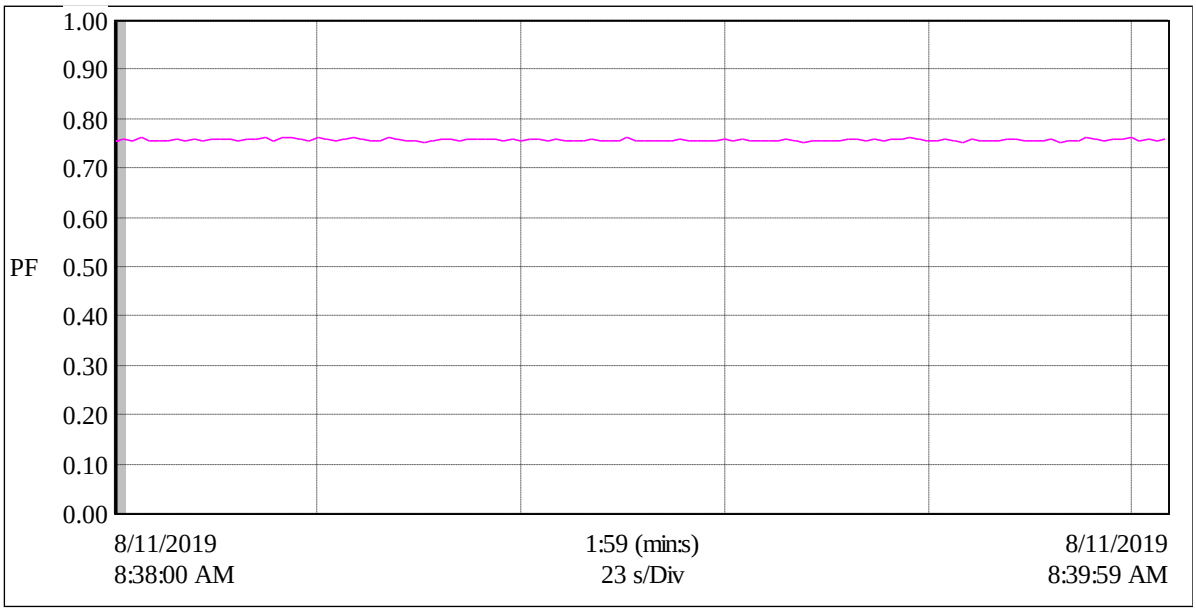

Fig. 3-37. Power factor of the three-phase CMLI

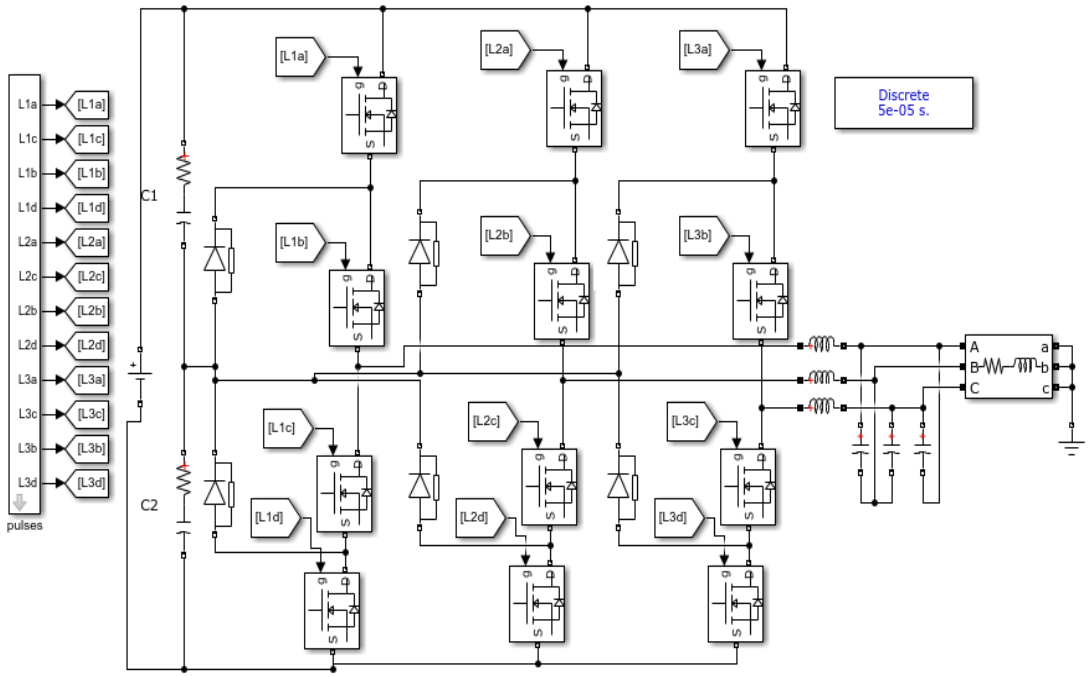

Fig. 3-38. Power factor improvement using capacitor bank [263].

Summary

The WECS proposed in this thesis presents a three-phase CMLI, and a SVPWM controller. The SVPWM controller has been simulated and experimented to suppress ripples from the dc-link voltage as well as to control the rectifier. The three-phase CMLI has been proposed, which requires four dc-link capacitors instead of dc supply to produce 5-level staircase output. The proposed SVPWM controller has been simulated and experimented to balance the dc-link voltage over non-isolated capacitors as well as to control the three-phase CMLI. The complete WECS has been designed and simulated in the MATLAB/Simulink software. An experimental prototype of the WECS has been constructed to validate the simulation result. The obtained results from simulation and experiment reveal that the proposed controllers and CMLI topology have shown excellent performance.

Chapter IV
Condition Monitoring of the DC-Link and Three-phase CMLI for a WECS over the industrial IoT

4.1 Introduction

Condition monitoring for wind energy conversion systems (WECS) has become an essential industry practice, as this helps improve wind farm reliability, overall performance, and productivity. If not detected and rectified in the early stages, some faults can be catastrophic with significant loss of revenue along with interruptions to businesses that primarily rely on wind energy [36]. A WECS failure results in system downtime and repair or replacement expenses that significantly reduce annual income. Such failures call for more systematised operation and maintenance schemes to ensure the reliability of the WECS. The condition monitoring and fault diagnosis systems for WECS play an important role in reducing maintenance and operational costs and increase system reliability [264]. This thesis proposes a condition monitoring algorithm, energy storage, and management system and industrial IoT algorithm to monitor the condition of switching devices in the three-phase CMLI, DC-link capacitors for the WECS as shown in the block diagram in Fig. 4-1. The block diagram is divided into six architectural layers, including the physical layer, data sensing layer, data processing layer, data-link layer, network layer, and application layer. The condition monitoring algorithm and energy storage system for the WECS are included in the physical layer, and the rest is divided between the data sensing layer, data processing layer, data-link layer, and application layer. The details of this architecture have been designed in the MATLAB and Protius software environment, which are presented in section 4.2. The design of the physical layer has been simulated and performances have been investigated, which are described in the earlier part of section 4.3.

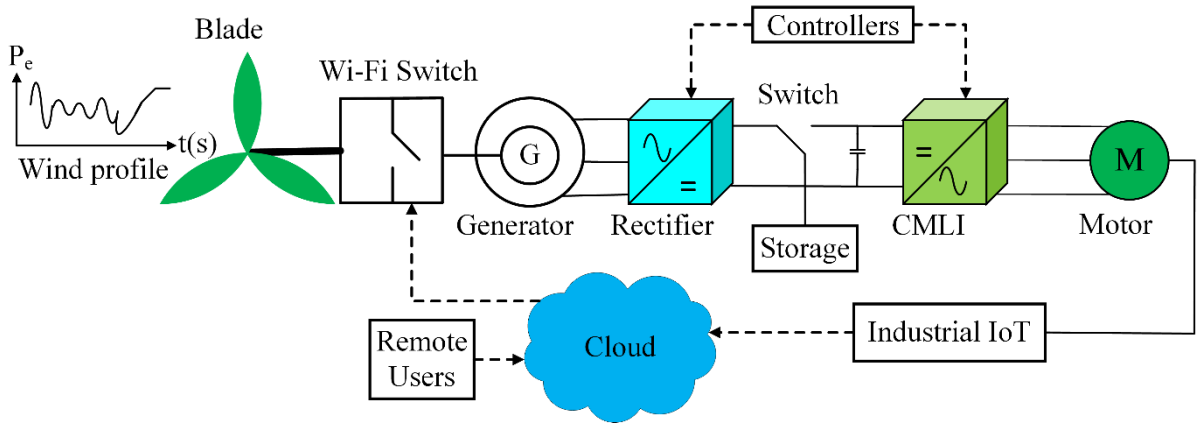

Fig. 4-1. The block diagram to monitor the condition of the WECS

A hardware prototype of the architecture has been developed and tested to validate the proposed condition monitoring algorithm and industrial IoT algorithm for the WECS, which is described in the middle part of section 4.3. The condition of the WECS has been monitored remotely via local area network and internet, which has been added at the end of section 4.3. A summary is included in section 4.4.

4.2 Proposed condition monitoring algorithm, energy storage and management system and industrial IoT algorithm for monitoring the condition of the WECS

The physical layer consists of several components and subsystems, which include turbine blades, generator, rectifier, three-phase cascaded multilevel inverter (CMLI), a motor, DC-link capacitors, energy storage and management system, and controllers as shown in Fig. 4-2. The full-scale power electronic converter (rectifier and CMLI) has been given much attention in the physical layer due to its flexibility and faster response, which facilitates the integration of various renewable energy sources and improves power system reliability [40].

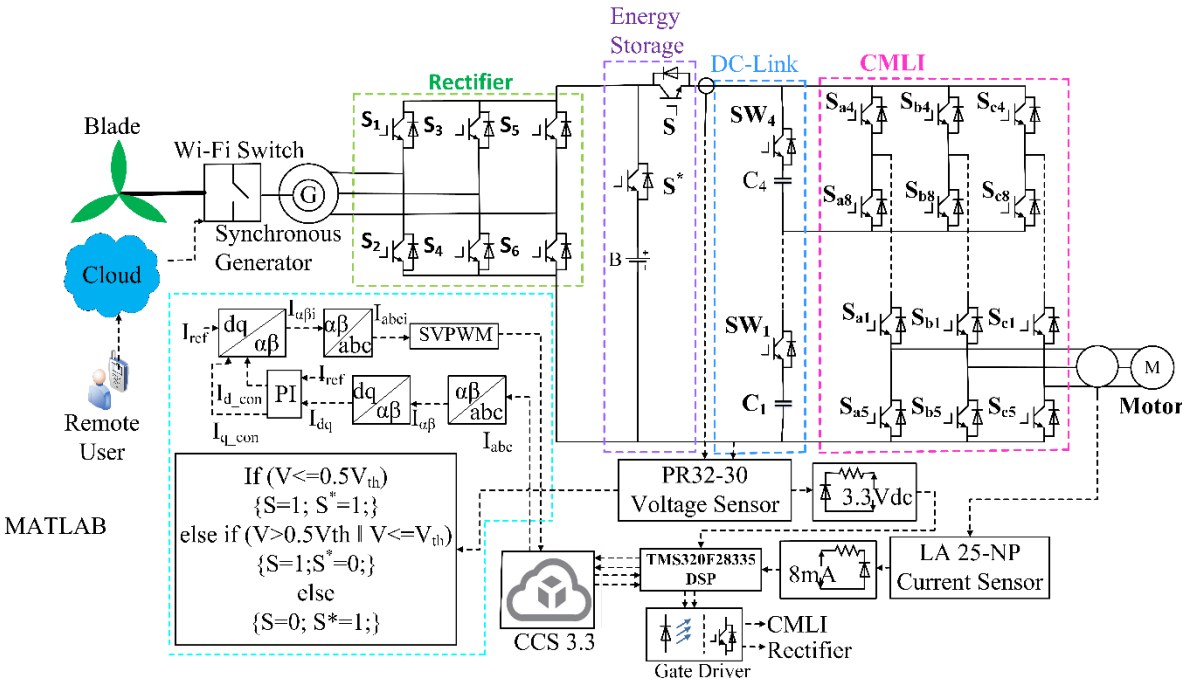

Fig. 4-2. Design of condition monitoring system for the wind energy conversion system

The 3-phase AC voltage in the wind generator is converted into intermittent DC voltage across the DC-link capacitor through 6 bi-directional switching devices which contain ripples. These ripples affect input voltage quality for the DC/AC converter [8]. A SVPWM controller is used to suppress such ripples and improves power quality as shown in Fig. 4-2. The rectifier is coupled through DC-link capacitors to the cascaded multilevel inverter (CMLI), which drives a 3-phase AC motor. The multilevel inverter (MLI) has brought tremendous change to high-

power medium-voltage industry applications, which is one of the new trends DC/AC converters [265]. MLIs have several advantages over conventional inverters, including less stress on switching devices, more utilisation of the DC-link voltage, and better power quality [53]. A PI-based space vector modulation (SVM) controller is used to control the three-phase CMLI as presented in Fig. 4-2.

An algorithm has been proposed here to monitor the condition of the switching devices in the three-phase CMLI and dc-link capacitors as depicted in Fig. 4-3.

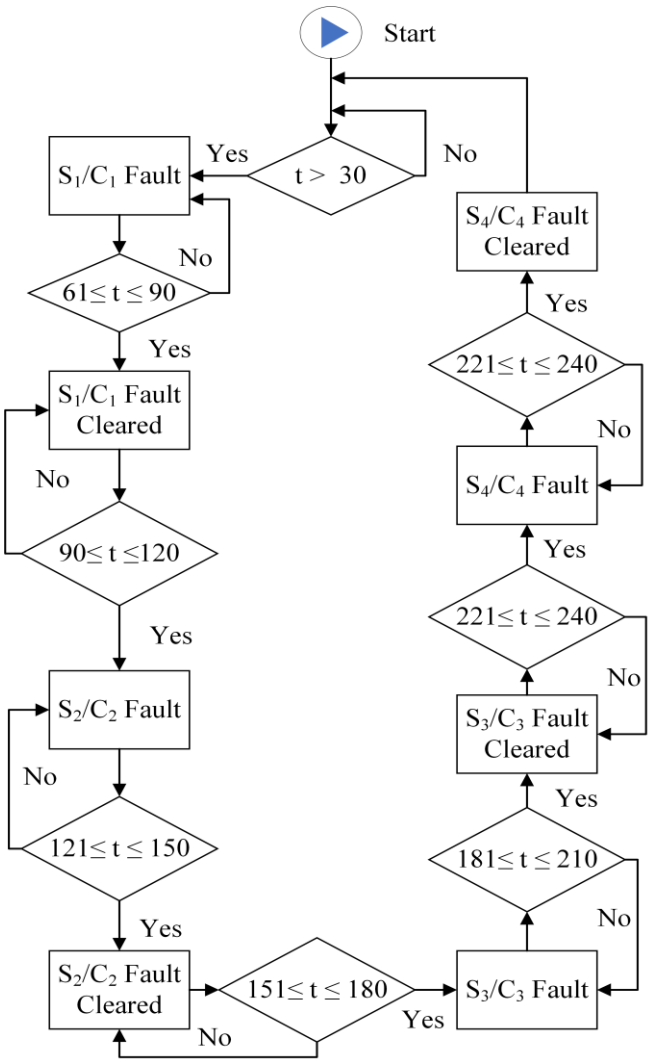

Fig. 4-3. Proposed condition monitoring algorithm

The condition monitoring algorithm generates faulty control pulses, which are used to control the semiconductor switching devices of the three-phase CMLI and the switches of the dc-link capacitors. Due to these faulty control pulses, three transitions have been displayed in the RMS output waveforms of the three-phase CMLI consecutively. The first transition continues for 30 seconds and the condition of the switching device has been monitored in real-time and indicates the healthy condition of the switching device. The second transition executes

just after the first transition and continues until 60 seconds. The condition of the switching device has been monitored during the second transition, which indicates the faulty condition of the switching device. The third transition begins just after the second transition and continues until 90 seconds. The condition of the switching device has been monitored in real-time and indicates the fault clearance of the switching device. The same process has been repeated for all the upper switching devices (i.e. S_{a1} to S_{a4}) of the three-phase CMLI. The creation and clearance of the faults are continued until 270 seconds and the condition of the WECS is monitored in each period.

In addition, the proposed algorithm has also been applied here to monitor the condition of the dc-link capacitors as presented in Fig. 4-3. The proposed generated faulty control pulses have been applied to control the dc-link switches (SW_1 to SW_4). Due to the faulty control pulses, three transitions have been displayed in the RMS output waveforms of the three-phase CMLI consecutively. The first transition continues for 30 seconds and the condition of the RMS output has been monitored in real time and indicates the healthy condition of the dc-link capacitor (C_1). The second transition executes just after the first transition and continues until 60 seconds. The condition of the dc-link capacitor (C_1) has been monitored during this transition and indicates an open circuit fault of the dc-link capacitor (C_1). The third transition begins just after second transition and continues until 90 seconds. The condition of dc-link capacitor (C_1) has been monitored in real time and indicates the open circuit fault clearance from the dc-link capacitor (C_1). The same process has been repeated for all the dc-link capacitors (C_1 to C_4). The creation and clearance of faults are continued until 270 seconds and the condition of the RMS output has been monitored in each period.

Moreover, the battery energy storage and management system play a vital role in the modern power sector in terms of the dual performance of storing electrical energy in dc form through the rectifier circuit and releasing the stored electrical energy through the inverter circuit at the required time [266]. This thesis proposes an energy storage and management system to improve the performances of the WECS. The proposed system consists of a battery (B, super capacitor), two switching devices (S and S^*), a voltage sensor, and a controller which is described in Fig. 4-2. The voltage (V) captured by the voltage sensor is compared with the threshold voltage (V_{th}). The following decisions are taken as a result of the comparison.

Decision 1: If $V \leq 0.5Vth$, both of the switches (S and S*) are made ON (1). The WECS operates in normal condition with low voltage and the battery starts to discharge through switch S*.

Decision 2: If $V>0.5Vth \parallel V \leq V_{th}$, switch (S) is made ON (1) and switch (S^*) is made OFF (0). The WECS is operating in normal condition.

Decision 3: If $V>V_{th}$, switch (S) is made OFF (0) and switch (S^*) is made ON (1). The WECS is operating in faulty condition, which increases the dc-link capacitor voltage. The three-phase cascaded MLI is isolated from the rectifier. The battery (super capacitor) is in charging mode and energy is stored.

The data sensing layer consists of a three-phase step down transformer and a three-phase full-bridge rectifier as shown in Fig. 4-4. The output voltage of the transformer is fed to the three-phase full bridge rectifier. The dc output voltage of the rectifier is fed to the data processing layer, which consists of an Arduino Uno board along with an integrated development environment (IDE), and a liquid crystal display (LCD). The data is processed in binary form after which it is transferred to the data-link layer. The data-link layer consists of a global system for mobile (GSM) module (SIM card), SIM800L module, and a global packet radio service (GPRS).

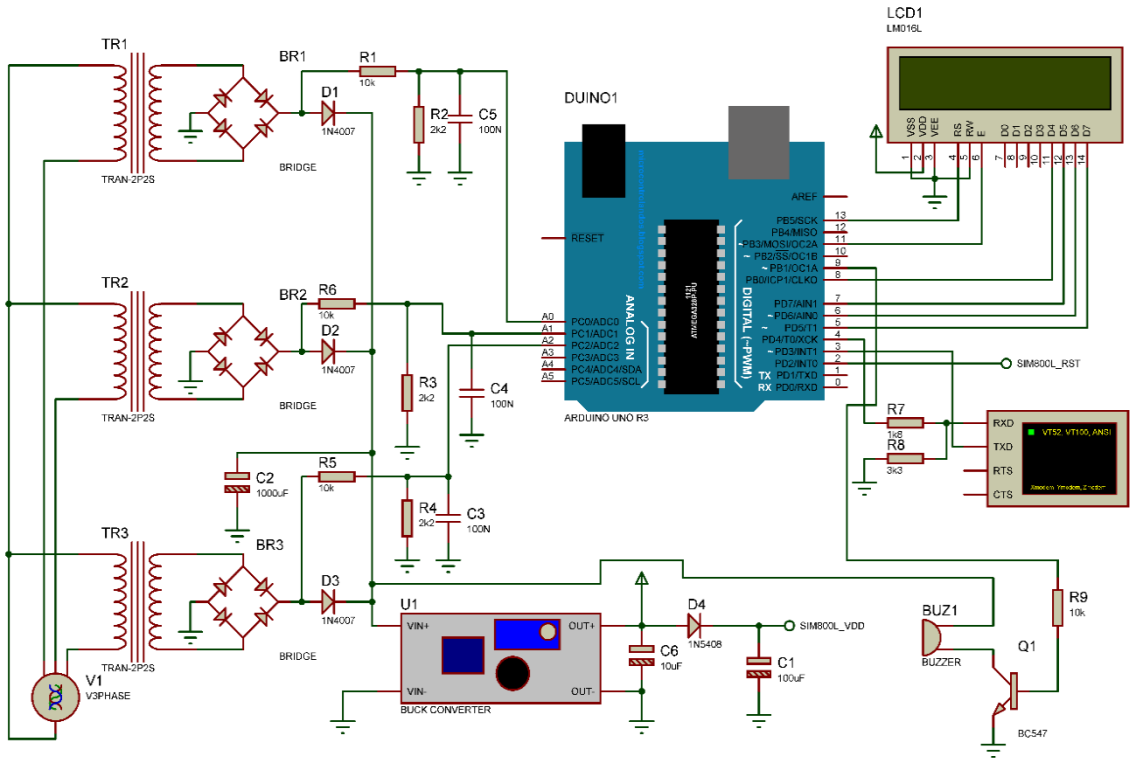

Fig. 4-4. Proposed industrial IoT module

The Arduino Uno board and SIM800L module are among the most popular smart devices, and are highly recommended when developing any industrial IoT system due to their small portable size, ease of development and excellent manufacturer support [267], [268], [269]. The SIM800L module can work like a cellular mobile phone with the integration of an

external peripheral, which can generate calls, SMS messages, emails, and build dual communications with the internet [270]. Data can be written to the internet and the web page can be read through the SIM800 module.

A UART (Universal Asynchronous Receiver/Transmitter) sends (T_X for SIM800 and D_8 for Arduino Uno) and receives (R_X for SIM800 and D_7 for Arduino Uno) lines. The required hardware components and software to develop the proposed industrial IoT system comprise a SIM800L, Arduino Uno, a mobile phone SIM card inserted into the back of the SIM800L device, and a USB cable for serial interface between the Arduino and the computer.

A program is developed in the Arduino IDE environment to control the data processing and send it to the SIM800 module along with the GSM module via the Arduino Uno board which is described here.

In the Arduino IDE, three libraries – Adafruit FONA Library (AFL), Software Serial Library (SSL), and Liquid Crystal Library (LCL) – are included. The AFL is used for GSM Breakouts. The Arduino Uno board possesses built-in supported serial of communication using SSL on pins 0 and 1, which is connected to computer through USB cable. The SSL is developed and allows serial communication to the other digital pins of the Arduino Uno via the IDE software for replicating the functionality. It could also be probable to build multiple software serial port connections with a speed of up to 115200 bps. A parameter allows device inverted signals requiring that protocol. The LCL allows the Arduino Uno board to print the message signal in the LCD display, which is developed based on the Hitachi HD44780 (LM016L) chipset. The LCL can work on 4/8 bits mode; for example,

LiquidCrystal (rs, rw, enable, d_0, d_1, d_2, d_3, d_4, d_5, d_6, d_7).

This is an 8-bit mode where bits (d_0–d_3) are optional. The rs, rw, and enabled bits are the number of the Arduino Uno board pins, which could be interfaced to the RS, RW and E pins on the LCD respectively. The d_0, d_1, d_2, d_3, d_4, d_5, d_6, and d_7 are the numbers of the Arduino Uno board pins which could be interfaced to the corresponding data pins to the LCD. The three-phase voltages (V_a, V_b, and V_c) are acquired from the Arduino analogue pins specified in the Arduino Uno board as A_0 to A_6 and are converted to digital data (binary) using an analogue to digital converter with limited resolution of 0–1023 pixel for 10 bits or 0–4095 pixel for 12 bits.

The Arduino library enables the Arduino board to run couple of operations using GSM, such as sending and receiving voice calls, SMS and MMS messages and even connecting to the internet all over the world through a General Packet Radio Service (GPRS) network.

The network layer is a dedicated server for hosting incoming data from the SIM800L module. The GPRS provides idealised data rates between 126 to 256 kbits/s for the server

domain. The posted data in the server are compared with the threshold voltage. If the posted data goes below the threshold voltage, a message is sent to the application layer. The application layer consists of authenticated remote users, email servers and Wi-Fi switches as shown in Fig. 4-2. The authenticated remote users can access data from the server directly over the internet. They are also notified instantly with fault information via their authenticated email server. The authenticated remote users can control the Wi-Fi switches of the WECS. A brief flow chart of the proposed industrial IoT for the WECS is shown in Fig. 4-5.

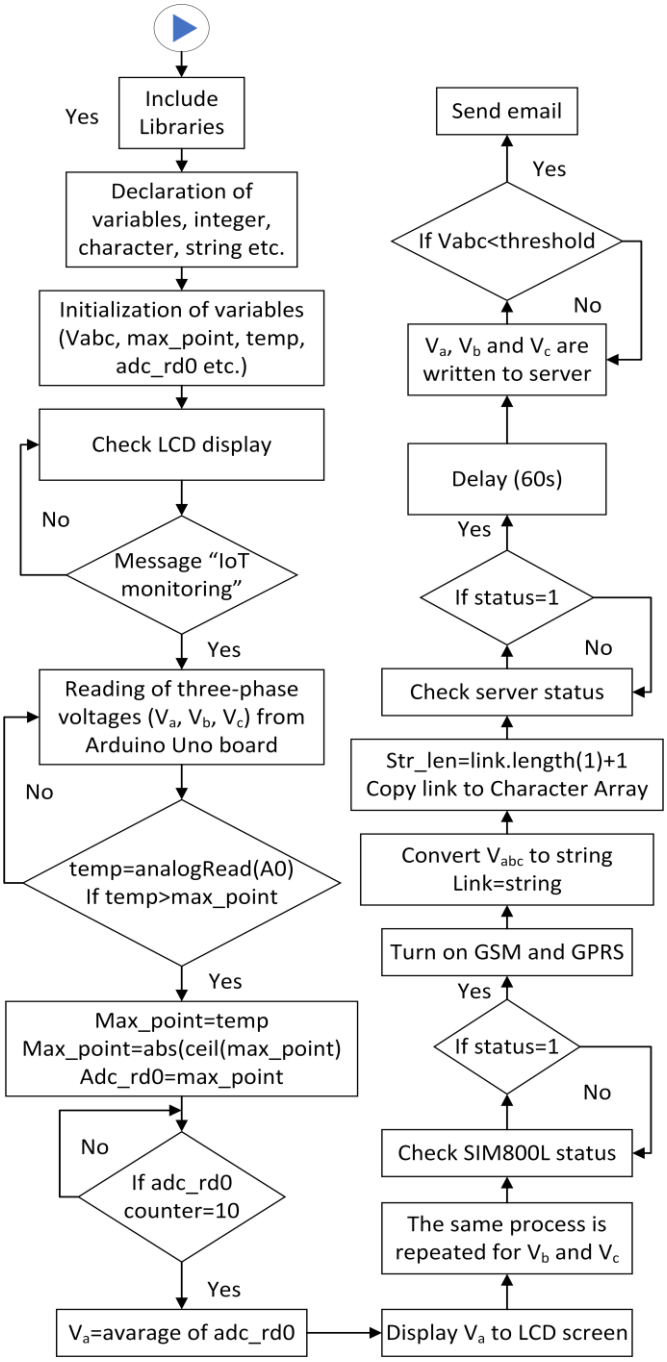

Fig. 4-5. Block diagram of proposed industrial IoT algorithm for WECS

4.3 Results and Discussion

4.3.1. Simulation Results

The proposed condition monitoring algorithm, and energy storage system for the WECS were designed and simulated in the MATLAB software environment. The simulation results were monitored and investigated. The three-phase CMLI output voltages were captured, as shown in Fig. 4-6 display fault information outlined with rectangles coloured in red. Due to the fault, the waveforms of output voltage (V_{ab} and V_{ca}) are affected and labelled with green circles when V_{bc} is in a healthy state. This indicates that the fault is located in the switching devices of either Phase-A or Phase-C. It can be observed that the positive peak of Phase-A and negative peak of Phase-C are affected, which confirms the fault to be located within Phase-A, not Phase-C. Furthermore, as the positive portion of Phase-A is affected, the fault is expected to be within the upper switching devices (S_{a1} to S_{a4}), since the upper switching devices execute the positive level of the output voltages. It must be noted that switching devices S_{a1}, S_{a2}, S_{a3}, and S_{a4} take part in generating levels 2, 3, 4, and 5 of the output voltages, respectively. The results show that the fifth level of Phase-A is affected, while the other levels maintain a normal condition. Therefore, it can be concluded that the fault is located within switch S_{a4}. Hence, the switch Sa4 should be replaced to mitigate the fault.

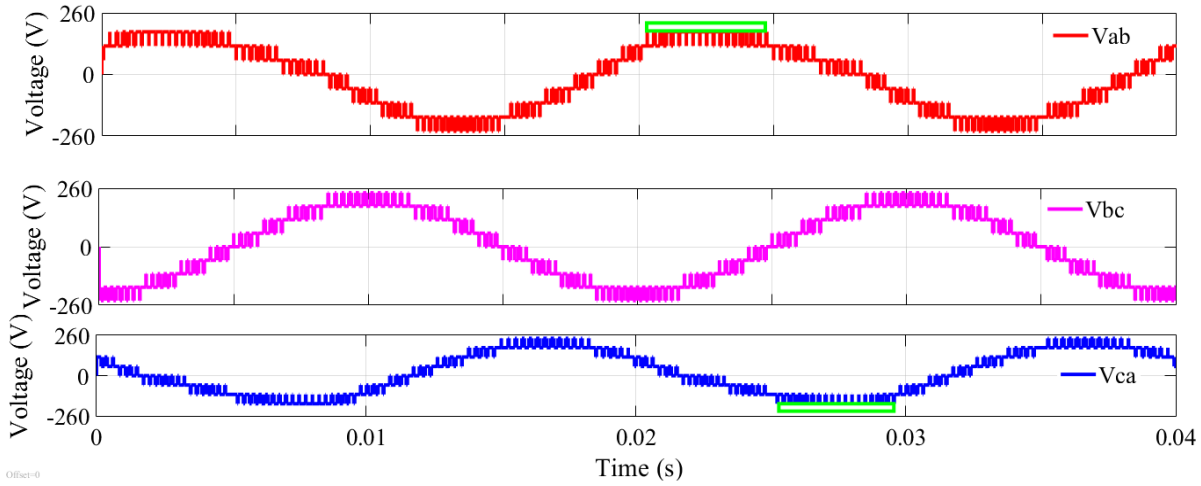

Fig. 4-6. Output voltages of the three-phase CMLI due to a fault at S_{a4}

The algorithm proposed in this thesis executes the control signals in such a way that demonstrates three transitions. Each transition stands for 30 seconds. In the1st transition, it generates the signal part which runs the CMLI in normal condition. In the 2nd transition, it generates the faulty signal to the switches while in the 3rd transition, it generates a signal to drive back the CMLI into normal condition. All considered faults are open circuit fault. The

dynamic performances of the three-phase CMLI was investigated by applying the proposed condition monitoring algorithm for semiconductor switching devices (S_{a1} to S_{a4}) located in the physical layer. A dynamic RMS voltage is shown in Fig. 4-7, which shows a different transition dynamically during the simultaneous faults. The first transition of the dynamic RMS voltage continued for 30 seconds with an amplitude of around 156V, which indicates the healthy condition of the switching device. The RMS voltage was flopped down and continued until 60 seconds during the second transition with an amplitude of around 146V, which indicates the faulty condition of switching device (S_{a1}). The dynamic RMS voltage returned to the normal position (healthy condition) and continued until 90 seconds during the third transition. The same process was repeated for all the upper switching devices of the three-phase CMLI. The creation and clearance of the faults were continued and investigated for the performance of the proposed condition monitoring algorithm until 270 seconds.

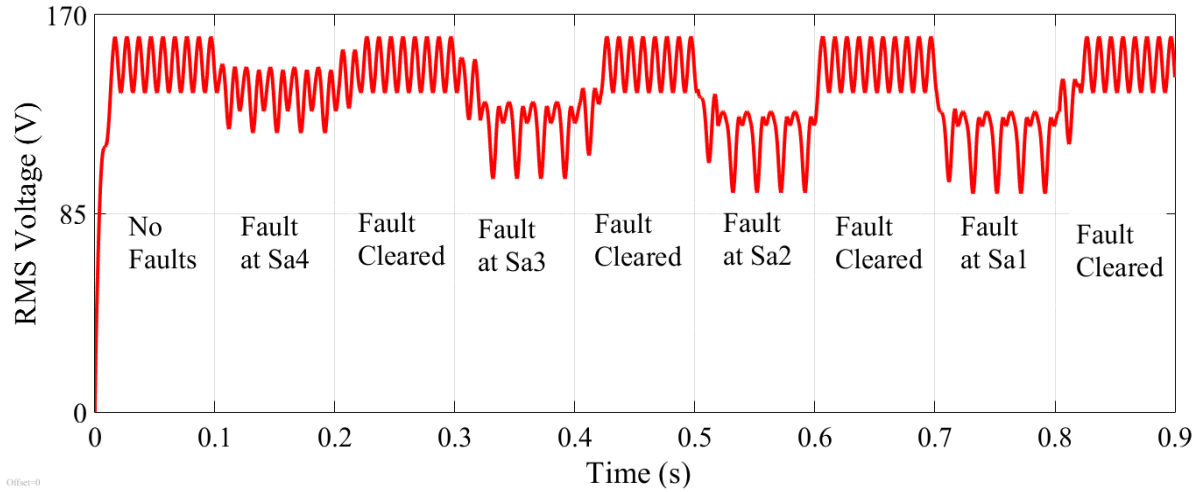

Fig. 4-7. Dynamic RMS voltage due to faults in the switching devices (S_{a1} to S_{a4})

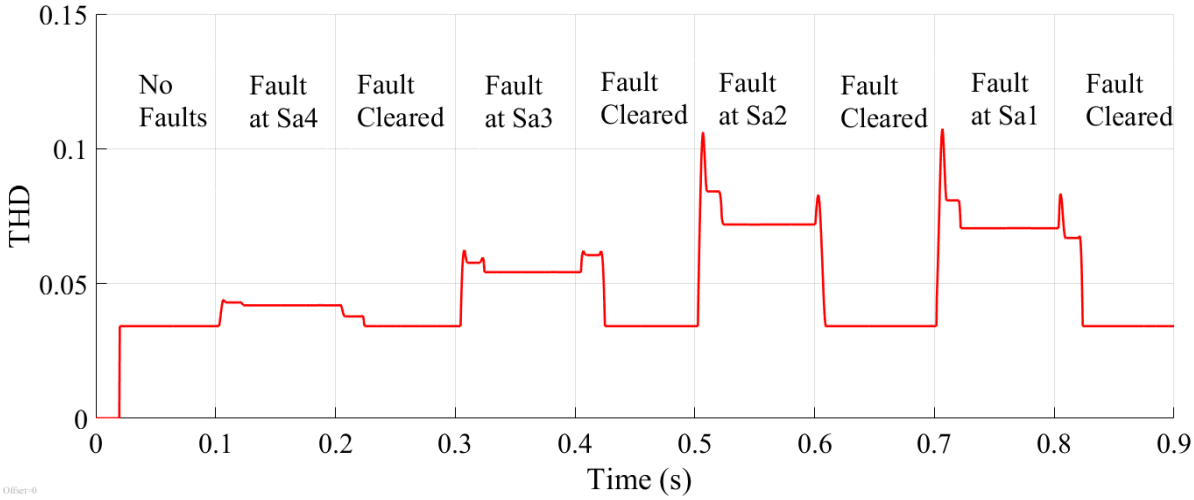

Fig. 4-8. Dynamic THD due to faults in the switching devices (S_{a1} to S_{a4})

The total harmonic distribution (THD) of the RMS voltage was below 5% during the healthy condition as depicted in Fig. 4-8, which satisfies the IEEE519 standard on harmonics [271]. The THD was increased to around 5% during the second transition due to the fault in the switching device (S_{a4}). The THD returned to the IEEE519 standard during the third transition, which proves the robustness of the proposed condition monitoring algorithm. The performance of the THD was continued and investigated until 270 seconds.

The conditions of the dc-link capacitors were also monitored in physical layer by applying the proposed condition monitoring algorithm. The three-phase output voltages were measured as depicted in Fig. 4-9, which highlight the fault information marked by red coloured rectangles. Due to such faults, the three-phase output voltage is dropped to around 180V (peak), which wipes out the 5th level. This missing 5th level of the three-phase voltage indicates faults in either of the dc-link capacitors (C_1 to C_4).

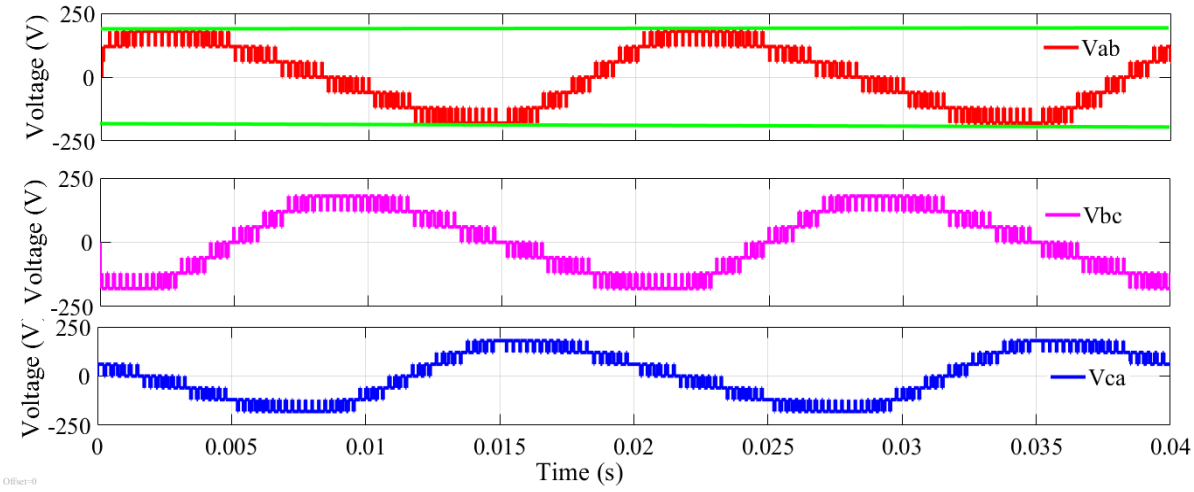

Fig. 4-9. Output voltages of the three-phase CMLI due to a fault in C_4

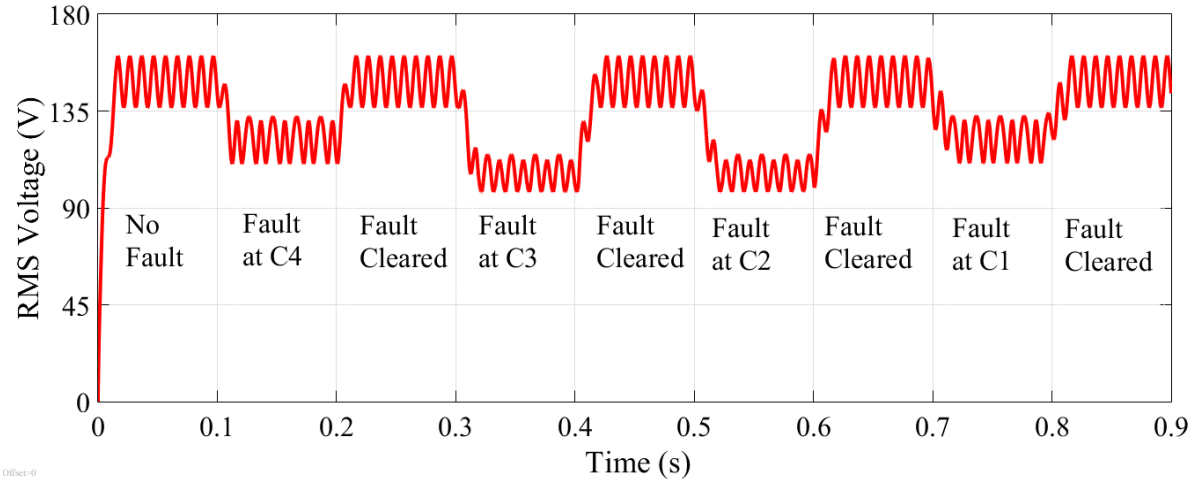

Fig. 4-10. Dynamic RMS voltage due to faults in the dc-link capacitors (C_1 to C_4)

The dynamic performances of the dc-link voltage were investigated by applying the proposed condition monitoring algorithm for the faults in the dc-link capacitors (C_1 to C_4) in physical layer. The dynamic RMS voltage due to faults in the dc-link capacitor is presented in Fig. 4-10. The first transition of the dynamic RMS voltage continued for 30 seconds with an amplitude of around 156V, which indicates the healthy condition of the dc-link capacitors. The RMS voltage is dropped and continued until 60 seconds during the second transition with an amplitude of around 124V, which indicates the faulty condition of the dc-link capacitor (C_4). The dynamic RMS voltage returned to the normal position (healthy condition) and continued until 90 seconds during the third transition. The same process is repeated for all the DC-link capacitors of the WECS. The creation and clearance of faults were continued, and the performance of the proposed condition monitoring algorithm investigated until 270 seconds. The total harmonic distribution (THD) of the RMS voltage is below 5% during the healthy condition as depicted in Fig. 4-11, which satisfies the IEEE519 standard on harmonics. The THD was increased to around 5% during the second transition due to the fault in the DC-link capacitor (C_4). The THD returned to the IEEE519 standard during the third transition, which proves the robustness of the proposed condition monitoring algorithm. The performance of the THD was continued and investigated until 270 seconds.

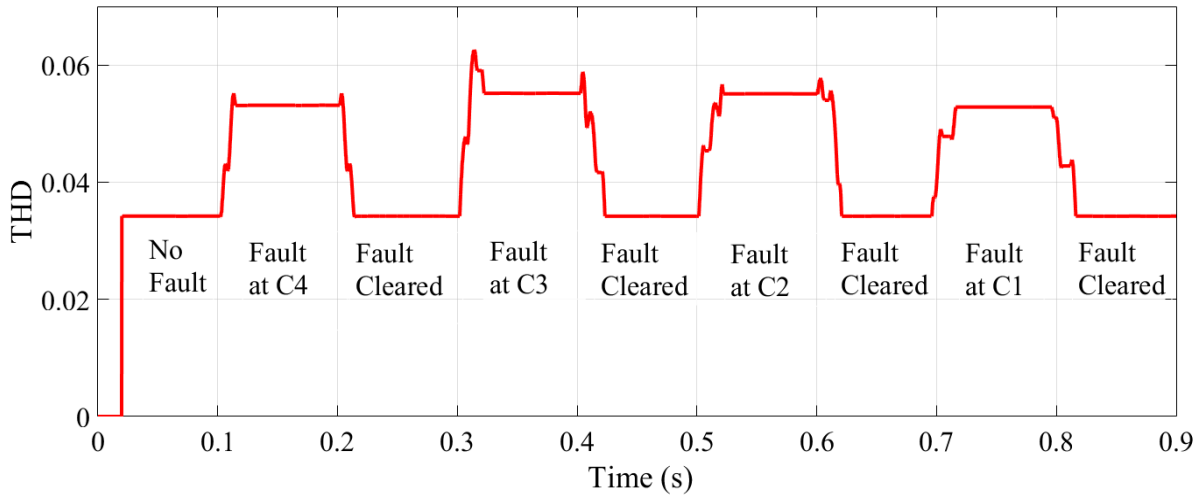

Fig. 4-11. Dynamic THD due to the faults in the dc-link capacitors (C_1 to C_4)

The battery storage and management system was designed and simulated in the MATLAB software environment as presented in Fig. 4-2. The characteristics of the super capacitor is shown in Fig. 4-12, where the shaded area denotes the nominal energy. Under the normal condition, the dc-link voltage is almost constant albeit with a slight overshoot and undershoot, which is presented in Fig. 4-13. The state of charge (SoC) in the super capacitor is also almost constant except for a slight discharging due to the fluctuation of the dc-link voltage.

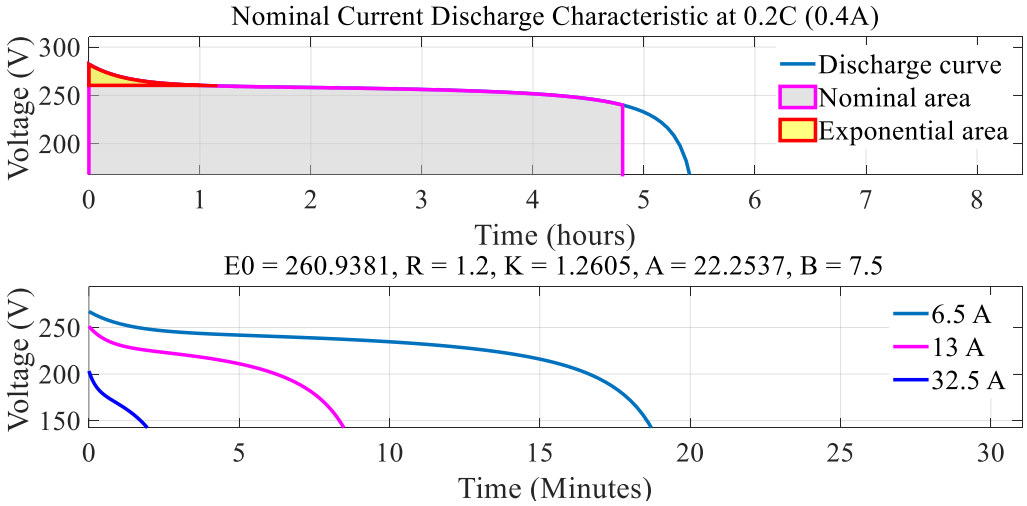

Fig. 4-12. Super capacitor characteristics

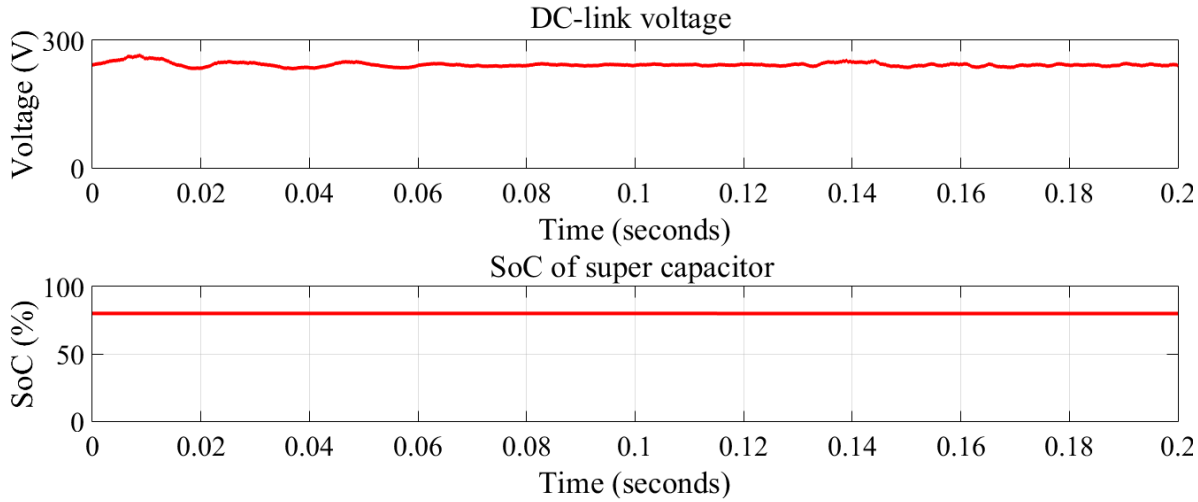

Fig. 4-13. dc-link voltage and SoC of super capacitor at normal operation of WECS

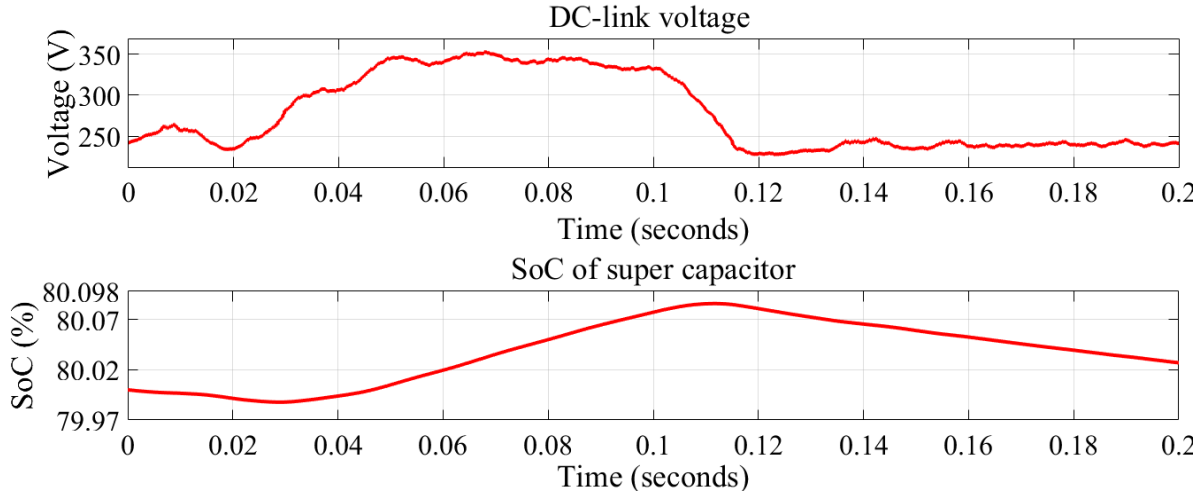

Fig. 4-14. Swing of the dc-link voltage and SoC of the super capacitor during the faulty condition of the WECS

The dc-link voltage was increased sharply between 0.025s to 0.1s due the three-phase faults as shown in Fig. 4-14. As the dc-link voltage goes above the maximum value, the super capacitor starts to charge for that faulty period, which is depicted in Fig. 4-14.

4.3.2. Experimental Results

To assess the robustness of the proposed algorithms for the WECS, a hardware prototype was developed, which contains six architectural layers. The physical layer consists of a synchronous generator, rectifier, three-phase cascaded multilevel inverter (CMLI), a squirrel cage induction motor, voltage sensor, current sensor, digital signal processing board (TMS320F28335), gate drivers, dc source, heat sink, and computer as presented in Fig. 4-15. The output voltages of the three-phase CMLI are captured as shown in Fig. 4-16, which indicates fault information marked by red coloured circles.

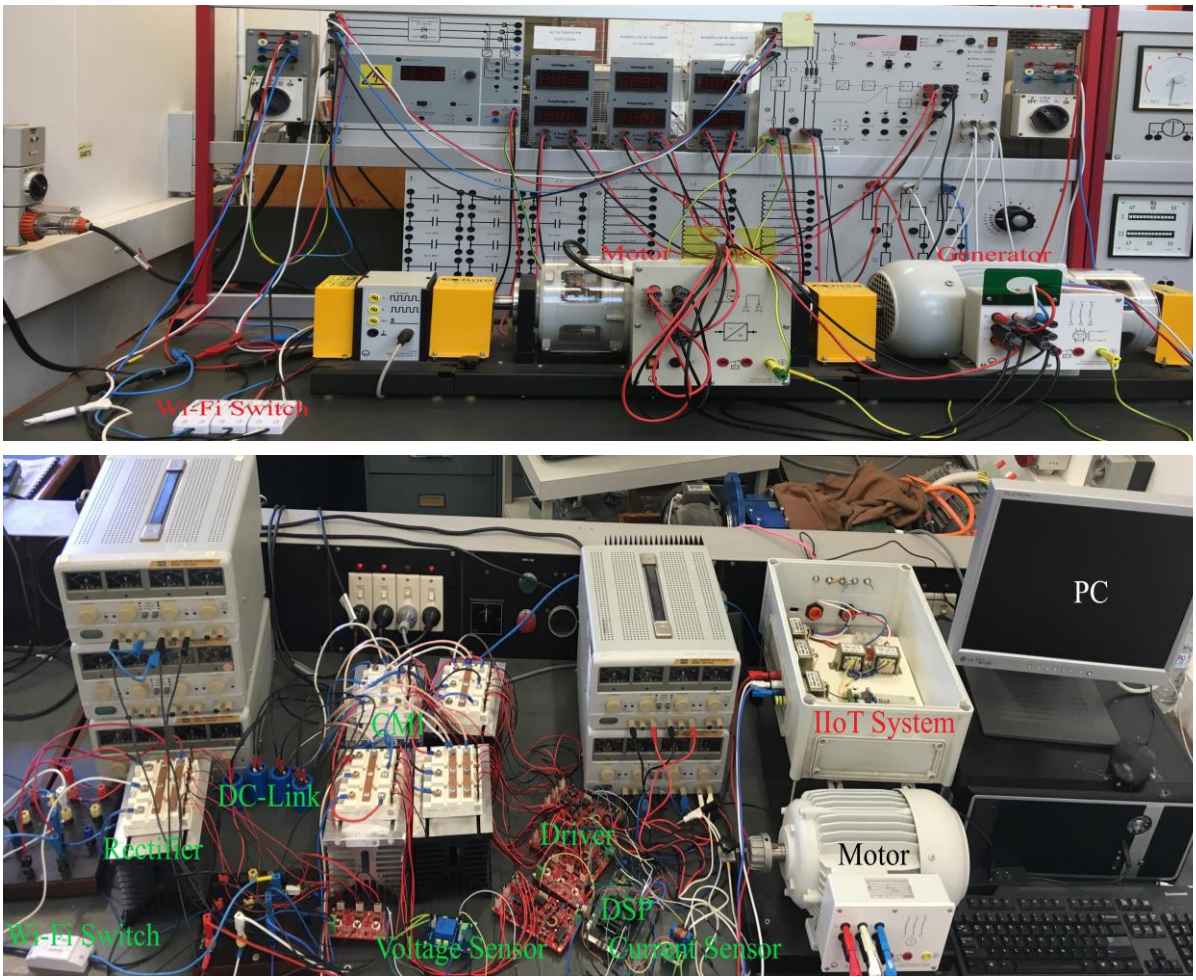

Fig. 4-15. Experimental setup of proposed algorithms for the WECS

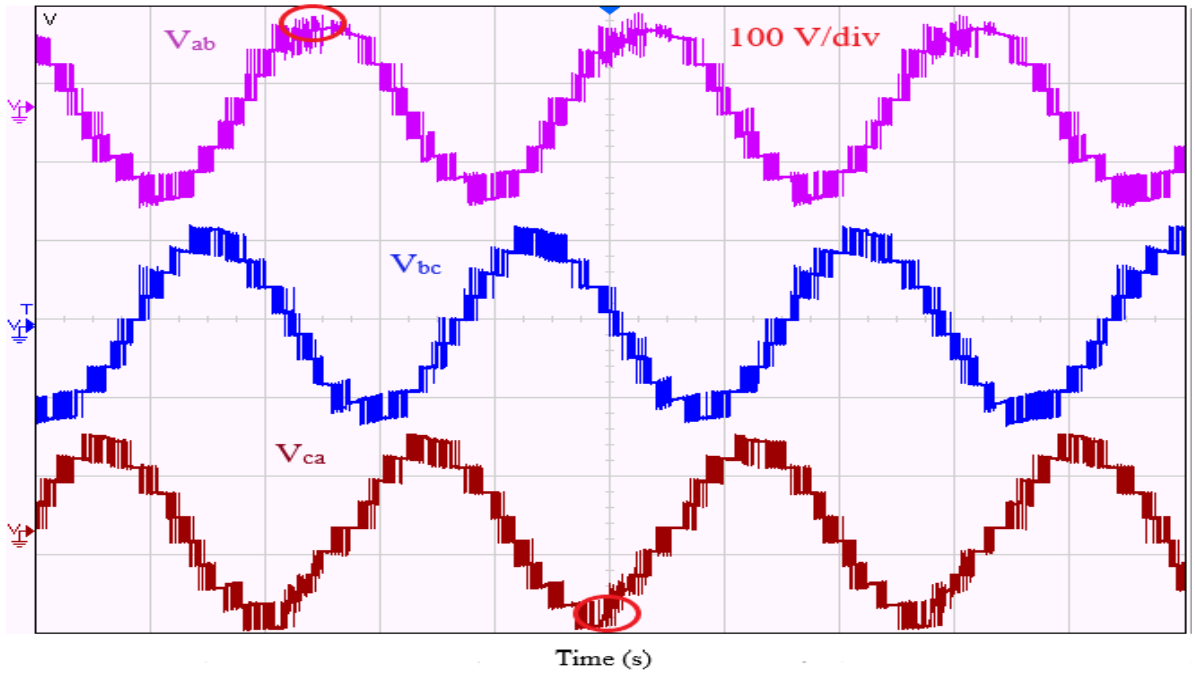

Fig. 4-16. Experimental output voltages of the three-phase CMLI due to fault at Sa4

The fifth level of Phase-A (positive peak) and Phase-C (negative peak) are affected while other levels remain at normal conditions, which is almost similar to the simulated results presented in Fig. 4-6. It can therefore be concluded that the fault location is within switch S_{a4}.

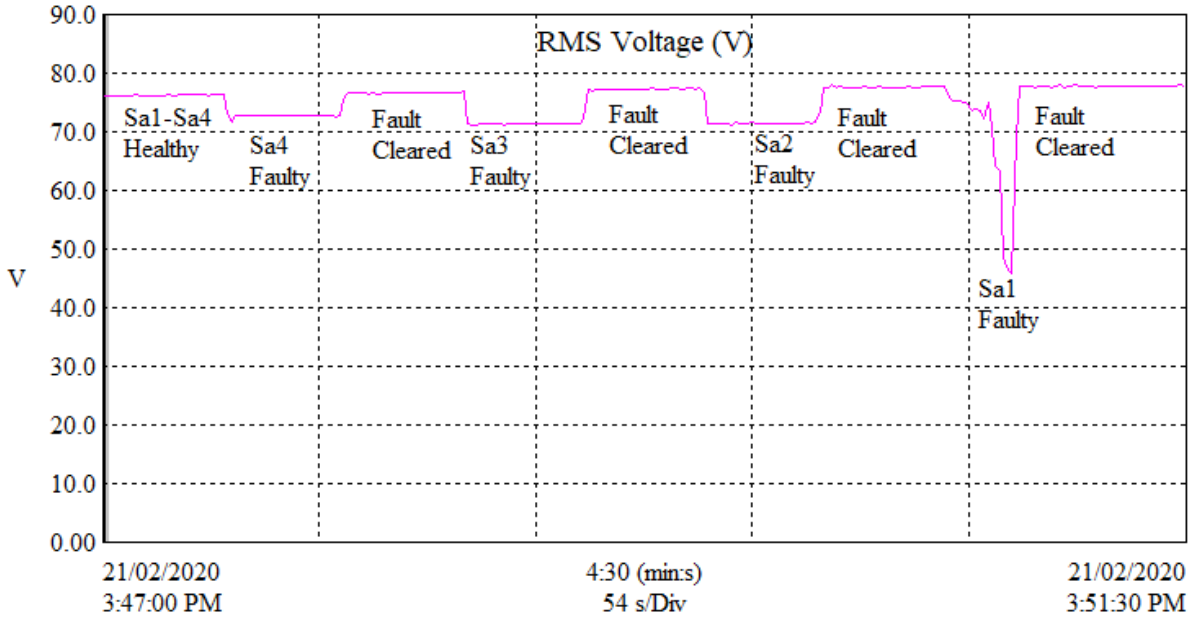

Fig. 4-17. Dynamic RMS voltage due to the faults in semiconductor devices (S_{a1} to S_{a4})

The dynamic performances of the three-phase CMLI were investigated by applying the proposed condition monitoring algorithm for the semiconductor switching devices (S_{a1} to S_{a4}) in physical layer. The dynamic RMS voltage is shown in Fig. 4-17, which is almost symmetrical with the simulated results as presented in Fig. 4-7. The dynamic total harmonic

distribution (THD) of the RMS voltage is shown in Fig. 4-18, which almost matches the simulated results depicted in Fig. 4-8.

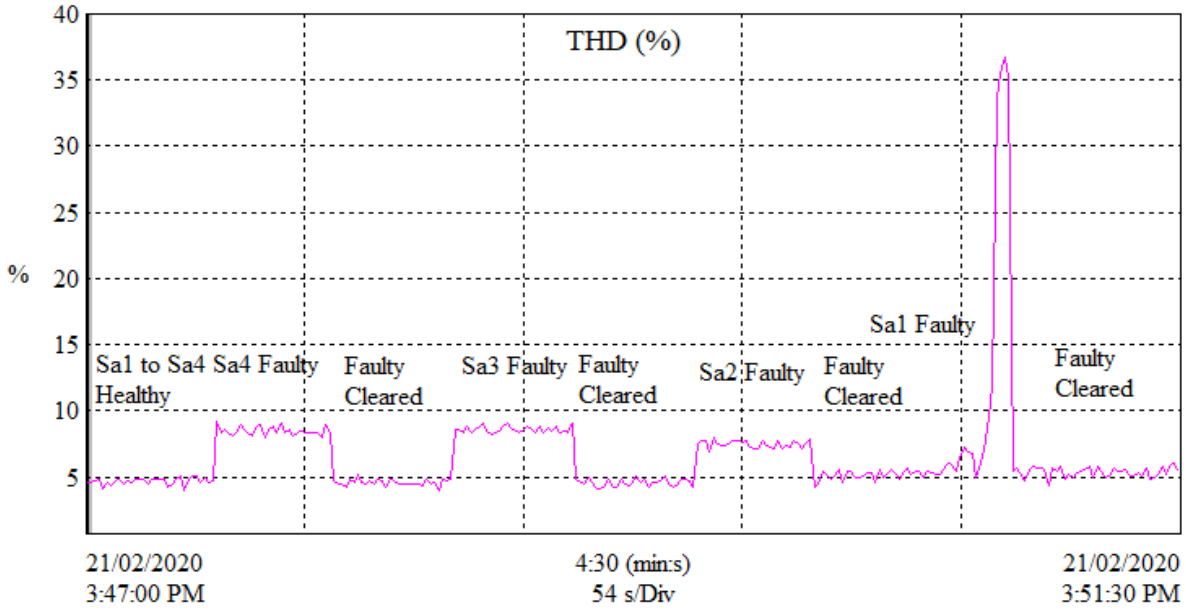

Fig. 4-18. Dynamic THD due to the faults in semiconductor switching devices (S_{a1} to S_{a4})

The crest factor of the RMS voltage was measured with an amplitude close to √2 until 30 seconds during the first transition as depicted in Fig. 4-19. This value indicates the almost sinusoidal nature of the output voltage of the WECS [272]. The crest factor shows a slight non-sinusoidal nature during the second transition and returns to the normal condition in the third transition. This process was continued and investigated until 270 seconds for all the upper switches. These results and investigations reveal the superior performance of the proposed condition monitoring algorithm for monitoring the condition of the switching devices of the three-phase CMLI.

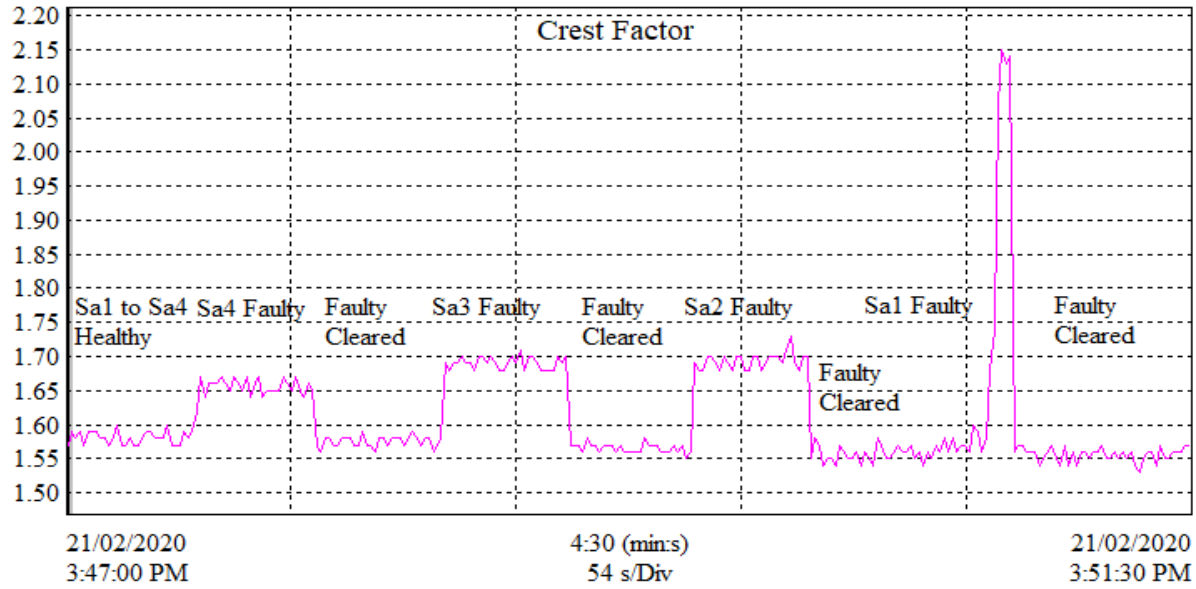

Fig. 4-19. Dynamic crest factor due to the faults in semiconductor devices (S_{a1} to S_{a4})

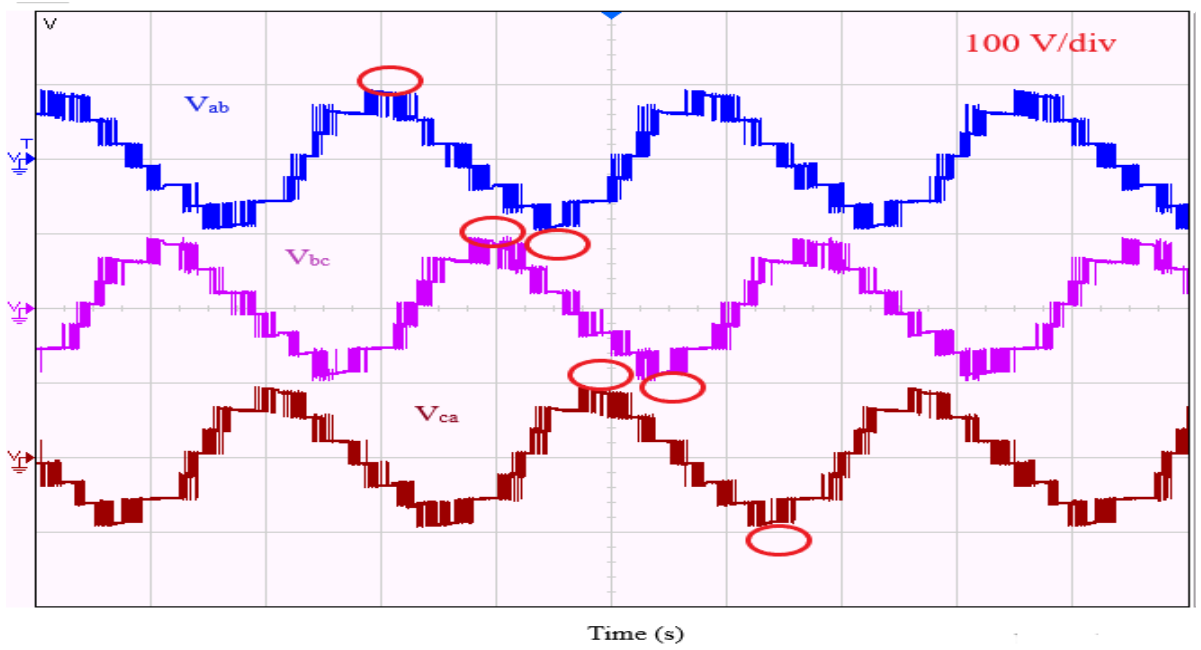

Fig. 4-20. Three-phase output voltage of the dc-link capacitor fault

The output voltages of the three-phase CMLI were captured as shown in Fig. 4-20, which indicate the fault information marked by red coloured circles. The fifth level of each voltage (positive and negative peak) was wiped out, while the other levels remain in normal condition, which was the same as the simulated results presented in Fig. 4-9. It can, therefore, be concluded that the fault location is at C_1.

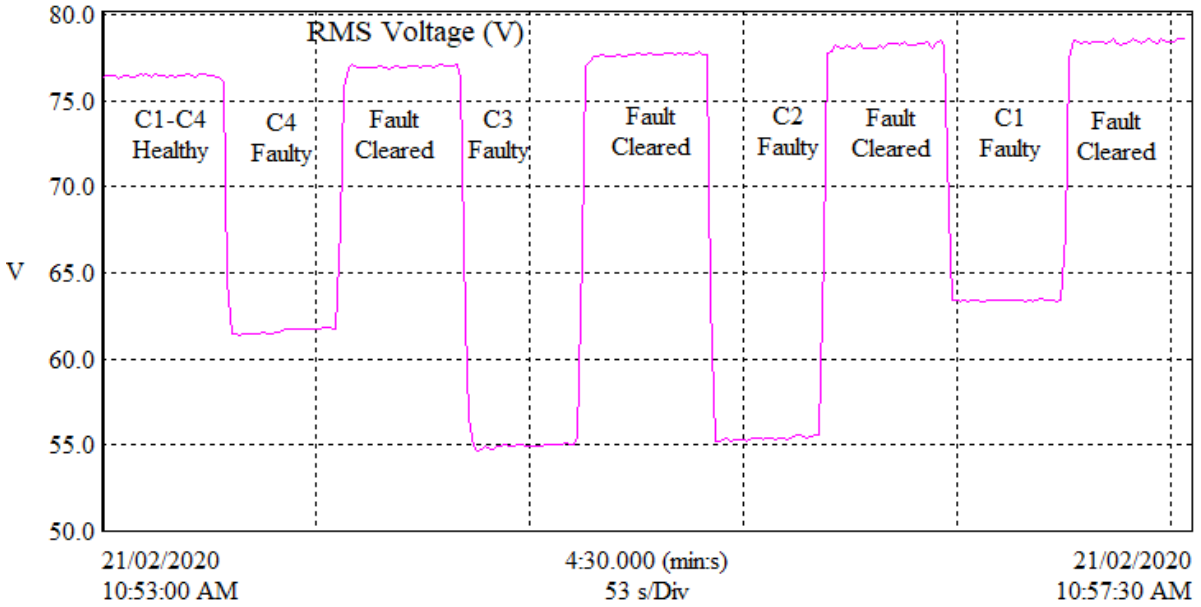

Fig. 4-21. Dynamic RMS voltage due to the faults in the dc-link capacitors (C_1 to C_4)

The dynamic performances of the three-phase CMLI were investigated by applying the proposed condition monitoring algorithm for the dc-link capacitors (C_1 to C_4) in physical layer.

The dynamic RMS voltage is shown in Fig. 4-21, which is almost symmetrical with the simulated results as presented in Fig. 4-10. The dynamic total harmonic distribution (THD) of the RMS voltage is shown in Fig. 4-22, which almost matches the simulated results as depicted in Fig. 4-11.

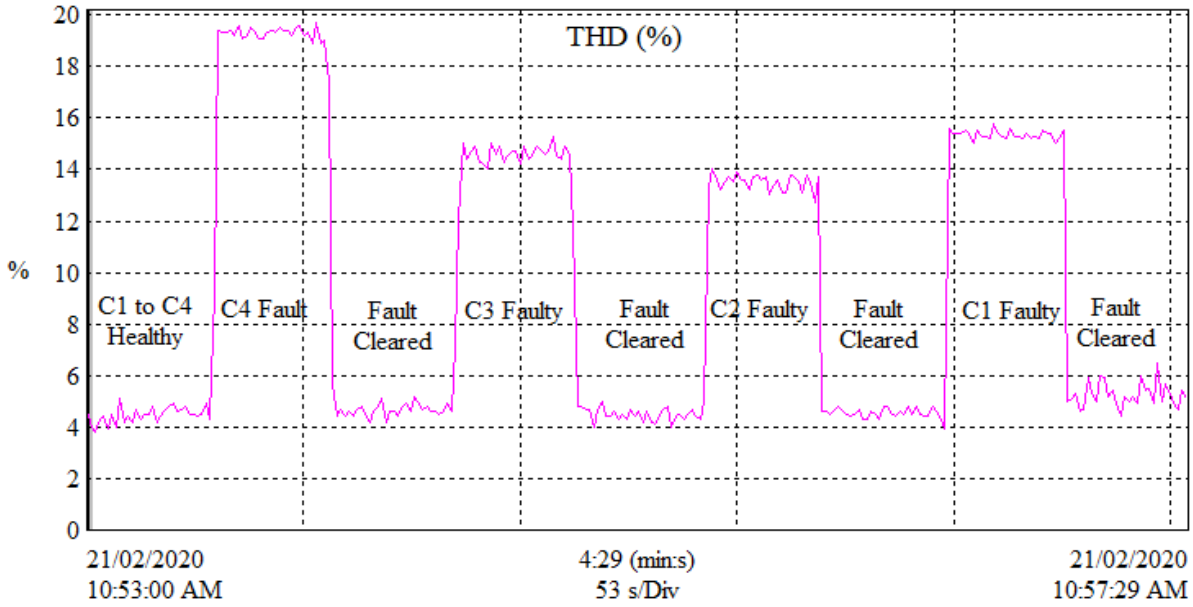

Fig. 4-22. Dynamic THD due to the faults in the dc-link capacitors (C1 to C4)

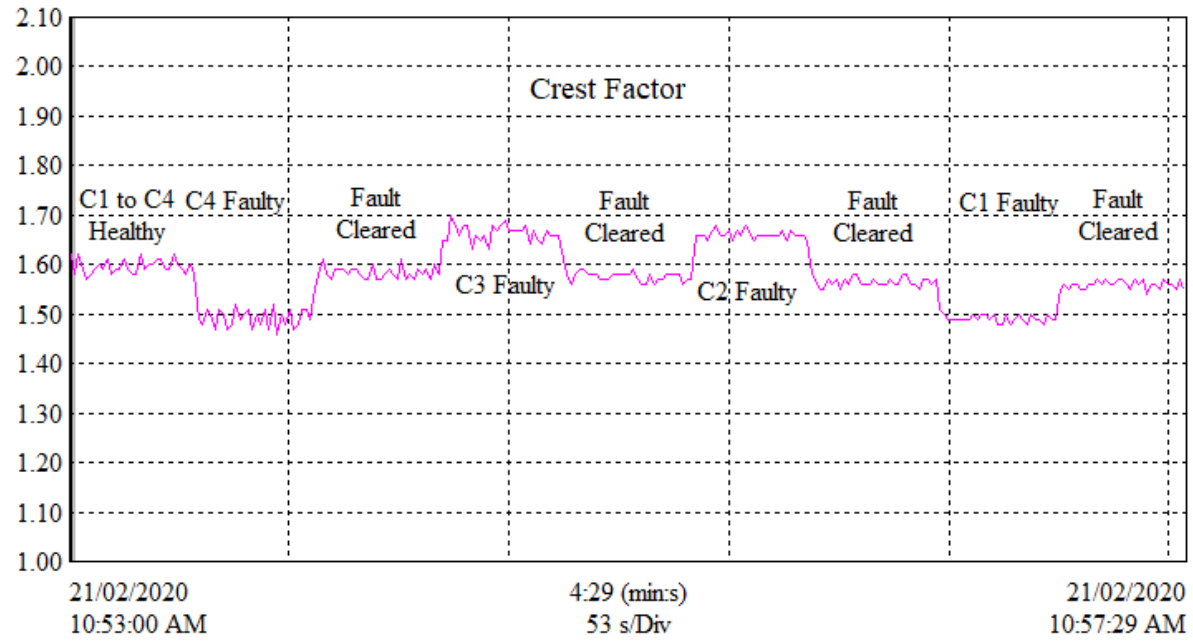

Fig. 4-23. Dynamic crest factor due to the faults in the dc-link capacitors (C1 to C4)

The crest factor of the RMS voltage was measured with an amplitude close to √2 until 30 seconds during the first transition as depicted in Fig. 4-23. This value indicates the almost sinusoidal nature of the output voltage of the three-phase CMLI [272]. The crest factor shows

the slight non-sinusoidal nature during the second transition and returns to normal conditions in the third transition. This process was continued and investigated until 270 seconds for all the dc-link capacitors. These results and investigations reveal the superior performance of the proposed condition monitoring algorithm for monitoring the condition of dc-link capacitors.

All the condition monitoring of the WECS described above could have been monitored remotely over the internet of things, including for the remaining five architectural layers. In the data sensing layer, a three-phase step-down transformer (220, 50Hz, 9V, 1000mA) is used to sense the three-phase voltage from the squirrel cage induction motor as depicted in Fig. 4-15. The three-phase bridge-rectifier (SP 9V, 2W10) is used to link the sensed three-phase voltage to the Arduino Uno board in the data processing layer. The data sensing layer processes the data in binary form and sends the processed data to the SIM800L in the data-link layer. The data-link layer posts and updates the three-phase processed data to the server in the network layer every 60 seconds as depicted in Fig. 4-24. The three-phase processed data generates sinusoidal output waveforms in the authenticated server, which identifies fault information for phases B and C. The fault information is being monitored in real-time by the authenticated remote users in the application layer.

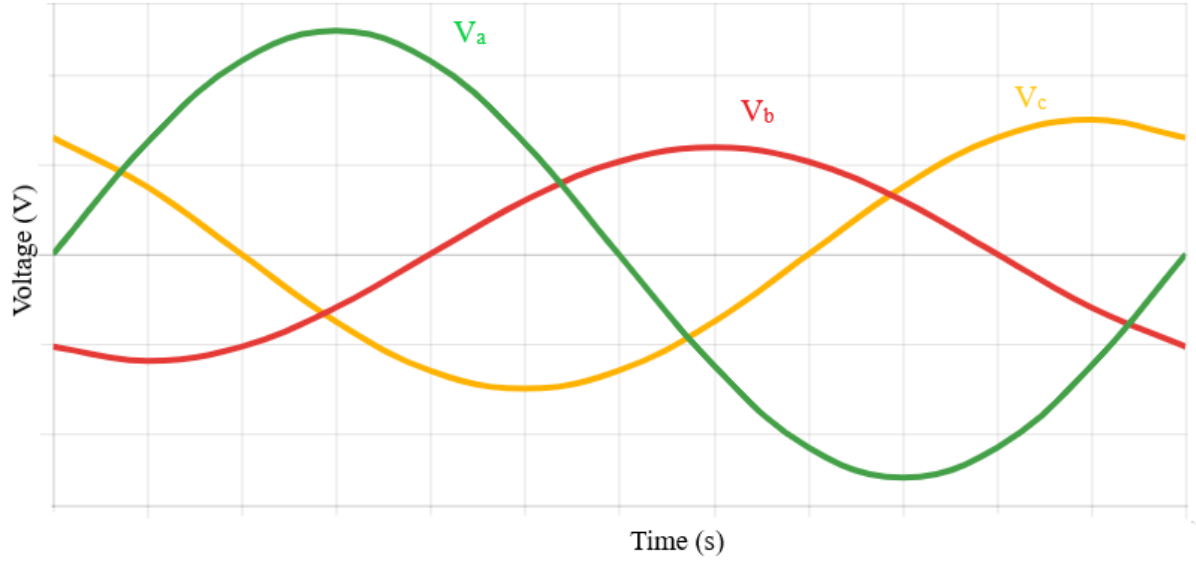

Fig. 4-24. Condition monitoring of the WECS using an industrial IoT algorithm

The authenticated remote users monitor this fault information by accessing the server over the internet. This faulty three-phase voltage has also gone below the threshold voltage, which is sent to the authenticated email servers every 60 seconds. The authenticated remote users may shut down the WECS through Wi-Fi switches over the internet or advise the local operating personnel of the fault correction through the ability of the WECS if the faults are not severe.

The condition of the WECS is also monitored remotely using the IoT via a local area network (LAN). The real-time output waveforms of the WECS are captured using a Keysight oscilloscope (PA2203a). Remote users can monitor the output waveform using Keysight oscilloscope local area network (LAN) connection. The rear panel LAN ports of the oscilloscope and remote computer communicate through an ethernet cable. The dynamic DNS option is enabled to allow each oscilloscope to register its hostname to discriminate multiple devices. When the oscilloscope is connected to the remote computer, screen images of the oscilloscope can be shown on the remote computer. The output of the oscilloscope can be monitored over the internet through its hostname or IP address as shown in Fig. 4-25. The web browser helps control the oscilloscope, capture screen images, save the captured images to the computer, print the web pages, and recall the files to the web page. The recommended browser is internet explorer; other java enabled browsers may also be applicable. The authenticated remote users can access the computer securely over the internet by launching the Chrome Remote Desktop app in both host computer and authenticated remote devices (computer, laptop, phone, etc.). The WECS could be controlled over IoT by the authenticated remote users. Once the remote users can access a local computer, they will be able to control and diagnose the WECS remotely.

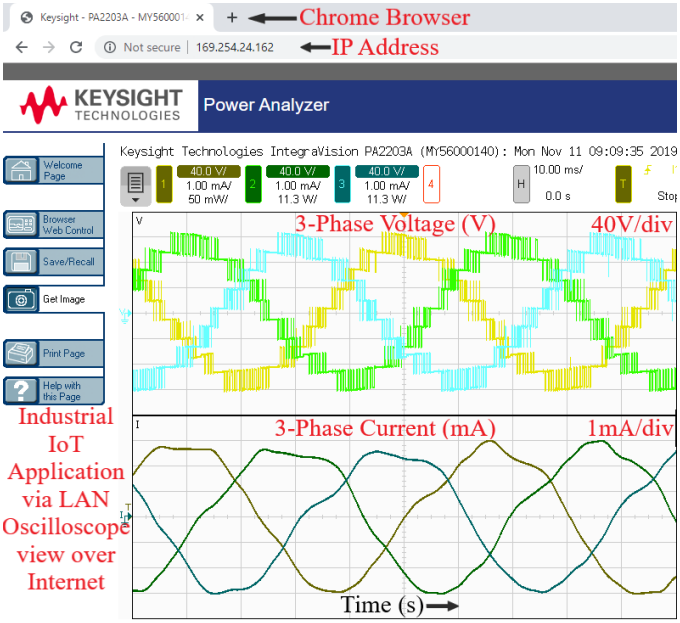

Fig. 4-25. Condition monitoring of the WECS via the LAN

4.3.3. Suggestions on how to mitigate the faults

The CMLI consists of four three-phase 2-level inverters connected in cascade. If a fault occurs in any switch of the three-phase 2-level inverter, its performances will be affected which could be monitored through industrial IoT system proposed in this thesis. The authenticated

remote users will allow the CMLI to operate if the nature of fault severe and within the fault right through ability of the CMLI. The authenticated remote users may shut down the system and instruct the local operators to replace the faulty section when the fault is in severe condition. Replacement of the faulty three-phase 2-level inverter by a new one is a rapid cost-effective solution due to the significant reduction in the prices of power electronic components. Authors of [273] proposed a novel switching technique based on selective harmonic elimination (SHE) controller to mitigate faults of multilevel cascaded H-bridge (CHB) inverters which could be implemented in future. Authors of [274] proposed a design of a fault-tolerant structure to mitigate the fault of cascaded H-bridge multilevel inverter. Failure mean time and reliability have been evaluated using Markov method in which rate of failures of switches are calculated. This fault tolerant structure could be also applied in future to mitigate the faults of CMLI."

Summary

Monitoring the condition of the WECS is mandatory for reducing downtime and obtaining an uninterrupted power supply. This thesis proposes an algorithm to monitor the condition of the dc-link and semiconductor switching devices in a three-phase CMLI for the WECS in real-time. The algorithm was designed in the MATLAB software environment and a hardware prototype was developed to test the algorithm. The experimental results reveal the superiority of the algorithm for monitoring the condition of the dc-link capacitors and semiconductor switching devices. The performances of the algorithm were also investigated remotely in real-time through an industrial IoT algorithm. A hardware prototype of the industrial IoT algorithm was also developed to monitor the condition of the dc-link capacitors and semiconductor switching devices remotely in real time. The real-time data of the dc-link capacitors and semiconductor switching devices was posted to the server so that authenticated remote users could monitor the condition and advise accordingly in real time. From the experimental results, it can be concluded that the proposed industrial IoT algorithm shows excellent performance.

Chapter V
Conclusions and Future work

5.1 Conclusion

This thesis proposes a three-phase cascaded multilevel inverter (CMLI) to produce a better quality of output voltage waveform, and a space vector pulse width modulation (SVPWM) controller to control the three-phase CMLI and balance the voltages across the dc-link capacitors. A hardware prototype has been developed to validate the proposed three-phase CMLI and SVPWM controller. In addition, this thesis proposes an algorithm to monitor the condition of the dc-link capacitors and switching devices of the three-phase CMLI, and energy storage and management system to protect the dc-link capacitors as well as store the energy during faulty periods of WECS function, and an industrial internet of things (IoT) algorithm to monitor the condition of the WECS remotely in real-time. A hardware prototype has also been developed to verify the proposed PI-based SVPWM embedded and industrial IoT algorithms. These significant contributions set out to improve system performance and reliability, which are separately covered in two chapters (Chapter 3 and Chapter 4). These contributions and key features are summarized here in section 5.2.

5.2. Main Contributions in the thesis

The main contributions of this thesis are summarized here.

1. The rectifier produces harmonic ripples in its output voltage waveform across the dc-link capacitors during conversion, which restricts the achievement of the desired input voltage waveform for the three-phase CMLI. Several ripple minimization techniques have been discussed with their limitations in the literature [275], [276], [277]. A SVPWM controller has been developed, which minimizes the ripples of the dc-link voltage. The SVPWM controller has self-rotating voltage vectors in each sector around the coordinates which can minimize the ripples of rectifier using the PI controller. The SVPWM controller has been designed and simulated in the MATLAB software environment. An experimental prototype has also been developed and tested to validate the SVPWM controller. The simulated and experimental results reveal the superiority of the SVPWM controller.
2. The multilevel inverter (MLI) has brought a tremendous revolution in industry for converting the dc-link voltage to three-phase ac voltage [278]. Several topologies of MLI have been discussed with their limitations in the literature [279]. The cascaded h-

bridge inverter (CHBI) is one of the promising topologies of MLI, since it requires the least number of components during its fabrication [280]. However, the CHBI requires a large number of isolated dc sources, which restricts its coupling with the dc-link. A three-phase CMLI has been proposed in this thesis, which requires four non-isolated dc-link capacitors and is easily coupled with the rectifier. The proposed three-phase CMLI has been designed and simulated in the MATLAB software environment. An experimental setup of the three-phase CMLI has been developed and tested to verify the simulated results. The simulation and experimental results reveal the robustness of the proposed CMLI.

3. The proposed three-phase CMLI suffers from voltage balancing issues across the non-isolated dc-link capacitors like capacitor clamped inverter [281]. A simplified SVPWM controller has been proposed to balance the dc-link voltage across the non-isolated dc-link capacitor. The proposed SVPWM controller has been simplified by reducing the switching vectors which contributes to balance the voltage across the dc-link capacitors. The SVPWM controller has been designed and simulated in the MATLAB software environment. Also, an experimental test rig has been developed to validate the simulation results. The proposed SVPWM controller shows excellent performance for balancing the dc-link voltage over non-isolated capacitors.
4. Condition monitoring and early fault diagnosis for the WECS have become essential industry practices, as they help improve wind farm reliability, overall performance and productivity. If not detected and rectified at an early stage, some faults can be catastrophic with significant loss of revenue along with interruptions for businesses that primarily rely on wind energy [23]. The failure of the WECS results in system downtime and repair or replacement expenses that significantly reduce annual income. This thesis proposed a condition monitoring system (CMS) for the WECS which comprises six architectural layers, including the physical layer, data sensing layer, data processing layer, data-link layer, network layer, and application layer. The physical layer consists of several components and subsystems, which include a synchronous generator, rectifier, proposed three-phase CMLI, a motor, and the proposed controllers. The data sensing layer consists of a three-phase step-down transformer and a three-phase full-bridge rectifier. The three-phase output voltage is sensed from the physical layer and fed to the three-phase step down transformer. The three-phase full bridge-rectifier converts the three-phase step downed voltage and feeds it to the data processing layer, which consists of an Arduino Uno board along with an integrated development

environment (IDE) and a liquid crystal display (LCD). The data is processed in a binary form after which it is transferred to the data link layer. The data link layer consists of a global system for mobile GSM module with SIM Card (SIM800L) and a global packet radio service (GPRS). The network layer is a dedicated server for hosting incoming data from the SIM800L module. The GPRS provides idealized data rates between 126 to 256 kbits/s for the server domain. The posted data on the server are compared with the threshold voltage. If the posted data goes below the threshold voltage, a message is sent to the application layer. The application layer consists of authenticated remote users, email servers and Wi-Fi switches. The authenticated remote users can access the data from the server directly over the internet. They are also notified instantly with information about the fault via their authenticated email server. The authenticated remote users can control the Wi-Fi switches of the WECS. The authenticated remote user can monitor the performances of WECS in real time over internet. The status of the WECS is also updated with the authenticated remote users via email.

5. The condition of the WECS is also monitored remotely using the internet of things (IoT) via a local area network (LAN). The real time output waveforms of the wind energy conversion system are captured using a Keysight oscilloscope (PA2203a). The remote users can monitor the output waveform using the local area network (LAN) connection. When the oscilloscope is connected to the remote computer, screen images on the oscilloscope can be shown on the remote computer. The output of the oscilloscope can be monitored over the internet through its dedicated web server. The web browser helps to control the oscilloscope, capture screen images, save the captured images to the computer, print web pages, and recall the files to the web page. The authenticated remote users can access the computer securely over the internet by launching the Chrome Remote Desktop app in both the host computer and the authenticated remote devices (computer, laptop, phone, etc.). The WECS can ultimately be controlled over the IoT by authenticated remote users. Once the remote users can access a local computer, they will be able to control and diagnose the WECS remotely.

5.3.Suggestions for future work

The proposed WECS along with condition monitoring system (CMS) will play a significant role in the future smart power sector. Despite its significant contribution, this research has some challenges, which could be investigated in future research. The key points for future research are as follows:

Renewable energy production has increased significantly now a days which needs to be integrated into the recent smart power grid system [282]. But integrations of renewable energies into smart power grid lead to several significant technical challenges. Power quality is an important factor in the integrations of renewable energies. One of the major power problem quality issues is harmonic distortion, which is caused by the power electronic converter utilized for the conversion of renewable energy [283]. The harmonic distortion is significant when renewable energy penetration is high. The harmonic distortion needs to be minimized, and this is recommended for future research.

Photovoltaic power generation has also increased in recent years due to the reduction in the price of solar PV panels along with support policies in many countries [284]. The integration of PV generation into power grids leads to several technical challenges, such as the impact of the power electronic converter along with controllers, reverse power flow, power quality issues, voltage fluctuations, dynamic stability, and big data challenges [285], [286]. Exploring these issues in greater depth in order to resolve them is recommended as a valuable direction for future research.

Renewable power generation is integrated into low-voltage or medium-voltage distribution networks, since renewable power plants are mostly located in remote areas, which are not planned properly. In some cases, the large-scale power plants are normally connected to high voltage transmission networks, which require advanced structures to combine these energies. There are numerous challenges related to the control, operation and protection involved in integrating these energies into the transmission grid, due to the power electronic converters implemented for grid connectivity [287]. These challenges could be investigated elaborately in future.

The condition of the dc-link capacitors and switching devices in the three-phase CMLI have been monitored in real time locally and remotely. Condition monitoring of other parts, such as the blade, generator, rectifier, controller, and squirrel case induction generator has not been covered in this research, which are recommended as future works [288], [289], [290]. Though some faults have been investigated and discussed, no fault tolerant techniques have been covered yet to mitigate the faults, and these could be explored in future research.

The energy storage and management system has been designed and simulated as part of looking at the three-phase faults in this thesis. But no experimental investigations have yet been covered, and this needs to be done in the future.

This thesis proposes an industrial IoT system to monitor the condition of the WECS remotely in real time, which only covers for the three-phase voltages. Other signals such as

gate pulse, dc-link voltage, synchronous generator output, and three-phase currents have not yet been covered, and these are recommended that these could be explored as future work.

This thesis uses a cellular network system to monitor the condition of the WECS. This network can post the data to the authenticated server, which has bandwidth limitations. Other networking systems such as wireless networks and satellite networks could be applied to monitor the WECS in the future.

However, industrial IoT based projects are facing several challenges such as real time data accessing interoperability, end to end secure data privacy management, prohibition of unauthorized network, integration and identification of authenticated remote users [291]. The major issue is the security challenges due to the exploitation of unauthorized network since the industrial IoT devices are liable to provide secure information to the authenticated remote users. Recently, IoT automated industries are suffering hacking or blocking services between transmission like hacking of automated banking currency or intellectual property which have been developed based on untrustworthy IoT technology. This issue needs to be addressed by developing a trustworthy security system to reduce security threats which are recommended as future work.

References

[1] A. Qazi *et al.*, "Towards Sustainable Energy: A Systematic Review of Renewable Energy Sources, Technologies, and Public Opinions," *IEEE Access*, vol. 7, pp. 63837–63851, 2019, doi: 10.1109/ACCESS.2019.2906402.

[2] K. S. Rani, "Environmental effects of burning fossil fuels," *J. Chem. Pharm. Sci.*, vol. 2, no. 3, pp. 63–67, 2014.

[3] A. Jahid, M. K. H. Monju, M. E. Hossain, and M. F. Hossain, "Renewable Energy Assisted Cost Aware Sustainable Off-Grid Base Stations with Energy Cooperation," *IEEE Access*, vol. 6, pp. 60900–60920, 2018, doi: 10.1109/ACCESS.2018.2874131.

[4]. "'Wind Power Capacity Worldwide Reaches 597 GW, 50,1 GW added in 2018,'" *World Wind Energy Association*. .

[5] M. Liton Hossain, A. Abu-Siada, and S. M. Muyeen, "Methods for advanced wind turbine condition monitoring and early diagnosis: A literature review," *Energies*, vol. 11, no. 5, 2018, doi: 10.3390/en11051309.

[6] Y. M. Jadan, M. E. Bolanos, F. D. Merlet, R. Hidalgo-Leon, G. S. Idrovo, and P. J. Ruiz, "Hardware-in-the-Loop for Wind Energy Conversion with Resonant Current Control and Active Damping," *IEEE Lat. Am. Trans.*, vol. 17, no. 7, pp. 1146–1154, 2019, doi: 10.1109/TLA.2019.8931203.

[7] A. Elkomy, A. Huzayyin, T. M. Abdo, A. A. Adly, and H. M. Yassin, "Enhancement of wind energy conversion systems active and reactive power control via flywheel energy storage systems integration," *2017 19th Int. Middle-East Power Syst. Conf. MEPCON 2017 - Proc.*, vol. 2018-Febru, no. December, pp. 1151–1156, 2018, doi: 10.1109/MEPCON.2017.8301327.

[8] P. Drabek and L. Poljak, "Metods for voltage ripple mitigation on DC side of single-phase AC\DC converters," *Int. Conf. Appl. Electron.*, vol. 2015-Octob, pp. 201–204, 2015.

[9] S. Kuo and Z. Lin, "Clamped Five-Level Inverter with Auto Equalization," pp. 2–6, 2018.

[10] R. Viju Nair, R. Chattopadhyay, S. Parashar, S. Bhattacharya, and K. Gopakumar, "Cascaded Active Neutral Point Clamped and Flying Capacitor Inverter Topology for Induction Motor Drives Applications," *2018 IEEE Energy Convers. Congr. Expo. ECCE 2018*, pp. 6696–6702, 2018, doi: 10.1109/ECCE.2018.8557745.

[11] K. K. Gupta, A. Ranjan, P. Bhatnagar, L. K. Sahu, and S. Jain, "Multilevel inverter topologies with reduced device count: A review," *IEEE Trans. Power Electron.*, vol. 31, no. 1, pp. 135–151, 2016, doi: 10.1109/TPEL.2015.2405012.

[12] N. Mittal, B. Singh, S. P. Singh, R. Dixit, and D. Kumar, "Multilevel inverters: A literature survey on topologies and control strategies," *ICPCES 2012 - 2012 2nd Int. Conf. Power, Control Embed. Syst.*, 2012, doi: 10.1109/ICPCES.2012.6508041.

[13] M. M. Hasan, A. Abu-Siada, and M. S. A. Dahidah, "A three-phase symmetrical DC-Link multilevel inverter with reduced number of DC Sources," *IEEE Trans. Power Electron.*, vol. 33, no. 10, pp. 8331–8340, 2018, doi: 10.1109/TPEL.2017.2780849.

[14] A. Karmakar, N. Dey, T. Baral, M. Chowdhury, and M. Rehan, "Industrial internet of things: A review," *2019 Int. Conf. Opto-Electronics Appl. Opt. Optronix 2019*, 2019, doi: 10.1109/OPTRONIX.2019.8862436.

[15] B. Radunovic and A. Proutiere, "On downlink capacity of cellular data networks with WLAN/WPAN relays," *IEEE/ACM Trans. Netw.*, vol. 21, no. 1, pp. 286–296, 2013, doi: 10.1109/TNET.2012.2198072.

[16] BP Statistical Review of World Energy, 68th edition, June, 2019, pp. 1-64.

[17] Renewable Capacity Statistics,*International Renewable Energy Agency*, March, 2019, pp.1-60.

[18] Renewables Information, International Energy Agency, August 2019.

[19] K. B. Tawfiq, A. S. Mansour, H. S. Ramadan, M. Becherif, and E. E. El-Kholy, "Wind energy conversion system topologies and converters: Comparative review," *Energy Procedia*, vol. 162, pp. 38–47, 2019, doi: 10.1016/j.egypro.2019.04.005.

[20] X. Yin and X. Zhao, "Composite hierarchical pitch angle control for a tidal turbine based on the uncertainty and disturbance estimator," *IEEE Trans. Ind. Electron.*, vol. 67, no. 1, pp. 329–339, 2020, doi: 10.1109/TIE.2019.2896261.

[21] Y. Gao, T. Yang, T. Dragicevic, S. Bozhko, P. Wheeler, and C. Zheng, "Optimal filter design for power converters regulated by FCS-MPC in the MEA," *IEEE Trans. Power Electron.*, vol. 36, no. 3, pp. 1–1, 2020, doi: 10.1109/tpel.2020.3017862.

[22] E. Wolfgang, "Examples for failures in power electronics systems," in *Proc. ECPE Tut. Rel. Power Electron. Syst.*, pp. 19–20.

[23] L. Hossain, A. Abu-siada, S. M. Muyeen, and M. Hasan, “Industrial IoT based condition monitoring for wind energy conversion system,” *CSEE J. Power Energy Syst.*, 2020, doi: 10.17775/cseejpes.2020.00680.

[24] I. Miladinovic and S. Schefer-Wenzl, “NFV enabled IoT architecture for an operating room environment,” *IEEE World Forum Internet Things, WF-IoT 2018 - Proc.*, vol. 2018-Janua, pp. 98–102, 2018, doi: 10.1109/WF-IoT.2018.8355128.

[25] “‘IDC Forecasts Worldwide Spending on the Internet of Things.’”

[26] R. Abdullah, N. A. Rahim, S. R. Sheikh Raihan, and A. Z. Ahmad, “Five-level diode-clamped inverter with three-level boost converter,” *IEEE Trans. Ind. Electron.*, vol. 61, no. 10, pp. 5155–5163, 2014, doi: 10.1109/TIE.2013.2297315.

[27] N. Bianchi and M. Dai Pre, “Active power filter control using neural network technologies,” *IEE Proceedings-Electric Power Appl.*, vol. 150, no. 2, pp. 139–145, 2003, doi: 10.1049/ip-epa.

[28] M. M. Hasan and A. Abu-Siada, “A novel three phase cascaded multilevel inverter topology,” *IEACon 2016 - 2016 IEEE Ind. Electron. Appl. Conf.*, pp. 31–35, 2017, doi: 10.1109/IEACON.2016.8067351.

[29] M. M. Hasan, A. Abu-Siada, and M. R. Islam, “Design and implementation of a novel three-phase cascaded half-bridge inverter,” *IET Power Electron.*, vol. 9, no. 8, pp. 1741–1752, 2016, doi: 10.1049/iet-pel.2015.0951.

[30] M. M. Hasan, A. Abu-Siada, S. M. Islam, and M. S. A. Dahidah, “A New Cascaded Multilevel Inverter Topology with Galvanic Isolation,” *IEEE Trans. Ind. Appl.*, vol. 54, no. 4, pp. 3463–3472, 2018, doi: 10.1109/TIA.2018.2818061.

[31] V. T. Somasekhar and K. Gopakumar, “No TitlThree-level inverter configuration cascading two two-level inverterse,” in *IEE Proceedings - Electric Power Applications, vol. 150, no. 3*, pp. 245–254.

[32] A. K. Gupta and A. M. Khambadkone, “A space vector PWM scheme for multilevel inverters based on two-level space vector PWM,” *IEEE Trans. Ind. Electron.*, vol. 53, no. 5, pp. 1631–1639, 2006, doi: 10.1109/TIE.2006.881989.

[33] Y. Liao, E. D. F. R. Loures, and F. Deschamps, “Industrial Internet of Things: A Systematic Literature Review and Insights,” *IEEE Internet Things J.*, vol. 5, no. 6, pp. 4515–4525, 2018, doi: 10.1109/JIOT.2018.2834151.

[34] Clean Energy Australia Report 2019, Clean Energy Council, 4 April, 2019, pp. 1-82.

[35] M. B. H. Kumar, B. Saravanan, P. Sanjeevikumar, and F. Blaabjerg, “Review on control techniques and methodologies for maximum power extraction from wind energy systems,” *IET Renew. Power Gener.*, vol. 12, no. 14, pp. 1609–1622, 2018, doi: 10.1049/iet-rpg.2018.5206.

[36] W. Qiao and D. Lu, “A Survey on Wind Turbine Condition Monitoring and Fault Diagnosis - Part II: Signals and Signal Processing Methods,” *IEEE Trans. Ind. Electron.*, vol. 62, no. 10, pp. 6546–6557, 2015, doi: 10.1109/TIE.2015.2422394.

[37] A. M. S. Yunus, M. A. S. Masoum, and A. Abu-Siada, “Application of SMES to enhance the dynamic performance of DFIG during voltage sag and swell,” *IEEE Trans. Appl. Supercond.*, vol. 22, no. 4, 2012, doi: 10.1109/TASC.2012.2191769.

[38] P. Qian, X. Ma, and P. Cross, “Integrated data-driven model-based approach to condition monitoring of the wind turbine gearbox,” *IET Renew. Power Gener.*, vol. 11, no. 9, pp. 1177–1185, 2017, doi: 10.1049/iet-rpg.2016.0216.

[39] H. M. Hasanien and S. M. Muyeen, “Affine projection algorithm based adaptive control scheme for operation of variable-speed wind generator,” *IET Gener. Transm. Distrib.*, vol. 9, no. 16, pp. 2611–2616, 2015, doi: 10.1049/iet-gtd.2014.1146.

[40] S. A. Taher, M. H. Karimi, and Z. D. Arani, “Improving Fault Ride Through Capability of Full-Scale WRSG Wind Turbines Using MPC-Based DVR,” *ICEE 2019 - 27th Iran. Conf. Electr. Eng.*, pp. 863–867, 2019, doi: 10.1109/IranianCEE.2019.8786566.

[41] A. S. Gadalla, X. Yan, and H. Hasabelrasul, “Active power analysis for the battery energy storage systems based on a modern cascaded multilevel converter,” *Proc. - 2nd IEEE Int. Conf. Energy Internet, ICEI 2018*, pp. 111–116, 2018, doi: 10.1109/ICEI.2018.00028.

[42] N. Mukherjee and D. Strickland, “Analysis and Comparative Study of Different Converter Modes in Modular Second-Life Hybrid Battery Energy Storage Systems,” *IEEE J. Emerg. Sel. Top. Power Electron.*, vol. 4, no. 2, pp. 547–563, 2016, doi: 10.1109/JESTPE.2015.2460334.

[43] L. Y. W. and J. L. M. Liu, W. Li, C. Wang, M. P. Polis, “Reliability Evaluation of Large-Scale Battery Energy Storage Systems,”

IEEE Trans. Smart Grid, vol. 8, no. 6, pp. 2733–2743.

[44] Y. Shen, H. Wang, Z. Shen, Y. Yang, and F. Blaabjerg, "A 1-MHz Series Resonant DC-DC Converter with a Dual-Mode Rectifier for PV Microinverters," *IEEE Trans. Power Electron.*, vol. 34, no. 7, pp. 6544–6564, 2019, doi: 10.1109/TPEL.2018.2876346.

[45] P. Garg, Priyanshi, and G. Bhuvaneswari, "Power electronic circuit based implementation of a solar PV emulator using a power factor corrected buck converter," *2018 IEEMA Eng. Infin. Conf. eTechNxT 2018*, pp. 1–6, 2018, doi: 10.1109/ETECHNXT.2018.8385297.

[46] L. Zhao, Q. Ge, Z. Zhou, B. Yang, and Y. Li, "Band Gap Power Semiconductor Devices for Rail Transit Electrical Drive," *2018 1st Work. Wide Bandgap Power Devices Appl. Asia (WiPDA Asia)*, pp. 1–4.

[47] A. Ramya, M. Balaji, and C. Bharatiraja, "Power quality improvement in BLDC motor drive using Bridgeless Modified Cuk converter," *Proc. 2018 IEEE Int. Conf. Power Electron. Drives Energy Syst. PEDES 2018*, vol. 4, no. d, 2018, doi: 10.1109/PEDES.2018.8707478.

[48] Y. Rozanov, K. Kryukov, M. Kiselev, M. Lepanov, Y. Tserkovsky, and E. Namestnikova, "Power Conditioning Unit for Direct-Drive Wave Energy Converter," *Proc. - 2018 IEEE 18th Int. Conf. Power Electron. Motion Control. PEMC 2018*, pp. 416–420, 2018, doi: 10.1109/EPEPEMC.2018.8521966.

[49] X. Zhao, L. Zhang, R. Born, and J. S. Lai, "Solution of input double-line frequency ripple rejection for high-efficiency high-power density string inverter in photovoltaic application," *Conf. Proc. - IEEE Appl. Power Electron. Conf. Expo. - APEC*, vol. 2016-May, no. 2, pp. 1148–1154, 2016, doi: 10.1109/APEC.2016.7468014.

[50] I. Castro, S. Member, and D. G. Lamar, "Optimized Design of a High," vol. 33, no. 6, pp. 5192–5205, 2018.

[51] P. Das, M. Pahlevaninezhad, J. Drobnik, G. Moschopoulos, and P. K. Jain, "A nonlinear controller based on a discrete energy function for an AC/DC boost PFC converter," *IEEE Trans. Power Electron.*, vol. 28, no. 12, pp. 5458–5476, 2013, doi: 10.1109/TPEL.2012.2232681.

[52] B. Veerasamy, W. Kitagawa, and T. Takeshita, "Output ripple minimization of single-stage power-factor-correction bidirectional buck AC/DC converter," *IEEJ J. Ind. Appl.*, vol. 4, no. 3, pp. 235–243, 2015, doi: 10.1541/ieejjia.4.235.

[53] J. Rodríguez, J. S. Lai, and F. Z. Peng, "Multilevel inverters: A survey of topologies, controls, and applications," *IEEE Trans. Ind. Electron.*, vol. 49, no. 4, pp. 724–738, 2002, doi: 10.1109/TIE.2002.801052.

[54] M. Vijeh, M. Rezanejad, E. Samadaei, and K. Bertilsson, "A General Review of Multilevel Inverters Based on Main Submodules: Structural Point of View," *IEEE Trans. Power Electron.*, vol. 34, no. 10, pp. 9479–9502, 2019, doi: 10.1109/TPEL.2018.2890649.

[55] A. R. Kumar and T. Deepa, "Multilevel Inverters: A Review of Recent Topologies and New Modulation Techniques," *Proc. IEEE Int. Conf. "Recent Trends Electr. Control Commun. RTECC 2018*, pp. 196–203, 2019, doi: 10.1109/RTECC.2018.8625667.

[56] J. Singh, R. Dahiya, and L. M. Saini, "Recent research on transformer based single DC source multilevel inverter: A review," *Renew. Sustain. Energy Rev.*, vol. 82, no. September 2017, pp. 3207–3224, 2018, doi: 10.1016/j.rser.2017.10.023.

[57] H. M. A. Antunes, I. A. Pires, and S. M. Silva, "Evaluation of Series and Parallel Hybrid Filters Applied to Hot Strip Mills with Cycloconverters," *IEEE Trans. Ind. Appl.*, vol. 55, no. 6, pp. 6643–6651, 2019, doi: 10.1109/TIA.2019.2932966.

[58] T. M. Thompkins, D. I. Kim, P. Stone, and Y. J. Shin, "Rolling Mill Cycloconverter Condition Assessment by Harmonic Current via Time-Frequency Signature," *IEEE Trans. Ind. Informatics*, vol. 14, no. 10, pp. 4376–4384, 2018, doi: 10.1109/TII.2017.2753282.

[59] S. Mondal and D. Kastha, "Input Reactive Power Controller with a Novel Active Damping Strategy for a Matrix Converter Fed Direct Torque Controlled DFIG for Wind Power Generation," *IEEE J. Emerg. Sel. Top. Power Electron.*, vol. 6777, no. c, pp. 1–1, 2019, doi: 10.1109/jestpe.2019.2938012.

[60] N. Prabaharan and K. Palanisamy, "A comprehensive review on reduced switch multilevel inverter topologies, modulation techniques and applications," *Renew. Sustain. Energy Rev.*, vol. 76, no. March, pp. 1248–1282, 2017, doi: 10.1016/j.rser.2017.03.121.

[61] M. T. Hagh, F. N. Mazgar, S. Roozbehani, and A. Jalilian, “THD minimisation of multilevel inverter with optimised dc sources magnitude and switching angles,” *CIRED - Open Access Proc. J.*, vol. 2017, no. 1, pp. 875–878, 2017, doi: 10.1049/oap-cired.2017.0341.

[62] P. Mehta and M. Kumar, “Capacitor voltage balancing and THD analysis in ANPC multilevel inverter,” *2018 IEEMA Eng. Infin. Conf. eTechNxT 2018*, pp. 1–5, 2018, doi: 10.1109/ETECHNXT.2018.8385376.

[63] A. Edpuganti and A. K. Rathore, “Optimal low-switching frequency pulsewidth modulation of medium voltage seven-level cascade-5/3H inverter,” *IEEE Trans. Power Electron.*, vol. 30, no. 1, pp. 496–503, 2015, doi: 10.1109/TPEL.2014.2313552.

[64] M. M. Hasan, A. Abu-Siada, S. M. Islam, and S. M. Muyeen, “A Novel Generalized Concept for Three Phase Cascaded Multilevel Inverter Topologies,” *IEEE Green Technol. Conf.*, no. MLI, pp. 110–117, 2017, doi: 10.1109/GreenTech.2017.22.

[65] S. Ouni, M. Khodabandeh, M. Zolghadri, J. Rodriguez, and H. Oraee, “A reduced switch cascaded transformer multi level inverter,” *2015 IEEE 15th Int. Conf. Environ. Electr. Eng. EEEIC 2015 - Conf. Proc.*, vol. 1, no. c, pp. 1013–1018, 2015, doi: 10.1109/EEEIC.2015.7165303.

[66] P. C. Sajith and K. Sunitha, “Asymmetrical cascaded 15-level inverter using single DC-source,” *2014 Annu. Int. Conf. Emerg. Res. Areas Magn. Mach. Drives, AICERA/iCMMD 2014 - Proc.*, 2014, doi: 10.1109/AICERA.2014.6908214.

[67] O. Lopez-Santos, C. A. Jacanamejoy-Jamioy, D. F. Salazar-D’Antonio, J. R. Corredor-Ramirez, G. Garcia, and L. Martinez-Salamero, “A Single-Phase Transformer-Based Cascaded Asymmetric Multilevel Inverter With Balanced Power Distribution,” *IEEE Access*, vol. 7, no. July, pp. 98182–98196, 2019, doi: 10.1109/access.2019.2930230.

[68] Y. Suresh and A. K. Panda, “Investigation on stacked cascade multilevel inverter by employing single-phase transformers,” *Eng. Sci. Technol. an Int. J.*, vol. 19, no. 2, pp. 894–903, 2016, doi: 10.1016/j.jestch.2015.11.008.

[69] S. G. Song, F. S. Kang, and S. J. Park, “Cascaded multilevel inverter employing three-phase transformers and single DC input,” *IEEE Trans. Ind. Electron.*, vol. 56, no. 6, pp. 2005–2014, 2009, doi: 10.1109/TIE.2009.2013846.

[70] J. Lyu, J. Wang, W. Hu, and Y. Yan, “a neutral-point voltage conytroller with hybrid parameters for NPC three-level Grid-connected inverters under unbalanced Grid conditions,” *IEEE J. Emerg. Sel. Top. Power Electron.*, vol. 6777, no. c, pp. 1–1, 2019, doi: 10.1109/jestpe.2019.2930570.

[71] L. He and C. Cheng, “A Flying-Capacitor-Clamped Five-Level Inverter Based on Bridge Modular Switched-Capacitor Topology,” *IEEE Trans. Ind. Electron.*, vol. 63, no. 12, pp. 7814–7822, 2016, doi: 10.1109/TIE.2016.2607155.

[72] X. Wu, C. Xiong, S. Yang, H. Yang, and X. Feng, “A Simplified Space Vector Pulsewidth Modulation Scheme for Three-Phase Cascaded H-Bridge Inverters,” *IEEE Trans. Power Electron.*, vol. 35, no. 4, pp. 4192–4204, 2020, doi: 10.1109/TPEL.2019.2934821.

[73] P. Kant and B. Singh, “A New Three-Phase to Five-Phase Transformer with Power Quality Improvement in Hybrid-Multilevel Inverter Based VCIMD,” *IEEE Trans. Power Deliv.*, vol. 35, no. 2, pp. 871–880, 2020, doi: 10.1109/TPWRD.2019.2930151.

[74] M. N. Raju, J. Sreedevi, R. P. Mandi, and K. S. Meera, “Modular multilevel converters technology: A comprehensive study on its topologies, modelling, control and applications,” *IET Power Electron.*, vol. 12, no. 2, pp. 149–169, 2019, doi: 10.1049/iet-pel.2018.5734.

[75] A. New, C. Osawa, and Y. Matsumoto, “PWM Inverter,” *... 1997., Proc. ...*, vol. I, no. 5, pp. 225–230, 1981, [Online]. Available: http://ieeexplore.ieee.org/xpls/abs_all.jsp?arnumber=645616.

[76] H. Wu, L. Zhu, F. Yang, T. Mu, and H. Ge, “Dual-DC-Port Asymmetrical Multilevel Inverters with Reduced Conversion Stages and Enhanced Conversion Efficiency,” *IEEE Trans. Ind. Electron.*, vol. 64, no. 3, pp. 2081–2091, 2017, doi: 10.1109/TIE.2016.2625772.

[77] M. Sharifzadeh, A. Sheikholeslami, H. Vahedi, H. Ghoreishy, P. A. Labbé, and K. Al-Haddad, “Optimised harmonic elimination modulation extended to four-leg neutral-point-clamped inverter,” *IET Power Electron.*, vol. 9, no. 3, pp. 441–448, 2016, doi: 10.1049/iet-pel.2015.0022.

[78] A. Fri, R. El Bachtiri, and A. El Ghzizal, “A comparative study of three topologies of three-phase (5L) inverter for a PV system,”

Energy Procedia, vol. 42, pp. 436–445, 2013, doi: 10.1016/j.egypro.2013.11.044.

[79] H. Peng *et al.*, "Improved Space Vector Modulation for Neutral-Point Balancing Control in Hybrid-Switch-Based T-Type Neutral-Point-Clamped Inverters With Loss and Common-Mode Voltage Reduction," *CPSS Trans. Power Electron. Appl.*, vol. 4, no. 4, pp. 328–338, 2019, doi: 10.24295/cpsstpea.2019.00031.

[80] T. Proctor, G. Company, Q. Evaluation, A. Press, N. York, and R. Cited, "United States Patent [19]," vol. 38, no. 4, pp. 195–201, 1985.

[81] José Rodríguez, Jih-Sheng Lai, Fang Zheng Peng, "Multilevel Inverters: A Survey of Topologies, Controls, and Applications", *IEEE Trans. on Ind. Electron.*, Vol. 49, No. 4, Aug, 2002.

[82] S. D. G. Jayasinghe, D. M. Vilathgamuwa, and U. K. Madawala, "An analysis on the possibility of using capacitors of a three-level capacitor clamped inverter as power smoothing elements for wind power systems," *IEEE Energy Convers. Congr. Expo. Energy Convers. Innov. a Clean Energy Futur. ECCE 2011, Proc.*, pp. 2963–2970, 2011, doi: 10.1109/ECCE.2011.6064168.

[83] J. S. Lai and F. Z. Peng, "Multilevel converters - A new breed of power converters," *IEEE Trans. Ind. Appl.*, vol. 32, no. 3, pp. 509–517, 1996, doi: 10.1109/28.502161.

[84] A. Bahrami, M. Narimani, M. Norambuena, and J. Rodriguez, "Current Control of a Seven-Level Voltage Source Inverter," *IEEE Trans. Power Electron.*, vol. 35, no. 3, pp. 2308–2316, 2020, doi: 10.1109/TPEL.2019.2926174.

[85] I. R. H. Baker and L. H. Bannister, "United States Patent (19)," no. 19, 1975.

[86] S. B. Veeranna, A. R. Beig, and U. R. Yaragatti, "Performance analysis of PWM strategies for cascaded H-bridge three-level inverter," *2011 IEEE GCC Conf. Exhib. GCC 2011*, pp. 81–84, 2011, doi: 10.1109/IEEEGCC.2011.5752629.

[87] R. Vasu, S. K. Chattopadhyay, and C. Chakraborty, "Asymmetric cascaded H-Bridge multilevel inverter with single DC source per phase," *IEEE Trans. Ind. Electron.*, vol. 67, no. 7, pp. 5398–5409, 2020, doi: 10.1109/TIE.2019.2934080.

[88] J. C. Kartick, B. K. Sujit, and K. C. Suparna, "Dual reference phase shifted pulse width modulation technique for a N-level inverter based grid connected solar photovoltaic system," *IET Renew. Power Gener.*, vol. 10, no. 7, pp. 928–935, 2016, doi: 10.1049/iet-rpg.2015.0393.

[89] A. Sinha, K. Chandra Jana, and M. Kumar Das, "An inclusive review on different multi-level inverter topologies, their modulation and control strategies for a grid connected photo-voltaic system," *Sol. Energy*, vol. 170, no. May, pp. 633–657, 2018, doi: 10.1016/j.solener.2018.06.001.

[90] E. Babaei and S. S. Gowgani, "Hybrid multilevel inverter using switched capacitor units," *IEEE Trans. Ind. Electron.*, vol. 61, no. 9, pp. 4614–4621, 2014, doi: 10.1109/TIE.2013.2290769.

[91] M. Abarzadeh and K. Al-Haddad, "Generalized Circuit Topology of Qn-Hybrid-NPC Multilevel Converter with Novel Decomposed Sensor-Less Modulation Method," *IEEE Access*, vol. 7, pp. 59813–59824, 2019, doi: 10.1109/ACCESS.2019.2913904.

[92] J. Zhang, S. Xu, Z. Din, and X. Hu, "Hybrid multilevel converters: Topologies, evolutions and verifications," *Energies*, vol. 12, no. 4, 2019, doi: 10.3390/en12040615.

[93] P. Lezana, J. Rodriguez, and D. A. Oyarzun, "Cascaded multilevel inverter with regeneration capability and reduced number of switches," *IEEE Trans. Ind. Electron.*, vol. 55, no. 3, pp. 1059–1066, 2008, doi: 10.1109/TIE.2008.917095.

[94] S. Inoue and H. Akagi, "A Bi-directional isolated DC/DC converter as a core circuit of the next-generation medium-voltage power conversion system," *PESC Rec. - IEEE Annu. Power Electron. Spec. Conf.*, vol. 22, no. 2, pp. 535–542, 2006, doi: 10.1109/PESC.2006.1711782.

[95] N. Hatti, K. Hasegawa, and H. Akagi, "A 6.6-kV transformerless motor drive using a five-level diode-clamped PWM inverter for energy savings of pumps and blowers," *IEEE Trans. Power Electron.*, vol. 24, no. 3, pp. 796–803, 2009, doi: 10.1109/TPEL.2008.2008995.

[96] L. Rmili, M. Hamouda, S. Rahmani, and K. Al-Haddad, "Advanced topologies of multilevel matrix converter," *16th Int. Conf. Sci. Tech. Autom. Control Comput. Eng. STA 2015*, no. 1, pp. 599–604, 2016, doi: 10.1109/STA.2015.7505221.

[97] B. P. McGrath, T. Meynard, G. Gateau, and D. G. Holmes, “Optimal modulation of flying capacitor and stacked multicell converters using a state machine decoder,” *IEEE Trans. Power Electron.*, vol. 22, no. 2, pp. 508–516, 2007, doi: 10.1109/TPEL.2006.889932.

[98] M. Ben Smida and F. Ben Ammar, “Modeling and DBC-PSC-PWM control of a three-phase flying-capacitor stacked multilevel voltage source inverter,” *IEEE Trans. Ind. Electron.*, vol. 57, no. 7, pp. 2231–2239, 2010, doi: 10.1109/TIE.2009.2030764.

[99] S. Busquets-Monge, J. Rocabert, P. Rodríguez, S. Alepuz, and J. Bordonau, “Multilevel diode-clamped converter for photovoltaic generators with independent voltage control of each solar array,” *IEEE Trans. Ind. Electron.*, vol. 55, no. 7, pp. 2713–2723, 2008, doi: 10.1109/TIE.2008.924011.

[100] M. M. Renge and H. M. Suryawanshi, “Five-level diode clamped inverter to eliminate common mode voltage and reduce dv/dt in medium voltage rating induction motor drives,” *IEEE Trans. Power Electron.*, vol. 23, no. 4, pp. 1598–1607, 2008, doi: 10.1109/TPEL.2008.925423.

[101] S. Busquets-Monge, S. Alepuz, J. Rocabert, and J. Bordonau, “Pulsewidth Modulations for the Comprehensive Capacitor Voltage Balance of n-Level Three-Leg Diode-Clamped Converters,” *IEEE Trans. Power Electron.*, vol. 24, no. 5, pp. 1364–1375, 2009, doi: 10.1109/TPEL.2009.2016661.

[102] J. Lavieville and G. S. Yvette, “Ika c Tik Tkly,” 1998.

[103] K. Kim, J. Han, and G. Moon, “Number of Switches,” vol. 36, no. 3, pp. 2505–2509, 2021.

[104] M. Lee, C. S. Yeh, and J. S. Lai, “A Hybrid Binary-Cascaded Multilevel Inverter with Simple Floating-Capacitor-Voltage Control,” *IEEE Trans. Power Electron.*, vol. 36, no. 2, pp. 2218–2230, 2021, doi: 10.1109/TPEL.2020.3007122.

[105] S. Pal *et al.*, “A Cascaded Nine-Level Inverter Topology with T-Type and H-Bridge with Increased DC-Bus Utilization,” *IEEE Trans. Power Electron.*, vol. 36, no. 1, pp. 285–294, 2021, doi: 10.1109/TPEL.2020.3002918.

[106] Z. Bin Ibrahim, M. L. Hossain, I. Bin Bugis, N. M. N. Mahadi, A. Shukri, and A. Hasim, “Simulation investigation of SPWM, THIPWM and SVPWM techniques for three phase voltage source inverter,” *Int. J. Power Electron. Drive Syst.*, vol. 4, no. 2, pp. 223–232, 2014, doi: 10.11591/ijpeds.v4i2.5833.

[107] C. Zang, Z. Pei, J. He, T. Guo, J. Zhu, and W. Sun, “Research on the application of CPS-SPWM technology in cascaded multilevel inverter,” *Proc. - 12th Int. Conf. Electr. Mach. Syst. ICEMS 2009*, pp. 8–11, 2009, doi: 10.1109/ICEMS.2009.5382769.

[108] Z. Bin Ibrahim, M. L. Hossain, S. B. Sanusi, N. M. B. N. Mahadi, and A. S. A. Hasim, “Performance of different topologies for three level inverter based on space vector pulse width modulation technique,” *IET Semin. Dig.*, vol. 2014, no. CP659, pp. 1–6, 2014, doi: 10.1049/cp.2014.1490.

[109] G. N. G. Prachi S Dharmadhikari, “Analysis & Hardware Implementation Of Three-Phase Voltage Source Inverter,” *Int. J. Eng. Res. Technol.*, vol. 2(5), no. 5, pp. 2209–2218, 2013.

[110] H. Gupta, A. Yadav, and S. Maurya, “Multi carrier PWM and selective harmonic elimination technique for cascade multilevel inverter,” *Proceeding IEEE - 2nd Int. Conf. Adv. Electr. Electron. Information, Commun. Bio-Informatics, IEEE - AEEICB 2016*, pp. 98–102, 2016, doi: 10.1109/AEEICB.2016.7538405.

[111] I. Colak, R. Bayindir, and E. Kabalci, “A modified harmonic mitigation analysis using Third Harmonic Injection PWM in a multilevel inverter control,” *Proc. EPE-PEMC 2010 - 14th Int. Power Electron. Motion Control Conf.*, pp. 215–220, 2010, doi: 10.1109/EPEPEMC.2010.5606607.

[112] H. Wang *et al.*, “Two-Stage Matrix Converter Based on Third-Harmonic Injection Technique,” *IEEE Trans. Power Electron.*, vol. 31, no. 1, pp. 533–547, 2016, doi: 10.1109/TPEL.2015.2413452.

[113] M. Srndovic, A. Zhetessov, T. Alizadeh, Y. L. Familiant, G. Grandi, and A. Ruderman, “Simultaneous Selective Harmonic Elimination and THD Minimization for a Single-Phase Multilevel Inverter with Staircase Modulation,” *IEEE Trans. Ind. Appl.*, vol. 54, no. 2, pp. 1532–1541, 2018, doi: 10.1109/TIA.2017.2775178.

[114] L. K. Haw, M. S. A. Dahidah, and H. A. F. Almurib, “SHE-PWM cascaded multilevel inverter with adjustable DC voltage levels control for STATCOM applications,” *IEEE Trans. Power Electron.*, vol. 29, no. 12, pp. 6433–6444, 2014, doi: 10.1109/TPEL.2014.2306455.

[115] Y. Deng and R. G. Harley, “Space-vector versus nearest-level pulse width modulation for multilevel converters,” *IEEE Trans. Power Electron.*, vol. 30, no. 6, pp. 2962–2974, 2015, doi: 10.1109/TPEL.2014.2331687.

[116] T. Inverters, “A New Simplified Space – Vector PWM Method for,” *IEEE Trans. Power Electron.*, vol. 16, no. 4, pp. 545–550, 2001, doi: 10.1109/APEC.1999.749730.

[117] M. Trabelsi, L. Ben-Brahim, T. Yokoyama, A. Kawamura, R. Kurosawa, and T. Yoshino, “An improved SVPWM method for multilevel inverters,” *15th Int. Power Electron. Motion Control Conf. Expo. EPE-PEMC 2012 ECCE Eur.*, pp. 1–7, 2012, doi: 10.1109/EPEPEMC.2012.6397476.

[118] M. Gendrin, J. Y. Gauthier, and X. Lin-Shi, “A predictive hybrid pulse-width-modulation technique for active-front-end rectifiers,” *IEEE Trans. Power Electron.*, vol. 32, no. 7, pp. 5487–5496, 2017, doi: 10.1109/TPEL.2016.2612832.

[119] E. Kannapiran, V. K. Chinnaiyan, and M. Gopinath, “A novel space vector pulse width modulation scheme for diode clamped multilevel inverters,” *Proceeding IEEE Int. Conf. Green Comput. Commun. Electr. Eng. ICGCCEE 2014*, pp. 8–14, 2014, doi: 10.1109/ICGCCEE.2014.6922446.

[120] W. Jiang, W. Li, Z. Wu, Y. She, and Z. Tao, “Space-vector pulse-width modulation algorithm for multilevel voltage source inverters based on matrix transformation and including operation in the overmodulation region,” *IET Power Electron.*, vol. 7, no. 12, pp. 2925–2933, 2014, doi: 10.1049/iet-pel.2013.0823.

[121] C. Hu *et al.*, “An Improved Virtual Space Vector Modulation Scheme for Three-Level Active Neutral-Point-Clamped Inverter,” *IEEE Trans. Power Electron.*, vol. 32, no. 10, pp. 7419–7434, 2017, doi: 10.1109/TPEL.2016.2621776.

[122] P. Muthukumar and P. M. Mary, “A co-simulation of random pulse width modulation generation,” *2014 Int. Conf. Circuits, Power Comput. Technol. ICCPCT 2014*, pp. 1296–1301, 2014, doi: 10.1109/ICCPCT.2014.7055033.

[123] M. Paramasivan, M. M. Paulraj, and S. Balasubramanian, “Assorted carrier-variable frequency-random PWM scheme for voltage source inverter,” *IET Power Electron.*, vol. 10, no. 14, pp. 1993–2001, 2017, doi: 10.1049/iet-pel.2016.0580.

[124] J. Rodríguez, L. Morán, P. Correa, and C. Silva, “A vector control technique for medium-voltage multilevel inverters,” *IEEE Trans. Ind. Electron.*, vol. 49, no. 4, pp. 882–888, 2002, doi: 10.1109/TIE.2002.801235.

[125] S. Kouro, R. Bernai, C. Silva, J. Rodríguez, and J. Pontt, “High performance torque and flux control for multilevel inverter fed induction motors,” *IECON Proc. (Industrial Electron. Conf.*, vol. 22, no. 6, pp. 805–810, 2006, doi: 10.1109/IECON.2006.347906.

[126] S. Kouro, J. Rebolledo, and J. Rodríguez, “Reduced switching-frequency-modulation algorithm for high-power multilevel inverters,” *IEEE Trans. Ind. Electron.*, vol. 54, no. 5, pp. 2894–2901, 2007, doi: 10.1109/TIE.2007.905968.

[127] M. Wu, Y. Li, and G. Konstantinou, “A Comprehensive Review of Capacitor Voltage Balancing Strategies for Multilevel Converters Under Selective Harmonic Elimination PWM,” *IEEE Trans. Power Electron.*, vol. 36, no. 3, pp. 1–1, 2020, doi: 10.1109/tpel.2020.3012915.

[128] S. Kouro *et al.*, “Recent advances and industrial applications of multilevel converters,” *IEEE Trans. Ind. Electron.*, vol. 57, no. 8, pp. 2553–2580, 2010, doi: 10.1109/TIE.2010.2049719.

[129] J. Rodríguez, S. Bernet, B. Wu, J. O. Pontt, and S. Kouro, “Multilevel voltage-source-converter topologies for industrial medium-voltage drives,” *IEEE Trans. Ind. Electron.*, vol. 54, no. 6, pp. 2930–2945, 2007, doi: 10.1109/TIE.2007.907044.

[130] P. Acuna, L. Moran, M. Rivera, J. Dixon, and J. Rodriguez, “Improved active power filter performance for renewable power generation systems,” *IEEE Trans. Power Electron.*, vol. 29, no. 2, pp. 687–694, 2014, doi: 10.1109/TPEL.2013.2257854.

[131] M. Carpita, D. Moser, M. Marchesoni, and M. Pellerin, “Multilevel converter for traction applications: Small-scale prototype tests results,” *IEEE Trans. Ind. Electron.*, vol. 55, no. 5, pp. 2203–2212, 2008, doi: 10.1109/TIE.2008.918645.

[132] I. S. Mohamed, S. A. Zaid, M. F. Abu-Elyazeed, and H. M. Elsayed, “Classical methods and model predictive control of three-phase inverter with output LC filter for UPS applications,” *2013 Int. Conf. Control. Decis. Inf. Technol. CoDIT 2013*, no. 1, pp. 483–488, 2013, doi: 10.1109/CoDIT.2013.6689592.

[133] R. José *et al.*, “Multilevel converters: An enabling technology for high-poer applications,” *Proc. IEEE*, vol. 97, no. 11, pp. 1786–1817, 2009, doi: 10.1109/JPROC.2009.2030235.

[134] N. A. Rahim, M. F. M. Elias, and W. P. Hew, “Transistor-clamped H-bridge based cascaded multilevel inverter with new method of capacitor voltage balancing,” *IEEE Trans. Ind. Electron.*, vol. 60, no. 8, pp. 2943–2956, 2013, doi: 10.1109/TIE.2012.2200213.

[135] Y. M. Alharbi, A. M. S. Yunus, and A. A. Siada, “Application of UPFC to improve the LVRT capability of wind turbine generator,” *2012 22nd Australas. Univ. Power Eng. Conf. "Green Smart Grid Syst. AUPEC 2012*, pp. 11–14, 2012, doi: 10.12720/ijoee.1.4.188-193.

[136] A. F. Abdou, A. Abu-Siada, and H. R. Pota, “Application of a STATCOM for damping subsynchronous oscillations and transient stability improvement,” *2011 21st Australas. Univ. Power Eng. Conf. AUPEC 2011*, pp. 1–5, 2011.

[137] M. F. M. Elias, N. A. Rahim, H. W. Ping, and M. N. Uddin, “Asymmetrical cascaded multilevel inverter based on transistor-clamped H-bridge power cell,” *IEEE Trans. Ind. Appl.*, vol. 50, no. 6, pp. 4281–4288, 2014, doi: 10.1109/TIA.2014.2346711.

[138] V. Vivek and S. Krishnakumar, “Cascaded multilevel H-Bridge inverter based DSTATCOM for voltage compensation,” *2014 Int. Conf. Comput. Power, Energy, Inf. Commun. ICCPEIC 2014*, pp. 348–352, 2014, doi: 10.1109/ICCPEIC.2014.6915388.

[139] Y. M. Alharbi, A. M. Shiddiq Yunus, and A. Abu-Siada, “Application of STATCOM to improve the high-voltage-ride-through capability of wind turbine generator,” *2011 IEEE PES Innov. Smart Grid Technol. ISGT Asia 2011 Conf. Smarter Grid Sustain. Afford. Energy Futur.*, pp. 6–10, 2011, doi: 10.1109/ISGT-Asia.2011.6167138.

[140] A. F. Abdou, A. Abu-Siada, and H. R. Pota, “Damping of subsynchronous oscillations and improve transient stability for wind farms,” *2011 IEEE PES Innov. Smart Grid Technol. ISGT Asia 2011 Conf. Smarter Grid Sustain. Afford. Energy Futur.*, pp. 1–6, 2011, doi: 10.1109/ISGT-Asia.2011.6167077.

[141] D. Sankar and C. A. Babu, “Cascaded H bridge multilevel inverter topologies for PV application: A comparison,” *Proc. IEEE Int. Conf. Circuit, Power Comput. Technol. ICCPCT 2016*, 2016, doi: 10.1109/ICCPCT.2016.7530140.

[142] R. Singh and J. Nakka, “Design, simulation and performance analysis of Fuel Cell based energy system with Cascaded H-Bridge Multilevel Inverter,” *1st IEEE Int. Conf. Power Electron. Intell. Control Energy Syst. ICPEICES 2016*, no. 2, pp. 9–14, 2017, doi: 10.1109/ICPEICES.2016.7853308.

[143] J. Amini and M. Moallem, “A capacitor voltage balancing method for cascaded H-bridge multilevel inverters with application to FACTS,” *IECON Proc. (Industrial Electron. Conf.*, pp. 6447–6452, 2016, doi: 10.1109/IECON.2016.7793653.

[144] B. P. Kadu and J. A. Khobragade, “Investigation of cascaded H-Bridge multilevel Inverter as Distribution Static Compensator in Power System for compensation of reactive power and harmonics,” *Int. Conf. Energy Syst. Appl. ICESA 2015*, no. Icesa, pp. 432–436, 2016, doi: 10.1109/ICESA.2015.7503386.

[145] S. Allebrod, R. Hamerski, and R. Marquardt, “New T ransformerless , S calable Modular Mu l tilevel Converters for HVDC- T ransmission,” pp. 174–179, 2008.

[146] S. Daher, J. Schmid, and F. L. M. Antunes, “Multilevel inverter topologies for stand-alone PV systems,” *IEEE Trans. Ind. Electron.*, vol. 55, no. 7, pp. 2703–2712, 2008, doi: 10.1109/TIE.2008.922601.

[147] R. González, E. Gubía, J. López, and L. Marroyo, “Transformerless Single-Phase Multilevel-Based,” vol. 55, no. 7, pp. 2694–2702, 2008.

[148] E. Ozdemir, S. Ozdemir, and L. M. Tolbert, “Fundamental-frequency-modulated six-level diode-clamped multilevel inverter for three-phase stand-alone photovoltaic system,” *IEEE Trans. Ind. Electron.*, vol. 56, no. 11, pp. 4407–4415, 2009, doi: 10.1109/TIE.2008.928096.

[149] T. Kerekes, R. Teodorescu, M. Liserre, C. Klumpner, and M. Sumner, “Evaluation of three-phase transformerless photovoltaic inverter topologies,” *IEEE Trans. Power Electron.*, vol. 24, no. 9, pp. 2202–2211, 2009, doi: 10.1109/TPEL.2009.2020800.

[150] F. S. Kang, S. J. Park, S. E. Cho, C. U. Kim, and T. Ise, “Multilevel PWM inverters suitable for the use of stand-alone photovoltaic power systems,” *IEEE Trans. Energy Convers.*, vol. 20, no. 4, pp. 906–915, 2005, doi: 10.1109/TEC.2005.847956.

[151] E. Villanueva, P. Correa, J. Rodriguez, and M. Pacas, “Control of a single-phase cascaded H-bridge multilevel inverter for grid-connected photovoltaic systems,” *IEEE Trans. Ind. Electron.*, vol. 56, no. 11, pp. 4399–4406, 2009, doi: 10.1109/TIE.2009.2029579.

[152] G. Grandi, C. Rossi, D. Ostojic, and D. Casadei, “A new multilevel conversion structure for grid-connected PV applications,” *IEEE Trans. Ind. Electron.*, vol. 56, no. 11, pp. 4416–4426, 2009, doi: 10.1109/TIE.2009.2029587.

[153] J. Selvaraj and N. A. Rahim, “Multilevel Inverter For Grid-Connected PV System Employing Digital PI Controller,” *IEEE Trans. Ind. Electron.*, vol. 56, no. 1, pp. 149–158, 2009, doi: 10.1109/TIE.2008.928116.

[154] S. Mariethoz, “Systematic design of high-performance hybrid cascaded multilevel inverters with active voltage balance and minimum switching losses,” *IEEE Trans. Power Electron.*, vol. 28, no. 7, pp. 3100–3113, 2013, doi: 10.1109/TPEL.2012.2222446.

[155] S. Mekhilef and M. N. Abdul Kadir, “Novel vector control method for three-stage hybrid cascaded multilevel inverter,” *IEEE Trans. Ind. Electron.*, vol. 58, no. 4, pp. 1339–1349, 2011, doi: 10.1109/TIE.2010.2049716.

[156] N. Sandeep and U. R. Yaragatti, “Simplified hybrid nine-level stacked multiceli converter with reduced part count for grid-connected applications,” *Asia-Pacific Power Energy Eng. Conf. APPEEC*, vol. 2017-Novem, pp. 1–6, 2018, doi: 10.1109/APPEEC.2017.8308984.

[157] K. Gnanasambandam, A. K. Rathore, A. Edpuganti, D. Srinivasan, and J. Rodriguez, “Current-Fed Multilevel Converters: An Overview of Circuit Topologies, Modulation Techniques, and Applications,” *IEEE Trans. Power Electron.*, vol. 32, no. 5, pp. 3382–3401, 2017, doi: 10.1109/TPEL.2016.2585576.

[158] M. S. Tahir, J. Xu, and Y. Wang, “Point-Clamping Inverter for Low and Medium Power Applications,” pp. 1949–1953, 2017.

[159] S. S. Priyan and K. Ramani, “Implementation of closed loop system for flying capacitor multilevel inverter with stand-alone Photovoltaic input,” *Proc. 2013 Int. Conf. Power, Energy Control. ICPEC 2013*, pp. 281–286, 2013, doi: 10.1109/ICPEC.2013.6527666.

[160] J. Rodriguez *et al.*, “Design and evaluation criteria for high power drives,” *Conf. Rec. - IAS Annu. Meet. (IEEE Ind. Appl. Soc.*, pp. 1–9, 2008, doi: 10.1109/08IAS.2008.341.

[161] D. Krug, S. Bernet, and S. S. Fazel, “Converters for Industrial Medium-Voltage Drives,” *IEEE Trans. Ind. Electron.*, vol. 54, no. 6, pp. 2979–2992, 2007.

[162] S. S. Fazel, S. Bernet, D. Krug, and K. Jalili, “Design and comparison of 4-kV neutral-point-clamped, flying-capacitor, and series-connected H-bridge multilevel converters,” *IEEE Trans. Ind. Appl.*, vol. 43, no. 4, pp. 1032–1040, 2007, doi: 10.1109/TIA.2007.900476.

[163] A. Ruderman, “About voltage total harmonic distortion for single- and three-phase multilevel inverters,” *IEEE Trans. Ind. Electron.*, vol. 62, no. 3, pp. 1548–1551, 2015, doi: 10.1109/TIE.2014.2341557.

[164] B. Rajesh and Manjesh, “Comparison of harmonics and THD suppression with three and 5 level multilevel inverter-cascaded H-bridge,” *Proc. IEEE Int. Conf. Circuit, Power Comput. Technol. ICCPCT 2016*, pp. 9–14, 2016, doi: 10.1109/ICCPCT.2016.7530116.

[165] J. He, R. Katebi, N. Weise, N. A. O. Demerdash, and L. Wei, “A Fault-Tolerant T-Type Multilevel Inverter Topology with Increased Overload Capability and Soft-Switching Characteristics,” *IEEE Trans. Ind. Appl.*, vol. 53, no. 3, pp. 2826–2839, 2017, doi: 10.1109/TIA.2017.2665630.

[166] K. Ma, H. Wang, and F. Blaabjerg, “New Approaches to Reliability Assessment,” *IEEE Power Electron. Mag.*, vol. 3, no. December, p. 13, 2016, doi: 10.1109/MPEL.2016.2615277.

[167] H. Soliman, H. Wang, and F. Blaabjerg, “A Review of the Condition Monitoring of Capacitors in Power Electronic Converters,” *IEEE Trans. Ind. Appl.*, vol. 52, no. 6, pp. 4976–4989, 2016, doi: 10.1109/TIA.2016.2591906.

[168] A. R. Biswas and R. Giaffreda, “IoT and cloud convergence: Opportunities and challenges,” *2014 IEEE World Forum Internet Things, WF-IoT 2014*, pp. 375–376, 2014, doi: 10.1109/WF-IoT.2014.6803194.

[169] M. Angel, L. Peña, and D. D. S. I. E. T. S. I. S. I, “SAT-IoT : An Architectural Model for a High- Performance Fog / Edge / Cloud IoT Platform,” pp. 633–638, 2020.

[170] S. Wang, Y. Hou, F. Gao, and X. Ji, “A novel IoT access architecture for vehicle monitoring system,” *2016 IEEE 3rd World Forum Internet Things, WF-IoT 2016*, pp. 639–642, 2017, doi: 10.1109/WF-IoT.2016.7845396.

[171] A. K. Gupta and R. Johari, “IOT based Electrical Device Surveillance and Control System,” *Proc. - 2019 4th Int. Conf. Internet Things Smart Innov. Usages, IoT-SIU 2019*, pp. 1–5, 2019, doi: 10.1109/IoT-SIU.2019.8777342.

[172] B. Hahn and M. Durstewitz, “Reliability of wind turbines - Experiences of 15 years with 1500 WTs,” *EUROMECH Colloq. 464b Wind Energy*, 2005, [Online].

[173] H. Malik and S. Mishra, “Artificial neural network and empirical mode decomposition based imbalance fault diagnosis of wind turbine using TurbSim, FAST and Simulink,” *IET Renew. Power Gener.*, vol. 11, no. 6, pp. 889–902, 2017, doi: 10.1049/iet-rpg.2015.0382.

[174] J. Zeng, D. Lu, Y. Zhao, Z. Zhang, W. Qiao, and X. Gong, “Wind turbine fault detection and isolation using support vector machine and a residual-based method,” *Proc. Am. Control Conf.*, pp. 3661–3666, 2013, doi: 10.1109/acc.2013.6580398.

[175] J. Helander, A. Ericsson, M. Gustafsson, T. Martin, D. Sjoberg, and C. Larsson, “Compressive Sensing Techniques for mm-Wave Nondestructive Testing of Composite Panels,” *IEEE Trans. Antennas Propag.*, vol. 65, no. 10, pp. 5523–5531, 2017, doi: 10.1109/TAP.2017.2738034.

[176] A. Salem, A. Abu-Siada, and S. Islam, “Improved condition monitoring technique for wind turbine gearbox and shaft stress detection,” *IET Sci. Meas. Technol.*, vol. 11, no. 4, pp. 431–437, 2017, doi: 10.1049/iet-smt.2016.0338.

[177] O. Blancke, A. Merkhouf, N. Amyot, J. Pedneault-Desroches, C. Hudon, and K. Haddad, “Strategic fault diagnosis approach for hydrogenerator shaft current discharges,” *Proc. - 2016 22nd Int. Conf. Electr. Mach. ICEM 2016*, pp. 2346–2351, 2016, doi: 10.1109/ICELMACH.2016.7732849.

[178] M. H. Marzebali, S. H. Kia, H. Henao, G. A. Capolino, and J. Faiz, “Planetary Gearbox Torsional Vibration Effects on Wound-Rotor Induction Generator Electrical Signatures,” *IEEE Trans. Ind. Appl.*, vol. 52, no. 6, pp. 4770–4780, 2016, doi: 10.1109/TIA.2016.2600599.

[179] X. Wu, Y. Li, F. Li, Z. Yang, and W. Teng, “Adaptive estimation-based leakage detection for a wind turbine hydraulic pitching system,” *IEEE/ASME Trans. Mechatronics*, vol. 17, no. 5, pp. 907–914, 2012, doi: 10.1109/TMECH.2011.2142400.

[180] L. Wang and C. Wen, “Fault diagnosis of wind turbine blade based on robust residual error design,” *Proc. 28th Chinese Control Decis. Conf. CCDC 2016*, pp. 574–577, 2016, doi: 10.1109/CCDC.2016.7531051.

[181] M. Entezami, S. Hillmansen, P. Weston, and M. P. Papaelias, “Fault detection and diagnosis within a wind turbine mechanical braking system using condition monitoring,” *Renew. Energy*, vol. 47, pp. 175–182, 2012, doi: 10.1016/j.renene.2012.04.031.

[182] G. Kilic and M. S. Unluturk, “Testing of wind turbine towers using wireless sensor network and accelerometer,” *Renew. Energy*, vol. 75, pp. 318–325, 2015, doi: 10.1016/j.renene.2014.10.010.

[183] W. Yucai and L. Yonggang, “Diagnosis of Short Circuit Faults Within Turbogenerator Excitation Winding Based on the Expected Electromotive Force Method,” *IEEE Trans. Energy Convers.*, vol. 31, no. 2, pp. 706–713, 2016, doi: 10.1109/TEC.2016.2521422.

[184] S. Djurovic, S. Williamson, P. J. Tavner, and W. Yang, “Condition monitoring artefacts for detecting winding faults in wind turbine DFIGs,” *Eur. Wind Energy Conf. Exhib. 2009, EWEC 2009*, vol. 1, no. April, pp. 491–512, 2009.

[185] H. Wang, M. Liserre, and F. Blaabjerg, “Toward reliable power electronics: Challenges, design tools, and opportunities,” *IEEE Ind. Electron. Mag.*, vol. 7, no. 2, pp. 17–26, 2013, doi: 10.1109/MIE.2013.2252958.

[186] J. Ribrant and L. Bertling, “Survey of failures in wind power systems with focus on Swedish wind power plants during 1997-2005,” *2007 IEEE Power Eng. Soc. Gen. Meet. PES*, vol. 22, no. 1, pp. 167–173, 2007, doi: 10.1109/PES.2007.386112.

[187] P. Mawby, P. McKeever, S. Konaklieva, and L. Ran, “Condition Monitoring of Power Electronics for Offshore Wind,” *Eng. Technol. Ref.*, no. September 2018, 2014, doi: 10.1049/etr.2014.0004.

[188] R. B. Sepe, C. Morrison, and J. M. Miller, “Fault-tolerant operation of induction motor drives with automatic Controller Reconfiguration,” *J. Fail. Anal. Prev.*, vol. 3, no. 1, pp. 64–70, 2003, doi: 10.1361/15298150377035141 8.

[189] M. Bourogaoui, H. Berriri, H. Ben Attia-Sethom, and I. Slama-Belkhodja, “Wavelets and parity equations methods comparison for faulty encoder detection in PMSM drives,” *Int. Multi-Conference Syst. Signals Devices, SSD’11 - Summ. Proc.*, no. 1, 2011, doi: 10.1109/SSD.2011.5767497.

[190] J. Wang, Y. Peng, and W. Qiao, “Current-Aided Order Tracking of Vibration Signals for Bearing Fault Diagnosis of Direct-Drive Wind Turbines,” *IEEE Trans. Ind. Electron.*, vol. 63, no. 10, pp. 6336–6346, 2016, doi: 10.1109/TIE.2016.2571258.

[191] P. Caselitz and J. Giebhardt, “Rotor condition monitoring for improved operational safety of offshore wind energy converters,” *J. Sol. Energy Eng. Trans. ASME*, vol. 127, no. 2, pp. 253–261, 2005, doi: 10.1115/1.1850485.

[192] J. W. He, M Y; Hutchinson, *Fundamentals for Remote Structural Health Monitoring of Wind Turbine Blades – a Preproject*, vol. 111, no. May. 1989.

[193] W. Yang, Z. Peng, K. Wei, and W. Tian, “Structural health monitoring of composite wind turbine blades: Challenges, issues and potential solutions,” *IET Renew. Power Gener.*, vol. 11, no. 4, pp. 411–416, 2017, doi: 10.1049/iet-rpg.2016.0087.

[194] B. Lu, Y. Li, X. Wu, and Z. Yang, “A review of recent advances in wind turbine condition monitoring and fault diagnosis,” *2009 IEEE Power Electron. Mach. Wind Appl. PEMWA 2009*, 2009, doi: 10.1109/PEMWA.2009.5208325.

[195] W. Yang, Z. Lang, and W. Tian, “Condition Monitoring and Damage Location of Wind Turbine Blades by Frequency Response Transmissibility Analysis,” *IEEE Trans. Ind. Electron.*, vol. 62, no. 10, pp. 6558–6564, 2015, doi: 10.1109/TIE.2015.2418738.

[196] J. W. He, M Y; Hutchinson, *Fundamentals for Remote Structural Health Monitoring of Wind Turbine Blades – a Preproject Annex B – Sensors and Non-Destructive Testing Methods for Damage Detection in Wind Turbine Blades Fundamentals for Remote Structural Health Monitoring of Wind Turbi*, vol. 111, no. May. 1989.

[197] M. R. Wilkinson, F. Spinato, and P. J. Tavner, “Condition monitoring of generators & other subassemblies in wind turbine drive trains,” *2007 IEEE Int. Symp. Diagnostics Electr. Mach. Power Electron. Drives, SDEMPED*, pp. 388–392, 2007, doi: 10.1109/DEMPED.2007.4393125.

[198] A. S. Zaher and S. D. J. McArthur, “A multi-agent fault detection system for wind turbine defect recognition and diagnosis,” *2007 IEEE Lausanne POWERTECH, Proc.*, pp. 22–27, 2007, doi: 10.1109/PCT.2007.4538286.

[199] Y. Qiu, Y. Feng, J. Sun, W. Zhang, and D. Infield, “Applying thermophysics for wind turbine drivetrain fault diagnosis using SCADA data,” *IET Renew. Power Gener.*, vol. 10, no. 5, pp. 661–668, 2016, doi: 10.1049/iet-rpg.2015.0160.

[200] Y. Qiu, W. Zhang, M. Cao, Y. Feng, and D. Infield, “An electro-thermal analysis of a variable-speed doubly-fed induction generator in a wind turbine,” *Energies*, vol. 8, no. 5, pp. 3386–3402, 2015, doi: 10.3390/en8053386.

[201] D. Astolfi, F. Castellani, and L. Terzi, “Fault prevention and diagnosis through SCADA temperature data analysis of an onshore wind farm,” *Diagnostyka*, vol. 15, no. 2, pp. 71–78, 2014.

[202] P. Sun, J. Li, C. Wang, and X. Lei, “A generalized model for wind turbine anomaly identification based on SCADA data,” *Appl. Energy*, vol. 168, pp. 550–567, 2016, doi: 10.1016/j.apenergy.2016.01.133.

[203] S. Sheng, “Investigation of oil conditioning, real-time monitoring and oil sample analysis for wind turbine gearboxes,” *Am. Wind Energy Assoc. Proj. Perform. Reliab. Work.*, 2011, [Online]. Available: http://www.nrel.gov/docs/fy11osti/50301.pdf.

[204] S. Savazzi, V. Rampa, and U. Spagnolini, “Wireless cloud networks for the factory of things: Connectivity modeling and layout design,” *IEEE Internet Things J.*, vol. 1, no. 2, pp. 180–195, 2014, doi: 10.1109/JIOT.2014.2313459.

[205] W. Liu, B. Tang, and Y. Jiang, “Status and problems of wind turbine structural health monitoring techniques in China,” *Renew. Energy*, vol. 35, no. 7, pp. 1414–1418, 2010, doi: 10.1016/j.renene.2010.01.006.

[206] L. M. Popa, B. B. Jensen, E. Ritchie, and I. Boldea, “Condition Monitoring of Wind Generators,” *Conf. Rec. - IAS Annu. Meet. (IEEE Ind. Appl. Soc.*, vol. 3, no. November, pp. 1839–1846, 2003, doi: 10.1109/ias.2003.1257819.

[207] O. Bennouna, N. Héraud, H. Camblong, and M. Rodriguez, “Diagnosis of the doubly-fed induction generator of a wind turbine,” *Wind Eng.*, vol. 29, no. 5, pp. 431–448, 2005, doi: 10.1260/030952405775992607.

[208] W. Yang, P. J. Tavner, C. J. Crabtree, and M. Wilkinson, “Research on a simple, cheap but globally effective condition monitoring technique for wind turbines,” *Proc. 2008 Int. Conf. Electr. Mach. ICEM’08*, pp. 1–5, 2008, doi: 10.1109/ICELMACH.2008.4799902.

[209] D. Lu, W. Qiao, and X. Gong, “Current-Based Gear Fault Detection for Wind Turbine Gearboxes,” *IEEE Trans. Sustain. Energy*,

vol. 8, no. 4, pp. 1453–1462, 2017, doi: 10.1109/TSTE.2017.2690835.

[210] L. Trilla, J. Pegueroles, J. Urresty, C. Muniz, and O. Gomis-Bellmunt, “Generator Short-Circuit Torque Compensation in Multichannel Wind Turbines,” *IEEE Trans. Ind. Electron.*, vol. 64, no. 11, pp. 8790–8798, 2017, doi: 10.1109/TIE.2017.2650870.

[211] W. Q. Jeffries, J. A. Chambers, and D. G. Infield, “Experience with bicoherence of electrical power for condition monitoring of wind turbine blades,” *IEE Proc. Vision, Image Signal Process.*, vol. 145, no. 3, pp. 141–148, 1998, doi: 10.1049/ip-vis:19982013.

[212] S. Watson and J. Xiang, “Real-time condition monitoring of offshore wind turbines,” *Eur. Wind Energy Conf. Exhib. 2006, EWEC 2006*, vol. 2, pp. 1733–1741, 2006.

[213] G. Qingding, “Turbine Based on the Neural Networks,” pp. 2007–2010, 2007.

[214] R. Khan, S. U. Khan, R. Zaheer, and S. Khan, “Future internet: The internet of things architecture, possible applications and key challenges,” *Proc. - 10th Int. Conf. Front. Inf. Technol. FIT 2012*, pp. 257–260, 2012, doi: 10.1109/FIT.2012.53.

[215] N. Pazos, M. Muller, M. Aeberli, and N. Ouerhani, “ConnectOpen - Automatic integration of IoT devices,” *IEEE World Forum Internet Things, WF-IoT 2015 - Proc.*, pp. 640–644, 2015, doi: 10.1109/WF-IoT.2015.7389129.

[216] Y. Benazzouz, C. Munilla, O. Gunalp, M. Gallissot, and L. Gurgen, “Sharing user IoT devices in the cloud,” *2014 IEEE World Forum Internet Things, WF-IoT 2014*, pp. 373–374, 2014, doi: 10.1109/WF-IoT.2014.6803193.

[217] L. Calderoni, A. Magnani, and D. Maio, “Iot manager: A case study of the design and implementation of an open source iot platform,” *IEEE 5th World Forum Internet Things, WF-IoT 2019 - Conf. Proc.*, pp. 749–754, 2019, doi: 10.1109/WF-IoT.2019.8767304.

[218] L. Salman *et al.*, “Energy efficient IoT-based smart home,” *2016 IEEE 3rd World Forum Internet Things, WF-IoT 2016*, pp. 526–529, 2017, doi: 10.1109/WF-IoT.2016.7845449.

[219] J. E. Siegel, S. Kumar, and S. E. Sarma, “The future internet of things: Secure, efficient, and model-based,” *IEEE Internet Things J.*, vol. 5, no. 4, pp. 2386–2398, 2018, doi: 10.1109/JIOT.2017.2755620.

[220] C. H. Li, K. W. Lao, and K. W. Tam, “A flooding warning system based on RFID tag array for energy facility,” *RFID-TA 2018 - 2018 IEEE Int. Conf. RFID Technol. Appl.*, pp. 7–10, 2018, doi: 10.1109/RFID-TA.2018.8552767.

[221] S. Singh and N. Singh, “Business Opportunities & Reference Architecture for E-commerce,” *Ieee*, pp. 1577–1581, 2015.

[222] J. Sun, S. Li, Q. Zhou, Y. Su, and Y. Fu, “Exploration and Research of Internet of Things Architecture Based on Fractal Theory,” *Proc. 2018 5th IEEE Int. Conf. Cloud Comput. Intell. Syst. CCIS 2018*, pp. 187–192, 2019, doi: 10.1109/CCIS.2018.8691200.

[223] C. Le Zhong, Z. Zhu, and R. G. Huang, “Study on the IOT architecture and gateway technology,” *Proc. - 14th Int. Symp. Distrib. Comput. Appl. Business, Eng. Sci. DCABES 2015*, pp. 196–199, 2016, doi: 10.1109/DCABES.2015.56.

[224] J. Guth, U. Breitenbucher, M. Falkenthal, F. Leymann, and L. Reinfurt, “Comparison of IoT platform architectures: A field study based on a reference architecture,” *2016 Cloudification Internet Things, CIoT 2016*, pp. 3–8, 2017, doi: 10.1109/CIOT.2016.7872918.

[225] C. Sharma, S. Mata, and V. Devi, “Constrained IoT Systems,” *2018 3rd Int. Conf. Internet Things Smart Innov. Usages*, pp. 1–6, 2018, doi: 10.1109/IoT-SIU.2018.8519904.

[226] A. H. Ngu, M. Gutierrez, V. Metsis, S. Nepal, and Q. Z. Sheng, “IoT Middleware: A Survey on Issues and Enabling Technologies,” *IEEE Internet Things J.*, vol. 4, no. 1, pp. 1–20, 2017, doi: 10.1109/JIOT.2016.2615180.

[227] F. Mutlu, M. A. Demir, and O. Ergul, “Improved Fonts for Chipless Radio-Frequency-Identification Tags Based on Letters,” *Mediterr. Microw. Symp.*, vol. 2018-Octob, pp. 247–250, 2019, doi: 10.1109/MMS.2018.8611948.

[228] M. Taouzari, A. Mouhsen, J. El Aoufi, H. Nasraoui, and O. El Mrabat, “Miniaturized design of passive ultra-high frequency Radio Frequency Identification tag,” *Proc. 14th Conf. Microw. Tech. Com. 2015*, no. 4, pp. 9–11, 2015, doi: 10.1109/COMITE.2015.7120231.

[229] J. Zheng, D. Simplot-Ryl, C. Bisdikian, and H. T. Mouftah, “The internet of things,” *IEEE Commun. Mag.*, vol. 49, no. 11, pp. 30–31, 2011, doi: 10.1109/MCOM.2011.6069706.

[230] Y. Liao, E. de Freitas Rocha Loures and F. Deschamps, "Industrial Internet of Things: A Systematic Literature Review and Insights," *IEEE Internet of Things Journal*, vol. 5, no. 6, pp. 4515-4525, Dec. 2018.

[231] G. Zhao, L. Lin, Y. Chen, S. Liu, J. Chu, and Z. Luo, "Barcode character defect detection method based on Tesseract-OCR," *2017 3rd IEEE Int. Conf. Comput. Commun. ICCC 2017*, vol. 2018-Janua, pp. 1767–1771, 2018, doi: 10.1109/CompComm.2017.8322843.

[232] N. Guo, X. Wang, Z. Wang, and J. Zhu, "GBVS Based 1D and 2D Barcodes Localization in Complex Scene," *Proc. - 2015 Int. Conf. Comput. Intell. Commun. Networks, CICN 2015*, pp. 352–356, 2016, doi: 10.1109/CICN.2015.76.

[233] M. R. Palattella *et al.*, "Standardized protocol stack for the internet of (important) things," *IEEE Commun. Surv. Tutorials*, vol. 15, no. 3, pp. 1389–1406, 2013, doi: 10.1109/SURV.2012.111412.00158.

[234] O. Horyachyy, "Comparison of Wireless Communication Technologies used in a Smart Home: Analysis of wireless sensor node based on Arduino in home automation scenario," no. June, p. 73, 2017, [Online]. Available: http://bth.diva-portal.org/smash/get/diva2:1118965/FULLTEXT02.pdf%0Ahttp://urn.kb.se/resolve?urn=urn:nbn:se:bth-14845.

[235] A. R. Jiménez and F. Seco, "Finding objects using UWB or BLE localization technology: A museum-like use case," *2017 Int. Conf. Indoor Position. Indoor Navig. IPIN 2017*, vol. 2017-Janua, no. September, pp. 1–8, 2017, doi: 10.1109/IPIN.2017.8115865.

[236] E. Khorov, A. Lyakhov, I. Nasedkin, and R. Yusupov, "Poster: Fast and reliable alert delivery in Wi-Fi HaLow sensor networks," *2019 IFIP Netw. Conf. IFIP Netw. 2019*, vol. 2019-Janua, 2019, doi: 10.23919/IFIPNetworking46909.2019.8999405.

[237] H. Su and S. Moh, "Comparative performance study of localization schemes in wireless sensor networks," *Int. J. Smart Home*, vol. 8, no. 1, pp. 95–102, 2014, doi: 10.14257/ijsh.2014.8.1.10.

[238] G. Pan, J. He, Q. Wu, R. Fang, J. Cao, and D. Liao, "Automatic stabilization of Zigbee network," *2018 Int. Conf. Artif. Intell. Big Data, ICAIBD 2018*, pp. 224–227, 2018, doi: 10.1109/ICAIBD.2018.8396199.

[239] R. P. Antonioli, M. Roff, Z. Sheng, J. Liu, and V. C. M. Leung, "A real-time MAC protocol for in-vehicle power line communications based on HomePlug GP," *IEEE Veh. Technol. Conf.*, vol. 2015, 2015, doi: 10.1109/VTCSpring.2015.7145642.

[240] M. Weyn, G. Ergeerts, R. Berkvens, B. Wojciechowski, and Y. Tabakov, "DASH7 alliance protocol 1.0: Low-power, mid-range sensor and actuator communication," *2015 IEEE Conf. Stand. Commun. Networking, CSCN 2015*, pp. 54–59, 2016, doi: 10.1109/CSCN.2015.7390420.

[241] A. J. Prawira, M. Abdurohman, and A. G. Putrada, "An Analysis on RPL Routing over IPv6 WSN Mobility and Transmission Range," *Proceeding - 2019 Int. Symp. Electron. Smart Devices, ISESD 2019*, pp. 8–12, 2019, doi: 10.1109/ISESD.2019.8909501.

[242] R. J. Tom, S. Sankaranarayanan, V. H. C. De Albuquerque, and J. J. P. C. Rodrigues, "Aggregator based RPL for an IoT-fog based power distribution system with 6LoWPAN," *China Commun.*, vol. 17, no. 1, pp. 104–117, 2020, doi: 10.23919/JCC.2020.01.008.

[243] B. T. Mi, X. Liang, and S. Sen Zhang, "A Survey on Social Internet of Things," *Jisuanji Xuebao/Chinese J. Comput.*, vol. 41, no. 7, pp. 1448–1475, 2018, doi: 10.11897/SP.J.1016.2018.01448.

[244] C. Mahmoud and S. Aouag, "Security for internet of things: A state of the art on existing protocols and open research issues," *ACM Int. Conf. Proceeding Ser.*, vol. 17, no. 3, pp. 1294–1312, 2019, doi: 10.1145/3361570.3361622.

[245] M. B. Yassein, M. Q. Shatnawi, and D. Al-Zoubi, "Application layer protocols for the Internet of Things: A survey," *Proc. - 2016 Int. Conf. Eng. MIS, ICEMIS 2016*, pp. 16–19, 2016, doi: 10.1109/ICEMIS.2016.7745303.

[246] S. Il Choi and S. J. Koh, "Use of Proxy Mobile IPv6 for Mobility Management in CoAP-Based Internet-of-Things Networks," *IEEE Commun. Lett.*, vol. 20, no. 11, pp. 2284–2287, 2016, doi: 10.1109/LCOMM.2016.2601318.

[247] O. Sadio, I. Ngom, and C. Lishou, "Lightweight Security Scheme for MQTT/MQTT-SN Protocol," *2019 6th Int. Conf. Internet Things Syst. Manag. Secur. IOTSMS 2019*, pp. 119–123, 2019, doi: 10.1109/IOTSMS48152.2019.8939177.

[248] M. H. Amaran, N. A. M. Noh, M. S. Rohmad, and H. Hashim, "A Comparison of Lightweight Communication Protocols in Robotic Applications," *Procedia Comput. Sci.*, vol. 76, no. Iris, pp. 400–405, 2015, doi: 10.1016/j.procs.2015.12.318.

[249] E. S. Llamuca, C. A. Garcia, J. E. Naranjo, and M. V. Garcia, "Cyber-physical production systems for industrial shop-floor

integration based on AMQP," *Proc. - 2019 Int. Conf. Inf. Syst. Softw. Technol. ICI2ST 2019*, pp. 48–54, 2019, doi: 10.1109/ICI2ST.2019.00014.

[250] A. Lavrenovs and F. J. R. Melón, "HTTP security headers analysis of top one million websites," *Int. Conf. Cyber Conflict, CYCON*, vol. 2018-May, pp. 345–370, 2018, doi: 10.23919/CYCON.2018.8405025.

[251] S. Mijovic, E. Shehu, and C. Buratti, "Comparing application layer protocols for the Internet of Things via experimentation," *2016 IEEE 2nd Int. Forum Res. Technol. Soc. Ind. Leveraging a Better Tomorrow, RTSI 2016*, 2016, doi: 10.1109/RTSI.2016.7740559.

[252] P. Koetket, T. Chaichana, Y. Auttawaitkul, W. Chiracharit, S. Khunkhet, and J. Waewsak, "Increasing efficiency in wind energy electricity generating by signal processing from wind measuring equipment on wind turbine for the determination of wind direction," *2018 Int. Work. Adv. Image Technol. IWAIT 2018*, pp. 1–4, 2018, doi: 10.1109/IWAIT.2018.8369735.

[253] T. Syskakis and M. Ordonez, "MPPT for small wind turbines: Zero-oscillation sensorless strategy," *PEDG 2019 - 2019 IEEE 10th Int. Symp. Power Electron. Distrib. Gener. Syst.*, pp. 1060–1065, 2019, doi: 10.1109/PEDG.2019.8807734.

[254] O. A. Morfin *et al.*, "Maximum wind energy capture in a wind system using a doubly-fed induction generator," *2018 IEEE Int. Autumn Meet. Power, Electron. Comput. ROPEC 2018*, no. Ropec, 2019, doi: 10.1109/ROPEC.2018.8661374.

[255] A. S. Kumar, T. Cermak, and S. Misak, "Modeling and experimentation of a 12kW direct driven PM synchronous generator of wind power," *3rd Int. Conf. Control. Eng. Inf. Technol. CEIT 2015*, 2015, doi: 10.1109/CEIT.2015.7233038.

[256] M. Gomez, E. Ribeiro, J. Estima, C. Boccaletti, and A. J. M. Cardoso, "Development of an effective MPPT method suitable to a stand-alone, low-cost wind turbine system," *IECON Proc. (Industrial Electron. Conf.*, no. 8, pp. 5550–5555, 2016, doi: 10.1109/IECON.2016.7793128.

[257] Y. Zhu, H. Zang, L. Cheng, and S. Gao, "Output power smoothing control for a wind farm based on the allocation of wind turbines," *Appl. Sci.*, vol. 8, no. 6, pp. 2–7, 2018, doi: 10.3390/app8060980.

[258] D. S. Wankhede and M. V. Aware, "Effective Switching Sequence Scheme for Space Vector Modulated Two-Level Inverter to Reduce the Current Distortion in Linear Operating Range," *India Int. Conf. Power Electron. IICPE*, vol. 2018-Decem, pp. 2018–2021, 2018, doi: 10.1109/IICPE.2018.8709596.

[259] M. A. Islam, M. B. Hossen, B. Banik, and B. C. Ghosh, "Field oriented space vector pulse width modulation control of permanent magnet brushless DC motor," *5th IEEE Reg. 10 Humanit. Technol. Conf. 2017, R10-HTC 2017*, vol. 2018-Janua, no. December, pp. 322–327, 2018, doi: 10.1109/R10-HTC.2017.8288966.

[260] K. N. V. Prasad, P. Parimitapradhan, B. Misra, and J. Surekha, "A modified space vector algorithm for 5-level cascaded multilevel inverter," *2017 Innov. Power Adv. Comput. Technol. i-PACT 2017*, vol. 2017-Janua, pp. 1–6, 2017, doi: 10.1109/IPACT.2017.8245107.

[261] P. Tinglong, J. Zhicheng, and J. Zhenhua, "Maximum power point tracking of wind energy conversion systems based on sliding mode extremum seeking control," *2008 IEEE Energy 2030 Conf. ENERGY 2008*, 2008, doi: 10.1109/ENERGY.2008.4781032.

[262] G. Kusic, *Computer-Aided Power Systems Analysis*. 2018.

[263] M. K. Islam, M. Abdullah-Al-Jobayer, M. J. H. Mahi, and K. Abdulla Al Mamun, "Pure sine wave gain and efficiency improvement of three-phase cascade multilevel inverter," *2016 5th Int. Conf. Informatics, Electron. Vision, ICIEV 2016*, pp. 287–292, 2016, doi: 10.1109/ICIEV.2016.7760012.

[264] J. Tautz-Weinert and S. J. Watson, "Using SCADA data for wind turbine condition monitoring - A review," *IET Renew. Power Gener.*, vol. 11, no. 4, pp. 382–394, 2017, doi: 10.1049/iet-rpg.2016.0248.

[265] A. Priyadarshi, P. K. Kar, and S. B. Karanki, "A Single Source Transformer-less Boost Multilevel Inverter Topology with Self Voltage Balancing," *IEEE Trans. Ind. Appl.*, vol. 9994, no. v, pp. 1–1, 2020, doi: 10.1109/tia.2020.2988012.

[266] M. Parchomiuk, R. Strzelecki, K. Zymmer, and A. Domino, "Modular power converter with superconducting magnetic energy storage for electric power distribution system- A nalysis and simulation," *2017 19th Eur. Conf. Power Electron. Appl. EPE 2017 ECCE Eur.*, vol. 2017-Janua, pp. 1–6, 2017, doi: 10.23919/EPE17ECCEEurope.2017.8099341.

[267] P. V. Vimal and K. S. Shivaprakasha, "IOT based greenhouse environment monitoring and controlling system using Arduino

platform," *2017 Int. Conf. Intell. Comput. Instrum. Control Technol. ICICICT 2017*, vol. 2018-Janua, pp. 1514–1519, 2018, doi: 10.1109/ICICICT1.2017.8342795.

[268] V. Romashchenko, M. Brutscheck, and I. Chmielewski, "Investigation and Implementation of Robust Wireless Zigbee Based Security System," *29th Irish Signals Syst. Conf. ISSC 2018*, 2018, doi: 10.1109/ISSC.2018.8585286.

[269] M. Pataky and P. Fecil'ak, "Remote arduino programming with blockly web interface," *Proc. - 2019 Int. Conf. Comput. Electron. Commun. Eng. iCCECE 2019*, pp. 22–25, 2019, doi: 10.1109/iCCECE46942.2019.8941764.

[270] S. S. Pawar, S. Pise, K. Walke, and R. Mohite, "Smart Garbage Monitoring System Using AVR Microcontroller," *Proc. - 2018 4th Int. Conf. Comput. Commun. Control Autom. ICCUBEA 2018*, pp. 2018–2021, 2018, doi: 10.1109/ICCUBEA.2018.8697585.

[271] E. Samadaei, S. A. Gholamian, A. Sheikholeslami, and J. Adabi, "An Envelope Type (E-Type) Module: Asymmetric Multilevel Inverters with Reduced Components," *IEEE Trans. Ind. Electron.*, vol. 63, no. 11, pp. 7148–7156, 2016, doi: 10.1109/TIE.2016.2520913.

[272] K. Zhou, J. Qu, Z. Zhou, and X. Xu, "Crest Factor Minimization for Multitone Waveform Synthesis Using the Clipping Algorithm," *CPEM 2018 - Conf. Precis. Electromagn. Meas.*, pp. 9–10, 2018, doi: 10.1109/CPEM.2018.8501139.

[273] M. Aleenejad, R. Ahmadi, and P. Moamaei, "A modified selective harmonic elimination method for fault-tolerant operation of multilevel cascaded H-bridge inverters," *2014 IEEE Power Energy Conf. Illinois, PECI 2014*, pp. 2–6, 2014, doi: 10.1109/PECI.2014.6804558.

[274] H. K. Jahan, F. Panahandeh, M. Abapour, and S. Tohidi, "Reconfigurable Multilevel Inverter with Fault-Tolerant Ability," *IEEE Trans. Power Electron.*, vol. 33, no. 9, pp. 7880–7893, 2018, doi: 10.1109/TPEL.2017.2773611.

[275] S. Gomathi, M. V. Suganyadevi, S. Kamalakannan, K. Ramash Kumar, and A. Deepak, "Active Bridges Based Bidirectional DC-DC Converter for Solar PV application," *Proc. - Int. Conf. Smart Electron. Commun. ICOSEC 2020*, no. Icosec, pp. 1087–1094, 2020, doi: 10.1109/ICOSEC49089.2020.9215300.

[276] H. Wu, D. Depernet, V. Lanfranchi, K. E. K. Benkara, and M. A. H. Rasid, "A Novel and Simple Torque Ripple Minimization Method of Synchronous Reluctance Machine Based on Torque Function Method," *IEEE Trans. Ind. Electron.*, vol. 68, no. 1, pp. 92–102, 2020, doi: 10.1109/tie.2019.2962490.

[277] W. Kang, C. Lee, S. Member, S. Bae, S. Oh, and S. Member, "Ripple Minimization for Harmonic-geared Series Elastic Actuator under Force Control," pp. 279–284, 2020.

[278] P. M. Lingom, J. Song-Manguelle, D. L. Mon-Nzongo, R. C. C. Flesch, and T. Jin, "Analysis and Control of PV Cascaded H-Bridge Multilevel Inverter with Failed Cells and Changing Meteorological Conditions," *IEEE Trans. Power Electron.*, vol. 36, no. 2, pp. 1777–1789, 2021, doi: 10.1109/TPEL.2020.3009107.

[279] A. Salem, H. Van Khang, K. G. Robbersmyr, M. Norambuena, and J. Rodriguez, "Voltage Source Multilevel Inverters With Reduced Device Count: Topological Review and Novel Comparative Factors," *IEEE Trans. Power Electron.*, vol. 36, no. 3, pp. 2720–2747, 2020, doi: 10.1109/tpel.2020.3011908.

[280] A. Lashab *et al.*, "A Cascaded H-Bridge with Integrated Boosting Circuit," *IEEE Trans. Power Electron.*, vol. 36, no. 1, pp. 18–22, 2021, doi: 10.1109/TPEL.2020.3000724.

[281] A. Khoshkbar-sadigh and K. Corzine, "Active Voltage-Balancing and Thermal Performance Analysis of Dual Flying-Capacitor Active Neutral- Point-Clamped (DFC-ANPC) Inverters," vol. 9994, no. c, 2020, doi: 10.1109/TIA.2020.3036570.

[282] Z. Tang, Y. Yang, and F. Blaabjerg, "An Interlinking Converter for Renewable Energy Integration Into Hybrid Grids," *IEEE Trans. Power Electron.*, vol. 36, no. 3, pp. 2499–2504, 2020, doi: 10.1109/tpel.2020.3018585.

[283] T. Sigamani, R. P. Ponraj, and V. Ravindran, "Modified single phase matrix converter with Z-source for renewable energy systems," *Proc. 3rd Int. Conf. Smart Syst. Inven. Technol. ICSSIT 2020*, no. Icssit, pp. 601–607, 2020, doi: 10.1109/ICSSIT48917.2020.9214138.

[284] D. Lopez Del Moral, A. Barrado, M. Sanz, A. Lazaro, and P. Zumel, "Analysis, Design, and Implementation of the AFZ Converter Applied to Photovoltaic Systems," *IEEE Trans. Power Electron.*, vol. 36, no. 2, pp. 1883–1900, 2021, doi:

10.1109/TPEL.2020.3010152.

[285] C. Lucas, M. Guemri, and Q. T. Tran, “Controlling consumption to reduce stress on grid infrastructure while enhancing PV penetration,” pp. 999–1006, 2020, doi: 10.1109/energycon48941.2020.9236567.

[286] X. Xu, Y. Jia, and C. S. Lai, “Bi-level optimal planning of voltage regulator in distribution system considering maximization of incentive-based photovoltaic energy integration,” *CSEE J. Power Energy Syst.*, 2020, doi: 10.17775/cseejpes.2020.01230.

[287] V. Kleinschmidt, T. Hamacher, V. Peric, and M. Reza Hesamzadeh, “Unlocking Flexibility in Multi-Energy Systems: A Literature Review,” *Int. Conf. Eur. Energy Mark. EEM*, vol. 2020-Septe, 2020, doi: 10.1109/EEM49802.2020.9221927.

[288] Y. Tang *et al.*, “WEC fault modelling and condition monitoring: A graph-theoretic approach,” *IET Electr. Power Appl.*, vol. 14, no. 5, pp. 781–788, 2020, doi: 10.1049/iet-epa.2019.0763.

[289] L. He, M. Attia, L. Hao, B. Fang, K. Younsi, and H. Wang, “Remote Monitoring and Diagnostics of Blade Health in Commercial MW-Scale Wind Turbines Using Electrical Signature Analysis (ESA),” pp. 808–813, 2020, doi: 10.1109/ecce44975.2020.9235984.

[290] J. Wang, W. Qiao, and L. Qu, “Wind Turbine Bearing Fault Diagnosis Based on Sparse Representation of Condition Monitoring Signals,” *IEEE Trans. Ind. Appl.*, vol. 55, no. 2, pp. 1844–1852, 2019, doi: 10.1109/TIA.2018.2873576.

[291] M. Moness and A. M. Moustafa, “A Survey of Cyber-Physical Advances and Challenges of Wind Energy Conversion Systems: Prospects for Internet of Energy,” *IEEE Internet Things J.*, vol. 3, no. 2, pp. 134–145, 2016, doi: 10.1109/JIOT.2015.2478381.

APPENDIX

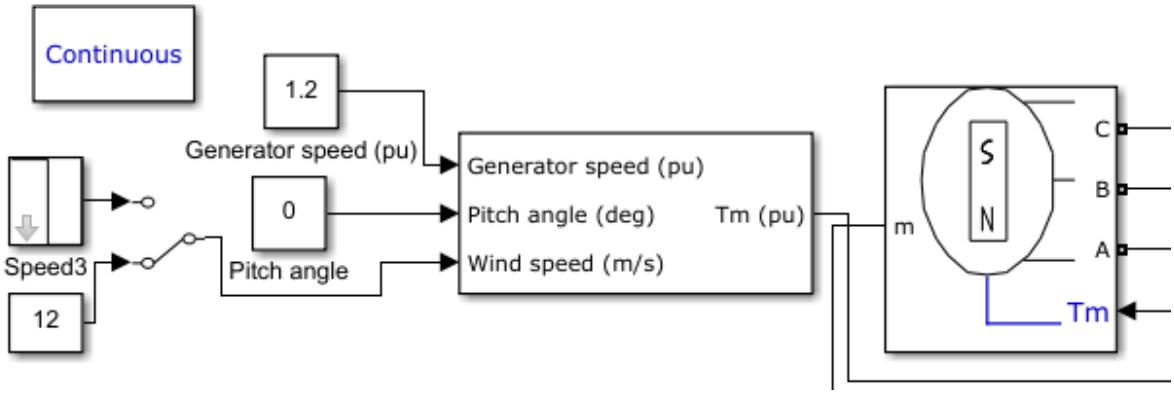

(1)

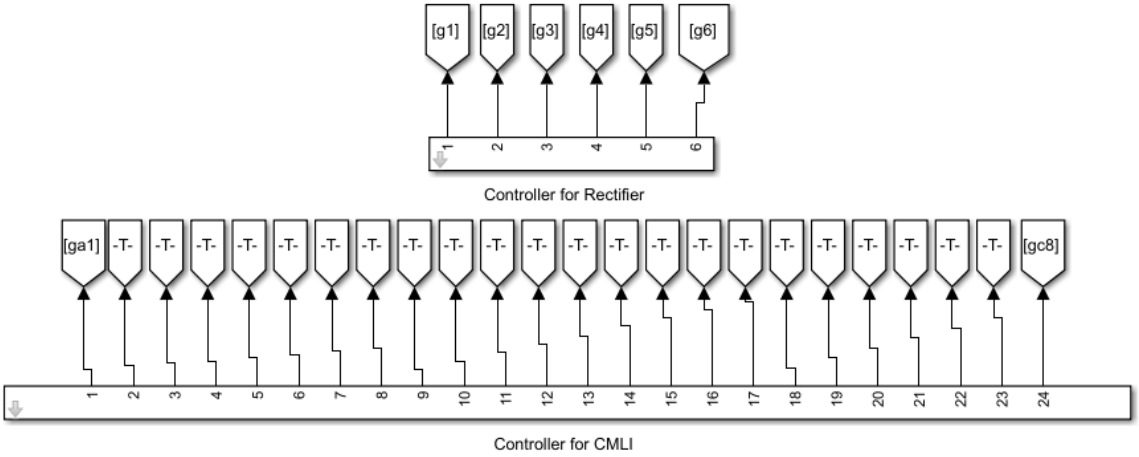

(2)

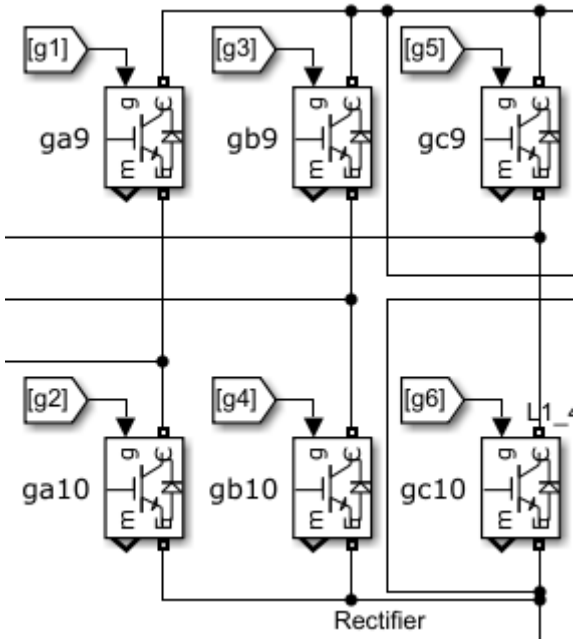

(3)

Fig. A (1). Wind Generator Model, A (2). Controllers, A (3). Rectifier

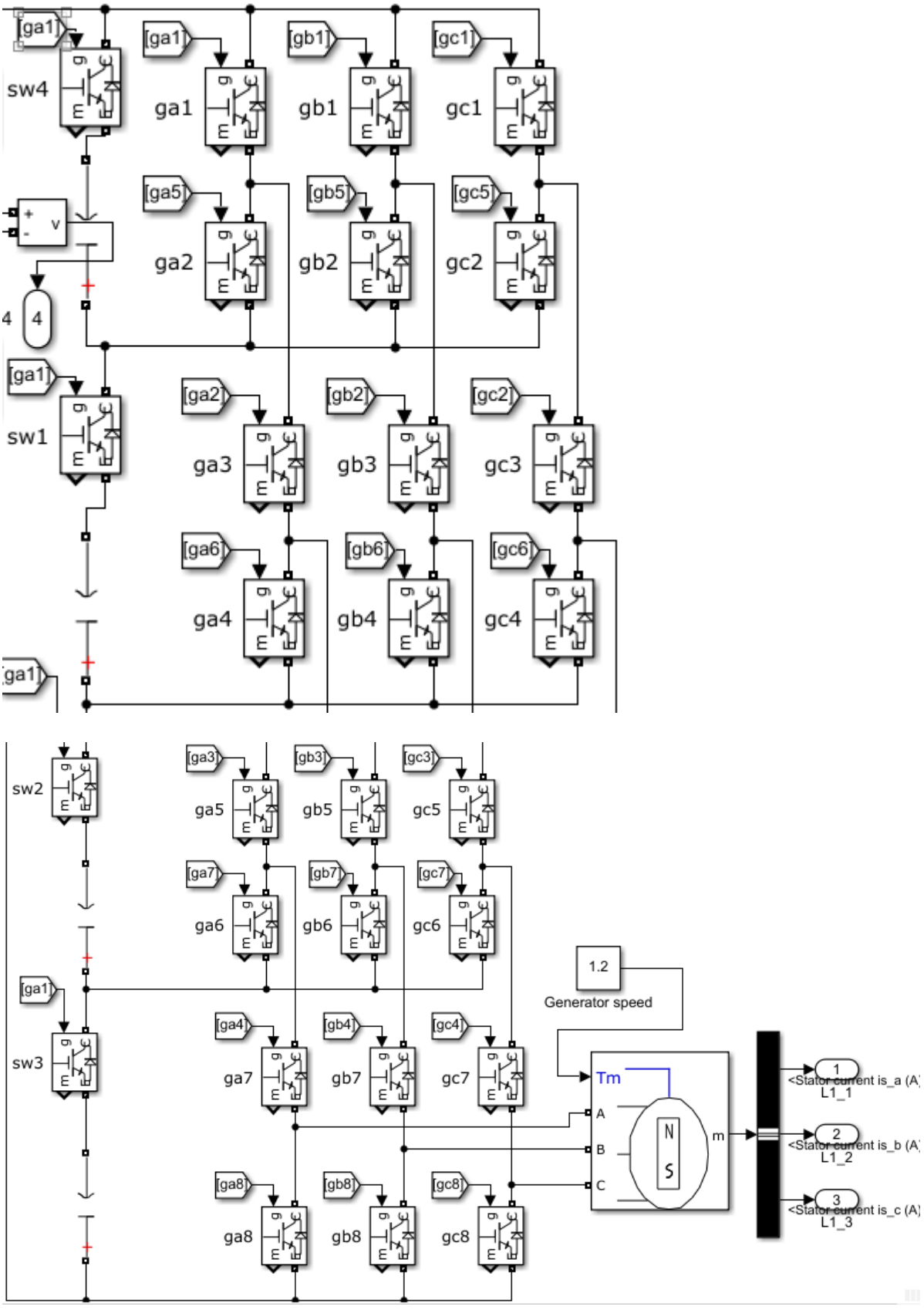
[ga1]
sw4
ga1
gb1
gc1
[ga5]
[gb5]
[gc5]
ga2
gb2
gc2
4
[ga1]
sw1
[ga2]
[gb2]
[gc2]
ga3
gb3
gc3
[ga6]
[gb6]
[gc6]
ga4
gb4
gc4
[ga1]
sw2
[ga3]
[gb3]
[gc3]
ga5
gb5
gc5
[ga7]
[gb7]
[gc7]
ga6
gb6
gc6
[ga1]
sw3
[ga4]
[gb4]
[gc4]
ga7
gb7
gc7
[ga8]
[gb8]
[gc8]
ga8
gb8
gc8
1.2
Generator speed
Tm
A
B
C
N
S
m
1
<Stator current is_a (A)
L1_1
2
<Stator current is_b (A)
L1_2
3
<Stator current is_c (A)
L1_3

Fig. A (4). CMLI

Authorship Statements

Authorship Statement

on

"A Hybrid Multilevel Power Electronic Inverter and Fault Location Identification of Switching Devices"

This study was designed, directed and coordinated by Md Liton Hossain, A. Au-Siada, S. M. Muyeen which is published in 2018 Condition Monitoring and Diagnosis (CMD), Perth, WA, 2018.

Contributors' of the paper:

I, Md Liton Hossain, PhD student at Curtin University have developed a hybrid multilevel power electronic inverter along with fault location identification technique. I have designed the inverter and fault identification technique which is validated through simulated results. I have written the manuscript based on the results.

Signature [redacted] ..... Date: 20/08/2020

I, Ahmed Abu-Siada, guided, supervised, and investigated necessity conditions of the work. I reviewed and corrected the manuscript written. I believe that I contributed 10% of the work.

Signature: [redacted] ..... Date: 20/08/2020

I, SM Muyeen, reviewed, and corrected the manuscript. I believe that I contributed 10% of the work.

Signature [redacted] ..... Date: 20/8/2020

Authorship Statement

on

"Methods for Advanced Wind Turbine Condition Monitoring and Early Diagnosis: A Literature Review"

This study was designed, directed and coordinated by Md Liton Hossain, A. Au-Siada, S. M. Muyeen which is published in Energies. 2018.

Contributors' of the paper:

I, Md Liton Hossain, PhD student at Curtin University have studied and investigated different existing methods and condition monitoring techniques of wind turbine. I have generated all the results based on literature investigation. I have written the manuscript based on the results.

Signature [redacted] Date: 20/08/2020

I, Ahmed Abu-Siada, guided, supervised, and investigated necessity conditions of the work. I reviewed and corrected the manuscript written. I believe that I contributed 15% of the work.

Signature: [redacted] Date: 20/8/2020

I, SM Muyeen, reviewed, and corrected the manuscript. I believe that I contributed 10% of the work.

Signature: [redacted] Date: 20/8/2020

Authorship Statement

on

"A Review on Wind Turbine Condition Monitoring and Fault Diagnosis"

This study was designed, directed and coordinated by Md Liton Hossain which is published in Proceedings of One Curtin International Postgraduate Conference in December 2017.

I, Md Liton Hossain, PhD student at Curtin University have studied and investigated the condition monitoring and fault diagnosis of wind turbine. I have written the manuscript based on the results.

Signature [redacted] Date: 20/08/2020

Authorship Statement

on

"Design and Validation of a Generalized Multilevel Inverter with Simplified Switching Technique"

This study was designed, directed and coordinated by Md Liton Hossain, A. Au-Siada, S. M. Muyeen, Zulkifilie Ibrahim, Frede Blaabjerg which is published in Electric Power Components and System in 07 April 2020.

Contributors' of the paper:

I, Md Liton Hossain, PhD student at Curtin University have developed a generalized multilevel inverter along with simplified space vector pulse width modulation. I have generated all the results based on my own simulation model. which is validated through my developed experimental hardware prototype. I have written the manuscript based on the results.

Signature [redacted] Date: 20/08/2020

I, Ahmed Abu-Siada, guided, supervised, and investigated necessity conditions of the work. I reviewed and corrected the manuscript written. I believe that I contributed 10% of the work.

Signature: [redacted] Date: 20/08/2020

I, SM Muyeen, reviewed, and corrected the manuscript. I believe that I contributed 10% of the work.

Signature: [redacted] Date: 20/8/2020

I, Zulkifilie Ibrahim, encouraged the idea from Md Liton Hossain, and motivated him to prepare a well-presented manuscript. I reviewed and corrected the manuscript. I believe that I contributed 10% of the work.

Signature: [redacted] Date: 21/8/2020.

I, Frede Blaabjerg, reviewed and corrected the manuscript. I believe that I contributed 5% of the work.

Signature: [redacted] Date: 22/8 - 2020

Authorship Statement

on

"Industrial IoT based Condition Monitoring for Wind Energy Conversion System"

This study was designed, directed and coordinated by Md Liton Hossain, A. Au-Siada, S. M. Muyeen, Md Mubashwar Hasan, and Md Momtazur Rahman which is accepted in 24.06.2020, CSEE Journal of Power and Energy Systems.

Contributors' of the paper:

I, Md Liton Hossain, PhD student at Curtin University have developed a wind energy conversion system along with an IoT monitoring system. I have generated all the results based on my own simulation model, which is validated through my developed experimental hardware prototype. I have written the manuscript based on the results.

Signatu[redacted] ..... Date: 20/08/2020

I, Ahmed Abu-Siada, guided, supervised, and investigated necessity conditions of the work. I reviewed and corrected the manuscript written. I believe that I contributed 15% of the work.

Signature:[redacted] ..... Date: 2./08/2020.....

I, SM Muyeen, reviewed, and corrected the manuscript. I believe that I contributed 10% of the work.

Signature[redacted] ..... Date: 20/8/2020

I, Md Mubashwar Hasan, encouraged the idea from Md Liton Hossain, and motivated him to prepare a well-presented manuscript. I reviewed and corrected the manuscript. I believe that I contributed 5% of the work.

Signature:[redacted] ..... Date: 20/08/2020

I, Md Momtazur Rahman, reviewed and corrected the manuscript. I believe that I contributed 5% of the work.

Signature:[redacted] ..... Date: 20/08/2020

Authorship Statement

on

"Topologies, Controllers, Applications and Future Challenges of Multilevel Inverters: A Comprehensive Review"

This study was designed, directed and coordinated by Md Liton Hossain, A. Au-Siada, S. M. Muyeen, and Md Mubashwar Hasan which is submitted to Journal of Energy Storage in August 2020.

Contributors' of the paper:

I, Md Liton Hossain, PhD student at Curtin University have studied and investigated different multilevel inverter topologies and controllers. I have written the manuscript based on the studied literatures.

Signature: [redacted] Date: 20/08/2020

I, Ahmed Abu-Siada, guided, supervised, and investigated necessity conditions of the work. I reviewed and corrected the manuscript written. I believe that I contributed 10% of the work.

Signature: [redacted] Date: 20/8/2020

I, SM Muyeen, reviewed, and corrected the manuscript. I believe that I contributed 5% of the work.

Signature: [redacted] Date: 20/8/2020

I, Md Mubashwar Hasan, encouraged the idea from Md Liton Hossain, and motivated him to prepare a well-presented manuscript. I reviewed and corrected the manuscript. I believe that I contributed 5% of the work.

Signature: [redacted] Date: 20/08/2020